

Aus dem
Department für Frauengesundheit Tübingen
Forschungsinstitut für Frauengesundheit

**Assessing Endometrial SARS-CoV-2 Infection with 3D
Spheroids and Organoids: Implications for Vertical
Transmission**

**Inaugural-Dissertation
zur Erlangung des Doktorgrades
der Medizin**

**der Medizinischen Fakultät
der Eberhard Karls Universität
zu Tübingen**

vorgelegt von

Liu, Anna

2024

Dekan: Professor Dr. B. Pichler

1. Berichterstatter: Professorin Dr. S. Brucker

2. Berichterstatter: Professor Dr. D. Sauter

Tag der Disputation: 23.07.2024

Für meine Eltern

Table of Contents

List of Figures	V
List of Tables.....	VIII
List of Abbreviations.....	IX
1 Introduction.....	1
1.1 Endometrial Anatomy and Physiology.....	1
1.1.1 The Human Endometrium and the Menstrual Cycle	1
1.1.2 Decidualization.....	2
1.1.3 Physiology of RAS and ACE2.....	4
1.1.4 The Role of ACE2 in the Endometrium and during Pregnancy.....	6
1.2 Pregnancy and the Immune System	8
1.2.1 Anatomical and Physiological Changes during Pregnancy.....	8
1.2.2 The Immune System during Pregnancy.....	10
1.3 SARS-CoV-2 and COVID-19.....	11
1.3.1 Structure and Pathophysiology of SARS-CoV-2.....	11
1.3.2 Clinical Characteristics of COVID-19	14
1.4 COVID-19 and Pregnancy.....	16
1.4.1 Maternal and Neonatal Outcomes	16
1.4.2 Possibility of Vertical Transmission.....	17
1.5 Models used in Biomedical Research	19
1.5.1 Monolayer Cell Culture and Animal Models.....	21
1.5.2 Three-Dimensional Cell Culture Models	22
1.5.3 3D Models in Reproductive Medicine	24
1.6 Hypothesis and Aims.....	26
2 Materials and Methods	27
2.1 Materials	27
2.2 Methods.....	36
2.2.1 2D Cell Culture.....	36
2.2.2 Culturing Endometrial Spheroids in Agarose-Coated Microplates....	36
2.2.3 Imaging and Growth Monitoring of Endometrial Spheroids	37

2.2.4	Viability Assay for Endometrial Spheroids	38
2.2.5	Endometrial Organoids Culture.....	38
2.2.6	Apical Out Assay of Endometrial Organoids.....	39
2.2.7	Immunostaining of Apical Out and Basal Out Endometrial Organoids	40
2.2.8	Decidualization Treatment	42
2.2.9	Infection of 2D Cells, Endometrial Spheroids and Endometrial Organoids with SARS-CoV-2.....	43
2.2.10	Immunostaining of Endometrial Spheroids	44
2.2.11	RNA Extraction, cDNA Synthesis and qPCR.....	46
2.2.12	RNA Extraction and RNA Sequencing after Infection	48
2.2.13	Protein Extraction, Gel Electrophoresis and Western Blot.....	50
2.2.14	Cytokine Quantification through Flow Cytometry.....	52
2.2.15	Statistics.....	53
3	Results	54
3.1	Decidualization of 2D HESC and ISK cells.....	54
3.1.1	Expression of Decidualization Markers in HESC and ISK cells	55
3.1.2	Effect of Decidualization on ACE2 and TMPRSS2 levels in 2D HESC and ISK cells	57
3.2	Establishment and Optimization of Endometrial Spheroids.....	59
3.3	Characterization of Endometrial Spheroids	63
3.3.1	Formation and Growth of Endometrial Spheroids.....	63
3.3.2	Viability of Endometrial Spheroids	65
3.3.3	Immunostaining for Epithelial and Stromal Cell Markers in Endometrial Spheroids.....	66
3.4	Decidualization of Endometrial Spheroids.....	67
3.4.1	Decidualization Markers in Endometrial Spheroids	67
3.4.2	Effect of Decidualization on ACE2 and TMPRSS2 Levels in Endometrial Spheroids.....	68
3.5	Culture and Growth of Endometrial Organoids.....	69
3.6	Characterization of Basal Out and Apical Out Endometrial Organoids.....	70
3.7	Expression of ACE2 and TMPRSS2 in Endometrial Organoids.....	73

3.8	Infection of Endometrial Organoids with SARS-CoV-2.....	74
3.9	Infectibility of 2D Endometrial Cells with SARS-CoV-2	75
3.10	Infection of Endometrial Spheroids with SARS-CoV-2.....	77
3.10.1	Immunostaining of Infected Endometrial Spheroids	77
3.10.2	Verification of Infection in Endometrial Spheroids through Western Blot	78
3.10.3	Cytokine Levels in Endometrial Spheroids after Infection with SARS-CoV-2.....	79
3.10.4	RNA Sequencing of Infected Endometrial Spheroids	81
3.10.5	Verification of RNA Sequencing Results of Infected Endometrial Spheroids through qPCR.....	90
4	Discussion.....	94
4.1	Endometrial Spheroids	94
4.1.1	Establishment and Optimization of Endometrial Spheroids	94
4.1.2	Formation and Growth of Endometrial Spheroids.....	96
4.1.3	Viability of Endometrial Spheroids	99
4.1.4	Epithelial and Stromal Cell Markers in Endometrial Spheroids.....	100
4.2	Endometrial Organoids.....	101
4.2.1	Culture and Growth of Endometrial Organoids.....	101
4.2.2	Basal Out and Apical Out Polarity of Endometrial Organoids.....	102
4.3	Decidualization and the Effect on ACE2 and TMPRSS2 in the Endometrium.....	103
4.3.1	Markers of Decidualization.....	103
4.3.2	Effect of Decidualization on ACE2 and TMPRSS2 Levels.....	106
4.4	SARS-CoV-2 Infection in the Endometrium.....	111
4.4.1	Susceptibility of Endometrial Monolayers and 3D Cultures to SARS-CoV-2.....	111
4.4.2	Cytokines in Endometrial Spheroids Infected with SARS-CoV-2....	115
4.4.3	Changes in Gene Expression in Endometrial Spheroids Infected with SARS-CoV-2	117
4.5	Conclusion and Outlook	128
5	Abstract	131
6	Zusammenfassung.....	133

7	Bibliography.....	135
8	Appendix	181
8.1	Supplementary Data: Materials and Methods	181
8.2	Supplementary Data: Results.....	184
9	Erklärung zum Eigenanteil	197
10	Publications	198
11	Acknowledgements	199

List of Figures and Supplementary Figures

Figure 1-1: The Renin-Angiotensin System (RAS) and the Role of the Angiotensin-Converting Enzyme 2 (ACE2)	5
Figure 1-2: Decidualization and ACE2 in the Human Endometrium	7
Figure 1-3: Structure and Cell Entry Mechanism of SARS-CoV-2	13
Figure 1-4: Vertical Transmission of Pathogens and Possible Consequences	19
Figure 3-1: Culture and Decidualization Treatment of Monolayer Cells	54
Figure 3-2: Decidualization Markers in HESC and ISK Cells.....	56
Figure 3-3: ACE2 and TMPRSS2 in 2D HESC and ISK Cells	58
Figure 3-4: Schematic Plan of the Optimization of Endometrial Spheroids	59
Figure 3-5: Liquid-Overlay Technique.....	60
Figure 3-6: Optimization of Endometrial Spheroids	62
Figure 3-7: Growth of Endometrial Spheroids.....	64
Figure 3-8: Growth Curve of Endometrial Spheroids	65
Figure 3-9: Viability Assay of Endometrial Spheroids	66
Figure 3-10: Immunostaining of Endometrial Spheroids for Epithelial and Stromal Cell Markers	67
Figure 3-11: Decidualization Markers in Endometrial Spheroids	68
Figure 3-12: ACE2 and TMPRSS2 Levels in Endometrial Spheroids.....	69
Figure 3-13: Formation and Growth of Endometrial Organoids	70
Figure 3-14: Comparison of the Morphology of Basal Out and Apical Out Endometrial Organoids.....	71
Figure 3-15: Immunostaining of Apical Out and Basal Out Endometrial Organoids.....	72
Figure 3-16: Protein Levels of ACE2 and TMPRSS2 in Endometrial Organoids	73
Figure 3-17: Infection of Endometrial Organoids with SARS-CoV-2.....	74
Figure 3-18: Infection of HESC and ISK with SARS-CoV-2.....	76
Figure 3-19: Experimental Set-Up for Infection of Endometrial Spheroids	77
Figure 3-20: Immunostaining of Non-Infected and Infected Endometrial Spheroids	78

Figure 3-21: Detection of SARS-CoV-2 Nucleocapsid Protein in Infected and Non-Infected Endometrial Spheroids	79
Figure 3-22: Cytokine Levels of Infected and Non-Infected Endometrial Spheroids	80
Figure 3-23: Volcano Plots of DEGs in Endometrial Spheroids Infected with SARS-CoV-2	83
Figure 3-24: Principal Component Analysis of RNA-Seq Data from Endometrial Spheroids after Infection with SARS-CoV-2.....	85
Figure 3-25: Heat Map Analysis of Gene Expression Profiles of Endometrial Spheroids after Infection with SARS-CoV-2	87
Figure 3-26: Gene Ontology Enrichment Analysis and Pathway Annotation of Endometrial Spheroids Infected with SARS-CoV-2.....	89
Figure 3-27: Validation of DEGs in SARS-CoV-2 Infected Endometrial Spheroids through qPCR	91
Figure 4-1: Spheroid Formation, Growth and Microenvironment.....	97
Figure 4-2: Hypothetical Pathway of ACE2 Upregulation during Decidualization	110
Figure 4-3: Potential Harmful Effects of SARS-CoV-2 Infection during Pregnancy	129
Supplementary Figure 8-1: Full Western Blot for ACE2 and TMPRSS2 in 2D HESC and ISK Cells	184
Supplementary Figure 8-2: Comparison of Endometrial Spheroids Grown in Agarose-Coated or Ultra-Low Attachment Wells.....	185
Supplementary Figure 8-3: Additional Images of the Growth of Endometrial Spheroids	186
Supplementary Figure 8-4: Additional Images of Viability Assay of Endometrial Spheroids	187
Supplementary Figure 8-5: Additional Images of Immunostaining of Endometrial Spheroids for Cytokeratin 7 and Vimentin.....	188
Supplementary Figure 8-6: Full Western Blot for ACE2 and TMPRSS2 in Endometrial Spheroids	189

Supplementary Figure 8-7: Full Western Blot for ACE2 and TMPRSS2 in Endometrial Organoids.....	190
Supplementary Figure 8-8: Full Western Blot for SARS-CoV-2 Nucleocapsid Protein in Infected Basal Out Organoids	191
Supplementary Figure 8-9: Full Western Blot for SARS-CoV-2 Nucleocapsid Protein in Infected Apical Out Organoids	192
Supplementary Figure 8-10: Full Western Blot for SARS-CoV-2 Nucleocapsid Protein in Infected 2D Cells	193
Supplementary Figure 8-11: Additional Images of Non-Infected and Infected Endometrial Spheroids	194
Supplementary Figure 8-12: Full Western Blot for SARS-CoV-2 Nucleocapsid Protein in Infected Endometrial Spheroids	195
Supplementary Figure 8-13: Heat Map with Dendrogram of DEGs from Endometrial Spheroids Infected with SARS-CoV-2.....	196

List of Tables and Supplementary Tables

Table 1-1: Comparison of 2D Cell Culture, Animal and 3D Cell Culture models	20
Table 2-1: List of Cells and Viruses, in Alphabetical Order.....	27
Table 2-2: List of Reagents and Chemicals, in Alphabetical Order	28
Table 2-3: List of Consumable Supplies, in Alphabetical Order.....	32
Table 2-4: List of Antibodies, in Alphabetical Order.....	33
Table 2-5: List of Primers, in Alphabetical Order	34
Table 2-6: List of Machines, in Alphabetical Order	35
Table 2-7: List of Software, in Alphabetical Order	35
Table 3-1: Number of Differentially Expressed Genes.....	82
Supplementary Table 8-1: Endometrial Organoids Medium, for 30 ml	181
Supplementary Table 8-3: Tri-Sodium Citrate Buffer, pH 6	181
Supplementary Table 8-4: Laemmli Buffer 2X, for 50 ml	182
Supplementary Table 8-5: Hand Casted Electrophoresis Gel, Volume for Two Gels	183
Supplementary Table 8-6: Tris Buffered Saline Tween 20 (TBST).....	183

List of Abbreviations

11 β HSD	11 β -Hydroxysteroid dehydrogenase
2D	Two-dimensional
3D	Three-dimensional
ACE	Angiotensin-converting enzyme
ACE2	Angiotensin-converting enzyme 2
<i>ACTB</i>	β -actin gene
Ang I/II	Angiotensin I/II
ANOVA	Analysis of variance
APS	Ammonium persulfate solution
BME	Basement membrane extract
CACO-2	Colorectal adenocarcinoma cell line, from <i>Cancer coli</i>
cAMP	Cyclic adenosine monophosphate
CCL20	Chemokine (C-C motif) ligand 20
CD38	Cluster of differentiation 38
cDNA	Complementary deoxyribonucleic acid
CMV	Cytomegalovirus
COVID-19	Coronavirus disease 2019
CRH	Corticotropin-releasing hormone
Ct	Threshold cycle (qPCR)
DAPI	4',6-Diamidino-2-phenylindole
DCC	Dextran coated charcoal
DEG	Differentially expressed genes
DMEM/F12	Dulbecco's modified eagle medium/Nutrient mixture F-12
DMSO	Dimethyl sulfoxide
ECM	Extracellular matrix
EDTA	Ethylenediaminetetraacetic acid
EGF	Epidermal growth factor
FBS	Fetal bovine serum

FC	Fold change
FDR	False discovery rate
FOXO1A	Forkhead box protein O1
GAPDH	Glyceraldehyde 3-phosphate dehydrogenase
GnRH	Gonadotropin-releasing hormone
GO	Gene ontology
hCG	Human chorionic gonadotropin
HEPES	4-(2-Hydroxyethyl)-1-piperazineethanesulfonic acid
HESC	Human endometrial stromal cells
HRP	Horseradish peroxidase
HSV	Herpes simplex virus
icSARS-CoV-2-mNG	Recombinant SARS-CoV-2 expressing mNeonGreen
ICU	Intensive care unit
IGFBP-1	Insulin-like growth factor-binding protein 1
IgG	Immunoglobulin G
IgM	Immunoglobulin M
IL-6	Interleukin 6
IL-8	Interleukin 8
IL1RL1	Interleukin 1 receptor-like 1
ISK	Ishikawa cells, a well-differentiated human endometrial adenocarcinoma cell line
IU	Infection units
JAK	Janus kinase
LCN2	Lipocalin 2
LEFTY1	Left-right determination factor 1
MCP-1	Monocyte chemoattractant protein 1
MERS-CoV	Middle East respiratory syndrome-related coronavirus
MOI	Multiplicity of infection
MPA	Medroxyprogesterone 17-acetate

mRNA	Messenger ribonucleic acid
NR4A3	Nuclear receptor 4A3
PBS	Phosphate buffered saline
PCA	Principal component analysis
PFA	Paraformaldehyde
<i>PRL</i>	Prolactin (gene)
PVDF	Polyvinylidene fluoride
qPCR	Quantitative polymerase chain reaction
RAS	Renin–angiotensin system
RNA	Ribonucleic acid
RNA-seq	RNA sequencing
SARS-CoV	Severe acute respiratory syndrome coronavirus
SARS-CoV-2	Severe acute respiratory syndrome coronavirus type 2
SDS-PAGE	Sodium dodecyl sulfate polyacrylamide gel electrophoresis
SEM	Standard error of the mean
STAT	Signal transducer and activator of transcription
TBST	Tris buffered saline Tween 20
TEMED	Tetramethylethylenediamine
TGF- β	Transforming growth factor beta
TMPRSS2	Transmembrane protease serine subtype 2
TNF	Tumor necrosis factor
uNK	Uterine natural killer cells
VOI	Variants of interest
VOC	Variants of concern
VTCN1	V-set domain-containing T-cell activation inhibitor 1
ZO-1	Zonula occludens-1

1 Introduction

Parts of the introduction are adopted from a previous publication: Liu, A., Raja Xavier, J., Singh, Y., Brucker, S. Y. & Salker, M. S. 2022. Molecular and Physiological Aspects of SARS-CoV-2 Infection in Women and Pregnancy. *Frontiers in Global Women's Health*, 3.

1.1 Endometrial Anatomy and Physiology

1.1.1 *The Human Endometrium and the Menstrual Cycle*

The female reproductive system is comprised of internal organs, including the vagina, uterus, fallopian tubes and ovaries, as well as the external vulva. The vagina serves as the female copulatory organ and the birth canal (Weber et al., 1995). Oogenesis and production of steroid hormones take place in the ovaries, while fertilization of the oocyte typically occurs in the fallopian tubes (Oktem and Oktay, 2008).

The uterus is a pear-shaped organ consisting of three layers, the outermost of which is the perimetrium, a smooth, serous coating that faces the pelvic cavity. The middle layer, the myometrium, mainly contains smooth muscle, which is also responsible for contractions during parturition (Wray and Prendergast, 2019). The uterine cavity is lined by a mucous membrane composed of a simple columnar epithelium and a multicellular stroma, the endometrium (Critchley et al., 2020). It is the endometrium that allows for embryo implantation, fetal development and therefore a successful pregnancy (Gellersen and Brosens, 2014). Further, this highly hormone-sensitive tissue is subject to morphological, functional as well as molecular and mechanical changes throughout the menstrual cycle (Gellersen and Brosens, 2014).

“The human menstrual cycle is approximately 28 days long and can be divided into two phases: the follicular (proliferative) phase and the luteal (secretory) phase (Ochoa-Bernal and Fazleabas, 2020, Critchley et al., 2020). The start of each cycle is marked by the onset of menstruation

(Brosens et al., 2009). During the first phase, estrogen is produced by granulosa cells in the ovaries, which leads to thickening of the endometrium (Ochoa-Bernal and Fazleabas, 2020). This thickening is the result of proliferating epithelial and stromal cells, as well as angiogenesis (Ochoa-Bernal and Fazleabas, 2020, Clancy, 2009). Ovulation marks the start of the second phase, when the corpus luteum produces progesterone, further preparing the endometrium for the possibility of embryo implantation and pregnancy; a process known as decidualization (Gellersen and Brosens, 2014, Suthaporn et al., 2021). In the case of no pregnancy, the corpus luteum deteriorates leading to a drop in progesterone levels, vasoconstriction in the endometrium with hypoxia and desquamation of the stratum functionalis (Suthaporn et al., 2021, Roberts et al., 1992, Gellersen and Brosens, 2014).” (Liu et al., 2022)

1.1.2 Decidualization

To accommodate pregnancies in species in which placentation involves the breaching of the luminal epithelium by the fetal trophoblast, the endometrium undergoes a process called decidualization (Brosens et al., 2002, Gellersen and Brosens, 2014). While decidualization in most eutherian (placental) mammals only occurs in the presence of a blastocyst, this process takes place spontaneously in higher primates, including humans, some bat species and the elephant shrew (Emera et al., 2012). It has been hypothesized that spontaneous decidualization and menstruation evolved as an adaptive response to conflicting maternal and fetal genomes (Emera et al., 2012).

“The process of decidualization involves the differentiation of endometrial stromal cells, which are of mesenchymal origin and resemble fibroblasts, into decidual cells, similar to epithelial cells (Gellersen et al., 2007, Okada et al., 2018, Ng et al., 2020). During this mesenchymal-epithelial transition, the cells become larger and rounder with an expansion of the rough endoplasmic reticulum and the Golgi apparatus (Gellersen et al., 2007, Gellersen and Brosens, 2014). There is an increase in the number of nucleoli and an

accumulation of lipid and glycogen droplets within the cytoplasm (Gellersen and Brosens, 2014, Okada et al., 2018). It was also shown that polyploidy is common among decidual cells, which might limit their lifespan but could benefit the growth of the embryo due to increased protein synthesis (Sachs and Shelesnyak, 1955, Sroga et al., 2012). Decidual cells produce large quantities of prolactin and insulin-like growth factor binding protein-1, among others, which can also be used as *bona fide* markers for decidualization (Gellersen et al., 2007, Gellersen and Brosens, 2014).” (Liu et al., 2022)

As aforementioned, a major hormonal regulator of decidualization is progesterone. Nonetheless, approximately 10 days of stimulation with progesterone are required for induction of decidualization (Critchley et al., 2020, de Ziegler et al., 1998). It is therefore conceivable that additional factors are critical for initiating the differentiation process. One of them is cyclic adenosine monophosphate (cAMP) (Gellersen et al., 2007, Gellersen and Brosens, 2014). Many local and endocrine cues make use of the cAMP pathway to modulate the endometrium, such as prostaglandin E2 and corticotropin-releasing hormone post-ovulation or human chorionic gonadotrophin during pregnancy (Brar et al., 1997, Gravanis et al., 1999, Gellersen and Brosens, 2003, Tang and Gurdip, 1993).

Besides prolactin and IGFBP-1, the enzyme 11 β -hydroxysteroid dehydrogenase (11 β HSD) is also known to increase during decidualization (Arcuri et al., 1996, Kuroda et al., 2013). Two isoforms of 11 β HSD exist (type 1 and 2) and while both can catalyze the oxidation of cortisol to the inactive metabolite cortisone, only 11 β HSD1 can reduce cortisone into active cortisol (McDonald et al., 2006). The effect of decidualization on 11 β HSD levels in the endometrium is relevant because glucocorticoids play a role in inflammation, maturation of fetal organs and preterm delivery (Marciniak et al., 2011, Damiani et al., 2017).

“The human endometrium is subject to cyclic transformations to provide an optimal environment for embryo implantation, however, the window of implantation is brief (Tan et al., 2018). The uterus is only receptive to a blastocyst during the limited duration of about 4 days, approximately 6 to

10 days after ovulation (Kimber, 2000, Achache and Revel, 2006). Not only does decidualization influence the timing of implantation but it also controls the extent of invasion by the embryo (Sharma et al., 2016). Some studies even suggest that decidual cells are not passively invaded by the trophoblast but actively encapsulate the embryo (Weimar et al., 2013a, Grewal et al., 2010, Grewal et al., 2008). Moreover, the endometrium has the capability to sense the quality of the conceptus and makes a distinction between healthy and impaired embryos (Teklenburg et al., 2010, Brosens et al., 2014). Therefore, the decidua promotes implantation of high-quality embryos while rejecting developmentally impaired ones through modulation of gene expression (Teklenburg et al., 2010, Brosens et al., 2014, Koot et al., 2012). Defective decidualization can lead to a plethora of pregnancy complications such as preeclampsia, preterm birth or even recurrent pregnancy loss, highlighting the importance of adequate decidualization in early pregnancy (Ng et al., 2020, Cha et al., 2012).“ (Liu et al., 2022)

1.1.3 Physiology of RAS and ACE2

The renin-angiotensin system (RAS) regulates systemic blood pressure as well as fluid and electrolyte balance (Hamming et al., 2007). Hypotonia, hypovolemia, hyponatremia as well as sympathetic activity stimulate renin secretion by renal juxtaglomerular cells (Hackenthal et al., 1990). The protease renin cleaves angiotensinogen, produced by the liver, into angiotensin (Ang) I, which is subsequently converted into Ang II by the angiotensin-converting enzyme (ACE) (Hamming et al., 2007). The effects of Ang II include vasoconstriction, aldosterone secretion by the adrenal cortex as well as fluid and sodium retention, which in turn lead to increased blood pressure and volume, resulting in negative feedback for renin secretion (Fyhrquist and Saijonmaa, 2008).

The angiotensin-converting enzyme 2 (ACE2) acts as a counterbalance to its homologue ACE by converting Ang I into Ang 1-9 and Ang II into Ang 1-7 (Donoghue et al., 2000, Wang et al., 2020b). ACE2 is ubiquitously expressed

throughout the human body, with the highest amounts found in the kidneys, heart, lungs, testes, intestines and vascular smooth muscle cells (Hamming et al., 2004, Gheblawi et al., 2020, Li et al., 2020b). Protective effects of ACE2 were demonstrated in diseases associated with dysregulated RAS activity, such as heart failure (Patel et al., 2016), hypertension (Crackower et al., 2002), renal damage (Shiota et al., 2010) and diabetes (Bindom and Lazartigues, 2009). The regulatory role of RAS and the function of ACE2 are illustrated in **Figure 1-1** (Liu et al., 2022).

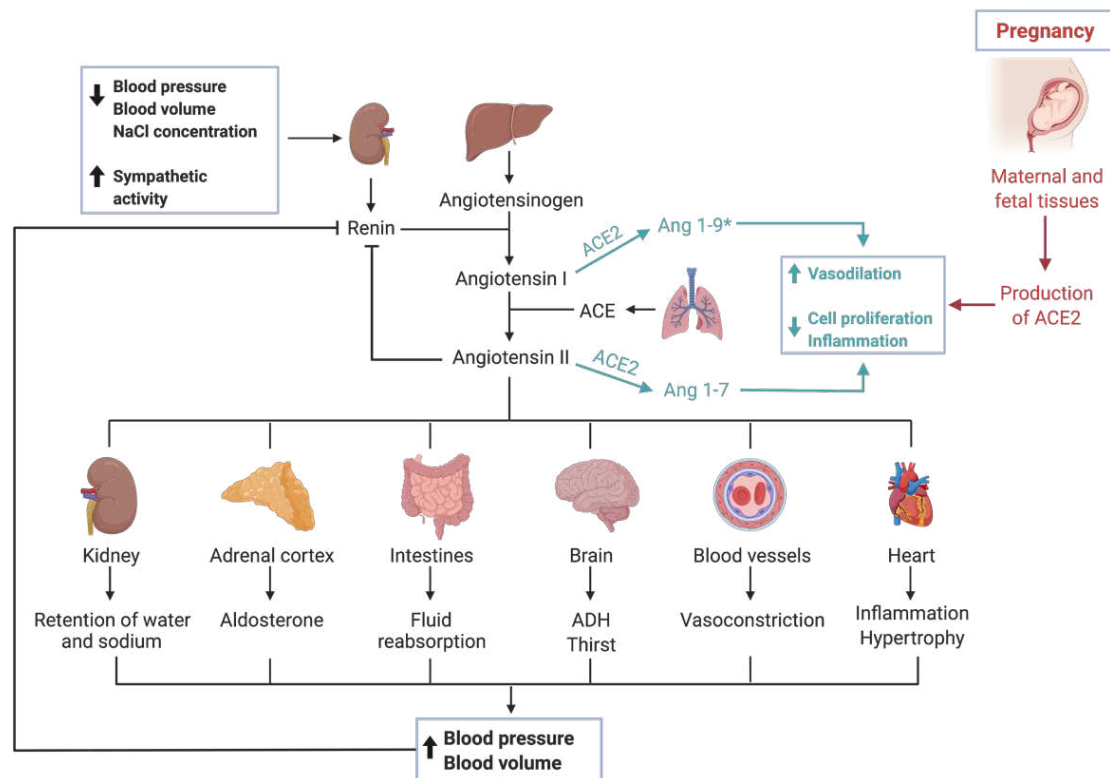


Figure 1-1: The Renin-Angiotensin System (RAS) and the Role of the Angiotensin-Converting Enzyme 2 (ACE2). Decrease in blood pressure, blood volume and sodium concentration as well as increase in sympathetic activity stimulate renin secretion from the kidney. The protease renin converts angiotensinogen, released from the liver, into angiotensin I, which is further cleaved into angiotensin II by the angiotensin-converting enzyme (ACE). ACE is mainly expressed on pulmonary and renal endothelial cells. Angiotensin II has various systemic effects, which ultimately result in increased blood pressure and volume. ACE2 exerts a regulatory role by converting angiotensin 1 and 2 into Ang 1-7 and Ang 1-9 (*Data on the effects of Ang 1-9 is limited but similarities to Ang 1-7 are hypothesized). Vasodilation, decreased cell proliferation and inflammation are caused by ACE2, which is amply produced during pregnancy. From Liu et al. (2022), CC BY 4.0.

Recently, ACE2 has received increased attention due to its role in severe acute respiratory syndrome coronavirus 2 (SARS-CoV-2) infection (Gheblawi et al., 2020, Lu et al., 2020, Chen et al., 2020). It was previously identified as a receptor for other human coronaviruses, such as severe acute respiratory syndrome coronavirus 1 (SARS-CoV-1) and human coronavirus NL63 (HCoV-NL63) (Li et al., 2003, Lin et al., 2008). Hence, tissues expressing ACE2 are potential targets for these viruses (Wiersinga et al., 2020).

1.1.4 The Role of ACE2 in the Endometrium and during Pregnancy

In addition to its local effects, RAS impacts the female reproductive system locally (Herr et al., 2013). All components of RAS have been found in the endometrium (Hagemann et al., 1994) and both their expression and distribution are subject to cyclic changes (Li and Ahmed, 1996). Chadchan et al. (2021) showed that ACE2 expression in human endometrial stromal cells (HESC) increases through decidualization and is highest during the secretory phase of the menstrual cycle. They further demonstrated that loss of ACE2 results in impaired decidualization. **Figure 1-2** illustrates physiological adaptations of the endometrium throughout the menstrual cycle as well as changes in hormone and ACE2 levels (Liu et al., 2022).

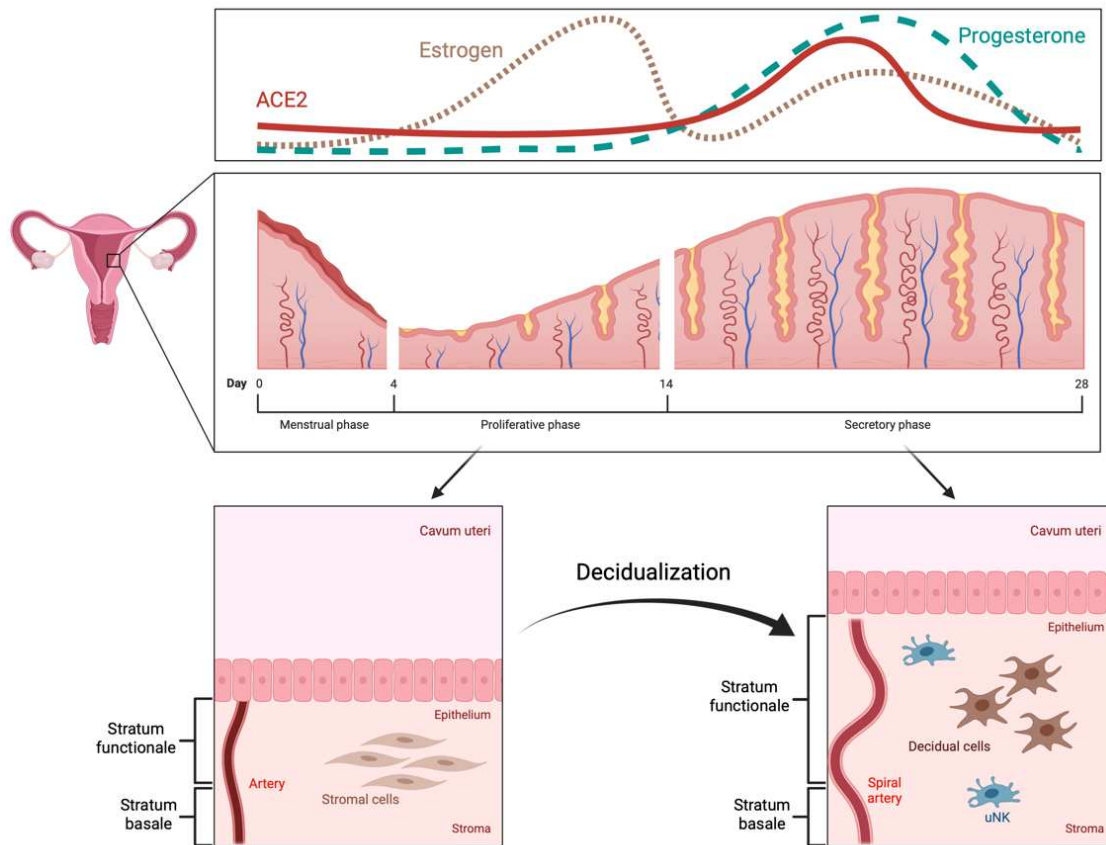


Figure 1-2: Decidualization and ACE2 in the Human Endometrium. Menstruation marks the beginning of each menstrual cycle, followed by the proliferative phase, which is characterized by the proliferation of endometrial cells. Decidualization in the secretory phase results in mesenchymal-epithelial transition of stromal cells, spiral artery formation and immunological adaptations (e.g., increase in uterine natural killer cells). During this 28-day long cycle, estrogen levels (pink, dotted line) are highest during the proliferative phase while progesterone (green, dashed line) and ACE2 levels (red, solid line) are elevated during the secretory phase. From Liu et al. (2022), CC BY 4.0.

“Furthermore, other studies have found that ACE2 and other components of RAS are expressed both in maternal and fetal tissues during pregnancy, suggesting their crucial role during implantation, vascular remodeling and labor (Marques et al., 2011, Weatherbee et al., 2020, Valdés et al., 2006, Valdés et al., 2013, Li et al., 2020a). During pregnancy, the uterus and placenta contribute substantially to ACE2 production, thus causing a twofold increase in ACE2 activity with subsequent systemic vasodilation (Levy et al., 2008). The upregulation of RAS in the maternal decidua as well as in the endothelial and perivascular stromal cells during the first trimester of pregnancy coincides with spiral artery remodeling and angiogenesis (Morgan

et al., 1998). Dysregulation of uteroplacental RAS is reported to alter the tightly regulated maternal homeostasis causing pregnancy complications such as miscarriage, stillbirth and preeclampsia (Irani and Xia, 2011, Irani and Xia, 2008, Verdonk et al., 2014). It was also shown that plasma Ang 1-7, a product of ACE2, is elevated during healthy pregnancies and that preeclamptic mothers had lower levels of Ang 1-7 (Merrill et al., 2002).

Remarkably, ACE2 is most abundant in the decidua in comparison with chorionic or amniotic tissues (Marques et al., 2011). Another compelling finding is that ACE2 expression is highest during early pregnancy and is negatively correlated with gestational age (Bloise et al., 2021, Neves et al., 2008). Moreover, fetal sex might affect maternal RAS and for instance, ACE2 mRNA levels were higher in decidual explants after 24h from women carrying a female fetus compared with those carrying a male fetus (Wang et al., 2012b).” (Liu et al., 2022)

1.2 Pregnancy and the Immune System

1.2.1 Anatomical and Physiological Changes during Pregnancy

During pregnancy, the female body is in a unique anatomical and physiological state with profound changes occurring throughout all organ systems (Kohlhepp et al., 2018). Pregnancy is a hypermetabolic state in which hormone levels are adjusted to support fetal growth (Mouzon and Lassance, 2015). The placenta itself is responsible for the production of hormones such as human chorionic gonadotropin (hCG), progesterone and estrogen as well as gonadotrophin-releasing hormone (GnRH) and corticotrophin-releasing hormone (CRH) (Costa, 2016, Tan and Tan, 2013). Hence, the placenta plays a major role not only in sustaining pregnancy but also in regulating the metabolism.

Physiologically, cardiovascular adaptations mediate an increase of cardiac output necessary to meet the elevated basal oxygen consumption level (Bamfo et al., 2007, Thornburg et al., 2000). Systemic vasodilation is another characteristic of hemodynamics during pregnancy, leading to a drop in blood

pressure (Chapman et al., 1998, Grindheim et al., 2012). Pregnancy is also marked by a hypercoagulable state with an increase in some procoagulant (e.g., factors VII, VIII, IX and fibrinogen) and anticoagulant (e.g., protein S activity, activated protein C resistance) factors (Simcox et al., 2015, Szecsi et al., 2010). This is also reflected in the increased risk of thromboembolism in pregnant and postpartum women (Heit et al., 2005).

Moreover, the respiratory system is altered during pregnancy. Breathing becomes more difficult due to swelling of the mucosa in the upper airways and uterine growth, which elevates the diaphragm (Munnur et al., 2005, Petrenko et al., 2021). Forced vital capacity (FVC) is decreased and gravid patients have a predisposition to lung edema and dyspnea (Jensen et al., 2021, Witry, 1992, Lee et al., 2017).

In addition to increased vulnerability to certain diseases due to the physiological adaptations during gestation, pregnancy also poses challenges for medical treatment and management. For instance, anesthesia is complicated by higher rates of failed endotracheal intubation in obstetric patients, which might be attributed to the aforementioned edema in the respiratory tract (Samsoon and Young, 1987). Additionally, pregnant patients are at higher risk for aspiration during intubation because of increased intra-abdominal pressure and lower esophageal sphincter tone (Maronge and Bogod, 2018). Thus, rapid sequence induction is recommended for general anesthesia (Devroe et al., 2015).

It is widely accepted that medication should be prescribed with caution during pregnancy as pharmacotherapy needs to be safe for both maternal health and fetal development (Mitchell et al., 2011). Gravid patients are commonly exposed to over-the-counter drugs, most frequently acetaminophen for treatment of fever and pain (Werler et al., 2005). While vaccination is a reliable strategy for the prevention of infectious diseases, some vaccines (e.g. live vaccines against measles, mumps, rubella or chickenpox) are contraindicated during pregnancy (Arora and Lakshmi, 2021). Since clinical trials for new treatment options usually exclude pregnant participants, data availability on teratogenicity of drugs is poor and much of the knowledge is derived from experiments using rodents

and primates (Adam et al., 2011). In low- and middle-income countries, low-quality drugs (e.g., due to problems in manufacturing or storage) for the treatment of obstetric complications pose a serious threat to expectant mothers and their offspring (Torloni et al., 2020).

Given these physiological changes and concomitant medical challenges, pregnant women are considered an especially vulnerable group of patients. This notion is of particular relevance during health crises such as pandemics.

1.2.2 *The Immune System during Pregnancy*

During pregnancy, the immune system is adapted to tolerate the semi-allogenic conceptus while simultaneously maintaining responsiveness against pathogens (Thellin and Heinen, 2003). Under normal circumstances, the immune system recognizes foreign antigens and responds promptly, as demonstrated by the rejection of organ transplants in the absence of sufficient immune suppression (Frohn et al., 2001). The mechanism by which a fetus, whose genome is half-paternal, is not rejected by the maternal immune system remains to be elucidated (Thellin et al., 2000).

One possible explanation lies in systemic changes in the immune system. Progesterone, which is amply produced by the placenta, reportedly inhibits T cell development and suppresses T cell activation during pregnancy (Tibbetts et al., 1999, Chien et al., 2007). Through binding to the glucocorticoid receptor, progesterone induces selective T cell death (Hierweger et al., 2019). Concurrently, progesterone promotes the development of dendritic cells which promote immunotolerance and are important for generating CD4⁺ and CD8⁺ regulatory T cells (Thiele et al., 2019). These mechanisms result in partial suppression of the maternal immune system, which increases pregnant women's susceptibility to infectious diseases and exacerbates influenza or hepatitis E severity. (Sappenfield et al., 2013, Terrault et al., 2021). Similarly, the activity of some autoimmune diseases, such as rheumatoid arthritis, is known to be reduced by pregnancy (Raine et al., 2020).

In addition to systemic effects, the maternal-fetal interface plays a critical role in balancing immune activity. During early pregnancy, immune cells make up to 40% of the decidual tissue and their spectrum is modulated by decidualized cells (Bulmer et al., 2010, Bonney, 2017, Erlebacher, 2013). Uterine natural killer cells (uNK) (70%) and macrophages (20-25%) are the most common leukocytes in the decidual tissue, while dendritic cells, B and T lymphocytes are rare (Gellersen and Brosens, 2014, Erlebacher, 2013, Ticconi et al., 2019). The number of uNK increases during decidualization and they are thought to play a role in spiral artery remodeling, clearance of senescent decidual cells, modulation of maternal immune tolerance and protection against pathogens (Ng et al., 2020, Sojka et al., 2019, Brighton et al., 2017). Decidualization further leads to entrapment and reduction of dendritic cells, which decreases T cell activation and inhibits immune reaction against the fetus (Collins et al., 2009).

1.3 SARS-CoV-2 and COVID-19

In March 2020, the World Health Organization declared Coronavirus disease 2019 (COVID-19) a global pandemic (WHO, 2020). The disease is caused by a virus called Severe Acute Respiratory Syndrome Coronavirus 2 (SARS-CoV-2) and, as of November 2023, there have been over 772 million confirmed cases and more than 6.9 million deaths (WHO, 2023b).

1.3.1 Structure and Pathophysiology of SARS-CoV-2

“SARS-CoV-2 belongs to the same genus betacoronavirus as SARS-CoV and MERS-CoV, which are all enveloped viruses with a single-stranded positive-sense RNA (Lu et al., 2020, Samudrala et al., 2020). Although the origin of SARS-CoV-2 has not been fully clarified yet, it is most likely that it originated from bats, which are a natural reservoir for coronaviruses, and was passed on to humans via an intermediate host such as pangolins (Zhang and Holmes, 2020, Hu et al., 2021).

SARS-CoV-2 consists of four structural proteins: spike (S), nucleocapsid (N), membrane (M) and envelope (E) protein (**Figure 1-3**) (Wang et al., 2020c). The S-protein is of utmost interest, as it facilitates virus entry into host cells (Li et al., 2003, Zhou et al., 2020b). Due to the similarity of their S-proteins, SARS-CoV and SARS-CoV-2 both utilize the cell surface receptor ACE2 for attachment and penetration of host cells (Zhou et al., 2020b). However, the receptor-binding domain (RBD) of the S-protein differs among SARS-CoV and SARS-CoV-2, resulting in higher binding affinity to ACE2 of the latter (Shang et al., 2020). A precondition for the interaction of SARS-CoV-2 with ACE2 is S-protein priming by host proteases, among which the most relevant seems to be transmembrane protease serine 2 (TMPRSS2) (Hoffmann et al., 2020).” (Liu et al., 2022)

After cell entry, the nucleocapsid is released into the cytoplasm of the host cell with subsequent uncoating, transcription and replication of the viral RNA (Baggen et al., 2021). The resulting negative-strand copies are translated into structural and accessory proteins (Nakagawa et al., 2016). The virions are assembled and released from the host cell, capable of infecting additional host cells and initiating yet another viral life cycle (de Haan et al., 2000, Baggen et al., 2021).

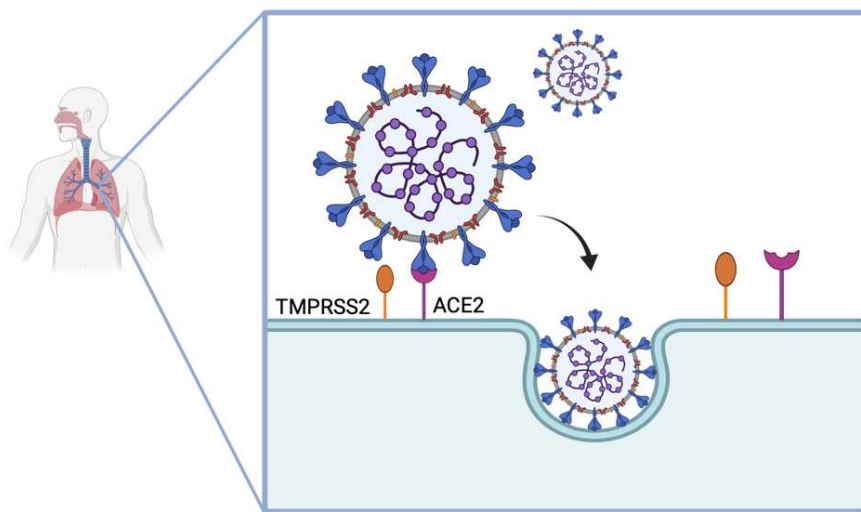
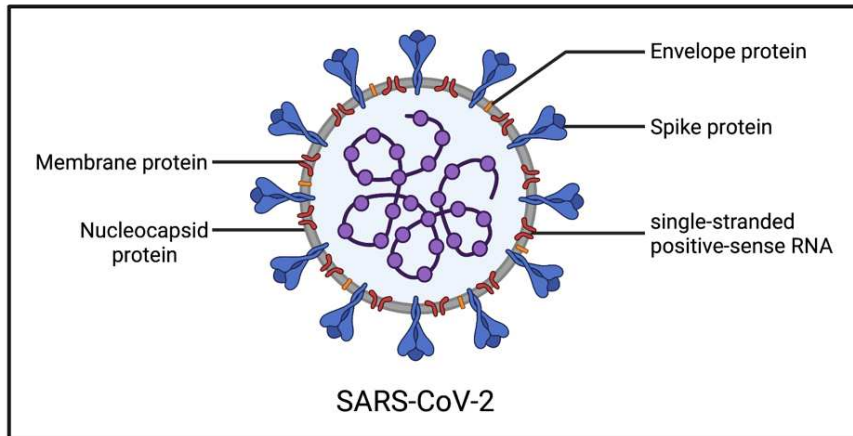


Figure 1-3: Structure and Cell Entry Mechanism of SARS-CoV-2. The Severe Acute Respiratory Syndrome Coronavirus 2 consists of four structural proteins (spike, nucleocapsid, membrane and envelope protein) and contains a single-stranded positive-sense RNA. Key factors of SARS-CoV-2 cell entry are the transmembrane protease serine 2 (TMPRSS2) and the angiotensin-converting enzyme 2 (ACE2) receptor, which are expressed on host cell membranes. After cleavage by TMPRSS2, the interaction of the spike protein with ACE2 leads to endocytosis of the virus by host cells. From Liu et al. (2022), CC BY 4.0.

The replication of RNA viruses generally is more error-prone than that of DNA viruses and as a result, mutation rates are high (Drake et al., 1998). However, coronaviruses possess an exceptionally large genome and express an exoribonuclease with a proofreading function (Minskaia et al., 2006, Graepel et al., 2017). Although the mutation rates of coronaviruses are lower compared to other RNA viruses, the WHO previously identified five variants of concern (VOC) and numerous variants of interest (VOI) of SARS-CoV-2 (Rambaut et al., 2020). Both VOI and VOC are genetically distinct from the index virus first identified in December 2019 or have a growth advantage over other circulating

variants, but VOC exhibit increased disease severity, reduced efficacy of available vaccines or require major public health interventions (WHO, 2023a). The previously circulating VOC were: Alpha (Pango lineage B.1.1.7, first detected in the UK), Beta (B.1.351, South Africa), Gamma (P.1, Brazil), Delta (B.1.617.2, India) and Omicron (B.1.1.529, multiple countries) (ECDC, 2023a). As of November 2023, no variants are categorized as VOC (ECDC, 2023b).

Mutations in the spike protein of SARS-CoV-2 are of great concern because they may affect viral interaction with ACE2 and entry into the host cell (Zhou et al., 2020b). All the previous VOC showed an increased transmission rate and the variants Alpha, Beta, Gamma and Delta were also more virulent than the index virus (Mistry et al., 2021). The Omicron variant has a higher rate of transmissibility compared to all other variants but also causes less severe diseases (Chatterjee et al., 2023). Due to over 30 mutations in the spike protein including 15 in the receptor binding domain, Omicron has elevated binding affinity to the ACE2 receptor (Shah and Woo, 2021). These mutations also explain the reduced neutralizing efficacy of antibody titers after vaccination, thus requiring a booster dose (Basile et al., 2022).

1.3.2 Clinical Characteristics of COVID-19

SARS-CoV-2 is mainly passed on via respiratory droplets, aerosols and contact transmission (Stadnytskyi et al., 2020, Tang et al., 2020). Initial estimates of the basic reproduction number (R_0) were around 2 to 3 but the new variants Delta and Omicron have significantly higher R_0 values with 5 and 8, respectively (Salzberger et al., 2021, Liu and Rocklöv, 2021, Liu and Rocklöv, 2022). The incubation period is approximately 4 to 5 days, but viral shedding can occur 3 days prior to the onset of symptoms (Lauer et al., 2020, McAloon et al., 2020, Widders et al., 2020).

“The clinical presentation of COVID-19 varies greatly from asymptomatic and mild to critical and even fatal cases (Cevik et al., 2020). Diagnosis is further impeded by unspecific symptoms, which resemble the clinical picture of the common cold, influenza or other respiratory diseases (Liu et al., 2020). The

most common manifestations are fever and cough, which are present in the majority of the patients, followed by fatigue and shortness of breath (Guan et al., 2020, Samudrala et al., 2020, Wiersinga et al., 2020). Anosmia, ageusia, myalgia and diarrhea are less frequent among COVID-19 patients (Adil et al., 2021, Spinato et al., 2020). Some symptoms, for instance fatigue or dyspnea, can persist despite microbiological recovery – a condition termed Long COVID (Carfi et al., 2020, Halpin et al., 2021).” (Liu et al., 2022)

“COVID-19 not only involves the lungs and the respiratory tract, but also multiple organ systems (Lai et al., 2020). This includes cardiovascular (e.g. acute cardiac injury, myocarditis), gastrointestinal (e.g. nausea and vomiting, diarrhea), neurological (e.g. dizziness, stroke) and hematological manifestations (e.g. lymphocytopenia, thrombotic events, disseminated intravascular coagulation (DIC)) (Lai et al., 2020, Magadum and Kishore, 2020, Mao et al., 2020, Orsini et al., 2020, Rahi et al., 2021). A case point feature of COVID-19 is, that it triggers an extensive inflammatory response, the “cytokine storm”, which further aggravates damage done by the virus (Ragab et al., 2020). A delay in immune response due to immune evasion of SARS-CoV-2 with consequentially unhindered virus replication is found in severe cases of COVID-19 (Felsenstein et al., 2020, Blanco-Melo et al., 2020, Keam et al., 2020). Virus-induced cell death prompts the recruitment of macrophages and neutrophils, followed by hyperinflammation (Felsenstein et al., 2020). Subsequent tissue damage and multi-organ failure are the main cause of death in COVID-19 (Melenotte et al., 2020, Wang et al., 2020a).” (Liu et al., 2022)

While over 80% of COVID-19 cases are either asymptomatic or mildly symptomatic, infections with the Delta variant were associated with significantly higher rates of oxygen requirement, ICU admission and mortality (Wu and McGoogan, 2020, Ong et al., 2021). The requirement of hospital admission and emergency care attendance was also higher in patients infected with the Delta variant (Twohig et al., 2022). The Omicron variant, on the other hand, is found to cause less severe COVID-19 cases with lower hospitalization rates (Wolter et al., 2022, Jassat et al., 2022).

1.4 COVID-19 and Pregnancy

1.4.1 Maternal and Neonatal Outcomes

According to a meta-analysis by Smith et al. (2023a) involving 13 136 cases, pregnant women infected with SARS-CoV-2 had a significantly higher risk of pneumonia, thromboembolic disease and death than uninfected pregnant women. Advanced maternal age, comorbidities (e.g., diabetes mellitus, hypertension and cardiovascular disease), pre-pregnancy obesity or underweight as well as low socioeconomic status have been identified as possible risk factors for adverse outcomes (Torres-Torres et al., 2021, Smith et al., 2023b). Notably, the majority of pregnant women only experience mild symptoms and fully recover from COVID-19, similar to the general population (Wang et al., 2021, Charuta et al., 2023).

Reported complications of neonates born to SARS-CoV-2 positive women include preterm delivery, admission to a neonatal care unit after birth, low birth weight and neonatal death (Simbar et al., 2023, Smith et al., 2023a). Recent studies underpin the fact that neonates exposed to SARS-CoV-2 during gestation are generally healthy and that most newborns do not show any manifestation of respiratory illness (Yan et al., 2020, Gale et al., 2021). Perinatal infection rate is low and the risk of transmission is not increased by rooming-in of the newborn with the mother (Morniroli et al., 2023).

The Delta variant is linked to higher transmission rates and disease severity among pregnant women (Seasely et al., 2021, Adhikari et al., 2022b). An increase in infection was also seen with the Omicron variant, but the severity was not increased or even decreased (Adhikari et al., 2022a, Birol Ilter et al., 2022).

To prevent both maternal and neonatal adverse outcomes, pregnant women are advised to be vaccinated against COVID-19 (Luxi et al., 2021). Multiple studies confirm that morbidity and mortality are significantly decreased through immunization during pregnancy (Vousden et al., 2022, Birol Ilter et al., 2022).

Vaccination reduces risk of stillbirth, preterm birth and neonatal ICU admission but not neonatal infection (Rahmati et al., 2023). A third vaccine dose is necessary to elicit an adequate neutralizing antibody response against the Omicron variant (Rottenstreich et al., 2022). Adverse events, such as miscarriage or fetal abnormalities, did not increase, indicating that vaccination during pregnancy is safe. Yet, many expectant mothers are hesitant to take up vaccination against COVID-19 and continuous effort is required to inform and encourage particularly vulnerable groups (Goncu Ayhan et al., 2021).

1.4.2 Possibility of Vertical Transmission

The process of ante-, peri- or postnatal mother-to-child transmission of infectious agents is termed vertical transmission (Arora et al., 2017).

“Several bacteria, viruses and parasites are known to cause congenital infection, the most common one being the cytomegalovirus (CMV) (Hughes and Gyamfi-Bannerman, 2016). The consequences of these infections depend on the pathogens, with some causing fetal death (e.g., parvovirus B19, mumps virus, rubella virus) and others leading to malformations or organ defects (e.g., *Chlamydia trachomatis*, *Treponema pallidum*, CMV, *Toxoplasma gondii*) (Adams Waldorf and McAdams, 2013). Another determinant of teratogenicity is the time of infection: the rubella virus causes cerebral, cardiac, ophthalmic and auditory defects when infection occurs in the first trimester of pregnancy (during organogenesis), whereas the fetus is most vulnerable to the hemolytic effect of parvovirus B19 and subsequent hydrops fetalis during the second trimester, due to heightened hematopoiesis in the fetal liver (Adams Waldorf and McAdams, 2013, Lamont et al., 2011).

While SARS-CoV-2 can be passed from mother to infant through respiratory droplets during labor or in the postnatal period, the question of *in utero* transmission remains unresolved (Karimi-Zarchi et al., 2020). Infection rates among neonates born to COVID-19 positive mothers are low (6%), however, cases of early-onset COVID-19 exist with infants testing positive via nasopharyngeal swabs within 12 h postpartum (Capobianco et al., 2020, Di

Toro et al., 2021). Further, antibodies against SARS-CoV-2 identified in newborns shed additional light on the possibility of prenatal vertical transmission (Zeng et al., 2020, Dong et al., 2020). In contrast to IgG, which is subject to physiological transplacental transfer and therefore could originate from maternal blood, elevated levels of IgM indicate infection of the fetus *in utero*, as IgM usually does not cross the placental barrier (Palmeira et al., 2012). Nevertheless, inflammatory processes can affect the placental barrier and result in altered transfer of immunoglobulin (Ben-Hur et al., 2005). Thus, elevated IgM levels in neonates are no definite proof for *in utero* transmission of SARS-CoV-2.

Furthermore, in a study from Hecht et al. SARS-CoV-2 RNA was detected in the syncytiotrophoblast and cytotrophoblast of placentas from COVID-19 positive mothers (Hecht et al., 2020). This demonstrates that SARS-CoV-2 can infect the placenta, however, it does not definitely confirm vertical transmission. Further, these women were tested (positive for COVID-19) peripartum, limiting the insights into late pregnancy infection.” (Liu et al., 2022)

Figure 1-4 gives an overview of pathogens with known vertical transmission and possible consequences.

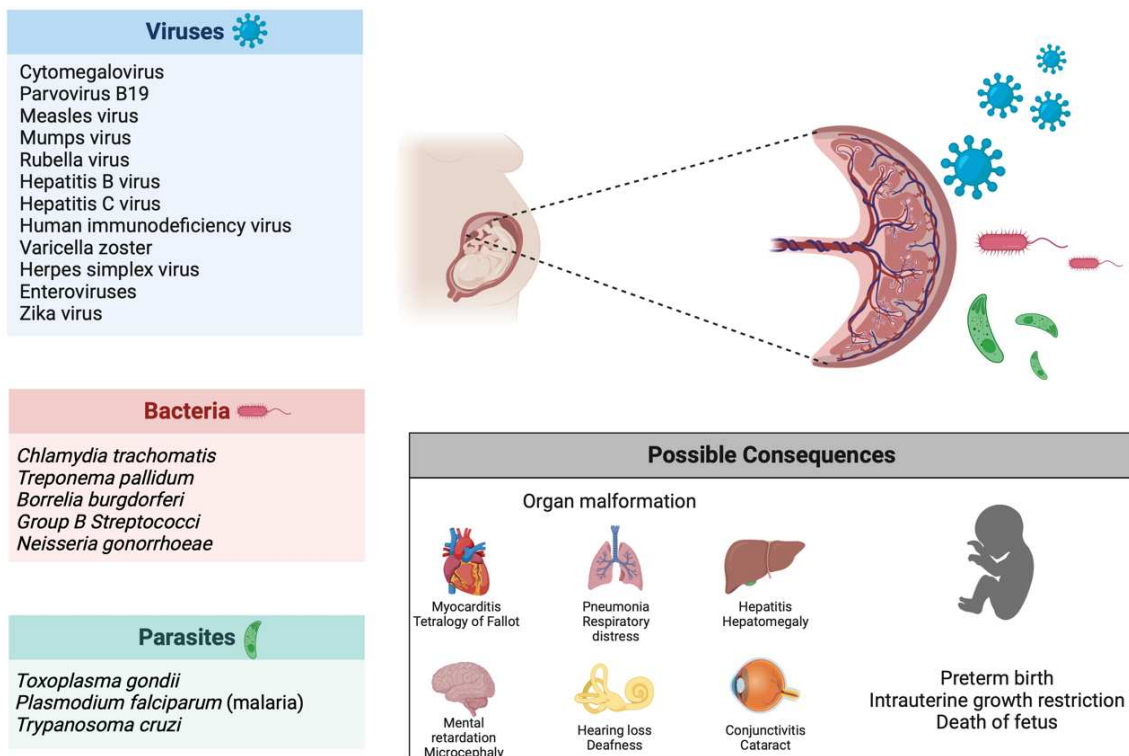


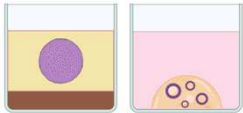


Figure 1-4: Vertical Transmission of Pathogens and Possible Consequences. Several viruses (blue), bacteria (red) and parasites (green) are known to be vertically transmitted during pregnancy. Infection during pregnancy can result in organ malformations, preterm birth, growth restriction and miscarriage. From Liu et al. (2022), CC BY 4.0..

1.5 Models used in Biomedical Research

Due to ethical and practical reasons, it is not always feasible to study the structure and function of the human body as well as the pathophysiology and treatment options for diseases directly in humans. Therefore, biomedical research relies heavily on models to enable research and scientific advances. The aim of these models is to replicate human *in vivo* conditions as best as possible while considering the requirements of specific experiments and research questions. In addition to well-established two-dimensional (2D) monolayer cell cultures and animal models, recent years have seen a surge in increasingly complex, three-dimensional (3D) cell culture models (de Dios-Figueroa et al., 2021). A brief overview of the various models including their advantages and disadvantages can be found in **Table 1-1**.

Table 1-1: Comparison of 2D Cell Culture, Animal and 3D Cell Culture models. Relative scores are represented as very good (+++), good (++) and poor (+). Pictograms created with BioRender.com.

	2D Cell Culture Models 	Animal Models 	3D Models (Spheroids and Organoids) 
Affordability	+++	+	++
Time Efficiency	+++	+	++
Accessibility	+++	++	++
Reproducibility and Controllability	+++	+	++
Replication of Human Cell Characteristics	+	+ / ++	++ / +++
Species Specificity	+++	+	+++
Complete Organism	+	+++	+
Ethics	+++	+	++ / +++
References	Bissell et al. (2002), Duval et al. (2017), Edmondson et al. (2014), de Dios-Figueroa et al. (2021), de Melo et al. (2021)	Demetrius (2006), Andersen and Winter (2019), Robinson et al. (2019), Bédard et al. (2020)	Pampaloni et al. (2007), Clevers (2019), Kim et al. (2020), Jensen and Teng (2020), de Dios-Figueroa et al. (2021), de Melo et al. (2021)

1.5.1 Monolayer Cell Culture and Animal Models

The most common *in vitro* approach is the use of monolayer cultures of cell lines grown on polystyrene plates (Duval et al., 2017, Bissell et al., 2002). Their application is uncomplicated, inexpensive and relatively fast. Experiments can be conducted in a tightly controlled manner and with high reproducibility (de Dios-Figueroa et al., 2021). Laboratories around the world have gained considerable experience in handling this easily accessible model, making monolayer cell cultures important tools in advancing knowledge in various biomedical fields of research (de Melo et al., 2021, Duval et al., 2017). However, accurate replication of living organisms is limited. The majority of 2D cultures consist of one single cell line and therefore lack the complexity of actual tissues and organs. Changes in morphology have been observed in adherent cells grown on a flat surface (Edmondson et al., 2014). In nature, cells do not grow as an isolated entity but in a context provided by cell-cell and cell-extracellular matrix (ECM) interactions, which both influence the structure and function of cells (Kleinman et al., 2003). Growing cells in 2D causes loss of tight junctions and abnormal polarity (de Dios-Figueroa et al., 2021, de Melo et al., 2021). The absence of a cell microenvironment not only causes phenotypic alterations but also changes in gene expression (Oda et al., 2008, Griffith and Swartz, 2006). Moreover, deviations from the natural cell cycle regarding migration, proliferation and cell death or apoptosis are another deficit in monolayer cell cultures (Bissell et al., 2002, Pampaloni et al., 2007).

Another classical model makes use of *in vivo* experiments in animals, predominantly mice and rats (Robinson et al., 2019). Since these models comprise of complete organisms, they allow for studying interactions between several organs and organ systems. Similarities in anatomy and physiology between animals, especially mammals, and humans enable conclusions from tests, such as on drugs and toxicity (Bédard et al., 2020). Due to a shorter life span, diseases can be studied fully over the course of an entire life cycle (Demetrius, 2006, Bédard et al., 2020). An advantage in comparison to tests in humans is the possibility of conducting experiments in a controlled environment. Nonetheless, many findings are not applicable to humans. For instance, human

cell tropism of viruses hinders the translation of results regarding infection and pathogenesis obtained from animal models (de Dios-Figueroa et al., 2021). A systematic review of highly cited animal studies showed that only a third of the research could be translated to humans at the level of randomized trials (Hackam and Redelmeier, 2006). Ethical concerns about the use of sentient beings as experimental models are also voiced. Consistent with the 3R principles in research, scientists should aim to replace animals with other suitable models, reduce animal testing and refine experiments to improve animal welfare (Bédard et al., 2020, Andersen and Winter, 2019). Further, experimenting on animals is cost- and time-consuming, rendering them inefficient, particularly considering their limited applicability to humans (Robinson et al., 2019). Despite these shortcomings, animal models remain the gold standard in drug testing (Ma et al., 2021).

1.5.2 Three-Dimensional Cell Culture Models

In contrast to the aforementioned approaches, 3D cell culture models use human cells grown in a spatial organization resembling *in vivo* tissues and organs. While various forms of 3D models exist, ranging from scaffold-free and scaffold-based to combinations of the two methods, they all have in common that the cells are grown in context (de Dios-Figueroa et al., 2021). This complexity allows for interactions of cells with each other and with their surroundings, which in turn influence cellular growth and function (Pampaloni et al., 2007). Hence, cells grown in the third dimension tend to retain tissue-specific phenotype better, express genes and proteins more similar to cells *in vivo* and have more cell-cell junctions. They also respond to stimuli, such as drugs or nutrients, more like cells *in vivo* than cells grown as monolayers (Jensen and Teng, 2020). An advantage over 2D cell culture models is seen in drug testing, as 3D models simulate aspects of cell mass penetration, diffusion gradients and barriers caused by tight junctions more realistically (Friedrich et al., 2009). These characteristics of 3D models could help develop drugs which are more efficient and better suitable for human application. However, creating

models with higher complexity is time-consuming because the cells grow more slowly and throughput is lower; 3D models are more difficult to implement on a large scale and are more cost-intensive than conventional cell culture (Jensen and Teng, 2020). In addition, 3D models lack vascular emulation and insights into organ-organ interactions or immune response are limited (de Dios-Figueroa et al., 2021). Since conventional microscopy is optimized for imaging of thinner 2D structures, the requirement of modern imaging techniques poses another obstacle to the implementation of 3D models (Pampaloni et al., 2007).

The most commonly used 3D models are spheroids, which were originally used in tumor research (de Dios-Figueroa et al., 2021). Spheroids consist of a scaffold-free system, in which adherent cells in suspension aggregate and compact into a multicellular structure (Lin and Chang, 2008). To generate spheroids, a non-adherent surface needs to be created in the culture ware. This can be achieved through various methods. Simple approaches include the liquid-overlay technique, which uses well plates with non-adhesive coatings, or the hanging drop method. For large-scale productions, rotary systems like the spinner flask can be employed (Lin and Chang, 2008). Since spheroids share many characteristics with avascular, solid tumors, such as a nutrient gradient from the periphery to the center and central hypoxia with necrosis, they realistically model tumor pathophysiology (Santini and Rainaldi, 1999). Further, Spheroids are used in drug screening, research on neurodegeneration and angiogenesis as well as tissue engineering (Bell et al., 2016, Yong et al., 2021, Heiss et al., 2015, Ong et al., 2018). Although most spheroids consist of commercially available, differentiated cell lines, stem cells can also form spheroids (Baptista et al., 2018, Ryu et al., 2019). Compared to other 3D models, spheroids are relatively inexpensive and can be generated in a short amount of time. Depending on the method used, spheroid formation can be labor-intensive with variations in size and shape (de Dios-Figueroa et al., 2021).

Another 3D cell culture model are organoids, which can be derived either from human embryonic stem cells, induced pluripotent stem cells or organ-restricted adult stem cells (Clevers, 2016). There are several methods to facilitate self-organization of stem cells. Solid matrices, such as natural Matrigel or chemically

defined hydrogels, mimic the ECM and support growth and differentiation (Rossi et al., 2018, Fujii et al., 2018). Organoids can also be cultured in suspension with and without additional ECM components (Eiraku et al., 2011, Kumar et al., 2019). To induce the development of organ-specific characteristics, stem cells are subjected to a complex interplay of exogenous (e.g., growth factors) and endogenous signals (e.g., morphogens from the starting cell culture) (Rossi et al., 2018). Thus, numerous protocols exist for establishing unique organoids as models for various tissues and organs. Since organoids originate from patient-derived primary cells, they are a promising tool in personalized medicine (Clevers, 2019). Another advantage is their ability to self-expand and self-renew which allows for a small amount of starting material, long-term culture and biobanking (Chen et al., 2021, Fatehullah et al., 2016). However, primary cells can be difficult to access and compared to monolayer models, organoids are more complicated and time-consuming to culture (Kim et al., 2020). In terms of complexity, organoids have limitations, such as a lack of vascularization and an immune system (de Melo et al., 2021). Due to their heterogeneity, replicating experiments can be challenging (de Dios-Figueroa et al., 2021).

Other more advanced and intricate 3D models aim to replicate not only a type of tissue or an organ but also the interactions between different organ systems. One such technology is the organ-on-a-chip, which incorporates both microfluidics and cell culture (Kimura et al., 2018). Not only can it mimic multiple organs but also human blood circulation, which is beneficial for studying the systemic effects of drugs or toxins (Ma et al., 2021). In addition to the previously discussed examples, various other 3D models are available for biomedical research, such as organotypic raft cultures or bioprinted models (Schweinfurth and Meyers, 2006, Mandrycky et al., 2016).

1.5.3 3D Models in Reproductive Medicine

Experimenting on humans often entails practical and ethical problems, which is especially true in reproductive medicine. While commonly used, animal models fail to duplicate certain characteristics of pregnancy unique to humans. In most

mammals, including mice and rats, decidualization occurs only in the presence of a conceptus, whereas the human endometrium decidualizes spontaneously and additionally undergoes menstruation (Gellersen et al., 2007). Compared to other mammals, the monthly fecundity rate in humans is very low (20%) and therefore insights on fertility from animal studies are limited (Evers, 2002). Other differences concern molecular mechanisms, such as contrasting expression of mucin during the window of implantation or variation in the distribution of progesterone receptors throughout the reproductive tract (Koot et al., 2012, Teilmann et al., 2006). Despite the knowledge gained by animal models, *in vitro* approaches are needed to further advance knowledge in reproductive medicine.

An optimal model for studying human reproduction should include both embryonic and maternal cells of human origin. Co-cultures of either endometrial stromal or epithelial cells with human embryo cells can be used to model different stages of implantation (Weimar et al., 2013b, Dominguez et al., 2003, Teklenburg et al., 2010, You et al., 2019). Due to ethical concerns and restrictions on the use of human embryos, mouse blastocysts or spheroids from trophoblast cells serve as substitutes (Domínguez et al., 2010, Holmberg et al., 2012). While these models permit interesting insights into the interactions between blastocyst and endometrium, some drawbacks remain. For instance, excluding one of the two endometrial cell types results in less complex cell-cell communication patterns. Further, culturing the cells in a monolayer leads to deviations from the original cell morphology and function (Jensen and Teng, 2020).

A higher degree of complexity is achieved by combining endometrial stromal and epithelial cells with collagen and Matrigel in between (Bentin-Ley et al., 1994, Park et al., 2003). This multilayer cell culture model enabled the formation of a polarized columnar epithelial layer with apical microvilli and cilia similar to *in vivo* morphology. Another study on embryo attachment applied a similar technique, in which endometrial epithelial cells were grown on a layer of endometrial stromal cells in a 3D fibrin matrix and spheroids consisting of a human choriocarcinoma cell line were seeded on top (Wang et al., 2012a).

While establishing such a culture is laborious, it provides valuable insights into the process of embryo implantation.

1.6 Hypothesis and Aims

Pregnant women infected with SARS-CoV-2 have higher rates of premature birth and reports of early onset COVID-19 in neonates born to infected gravid patients exist. While it remains unclear whether SARS-CoV-2 can be transmitted vertically, key entry factors for infection have been found in maternal and fetal tissues. Therefore, we hypothesize that SARS-CoV-2 can infect the endometrium, which leads to dysregulation of pathways associated with inflammation, immune evasion and, ultimately, pregnancy loss. We further postulate that decidualization has an impact on the effects of SARS-CoV-2 infection in the endometrium.

The aims of this dissertation are **I** to confirm the presence of key entry factors for SARS-CoV-2 in the endometrium, **II** to investigate the effect of decidualization on the expression of these factors, **III** to establish a three-dimensional *in vitro* endometrial spheroid model to study vertical transmission, **IV** to determine the susceptibility for SARS-CoV-2 of endometrial cells and **V** to study the effect of SARS-CoV-2 infection on the endometrium.

2 Materials and Methods

2.1 Materials

Table 2-1: List of Cells and Viruses, in Alphabetical Order

Item	Catalog number	Company
Benign human endometrial stromal cells (HESC)	#T0533	Applied Biological Materials Inc., Richmond, Canada
CACO-2	A KRAS wildtype colorectal cancer cell line (ATCC, HTB-37), stably transfected with a doxycycline-inducible KRASG12V expression system (Kuhn et al., 2021)	
Endometrial organoid lines	Derived from primary stem cells isolated from tissue biopsies of healthy premenopausal subjects at the Department of Women's Health, University Women's Hospital Tübingen (Brucker et al., 2022)	
Ishikawa cell line, a well-differentiated human endometrial adenocarcinoma cell line (ISK)	#99040201	Merck, UK
Recombinant SARS-CoV-2 expressing mNeonGreen (icSARS-CoV-2-mNG)	Obtained from the World Reference Center for Emerging Viruses and Arboviruses at the University of Texas Medical Branch (Xie et al., 2020)	
SARS-CoV-2 B.1 (Wildtype)	Isolated from a throat swab collected in March 2020 at the Institute for Medical Virology and Epidemiology of Viral	

	Diseases, University Hospital Tübingen, from a PCR-positive patient (Ruetalo et al., 2021)
SARS-CoV-2 B.1.617.2 (Delta)	Isolated from a throat swab collected in May 2021 at the Institute for Medical Virology and Epidemiology of Viral Diseases, University Hospital Tübingen, from a PCR-positive patient (Wagner et al., 2022)

Table 2-2: List of Reagents and Chemicals, in Alphabetical Order

Item	Catalog number	Company
2-Mercaptoethanol	#31350010	ThermoFisher Scientific, Germany
8-Bromo-cAMP, sodium salt	#1140	Tocris, UK
A 83-01	#2939	Tocris, UK
Advanced DMEM/F-12	#12634010	ThermoFisher Scientific, Germany
Ammonium persulfate solution (APS)	#9592.3	Carl Roth, Germany
Animal-free recombinant human EGF	#AF-100-15	Peprtech, Germany
Antibiotic/antimycotic solution	#15240062	Invitrogen, Germany
B-27 supplement (50x)	#17504044	ThermoFisher Scientific, Germany
Bromophenol blue	#15375.01	SERVA Electrophoresis GmbH, Germany

Collagenase/Dispase	#10269638001	Merck, Germany
Cultrex organoid harvesting solution	#3700-100-01	Bio-Techne, Germany
Cultrex reduced growth factor basement membrane extract (BME), Type 2, Select	#3536-005-02	Bio-Techne, Germany
DAPI (4',6-Diamidino-2-phenylindole, dihydrochloride)	#D1306	Invitrogen, Germany
Dextran coated charcoal (DCC)	#C6241	Sigma-Aldrich, USA
Dimethyl sulfoxide (DMSO)	#D12345	Invitrogen, Germany
Dulbecco's modified eagle medium/Nutrient mixture F-12 (DMEM/F12)	#11039021	Invitrogen, Germany
Dulbecco's phosphate buffered saline (PBS)	#D8537	Sigma-Aldrich, UK
Fetal bovine serum (FBS)	#10270106	Invitrogen, Germany
GlutaMAX supplement	#35050061	Thermofisher Scientific, Germany
Glycerol	#3783	Carl Roth, Germany
HEPES (4-(2-Hydroxyethyl)-1-piperazineethanesulfonic acid)	#15630056	Thermofisher Scientific, Germany
L-glutamine	#25030024	Invitrogen, Germany
LEGENDplex human inflammation panel 1 (13-plex) with V-bottom plate	#740809	BioLegend, USA
LIVE/DEAD viability/cytotoxicity kit, for mammalian cells	#L3224	Invitrogen, Germany

LWRN 10% conditioned medium (RN8)		Kindly provided by Dr. André Koch
Maxima H Minus cDNA synthesis master mix, with dsDNase	#M1681	ThermoFisher Scientific, Germany
Medroxyprogesterone 17-acetate (MPA)	#M1629	Sigma-Aldrich, Germany
Methanol	#32213	Honeywell, USA
N-2 supplement (100x)	#17502048	ThermoFisher Scientific, Germany
<i>N</i> -Acetyl-L-cystein	#A9165	Sigma-Aldrich, Germany
Nicotinamide	#N0636	Sigma-Aldrich, Germany
Paraformaldehyde (PFA), 4% in PBS	#J19943.K2	ThermoFisher Scientific, Germany
Pierce 10X western blot transfer buffer, methanol-free	#35045	ThermoFisher Scientific, Germany
PowerUp SYBR Green master mix	#A25742	ThermoFisher Scientific, Germany
ProLong Gold antifade mountant with DAPI	#P36931	Invitrogen, Germany
ProSieve QuadColor protein marker	#00193837	Lonza, USA
PureLink RNA mini kit	#12183020	Invitrogen, Germany
Recombinant human FGF-10	#100-26	Peptidech, Germany
RNeasy mini kit	#74104	Qiagen, Germany

ROTIPHORESE 10x SDS-PAGE	#3060.2	Carl Roth, Germany
ROTIPHORESE NF-acrylamide/bis-solution 30 (29:1)	#A124.2	Carl Roth, Germany
SB 202190 monohydrochloride hydrate	#S7076	Sigma-Aldrich, Germany
Sodium chloride (NaCl)	#27810.295	VWR International, USA
Sodium dodecyl sulfate (SDS)	#L5750	Sigma-Aldrich, Germany
TEMED	#2367.3	Carl Roth, Germany
Tri-sodium citrate dihydrate	#1370421000	Merck, Germany
Triton X-100	#A16046.0F	Thermofisher Scientific, Germany
Trizma base	# T1503	Sigma-Aldrich, Germany
Trypan blue	#T8154	Sigma-Aldrich, Germany
Trypsin-EDTA, 0.25%	#25200056	Invitrogen, Germany
Tween 20	#P1379	Sigma-Aldrich, Germany
UltraPure agarose	#16500100	Invitrogen, Germany
Water for molecular biology, sterile filtered	#95284	Sigma-Aldrich, Germany
WesternBright ECL HRP substrate	#K-12045-D50	Advansta, USA
Xylol	#131769.1611	AppliChem, Germany
Y-27632 dihydrochloride	#M1817	AbMole, USA

Table 2-3: List of Consumable Supplies, in Alphabetical Order

Item	Catalog number	Company
48-well plate	#353230	Corning, USA
6-well plate	#353224	Corning, USA
96-well plate	#353072	Corning, USA
Amersham Hybond P western blotting membranes, PVDF	#GE10600023	Sigma-Aldrich, Germany
Cell counting slides	#1450015	Bio-Rad, Germany
Cell culture flask (T75)	#658175	Greiner Bio-One, Germany
Cell lifter	#3008	Corning, USA
Corning Falcon 15 mL conical centrifuge tubes	#10773501	Thermofisher Scientific, Germany
Corning Falcon 50 mL conical centrifuge tubes	#10788561	Thermofisher Scientific, Germany
Cover slips	#474030-9000-000	Carl Zeiss, Germany
Gel cassettes, 1.5 mm	#NC2015	Invitrogen, Germany
Glass slide	#03-0004	R. Langenbrick GmbH, Germany
ImmEdge hydrophobic barrier PAP pen	#H-4000	Vector laboratories, Germany
MicroAmp fast optical 96-Well reaction plate, 0.1 mL	#4346907	Life Technologies, Germany
Microcentrifuge tubes	#0030125150	Eppendorf, Germany
Optical adhesive covers, PCR compatible	#4360954	Thermofisher Scientific, Germany

Xcell SureLock Mini-Cell electrophoresis system	#EI0001	Life Technologies, Germany
---	---------	----------------------------

Table 2-4: List of Antibodies, in Alphabetical Order

Item	Catalog number	Company
ACE2 rabbit, polyclonal antibody	#21115-1-AP	Proteintech, Germany
Anti-rabbit IgG, HRP-linked	#7074	Cell Signaling Technology, Germany
GAPDH (14C10) rabbit, monoclonal antibody	#2118	Cell Signaling Technology, Germany
Goat anti-mouse IgG (H+L) cross-adsorbed secondary antibody, Alexa Fluor 594	#A-11005	Invitrogen, Germany
Goat anti-rabbit IgG (H+L) cross-adsorbed secondary antibody, Alexa Fluor 488	#A-11008	Invitrogen, Germany
Goat anti-rabbit IgG (H+L) cross-adsorbed secondary antibody, Alexa Fluor 594	#A-11012	Invitrogen, Germany
Keratin 7 (D1E4) rabbit mAb	#4465	Cell Signaling Technology, Germany
SARS-CoV/SARS-CoV-2 nucleocapsid antibody, rabbit mAb	#40143-R001	SinoBiological, Germany
TMPRSS2 rabbit, polyclonal antibody	#14437-1-AP	Proteintech, Germany
Vimentin monoclonal antibody, mouse	#60330-1-Ig	Proteintech, Germany
ZO-1 polyclonal antibody	#61-7300	Invitrogen, Germany
β -catenin monoclonal antibody (E-5)	#sc-7963	Santa Cruz Biotechnology, Germany

Table 2-5: List of Primers, in Alphabetical Order

Gene	Forward Primer	Reverse Primer
<i>ACTB</i>	5'-ATGGAGAAAATCTGGCACCCAC-3'	5'- TTGAAGGTCTCAAACATGATCTGG -3'
<i>CCL20</i>	5'-TGTGCGTCTCCTCAGTAAAA-3'	5'-ACAAGTCCAGTGAGGCACAA-3'
<i>CD38</i>	5'-AGCACTTTTGGGAGTGTGGAA-3'	5'- GATCCTGGCATAAGTCTCTGGA-3'
<i>HSD11B1</i>	5'-AGCAAGTTTGCTTTGGATGG-3'	5'-AGAGCTCCCCCTTTGATGAT-3'
<i>IGFBP1</i>	5'-CGAAGGCTCTCCATGTCACCA-3'	5'- TGTCTCCTGTGCCTTGGCTAAAC- 3'
<i>IL1RL1</i>	5'-TCCAAAATTTATTGTCCTACCAT-3'	5'- GATCCTTGAAGAGCCTGACAATT- 3'
<i>LCN2</i>	5'-CACCTCCGTCCTGTTTAGGAAA-3'	5'-TGCTGGTTGTAGTTGGTGCT-3'
<i>LEFTY1</i>	5'-TGGACAAATGCTCTGTGCTCT-3'	5'-TCCAGTGGCCAAAGATTCTCA- 3'
<i>NR4A3</i>	5'-GCAAGATACCCTCCAGATATGC-3'	5'-TTGGTGTAGTCGGGGTTCAT-3'
<i>PRL</i>	5'- AAGCTGTAGAGATTGAGGAGCAAAC -3'	5'- TCAGGATGAACCTGGCTGACTA-3'
<i>VTCN1</i>	5'-GCAGATCCTCTTCTGGAGCATAA- 3'	5'-AGTGCAGCTCAGGATTCCAT-3'

Table 2-6: List of Machines, in Alphabetical Order

Item	Catalog number	Company
Electrophoresis power supply	#E831	Consort, Belgium
EVOS M7000	#AMF7000	Invitrogen, Germany
iBright CL1000	#A32749	Invitrogen, Germany
Incubator	#9040-0012	Binder, Germany
QuantStudio 3 PCR system		ThermoFisher Scientific, Germany
Soluva Pro UV disinfection chamber		Heraeus, Germany
T100 thermal cycler	#621BR57740	Bio-Rad, Germany
TC20 automated cell counter	#1450102	Bio-Rad, Germany
Tilt/roller mixer RS-TR 05	#XK30.1	Carl Roth, Germany
Varioklav autoclave	#23330902	H+P Labortechnik, Germany
Varioskan LUX multimode microplate reader	#VLBL0TD2	Thermofisher Scientific, Germany
Vortex mixer	#K550GE	Bender & Hobein, Switzerland

Table 2-7: List of Software, in Alphabetical Order

Item	Company
BioRender	BioRender, Canada
Excel 16.51	Microsoft Corporation, USA
FIJI 2.1.0	Open source
FlowJo v10.8	Becton, Dickinson & Company, USA
Metascape.org	Open access (Zhou et al., 2019b)
GraphPad Prism 9	GraphPad Software, USA
Skant	Thermofisher Scientific, Germany

2.2 Methods

2.2.1 2D Cell Culture

The benign human endometrial stromal cells (HESC) and the Ishikawa cell line (ISK, a well-differentiated endometrial carcinoma cell line) were cultured in medium consisting of Dulbecco's modified eagle medium/Nutrient mixture F-12 (DMEM/F-12) supplemented with 10% dextran coated charcoal stripped fetal bovine serum (DCC-FBS), 1% L-glutamine and 1% antibiotic/antimycotic solution. The cells were maintained in an incubator at 37°C with a humidified atmosphere of 5% CO₂.

Upon reaching 80% confluency, the cells were passaged by removing the old medium and detaching the cells using 0.25% trypsin-EDTA. After incubating for 3 min, the suspension was diluted with DMEM/F12 medium. The mixture was transferred to a centrifuge tube and centrifuged at $171 \times g$ for 3 minutes. After discarding the supernatant, the cell pellet was resuspended in DMEM/F12 medium. 10 μ l of the cell suspension was mixed with 10 μ l of Trypan blue. Of this mixture, 10 μ l was added to a counting slide and cell counting was carried out using the TC20 cell counter. The amount of cell suspension required for the specific experiment was added to a new cell culture flask containing fresh medium.

2.2.2 Culturing Endometrial Spheroids in Agarose-Coated Microplates

Based on descriptions of the liquid-overlay method for spheroid culture (Friedrich et al., 2009, Li et al., 2011a, Kyffin et al., 2019), the following protocol was optimized for endometrial spheroids.

To produce agarose-coated 48- and 96-well plates, a 1% (w/v) agarose gel solution was prepared in a glass bottle using distilled water. After autoclaving, the agarose gel was used immediately or stored at room temperature and microwaved before use. The following steps took place in a sterile environment. The glass bottle containing the agarose gel was put on a heating plate set at 100°C and constantly stirred with a magnet to prevent solidification. Cut pipette

tips were used to add 50 μ l or 150 μ l of agarose gel to each well of a 96-well plate or 48-well plate, respectively. The pipette tips were replaced when solid gel droplets formed inside. During the pipetting process, the microplate was tapped intermittently to ensure even distribution. The low-attachment well plates were then used after 5 min or stored in a plastic bag for later usage.

During the optimization process, various cell numbers (ranging from 150 to 6000 cells per cell type and spheroid) and ratios (1:10 to 2:1) of HESC and ISK were used. ISK were seeded either with HESC or the day after.

In the optimized protocol, which was used to generate spheroids for all experiments after **3.2**, a cell suspension containing 60 000 HESC and 30 000 ISK cells per ml was prepared in 5% DCC-FBS medium containing 1% L-glutamine and 1% antibiotic/antimycotic solution. 100 μ l of the suspension was added to each well of a 96-well plate. The spheroids were cultured in an incubator at 37°C with a humidified atmosphere of 5% CO₂. After 2 days, another 100 μ l of medium was added to each well. To maintain the spheroids, 100 μ l of medium was changed every 2 to 3 days.

2.2.3 Imaging and Growth Monitoring of Endometrial Spheroids

Immediately after starting the endometrial spheroid culture and over the course of 11 days, phase-contrast images were captured using the EVOS M7000 with a magnification of 4x and 10x.

The area of the spheroids was measured using the FIJI software. Based on the obtained values, the diameter and volume of the spheroids were calculated on the assumption that the image of a spheroid approximates a circle and the spheroid approximates a sphere.

The area A of a circle of radius r is:

$$A = \pi r^2$$

The diameter d was calculated from the Area A as:

$$d = 2r = 2 \sqrt{\frac{A}{\pi}}$$

The volume V of a sphere is:

$$V = \frac{4}{3}\pi r^3 = \frac{4}{3}\pi \left(\sqrt{\frac{A}{\pi}}\right)^3$$

The results for spheroid diameter and volume are presented as arithmetic mean and standard error of the mean (SEM).

2.2.4 Viability Assay for Endometrial Spheroids

For the viability assay, the LIVE/DEAD Viability/Cytotoxicity Kit for mammalian cells was used and the protocol of the manufacturer was followed. Spheroids were removed from their original wells with 100 μ l of medium and added to a new 96-well plate. For the dead control, spheroids were incubated with 100 μ l of DMSO or 100% ethanol per well for 1 h at room temperature. Afterwards, 100 μ l of medium with DMSO or ethanol was removed from the dead controls and 100 μ l of Dulbecco's Phosphate Buffered Saline (PBS) was used for washing of all the wells. The LIVE/DEAD assay reagents were removed from the freezer and thawed. A dilution of 2 μ M of calcein-AM and 8 μ M of ethidium-homodimer-1 per ml was prepared in PBS. 100 μ l of combined LIVE/DEAD assay reagents were added to each well and the spheroids were incubated for 45 min in the dark at room temperature. Finally, the reagents were removed and the spheroids were washed with 100 μ l of PBS. The labeled spheroids were imaged with the EVOS M7000 at a magnification of 10x.

2.2.5 Endometrial Organoids Culture

Organoid lines as well as the following protocol were kindly provided by Dr. André Koch (Brucker et al., 2022). The organoids were derived from primary

stem cells obtained from tissue biopsies of healthy premenopausal subjects of University Women's Hospital Tübingen. All tissue biopsies were obtained with informed written consent. The study was conducted according to the guidelines of the Declaration of Helsinki, was approved by the Ethics Committee of the Eberhard Karls University of Tübingen (Ethical approval 01/2022BO2) and is compliant with all relevant ethical regulations regarding research involving human participants.

Frozen organoid lines were thawed and 2 ml of Advanced DMEM/F-12 containing 10 mM HEPES, 1% GlutaMAX and 1% antibiotic/antimycotic solution was added. The cell suspension was centrifuged at $385 \times g$ for 5 min. The supernatant was removed and the amount of cell suspension was measured with a pipette. The required amount of Advanced DMEM/F-12 was added for a final volume of 60 μ l. This cell suspension was transferred to a separate microcentrifuge tube on ice and 70 μ l of basement membrane extract (BME) was added. In a 48-well plate, 20 μ l of the solution was slowly pipetted into the middle of five central wells. After 1 min, the plate was inverted and put into the incubator for 30 min to form BME domes. The well plate was flipped back and 300 μ l of pre-heated endometrial organoid medium (for composition see **Supplementary Table 8-1**) was added to the wells containing BME domes. To the surrounding wells, 500 μ l of PBS was added. The endometrial organoid cultures were maintained in a humidified atmosphere at 37°C with 5% CO₂ and medium was changed every 3 days. Pictures were taken over 9 days with the EVOS M7000 using the tile-stitching technique.

2.2.6 Apical Out Assay of Endometrial Organoids

Based on the method described by Co et al. (2019), the following protocol was developed and optimized.

Endometrial organoids were cultured until 80% confluency. Endometrial organoids medium was discarded and 500 μ l of PBS was added to each well. The BME domes were gently scraped off using a pipette tip and the suspension

was transferred to a centrifuge tube. After centrifuging at $385 \times g$ for 5 min, the supernatant was discarded. 2 ml of organoid harvesting solution was added to the tube and pipetted up and down ten times. The tube was put on ice and on a shaker for 1 h. After incubation, the suspension was diluted using 3 ml of PBS and centrifuged at $385 \times g$ for 5 min. The supernatant was removed and the pellet was resuspended in endometrial organoid medium (500 μ l per number of original wells). 500 μ l of the suspension was transferred into each well of an agarose-coated 48-well plate (prepared according to the method described in **2.2.2**). To the surrounding wells, 500 μ l of PBS was added. The apical out endometrial organoid cultures were maintained in a humidified atmosphere with 5% CO₂ and at 37°C. Medium was changed every 3 days. Phase-contrast images were taken with the EVOS M7000 at a magnification of 10x and 20x.

2.2.7 Immunostaining of Apical Out and Basal Out Endometrial Organoids

For immunostaining of whole organoids, apical out endometrial organoids were cultured in suspension for 6 days prior to collection in microcentrifuge tubes. After centrifuging at $96 \times g$ for 3 min, the supernatant was discarded. Basal out organoids were cultured embedded in BME on chamber slides for 10 days before medium removal. The following steps were the same for apical out and basal out organoids. The organoids were washed with 500 μ l of PBS, fixed with 1 ml of 4% PFA in PBS for 30 min at room temperature and washed twice with 500 μ l. Blocking was carried out with 1 ml of PBST (0.1% Triton X-100) and 3% BSA at 4°C overnight, followed by two washes with PBST. The organoids were incubated with primary antibodies (ZO-1 and β -catenin, both 1:100) in 500 μ l PBST for 24 h at 4°C (apical out) or 1 h at room temperature (basal out) on a shaker. After three 10 min washes in PBST, the organoids were incubated with secondary antibodies (Alexa Fluor 488 anti-rabbit and Alexa Fluor 594 anti-mouse, both 1:500) in 200 μ l of PBST for 1 h at room temperature on a shaker and washed three times for 10 min in PBST. The organoids were mounted on glass slides using ProLong Gold Antifade mountant with DAPI, covered with

cover slips, sealed with nail polish and left to dry overnight in the dark. Z-stacks were captured using the EVOS M7000 at a magnification of 10x and 20x.

For immunostaining of organoid sections after paraffin-embedding, apical out organoids were collected in centrifuge tubes and centrifuged at $385 \times g$ for 5 min before discarding the supernatant. To prepare the basal out organoids, medium was removed and the BME domes were washed with 1 ml of PBS in the 48-well cell culture plate. 250 μ l of collagenase/dispase (1 mg/ml) was added to each well and the BME domes were scraped off with a pipette tip. After incubating for 15 min at 37°C, the suspension containing the organoids was transferred into a centrifuge tube filled with PBS. Each well was rinsed with 1 ml of PBS, which was also added to the tube. Following centrifugation at $216 \times g$ for 5 min, supernatant was removed. The following steps were the same for both types of organoids. The samples were fixed with 1 ml of 4% PFA in PBS for 30 min at room temperature and washed with 1 ml of PBS for 5 min. Following centrifuging at $216 \times g$ for 5 min and supernatant removal, 250 μ l of 25% ethanol was added. After 10 min, 300 μ l of 70% ethanol and after another 10 min 600 μ l of 96% ethanol were added. The samples were stored at 4°C before paraffin embedding and sectioning (4 μ m, done by Ingrid Teufel).

Deparaffinization of the sections was carried out by incubating three times in xylol for 10 min, twice in 100% ethanol for 3 min, twice in 96% ethanol for 3 min, once in 75% ethanol for 3 min, once in 75% ethanol for 5 min and once in distilled water for 5 min. Heat-induced antigen retrieval was performed by submerging the slides in citrate buffer (pH 6, for composition see **Supplementary Table 8-2**), followed by heating to 93°C in a glass beaker and microwaving at 180 W for 10 min. The slides were cooled to room temperature by placing the glass beaker on ice.

For antibody staining, a hydrophobic circle was created on the slides around the sections using a PAP pen. Incubations were carried out in the dark with sufficient amount of the following reagents to fully cover the sections. Sections were washed with PBS-T (0.1% Tween in PBS) for 5 min and permeabilized with 0.2% Triton X-100 in PBS for 3 min. After washing three times with PBS-T

for 5 min, the samples were blocked with 4% BSA in PBS-T for 30 min. The slides were incubated with primary antibodies (ZO-1 and β -catenin, both 1:100) in PBS-T containing 4% BSA for 1 h. Three washing steps with PBS-T for 5 min were performed. Incubation with secondary antibodies (Alexa Fluor 488 anti-rabbit and Alexa Fluor 594 anti-mouse, both 1:500) was carried out for 1 h. Following three washes with PBS-T for 5 min, the samples were mounted using ProLong Gold Antifade mountant with DAPI, covered with cover slips and sealed with nail polish. After drying overnight, the slides were imaged using the EVOS M7000 at a magnification of 10x and 20x.

2.2.8 Decidualization Treatment

Decidualization treatment was carried out according to the protocol described by Brosens et al. (1999), which was modified for endometrial spheroids and organoids. All incubation steps were carried out in an incubator providing a humidified atmosphere of 5% CO₂ and at 37°C.

HESC and ISK were cultured until reaching 80% confluency as described in **2.2.1** before being split into 6-well plates at a concentration of 1×10^5 cells per ml and 1 ml per well. The cells were cultured in a monolayer for 2 days in 10% DCC-FBS DMEM/F12 medium containing 1% L-glutamine and 1% antibiotic/antimycotic solution prior to treatment. Afterwards, medium was replaced with 2% DCC-FBS DMEM/F12 medium, which contained 1 μ M medroxyprogesterone 17-acetate (MPA) and 0.5 mM 8-bromo-cAMP for the treatment group. Medium was changed every 48 h for 6 days, after which the cells were used for downstream experiments.

Spheroids were cultured for 2 days in a 96-well plate and using 5% DCC-FBS DMEM/F12 medium containing 1% L-glutamine and 1% antibiotic/antimycotic solution medium as described in **2.2.2**. For the first treatment, a solution of 2 μ M MPA and 1 mM 8-bromo-cAMP in 2% DCC-FBS medium was prepared. 100 μ l of medium was removed from each well and 100 μ l of treatment medium was added. For the control group, 100 μ l of 2% DCC-FBS medium was added. Treatment was repeated every 48 h with 1 μ M MPA and 0.5 mM 8-bromo-cAMP

in 2% DCC-FBS medium. After 6 days, the spheroids were prepared for protein or RNA extraction.

Treatment of basal out endometrial organoids grown to 80% confluency as detailed in **2.2.5** was similar to that of 2D cells except for the usage of endometrial organoids medium instead of 2% DCC-FBS DMEM/F12 medium. Apical out organoids were treated in the same way as the spheroids except for using endometrial organoids medium in place of 5% DCC-FBS DMEM/F12 medium.

2.2.9 Infection of 2D Cells, Endometrial Spheroids and Endometrial Organoids with SARS-CoV-2

Monolayer HESC and ISK as well as endometrial spheroids were cultured for a total of 7 days and decidualization treatment was performed for 5 days prior to infection. Basal out endometrial organoids were cultured until 80% confluent followed by 5 days of decidualization treatment before infection. Apical out assay was performed on endometrial organoids cultured to 80% confluency, after which the organoids were cultured in suspension for 2 days prior to 5 days of decidualization treatment and infection.

All experiments involving SARS-CoV-2 viruses were conducted by Dr. Natalia Ruetalo-Buschinger in a Biosafety level 3 laboratory. Incubation was carried out in a humidified atmosphere with 5% CO₂ and at 37°C.

On the day of infection, medium was removed from monolayer cells and replaced with 2% DCC-FBS medium with or without 0.5 mM 8-bromo-cAMP and 1 µM MPA containing icSARS-CoV-2-mNG (mNG), a recombinant SARS-CoV-2 expressing mNeonGreen, at a multiplicity of infection (MOI) of 10 or with wildtype SARS-CoV-2 B.1 (WT, MOI = 40), respectively. Infection was monitored through fluorescence microscopy for 48 h. Protein was extracted after 48 h or 72 h. Infected CACO-2 lysate was used as positive control.

For the infection of endometrial spheroids, half of the medium (100 µl) was replaced with 5% DCC-FBS medium with or without 0.5 mM 8-bromo-cAMP and

1 μ M MPA containing SARS-CoV-2 B.1.617.2 (Delta, 648 267 898 IU/ml, diluted 1:20). After 24 h and 48 h, 10 μ l of supernatant was collected per well totaling 120 μ l per sample (12 spheroid wells per sample). 48 h post-infection, spheroids were collected for downstream experiments (12 spheroids per sample).

Basal out endometrial organoids were infected by complete medium removal and incubating with SARS-CoV-2 B.1 (WT, 200 930 034 IU/ml, diluted 1:100) in endometrial organoids medium with or without 0.5 mM 8-bromo-cAMP and 1 μ M MPA for 48 h. For apical out endometrial organoids, half of the medium (100 μ l) was replaced by endometrial organoids medium with or without 0.5 mM 8-bromo-cAMP and 1 μ M MPA containing SARS-CoV-2 B.1.617.2 (Delta, 648 267 898 IU/ml, diluted 1:100) for 72 h.

Remaining viral particles were neutralized through Laemmli buffer (for protein extraction, see **2.2.13**), lysis buffer (for RNA extraction, see **2.2.11** and **2.2.12**), PFA (for immunostaining, see **2.2.10**) or UV-radiation (for cytokine measurement, see **2.2.14**) and samples were further processed in an S2 biosafety laboratory.

2.2.10 Immunostaining of Endometrial Spheroids

The protocol of Weiswald et al. (2010) was followed with modifications. For staining of vimentin and cytokeratin 7, spheroids were cultured for 7 days prior to collection. For staining of ACE2 and SARS-CoV-2 nucleocapsid protein, spheroids were cultured, treated and infected as described in **2.2.9**.

The spheroids were collected in centrifugation tubes using pipette tips which were first coated in PBS to prevent the spheroids from sticking to the wall. The spheroids were centrifuged at $96 \times g$ for 5 min and the supernatant was discarded. The pellet was resuspended in 1 ml of PBS and centrifuged again at $96 \times g$ for 3 min. The supernatant was removed and the spheroids were incubated in 200 μ l of PBS with 4% paraformaldehyde (PFA) and 1% Triton X-100 for 3 h at 4°C. The spheroids were washed three times in 500 μ l of PBS for

10 min and left in PBS overnight. The spheroids were dehydrated using 500 μ l of increasing concentrations of methanol in PBS (25%, 50%, 75% and 95%) for 30 min each in 4°C. To each tube, 500 μ l of 100% methanol was added and the spheroids were incubated at 4°C for 5 h. The spheroids were rehydrated with 500 μ l of descending concentrations of methanol in PBS (95%, 75%, 50% and 25%) for 30 min each in 4°C. After washing for three times in PBS for 10 min, the spheroids were blocked with 500 μ l of PBST (0.1% Triton X-100 in PBS) containing 3% bovine serum albumin (BSA) at 4°C overnight. The next day, the spheroids were washed twice with 500 μ l of PBST for 15 min and incubated with 200 μ l of primary antibodies against cytokeratin 7 (rabbit anti-human, 1:100) and vimentin (mouse anti-human, 1:50) or SARS-CoV-2 nucleocapsid (rabbit anti-SARS-CoV/SARS-CoV-2, 1:100), respectively, diluted in PBST for 48 h on a rotator at 4°C. Afterwards, the spheroids were washed four times for 30 min in 500 μ l of PBST and incubated with 200 μ l of secondary antibodies (Alexa Fluor 488 anti-rabbit (1:300) and Alexa Fluor 594 anti-mouse (1:400) or Alexa Fluor 594 anti-rabbit (1:400), respectively) for 24 h at 4°C and wrapped in aluminum foil.

To detect ACE2 in infected endometrial spheroids, sequential staining was performed by washing three times for 15 min in PBST, followed by 48 h incubation with primary antibody against ACE2 (200 μ l, 10:100), 24 h incubation with secondary antibody (Alexa Fluor 488 anti-rabbit, 1:400) and washing steps in between. After washing the spheroids three times for 15 min in PBST, 400 μ l of DAPI (1:500) was added for 1 h at room temperature to the spheroids stained for cytokeratin 7 and vimentin.

The spheroids were washed once in PBST for 15 min and the supernatant was discarded. The spheroids were dissolved in a small amount of PBS and carefully dotted on a glass slide. A pipette was used to remove excess fluid and the slides were left to dry for 10 min. The spheroids were mounted using 90% glycerol (v/v) and covered with cover slips. The corners were sealed using nail polish. The slides were viewed and Z-stacks were captured using the EVOS M7000 at a magnification of 10x and 20x.

2.2.11 RNA Extraction, cDNA Synthesis and qPCR

The RNeasy Mini Kit was used for RNA extraction according to the manufacturer's protocol with slight modifications.

For HESC and ISK cells cultured in a monolayer, medium was removed and wells were briefly washed with PBS. 350 μ l of Buffer RLT containing 1% β -mercaptoethanol was added to each well and cell scrapers were used. The lysates were collected with a pipette and transferred into Eppendorf tubes. The subsequent steps were identical to the method used for spheroids.

Spheroids in two rows were carefully removed from the wells and added to an Eppendorf tube. Each tube contained one sample consisting of 24 spheroids. After centrifuging at $865 \times g$ for 1 min, the supernatant was discarded and 300 μ l of PBS was added to each sample. This washing step was repeated once. For lysis, 350 μ l of Buffer RLT containing 1% β -mercaptoethanol was added to each tube.

The samples were vortexed for 1 min, 350 μ l of 70% ethanol in RNase-free water was added to each tube and the homogenate was mixed by pipetting up and down. Each sample was transferred to a spin column in a 2 ml collection tube and centrifuged at $17\,000 \times g$ for 1 min at room temperature. The flow-through was discarded, the spin cartridge was reinserted into the collection tube and 700 μ l of Buffer RW1 was added. The tubes were centrifuged again at $17\,000 \times g$ for 1 min and the flow through was disposed of. 500 μ l of Buffer RPE containing ethanol was added and the tubes were centrifuged at $17\,000 \times g$ for 1 min. This wash step was repeated once. The collection tube was replaced with a fresh one and the samples were centrifuged at $17\,000 \times g$ for 1 min. The spin column was placed into a 1.5 ml collection tube and 30 μ l of RNase-free water was added to the center of the column. After incubating for 1 min at room temperature, the tubes were centrifuged at $17\,000 \times g$ for 2 min. The eluted RNA in the collection tube was stored on ice and the spin column was discarded.

Immediately after extraction, the RNA concentration was measured using a μ Drop plate and following the user manual. After cleaning the low-volume area, 1 μ l of sterile-filtered water or sample was added to the blank or sample positions. Absorbance measurement was performed with the Varioskan LUX and the SkanIt Software. The samples were only further processed, if the ratio of absorbances at 260 nm and 280 nm after blank subtraction (A_{260}/A_{280}) was above 1.8, indicating low protein contamination of the RNA. RNA concentration was calculated using the Beer Lambert Law (A_{260} of 1.0 is equivalent to 40 μ g/mL of RNA).

For cDNA synthesis, the Maxima H Minus cDNA Synthesis Master Mix was used. All reagents were thawed and stored on ice. To a tube on ice, 1 μ l of 10X dsDNase Buffer and 1 μ l of dsDNase were added. The required amount of RNA solution for 1 μ g of template RNA was calculated and nuclease-free water was added for a total volume of 10 μ l per tube. The tubes were briefly centrifuged and incubated at 37°C for 2 min in a thermal cycler. The samples were put on ice and 4 μ l of Maxima cDNA H Minus Synthesis Master Mix (5X) as well as 6 μ l of nuclease-free water were added to each tube. After briefly centrifuging, the tubes were incubated at 25°C for 10 min, then at 50°C for 15 min and finally at 85°C for 5 min in a thermal cycler. The obtained cDNA was diluted with 80 μ l of nuclease-free water and stored on ice.

For qPCR, all required reagents were placed on ice. Forward and reverse primer solutions were diluted separately with sterile-filtered water for a concentration of 10 μ M each. For each target gene, a master mix was prepared containing 5 μ l Powerup SYBR Green Master Mix, 0.8 μ l of forward and 0.8 μ l of reverse primers and 2.4 μ l of sterile-filtered water multiplied with the number of required reactions. The master mix was briefly vortexed. A 96-well reaction plate was placed on ice and 9 μ l of the master mix was added to the respective wells. The samples were run in triplicates and 1 μ l of cDNA sample was added to each respective well. For every target gene, non-template controls were run in duplicates, for which 1 μ l of sterile-filtered water was added. The reaction plate was sealed with an adhesive cover and centrifuged at $171 \times g$ for 1 min.

The qPCR was carried out using the QuantStudio 3 system with an initial denaturation step (20 s at 95°C), followed by 40 cycles of denaturation (1 s at 95°C), annealing (20 s at 60°C) and extension (10 s at 72°C). Relative gene expression was calculated using the $2^{-\Delta\Delta C_t}$ method, normalizing to the expression of the reference gene and the non-decidualized and/or non-infected control sample. The value of the control group was set at 1.0.

2.2.12 RNA Extraction and RNA Sequencing after Infection

A total of five spheroid samples were collected. The PureLink RNA Mini Kit was used for RNA extraction following the manufacturer's manual with slight modifications. Briefly, the samples were placed on ice and 300 μ l of Lysis Buffer containing 1% 2-mercaptoethanol was added to each tube. The samples were briefly vortexed and centrifuged at $17\,000 \times g$ for 2 min. 300 μ l of 70% ethanol in RNase-free water was added to each tube and the homogenate was briefly vortexed. Each sample was transferred to a spin cartridge in a collection tube. After centrifuging at $17\,000 \times g$ for 15 s at room temperature, the flow-through was discarded. The spin cartridge was reinserted into the collection tube and 700 μ l of Wash Buffer I was added. The tubes were centrifuged again at $17\,000 \times g$ for 15 s and the flow through was removed. Another 700 μ l of Wash Buffer I was added and after centrifuging at $17\,000 \times g$ for 15 s, the collection tube was replaced with a new tube. To the spin cartridge, 500 μ l of Wash Buffer II containing ethanol was added and the tubes were centrifuged at $17\,000 \times g$ for 15 s. The flow-through was discarded and this washing step was repeated once. Afterwards, the samples were centrifuged at $17\,000 \times g$ for 2 min and the collection tube was replaced by a recovery tube. 30 μ l of RNase-free water was pipetted into the center of the spin cartridge and the tubes were incubated for 1 min at room temperature. The tubes were centrifuged at $17\,000 \times g$ for 2 min to collect the purified RNA in the collection tube. The spin cartridge was discarded and the eluates were stored on ice.

RNA concentration was measured using a μ Drop plate as described in **2.2.11** and RNA quality was assessed with Agilent 2100 Bioanalyzer. The three samples with the best quality were selected for further processing. The following steps were performed at the Institute for Medical Genetics and Applied Genomics.

RNA sequencing (RNA-seq) libraries were generated using the NEBNext Ultra II Directional RNA Library Prep Kit for Illumina, with 100 ng of RNA utilized for each library. The library preparation protocol followed the manufacturer's instructions and involved poly(A) selection to enrich for mRNA transcripts. The Illumina NovaSeq 6000 platform was employed for sequencing in paired-end mode with a read length of 50 bp and an approximate depth of 70 million clusters per library. To minimize technical batch effects, library preparation and sequencing procedures were performed by the same individual. The quality of raw RNA-seq data in FASTQ files was assessed using ReadQC (ngs-bits version 2018_06) to identify potential sequencing cycles with low average quality and base distribution bias. Subsequently, reads were pre-processed using skewer (version 0.2.2) and aligned to the human reference genome (GRCh37) with STAR (version 2.5.4a), allowing spliced read alignment. Alignment quality was further evaluated using MappingQC (ngs-bits version 2018_06) and visually inspected using the Broad Integrative Genome Viewer (IGV, version 2.3.1). For gene-level quantification, read counts were obtained using subread (version 1.6.0) and the Ensembl genome annotation (GRCh37 v75).

For the differential gene expression (DGE) analysis, raw gene read counts were filtered to retain genes with at least 1 count per million (cpm) in at least three samples. This filtering step resulted in more than 15000 genes being considered for determining differential expression in the pair-wise comparisons between experimental groups. The analysis was conducted by Miguel Camarena-Sainz using edgeR (version 3.22.3), which employs a statistical framework based on negative binomial distributions and gene-wise testing through generalized linear models.

2.2.13 Protein Extraction, Gel Electrophoresis and Western Blot

For protein extraction, Laemmli buffer (see **Supplementary Table 8-3**) was used. The following steps were carried out on ice and the protein samples were stored at -20°C until usage.

Medium was removed from cells cultured in a monolayer and ice-cold PBS was used for a brief wash. 120 µl of Laemmli buffer 1X heated at 95°C was added to each well and the bottom was scraped using a cell scraper. The samples were transferred to Eppendorf tubes, vortexed and boiled at 95°C for 5 min.

For basal out organoids, medium was removed, the BME domes were washed with ice-cold PBS and 240 µl of Laemmli buffer 1X heated at 95°C was added to each well. A cell scraper was used and the lysate was transferred to Eppendorf tubes, vortexed and boiled at 95°C for 5 min. For apical out organoids, the medium containing organoids was transferred to Eppendorf tubes and centrifuged at 500 × *g* for 5 min. The supernatant was discarded and the pellet was washed with 500 µl of ice-cold PBS, followed by another centrifugation step. The PBS was removed and 120 µl of Laemmli buffer 1X heated to 95°C was added to each tube. After vortexing, the lysate was boiled at 95°C for 5 min.

The spheroids of one row of a 96-well plate were collected in an Eppendorf tube resulting in 12 spheroids per sample. The tubes were centrifuged at 500 × *g* for 5 min at 4°C. As much of the supernatant as possible was discarded while avoiding the cell pellet. To each tube, 500 µl of ice-cold PBS was added and the tubes were centrifuged again at 500 × *g* for 5 min at 4°C. The PBS was removed and 120 µl of Laemmli buffer 1X heated to 95°C was added to each tube. The mixture was briefly vortexed and boiled at 95°C for 5 min. The samples were stored at -20°C until usage.

To perform gel electrophoresis, hand-casted 10% SDS-polyacrylamide gels with 10-well combs were used (see **Supplementary Table 8-4** for details). The wells were loaded with 10 µl of protein ladder and 20 µl (spheroids and organoids) or 15 µl (2D cells) of each sample, respectively. The electrophoresis chambers

were filled with 1X electrophoresis buffer (diluted from ROTIPHORESE 10x SDS-PAGE) and electrophoresis was initiated at 80 V for 30 min, followed by 125 V for 90 min.

In preparation of the wet transfer, sponges and filter paper were soaked in wet transfer buffer. The gel was removed from the cassettes and a PVDF membrane, activated in methanol, was placed on it. The gel and membrane were sandwiched between filter paper and sponges on both sides. After arranging the blot module and removing air bubbles with a roller, the tank was filled with transfer buffer. The transfer was carried out on ice at 25 V for 90 min.

Following transfer, the membrane was placed in a Falcon tube and blocked with 10 ml of 5% milk in TBST (for composition see **Supplementary Table 8-5**) on a horizontal roller at room temperature for 1 h. The membrane was washed twice in 10 ml of TBST for 5 min. After removal of TBST, the membrane was incubated with 10 ml of primary antibody solution (ACE2 1:700 and TMPRSS2 1:1000 or SARS-CoV-2 nucleocapsid protein 1:1000 in 3% milk in TBST, respectively) on a horizontal roller at 4°C overnight. The following day, the membrane was washed quickly in 10 ml of TBST and then three times for 10 min. Afterwards, secondary antibodies (HRP-linked anti-Rabbit IgG, 1:2000 in 3% milk in TBST) were added for 1 h at room temperature. Post incubation, the membrane was washed quickly in 10 ml of TBST and then three times for 10 min.

For detection, the membrane was placed onto a plastic film and a mixture of 500 µl of each ECL reagent was distributed evenly on the membrane. After 1 min of incubation, a second plastic film was used to cover the membrane and excess solution was removed with a roller. The bands were detected with iBright CL1000.

Subsequently, the membrane was washed twice in 10 ml of TBST for 10 min and incubated with primary GAPDH antibodies (1:2000 in 3% milk in TBST) on a horizontal roller at 4°C overnight. The washing procedure, incubation with secondary antibodies and detection of bands were performed as described above. Protein quantity was analyzed by band signal intensity using FIJI.

Relative protein quantity was compared to the non-decidualized and/or non-infected control group, for which the value was set at 1.0.

2.2.14 Cytokine Quantification through Flow Cytometry

To inactivate viral particles in the supernatant samples collected during the infection experiments, the samples were thawed and exposed to UV-C light (254 nm) in a UV disinfection chamber for 10 min. This inactivation was kindly performed by Mirjam Hohner. The samples were stored on ice and further processed in an S2-lab.

The LEGENDplex Human Inflammation Panel 1 (13-plex) with V-bottom Plate was used to prepare the samples for cytokine quantification through flow cytometry according to the manufacturer's protocol. All reagents were warmed to room temperature prior to use and all incubation steps were performed in the dark by wrapping the plate in aluminum foil and at room temperature.

Per well of the provided 96-well V-bottom plate, 25 μ l of assay buffer, 25 μ l of supernatant and 25 μ l of mixed beads were added. The plate was covered with a plate sealer and incubated on a plate shaker for 2 h at 800 rpm. The plate was centrifuged at $250 \times g$ for 5 min, after which the supernatant was removed by a quick inversion and flick of the plate. The bead pellets were washed with 200 μ l of 1X wash buffer per well and centrifuged again at $250 \times g$ for 5 min followed by supernatant removal. To each well, 25 μ l of detection antibodies was added. The plate was sealed and incubated on a plate shaker for 30 min at 800 rpm. 25 μ l of SA-PE per well was added and incubation was continued for another 30 min. After centrifugation at $250 \times g$ for 5 min, supernatant was removed and 200 μ l of 1X wash buffer was dispensed per well. This wash step was repeated a second time. Then, the bead pellets were resuspended in 150 μ l of 1X wash buffer per well and stored at 4°C in the dark overnight.

The samples were read on a flow cytometer and the data was processed with FlowJo, which was kindly performed by Dr. Yogesh Singh.

2.2.15 Statistics

Statistical analysis was performed using GraphPad Prism software. A Shapiro-Wilk test and a QQ-plot were used to test whether the data fits normal distribution. For the majority of the data, only a small deviation from the normal distribution was observed, thus the following statistical hypothesis tests were performed.

Cytokine levels in endometrial spheroids infected with SARS-CoV-2 were analyzed with ANOVA followed by a Tukey's multiple comparisons test.

For the analysis of the RNA-seq results, the Benjamini-Hochberg method was applied to control the false discovery rate (FDR) during multiple testing correction in both differential expression and enrichment analysis. Genes meeting this criterion were ranked according to their adjusted p-values and log₂-fold change values were used to identify upregulated or downregulated transcripts. Genes with an adjusted p-value < 0.05 and a fold change ≥ 1.5 were considered significantly differentially expressed. Gene ontology (GO) enrichment analysis and pathway annotation were performed using the Metascape database (Zhou et al., 2019b). Significantly enriched terms were determined based on an adjusted p-value < 0.05.

All other experiments were tested for statistical significance by performing unpaired two-tailed student's t-tests. Data is presented as arithmetic mean and standard error of the mean (SEM). *p < 0.05, **p < 0.01 ***p < 0.001 and ****p < 0.0001 indicate statistical significance whereas ns means non-significant.

3 Results

3.1 Decidualization of 2D HESC and ISK cells

The first set of experiments aimed to investigate the effect of decidualization on protein levels of key entry factors for SARS-CoV-2 in endometrial stromal and epithelial cells (**Figure 3-1**). HESC and ISK were seeded in a 6-well plate at a concentration of 1×10^5 cells per well and cultured in duplicates in a monolayer. The sample size was $n = 6$ for each cell type. The experimental group was treated with 0.5 mM 8-bromo-cAMP and 1 μ M MPA in 2% DCC-FBS DMEM medium, whereas the control group received fresh medium. Decidualization treatment or medium change was repeated every 48 h for 6 days. Decidualization markers were examined using qPCR, while protein levels of ACE2 and TMPRSS2 were assessed through western blotting.

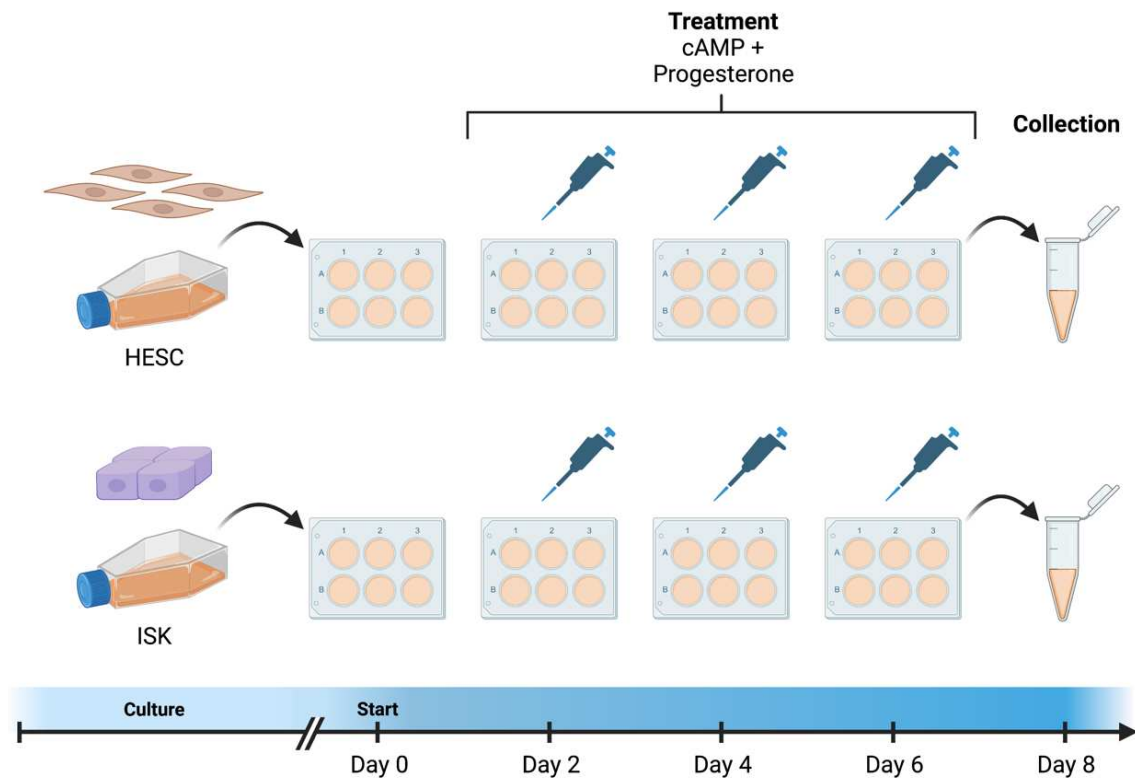


Figure 3-1: Culture and Decidualization Treatment of Monolayer Cells. HESC and ISK cells were cultured in cell culture flasks to 80% confluency. Cells were split to 6-well plates 2 days prior to treatment. Cells were treated with 0.5 mM 8-bromo-cAMP and 1 μ M MPA every 48 h for 6 days. Afterwards, cells were collected and prepared for downstream experiments. Created with BioRender.com.

3.1.1 Expression of Decidualization Markers in HESC and ISK cells

Following decidualization treatment, the cells were harvested and RNA isolation was performed. Average RNA concentrations were 74.6 ng/ μ L (\pm 4.6) and 360.8 ng/ μ L (\pm 24.7) for HESC diluted in a volume of 30 μ L and ISK diluted in 50 μ L, respectively.

After cDNA synthesis, qPCR was performed for decidualization markers *PRL*, *IGFBP1* and *HSD11B1* with *ACTB* as the reference gene. The qPCR results were analyzed using the $2^{-\Delta\Delta C_t}$ method and the value of the control group was set to 1.0. An unpaired two-tailed student's t-test was performed after testing for normality with the Shapiro-Wilk test and a QQ-plot.

Compared to the control group, *PRL* was significantly increased 9.8×10^4 -fold ($\pm 2.6 \times 10^4$, $p = 0.004$) in decidualized HESC (**Figure 3-2A**). In treated HESC, *IGFBP1* was significantly increased 6.6×10^4 -fold ($\pm 1.8 \times 10^4$, $p = 0.005$) compared to non-treated HESC (**Figure 3-2B**). Similarly, a significant 5.4×10^2 -fold ($\pm 9.9 \times 10^1$, $p = 0.0003$) increase was observed for *HSD11B1* following decidualization (**Figure 3-2C**). Thus, all three decidualization markers were significantly upregulated in HESC treated with 8-bromo-cAMP and MPA.

In ISK cells, decidualization treatment significantly lowered the *PRL* value to 20% of the control group ($p < 0.0001$, **Figure 3-2A**). No significant difference between the control and the decidualization group was found for *IGFBP1* ($p = 0.271$) and *HSD11B1* ($p = 0.065$) mRNA levels (**Figure 3-2B, C**).

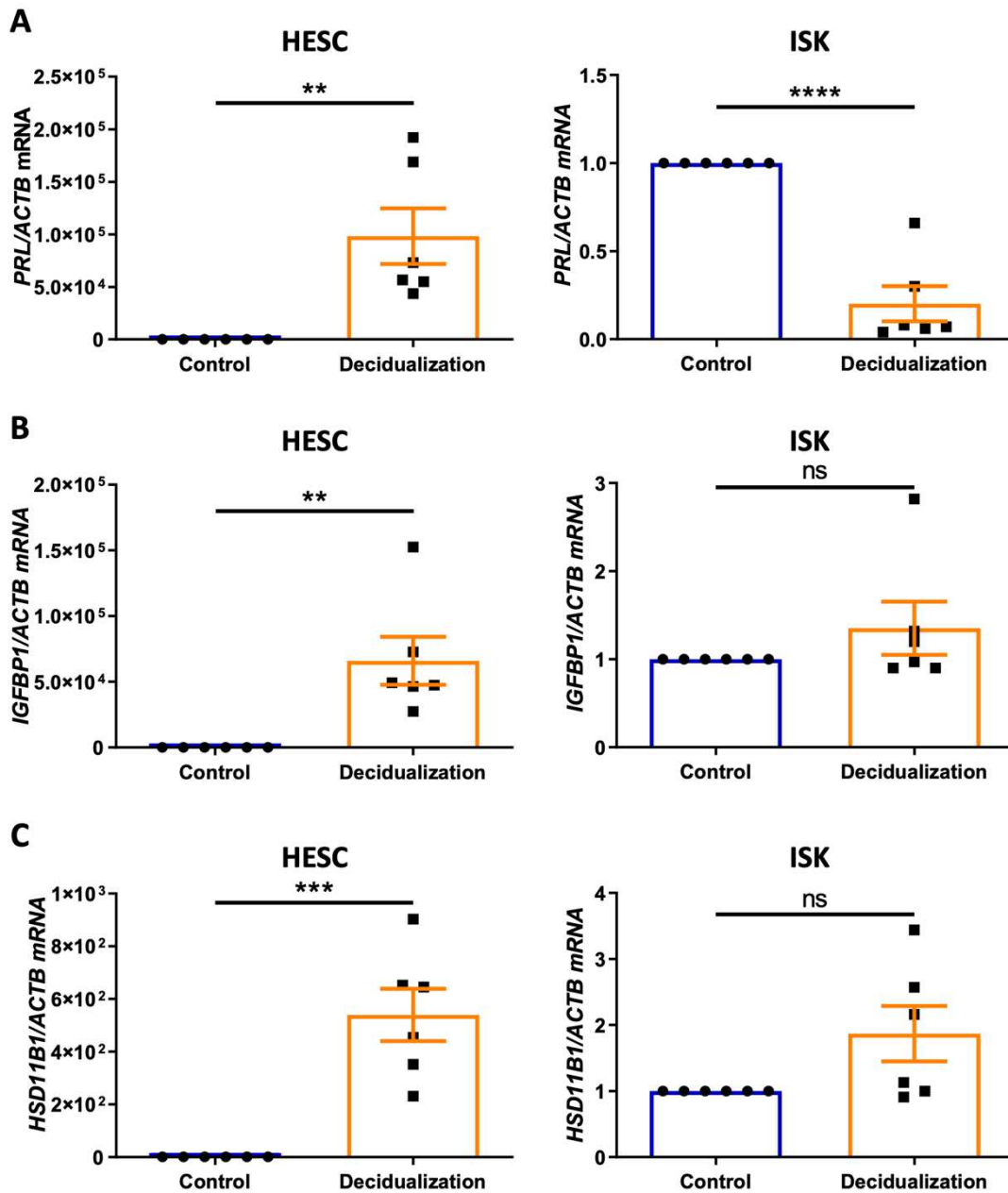


Figure 3-2: Decidualization Markers in HESC and ISK Cells. HESC and ISK cells were cultured as monolayers and treated with 0.5 mM 8-bromo-cAMP and 1 μ M MPA for 6 days. The cells were lysed and RNA extraction as well as qPCR were performed. The mRNA amount of PRL (A), IGFBP1 (B) and HSD11B1 (C) was normalized to ACTB and compared between decidualized and control groups ($n = 6$). Unpaired student's t-tests were applied. Data is presented as the arithmetic mean with SEM. ** $p < 0.01$; *** $p < 0.001$; **** $p < 0.0001$; ns, non-significant.

3.1.2 Effect of Decidualization on ACE2 and TMPRSS2 levels in 2D HESC and ISK cells

Subsequently, cells were collected for protein isolation using Laemmli buffer. Gel electrophoresis and western blot were performed with GAPDH as a loading control and human colorectal adenocarcinoma (CACO-2) cells as a positive control (**Figure 3-3A**). Relative protein quantity was compared to the control group, for which the value was set to 1.0. An unpaired two-tailed student's t-test was used to test for statistical significance. The full blot is shown in **Supplementary Figure 8-1**.

Protein levels of ACE2 showed a significant 177.0-fold increase (± 51.9 , $p = 0.007$) in decidualized HESC compared to the control group (**Figure 3-3B**). In ISK cells, a 1.3-fold increase (± 0.1 , $p = 0.033$) was observed after decidualization treatment. No significant change in TMPRSS2 protein levels were found in HESC ($p = 0.742$) or ISK cells ($p = 0.632$) compared to the control group (**Figure 3-3C**).

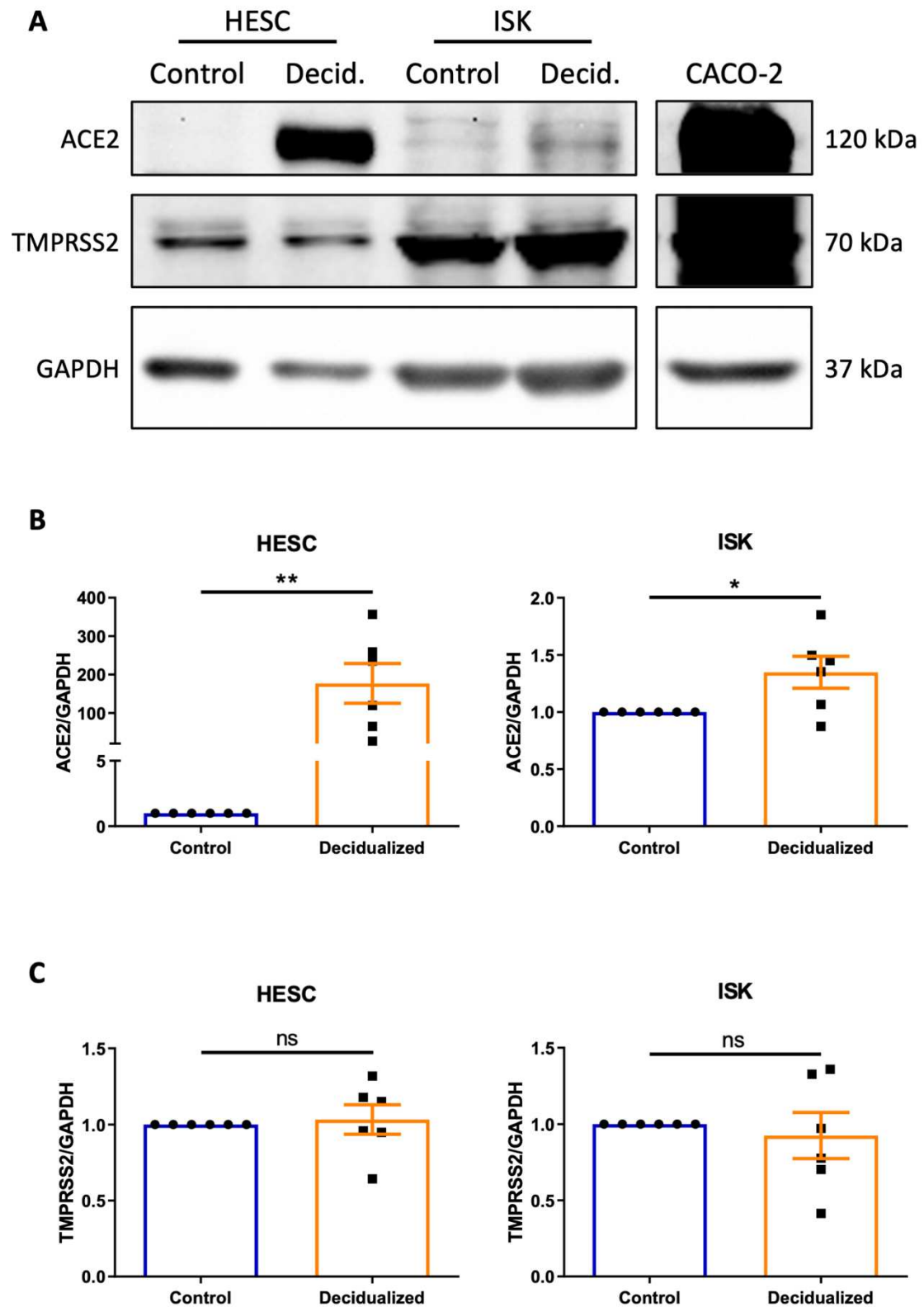


Figure 3-3: ACE2 and TMPRSS2 in 2D HESC and ISK Cells. HESC and ISK ($n = 6$) were cultured in a monolayer and treated with 0.5 mM 8-bromo-cAMP and 1 μ M MPA for 6 days. The cells were lysed and protein was extracted. A western blot was performed (A) with GAPDH as a loading control and CACO-2 cells as a positive control. Relative expression levels of ACE2 (B) and TMPRSS2 (C) were calculated and unpaired student's t-tests were performed. Data is presented as the arithmetic mean with SEM. * $p < 0.05$; ** $p < 0.01$; ns, non-significant.

3.2 Establishment and Optimization of Endometrial Spheroids

To establish a new three-dimensional cell culture model of the human endometrium, a stromal cell type (HESC) and an epithelial cell type (ISK) were included. Several variables were optimized, including the well size, cell number, ratio of HESC to ISK cells and timepoints of seeding the cell types (**Figure 3-4**).

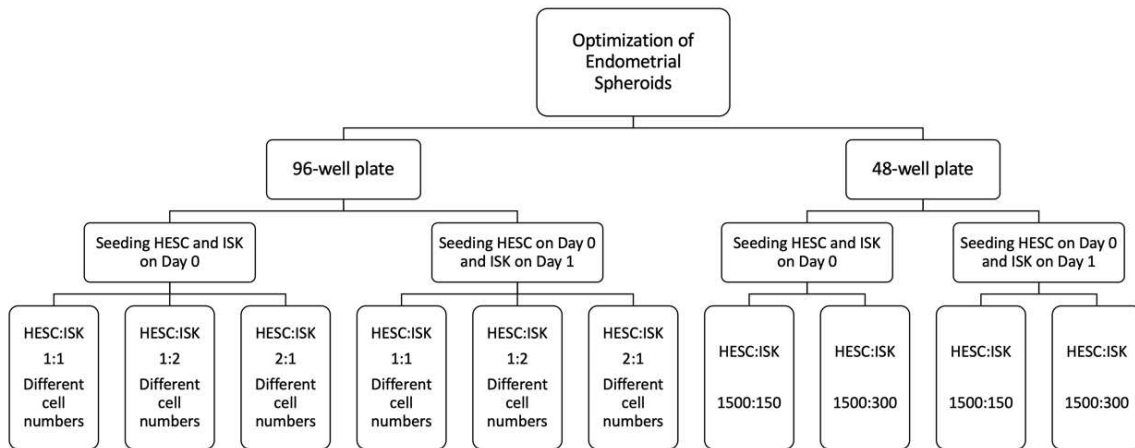


Figure 3-4: Schematic Plan of the Optimization of Endometrial Spheroids. Endometrial spheroids were cultured using the liquid-overlay technique. Different conditions, including well size, timepoint of seeding ISK cells, stromal to epithelial cell ratio and cell number, were compared.

HESC and ISK were cultured separately in cell culture flasks until reaching 80% confluency. The cells were collected, counted and seeded in agarose-coated flat-bottom well plates. Spheroids were created using the liquid-overlay technique (**Figure 3-5**).

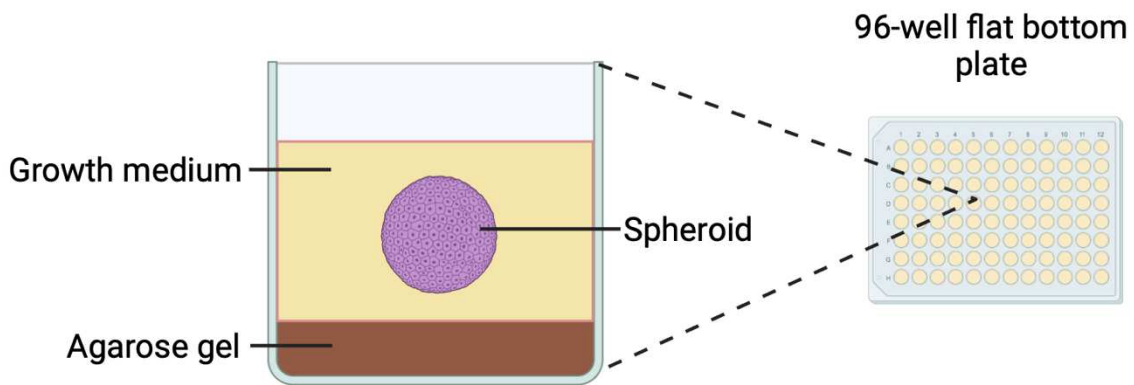


Figure 3-5: Liquid-Overlay Technique. Agarose gel was added to the wells of a 96-well flat bottom plate to create a non-adherent surface. Cells were added in suspension with medium and a spheroid is formed. Created with BioRender.com.

Microwell plates with growth areas of 0.32 cm² (96-well plate) and 0.75 cm² (48-well plate) were used (**Figure 3-6A**). ISK cells were either seeded together with HESC or the day after (**Figure 3-6B**). Ratios of HESC to ISK varied from 1:1, 1:2 to 2:1. Different cell numbers were tested for each cell type ranging from 150 to 6000 cells (**Figure 3-6C**). The medium was changed every 2 days and growth was monitored by phase-contrast imaging at a magnification of 10x.

Criteria for the optimization of the spheroid model were:

- Stable and uniform spheroid formation
- The ratio of stromal to epithelial cells similar to *in vivo* endometrium
- Sufficient cell number for downstream experiments
- Minimal nutrient deficiency or necrosis in the center

Comparison of different well sizes showed that the large volume in 48-well plates hindered the congregation of the cells. The cultures in 96-well plates yielded more stable and uniform spheroid formation (**Figure 3-6A**).

In an attempt to create spheroids with stromal cells at the core and epithelial cells in the periphery, HESC and ISK cells were seeded on sequential days. However, when the ISK cells were added later, they did not attach to the stromal cells. Instead, two separate cell clusters were formed. This

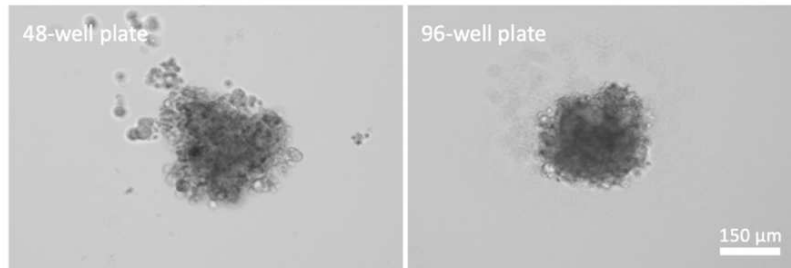
phenomenon was not observed when both cell types were seeded at the same time (**Figure 3-6B**).

The ratio of the HESC to ISK cells and the cell number had an impact on the shape, size and stability of the spheroids. A low proportion of ISK, such as 10:1 or 6:1 (ratio of HESC to ISK), led to an uneven and irregular spheroid surface. Small cell numbers resulted in less stable spheroid formation, comparable to the effect seen in larger well volumes (**Figure 3-6C**). More cells also meant more protein or RNA material for downstream experiments.

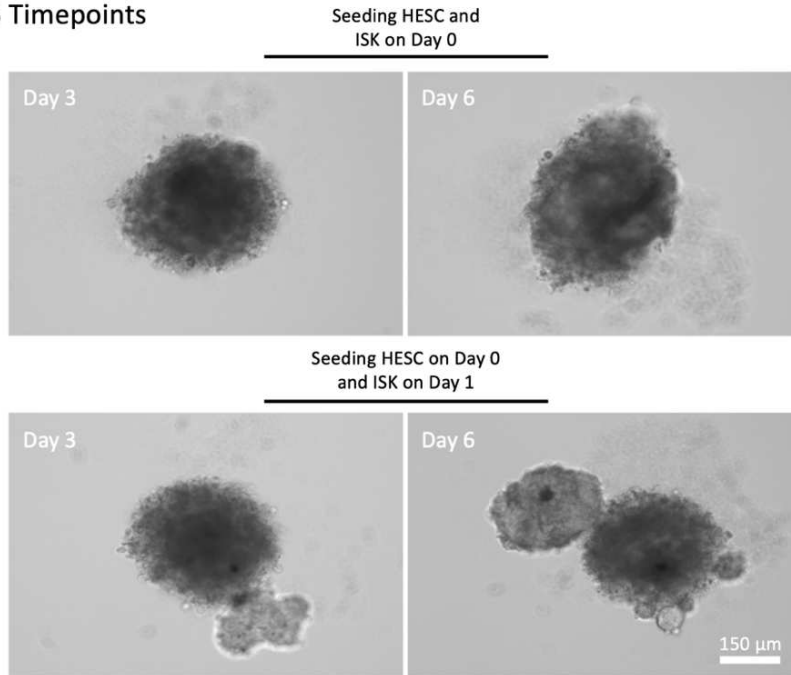
Furthermore, spheroids grown in agarose-coated wells were compared with those grown in prefabricated ultra-low attachment well plates (**Supplementary Figure 8-2**). No difference was observed in growth and morphology.

The optimized protocol is described in **2.2.2**.

A Well Size



B Timepoints



C Cell Number

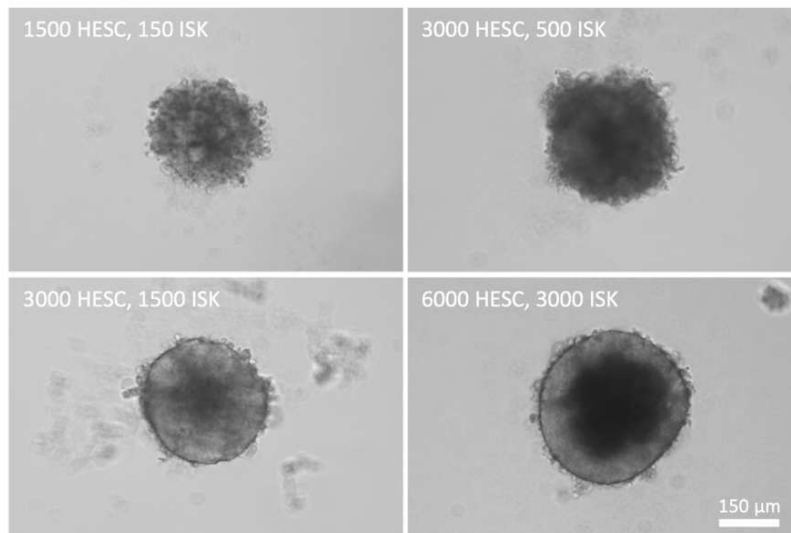


Figure 3-6: Optimization of Endometrial Spheroids. HESC and ISK cells were cultured using the liquid overlay technique to form endometrial spheroids. Comparison of endometrial spheroids (1500 HESC, 300 ISK) cultured in 48- and 96-well plates for 3 days (A). Comparison of endometrial spheroids (3000 HESC, 500 ISK) with ISK cells seeded on day 0 or day 1 (B). Spheroids of various cell numbers after 3 days in culture (C).

3.3 Characterization of Endometrial Spheroids

3.3.1 Formation and Growth of Endometrial Spheroids

To monitor their growth and morphology, endometrial spheroids were cultured using the liquid-overlay technique (n = 12). Growth was observed over the course of 11 days through phase-contrast microscopy (**Figure 3-7**).

Immediately after starting the culture (day 0, 0 h), the cells were single and in suspension. After 6 h, most of the cells migrated to the center of the well, forming loose clusters of cells. The following day, a spheroid with a diffuse shape and uneven surface was formed. A distinct border and a dense core were observed after 2 days. The morphology of the spheroid continued to change as it grew and after 8 days, the spheroid attained a solid, spherical shape, which persisted despite the further increase in size. Additional images can be seen in **Supplementary Figure 8-3**.

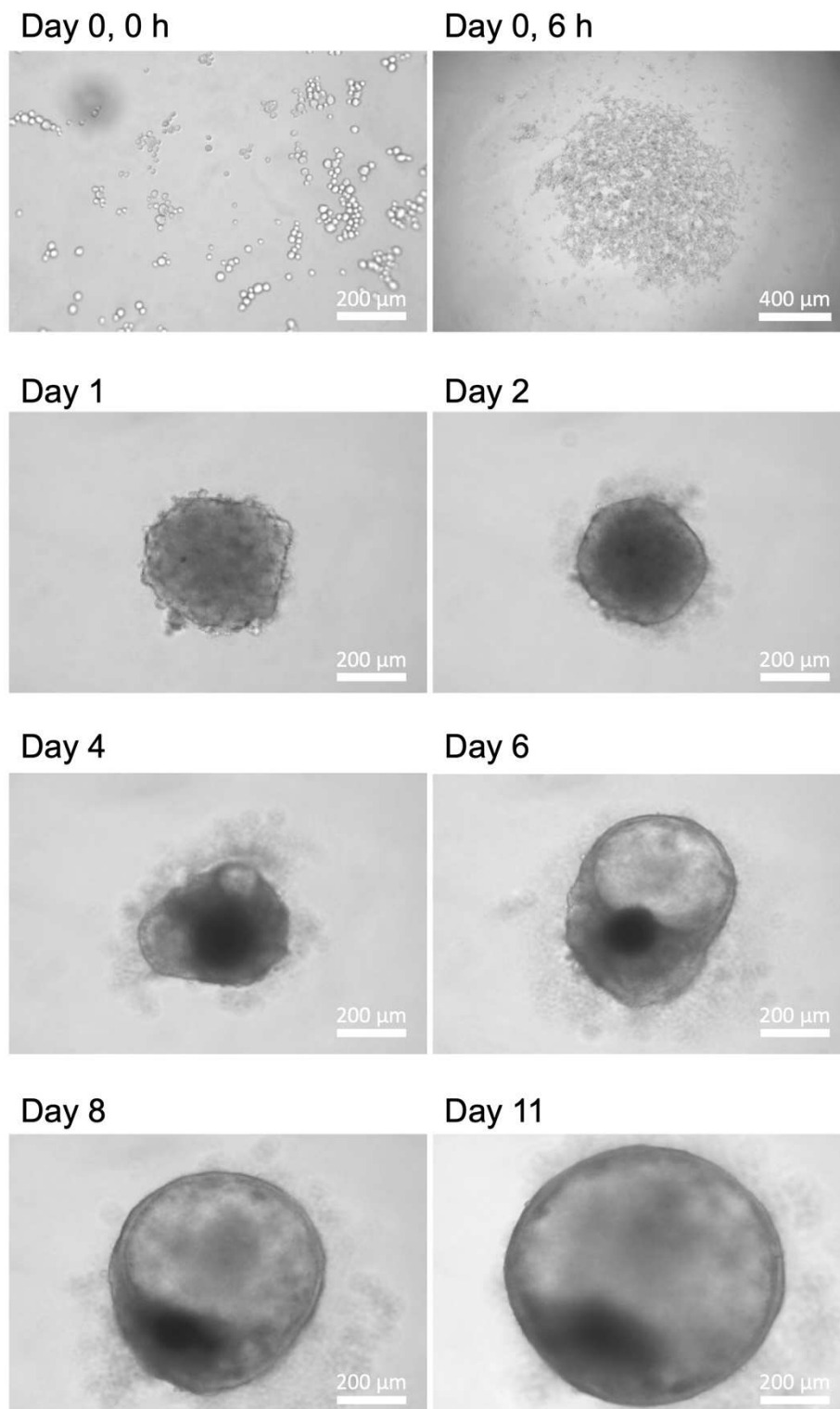


Figure 3-7: Growth of Endometrial Spheroids. 6000 HESC and 3000 ISK cells were cultured in an agarose-coated 96-well plate. Over 11 days, the formation and growth of the endometrial spheroids were documented through phase-contrast microscopy. The scale bar for day 0, 6 h is 400 μm , for the rest 200 μm . $n = 12$, images are representative of at least 100 spheroids.

The area of the endometrial spheroids ($n = 8$) was measured for 11 days (**Figure 3-8A**). On day 1, the mean area was $1.55 \times 10^5 \pm 6.28 \times 10^3 \mu\text{m}^2$, which slightly decreased on day 2 ($1.34 \times 10^5 \pm 1.32 \times 10^4 \mu\text{m}^2$). Afterwards, the area increased continuously reaching $2.35 \times 10^5 \pm 2.81 \times 10^4 \mu\text{m}^2$ after 6 days and $5.45 \times 10^5 \pm 3.88 \times 10^4 \mu\text{m}^2$ after 11 days.

The diameter (**Figure 3-8B**), an intuitive dimension of 2D images, and the volume (**Figure 3-8C**), which describes 3D growth, were calculated with the known mathematical formulas for circles and spheres. On day 6, the mean diameter was $540 \pm 32 \mu\text{m}$ and the mean volume was $8.86 \times 10^7 \pm 1.61 \times 10^7 \mu\text{m}^3$.

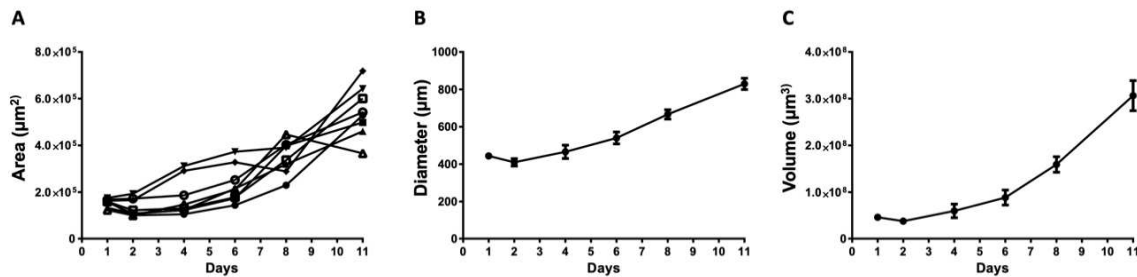


Figure 3-8: Growth Curve of Endometrial Spheroids. Endometrial Spheroids (6000 HESC and 3000 ISK cells) were cultured in an agarose-coated 96-well plate and imaged ($n = 8$). The area (A) was measured for 11 days. Each symbol represents a different spheroid on the respective days. The diameter (B) and volume (C) of the spheroids were calculated. Data is presented as the arithmetic mean and SEM.

3.3.2 Viability of Endometrial Spheroids

To confirm cell viability after spheroid formation and for several days, a viability assay was performed. Endometrial spheroids ($n = 4$) were grown for 2 days and stained with the LIVE/DEAD cytotoxicity kit. Some spheroids were treated with cytotoxic DMSO or 100% ethanol prior to staining. The same procedure was repeated 8 days later.

Green-fluorescent calcein-AM stained live cells through intracellular esterase activity and red-fluorescent ethidium homodimer-1 stained dead cells due to loss of plasma membrane integrity (**Figure 3-9**). On both day 2 and day 10, no red fluorescence was observed and the whole spheroids were stained green.

After treatment with DMSO or ethanol, however, almost the whole spheroids were stained red and only the cells at the center of the spheroids remained alive. The dead spheroids also appeared smaller in size. More images can be found in **Supplementary Figure 8-4**.

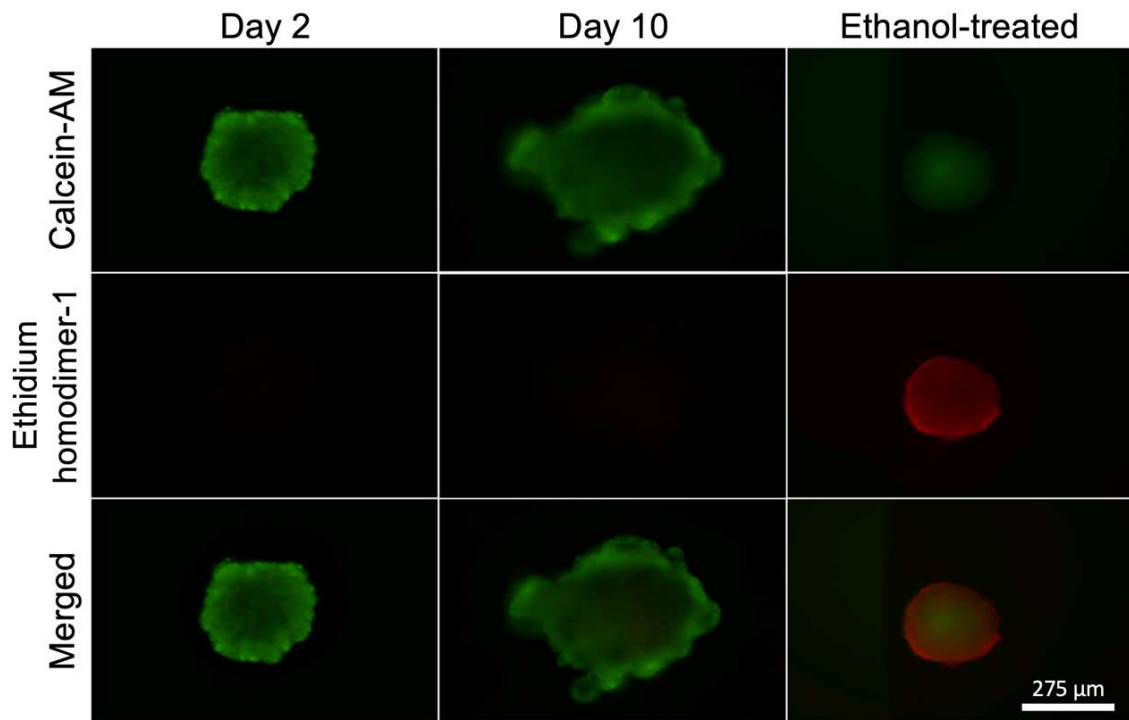


Figure 3-9: Viability Assay of Endometrial Spheroids. After 2 and 10 days in culture, respectively, endometrial spheroids were tested for viability using the LIVE/DEAD Viability/Cytotoxicity Kit. Live cells were stained with calcein-AM (green) and dead cells were stained with ethidium-homodimer-1 (red). Ethanol-treated spheroids were used as dead control. The scale bar is 275 μm , $n = 4$, images are representative of at least 12 spheroids per group.

3.3.3 Immunostaining for Epithelial and Stromal Cell Markers in Endometrial Spheroids

To validate the presence of both endometrial stromal and epithelial cells in the endometrial spheroids, immunostaining for stromal and epithelial cell markers was performed. Endometrial spheroids were cultured for 7 days prior to collection and fixation ($n = 2$). They were then dehydrated and rehydrated, blocked and stained with primary antibodies against cytokeratin 7 and vimentin as well as counterstained with DAPI. After incubation with the corresponding

secondary antibodies, the spheroids were imaged under the fluorescent microscope (**Figure 3-10**).

Cytokeratin (green) and vimentin (red) were both present in endometrial spheroids. Cell nuclei were stained with DAPI (blue). Additional images are shown in **Supplementary Figure 8-5**.

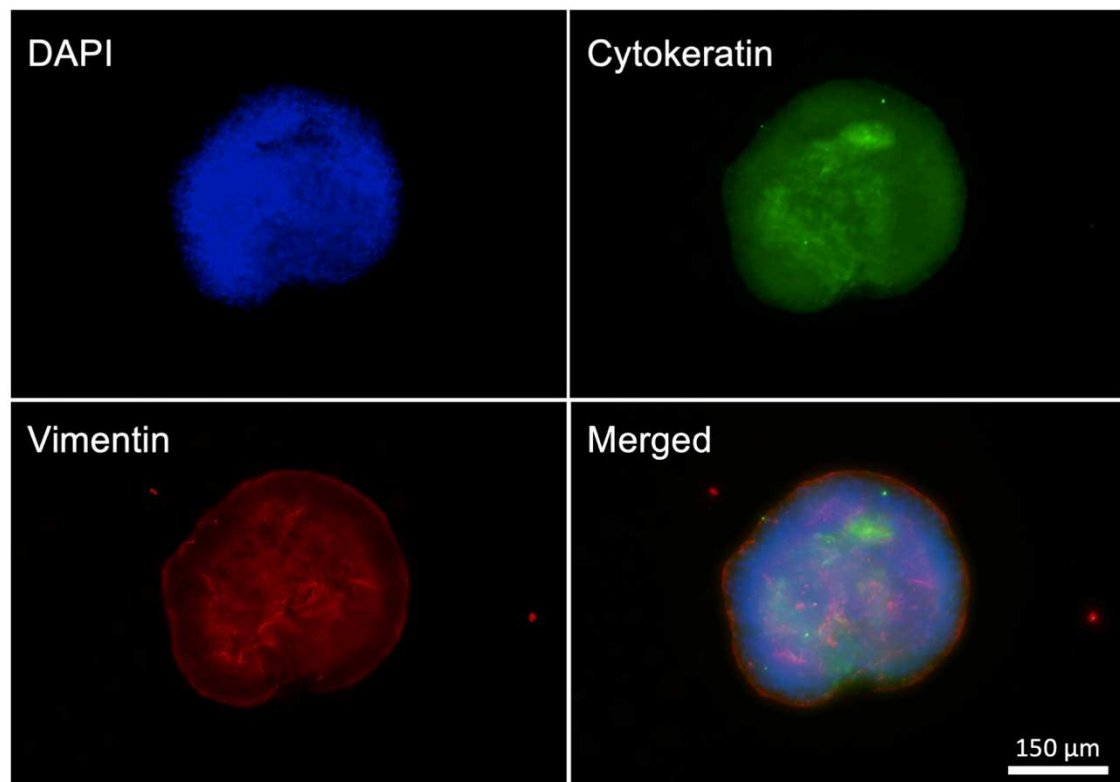


Figure 3-10: Immunostaining of Endometrial Spheroids for Epithelial and Stromal Cell Markers. After 7 days of culture, endometrial spheroids were fixed and immunostained using antibodies against cytokeratin 7 (green), an epithelial cell marker, and vimentin (red), a stromal cell marker. The nuclei were counterstained with DAPI (blue). The scale bar is 150 μm , $n = 2$, images are representative of at least 4 spheroids per group.

3.4 Decidualization of Endometrial Spheroids

3.4.1 Decidualization Markers in Endometrial Spheroids

The purpose of the fourth set of experiments was to investigate how endometrial spheroids respond to decidualization treatment and whether this has an impact on the expression of key entry factors for SARS-CoV-2.

Endometrial spheroids (n = 8) were cultured for 2 days prior to treatment with 5% DCC-FBS medium containing 0.5 mM 8-bromo-cAMP and 1 μ M MPA. Treatment or medium changes were repeated every 48 h for 6 days, after which the spheroids were collected. qPCR was performed and RNA levels of *PRL*, *IGFBP1* and *HSD11B1* were compared to *ACTB* as a reference gene (**Figure 3-11**). The qPCR results were analyzed using the $2^{-\Delta\Delta C_t}$ method and the value of the control group was set to 1.0. After testing for normality, an unpaired two-tailed student's t-test was performed.

No statistically significant difference in *PRL* expression was observed between decidualized endometrial spheroids and the control group (p = 0.107). However, decidualized spheroids had a significant 1.7-fold (± 0.2 , p = 0.0007) increase in *IGFBP1* expression. RNA levels of *HSD11B1* were 3.0-fold (± 0.8 , p = 0.028) higher in the treatment group compared to the control group.

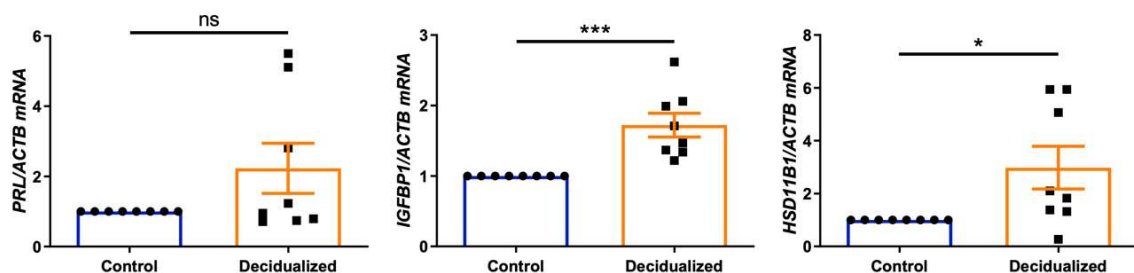


Figure 3-11: Decidualization Markers in Endometrial Spheroids. Endometrial spheroids (n = 8) were cultured for 2 days and treated for 6 days with 0.5 mM 8-bromo-cAMP and 1 μ M MPA. RNA was extracted and qPCR was performed. RNA levels of *PRL*, *IGFBP1* and *HSD11B1* were normalized to *ACTB* and unpaired student's t-tests were performed. Data is presented as the arithmetic mean and SEM. *p<0.05; ***p<0.001; ns, non-significant.

3.4.2 Effect of Decidualization on ACE2 and TMPRSS2 Levels in Endometrial Spheroids

After 2 days of culture and 6 days of decidualization treatment, endometrial spheroids (n = 5) were collected and lysed. Protein extraction and western blot for the detection of ACE2 and TMPRSS2 were performed. (**Figure 3-12A**). GAPDH was used as loading and CACO-2 cells as positive control,

respectively. Relative protein quantity was compared to the control group (defined as 1.0).

Only faint bands were visible for ACE2 in both control and decidualized samples, which did not allow reliable quantitative analyses and therefore, no quantitative data was obtained. TMPRSS2 was detected in both groups, but no significant difference was observed in TMPRSS2 protein levels between control and decidualized endometrial spheroids after testing for significance with an unpaired student's t-test ($p = 0.075$) (**Figure 3-12B**). The full blot is shown in **Supplementary Figure 8-6**.

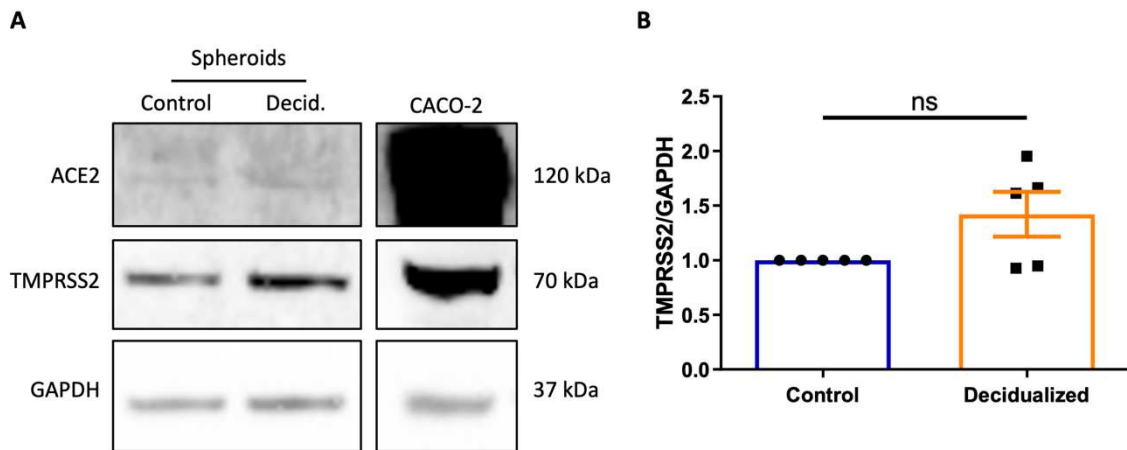


Figure 3-12: ACE2 and TMPRSS2 Levels in Endometrial Spheroids. Endometrial spheroids ($n = 5$) were treated with 0.5 mM 8-bromo-cAMP and 1 μ M MPA for 6 days. The cells were lysed and protein was extracted. A western blot was performed (**A**) with GAPDH as a loading control and CACO-2 cells as a positive control. Relative expression of TMPRSS2 was calculated and an unpaired student's t-test was performed (**B**). Data is presented as the arithmetic mean with SEM. ns, non-significant.

3.5 Culture and Growth of Endometrial Organoids

As an alternative model, already established endometrial organoids were cultured and characterized for comparison with endometrial spheroids. The organoid lines were derived from primary stem cells obtained from endometrial biopsies of the university clinic Tübingen and kindly provided by Dr. André Koch. Endometrial organoids were cultured embedded in basement membrane extract (BME). Organoid growth was monitored as a stitched overview image of

the well (**Figure 3-13**, upper row) as well as an image of the same position (**Figure 3-13**, lower row) over 9 days ($n = 6$).

At the beginning of the organoid culture, single cells were distributed throughout the BME. These cells then proliferated and formed cystic, gland-like organoids. The separate organoids continued to grow and merged with others in the vicinity while still maintaining a single lumen.

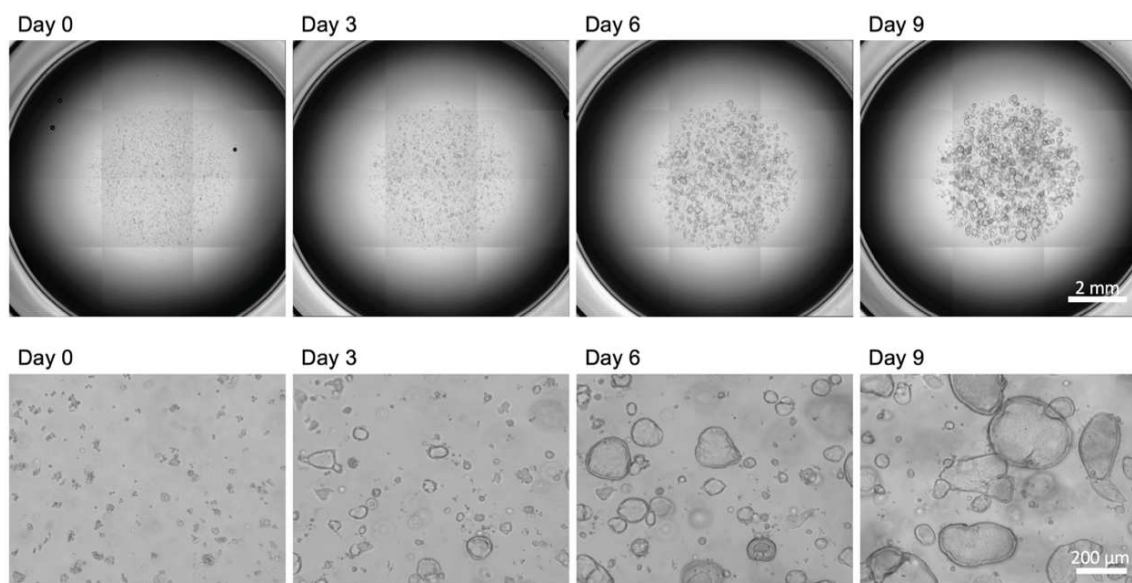


Figure 3-13: Formation and Growth of Endometrial Organoids. Endometrial organoids were cultured embedded in BME in a 48-well plate. Formation and growth were tracked by phase contrast images of an overview of the well (upper row) or in higher magnification (lower row). Scale bars are 2 mm (upper row) and 200 μm (lower row), respectively. $n = 6$.

3.6 Characterization of Basal Out and Apical Out Endometrial Organoids

To enable pathogen interaction with the apical side of the endometrial organoids, an apical-out assay was performed. To this end, basal out organoids cultured in BME were transferred to suspension culture to establish apical out polarity (**Figure 3-14A**).

For 6 days, organoids were cultured in BME before being removed and suspended in medium ($n = 5$). The organoid suspension was added to 48-well

plates coated with agarose gel. Morphology and growth were analyzed with the help of phase-contrast microscopy.

Organoids embedded in BME have a large, clear central lumen as well as a smooth outer and inner border (**Figure 3-14B**). After 3 days in suspension culture, organoids were smaller in size, displayed higher density and contained a small, dark lumen.

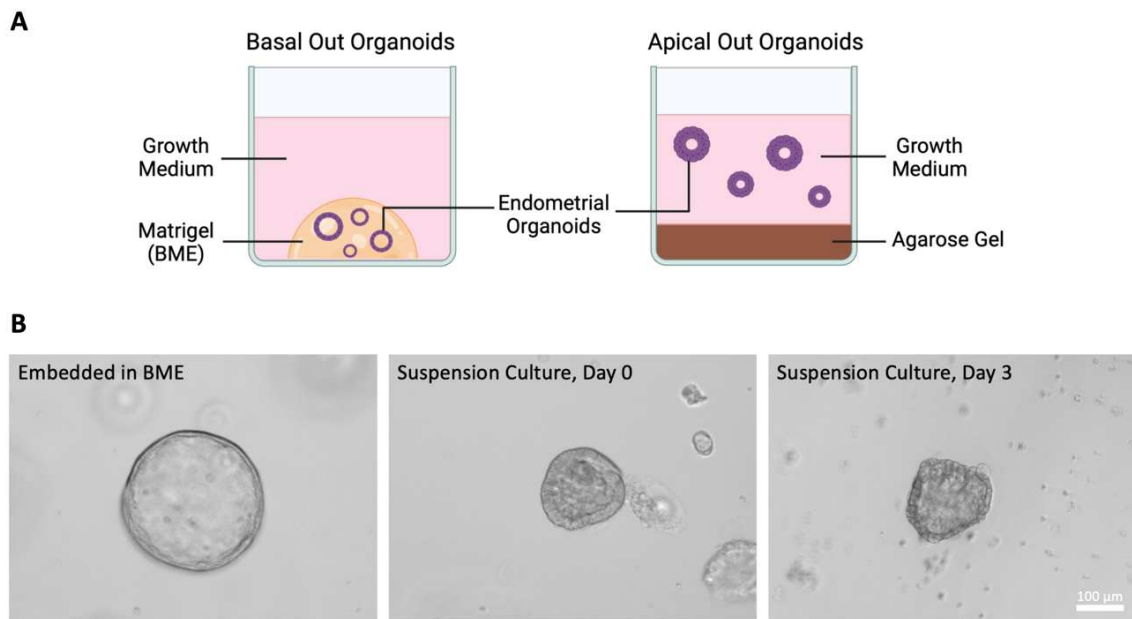


Figure 3-14: Comparison of the Morphology of Basal Out and Apical Out Endometrial Organoids. Schematic depiction (A) and phase contrast images (B) of endometrial organoids cultured in BME and in suspension. Single organoids were imaged after 6 days of culture embedded in BME. After removal from BME, organoids were cultured in suspension and change in morphology was observed through phase-contrast microscopy. $n = 5$, panel A created with BioRender.com.

To further characterize basal out and apical out endometrial organoids, whole organoids (**Figure 3-15A**) or sections (**Figure 3-15B**) were stained with antibodies targeting Zonula occludens-1 (ZO-1, a tight junction protein, green) and β -catenin (associated with adherens junctions, red). The nuclei were counterstained with DAPI (blue).

In the apical out organoids, ZO-1 was mainly located towards the outside and β -catenin towards the inside of the organoids. This pattern was different from the one observed in the basal out organoids.

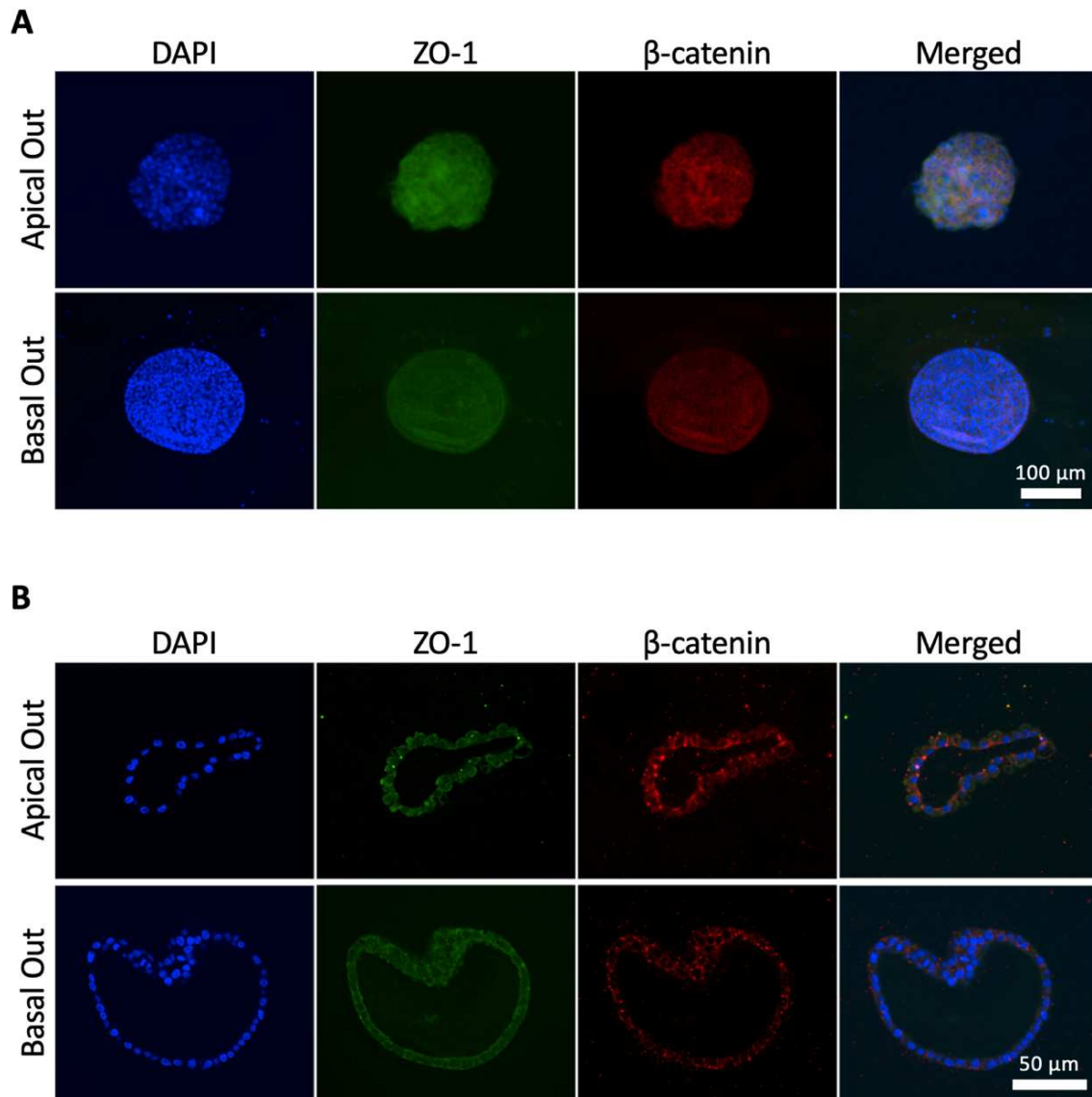


Figure 3-15: Immunostaining of Apical Out and Basal Out Endometrial Organoids. Endometrial organoids were cultured either embedded in BME (basal out) or in suspension (apical out). Immunofluorescence for structural proteins (ZO-1 in green and β -catenin in red) was performed on whole organoids (A) or after embedding in paraffin and sectioning (B). Nuclei were counterstained with DAPI (blue). Scale bars represent 100 μ m (A) and 50 μ m (B), respectively. $n = 1$, images are representative of at least 10 organoids per group.

3.7 Expression of ACE2 and TMPRSS2 in Endometrial Organoids

To assess the suitability of endometrial organoids as a model to study SARS-CoV-2 infection, protein expression of ACE2 and TMPRSS2 was examined. Endometrial organoids (n = 3) were cultured in BME and received decidualization treatment for 6 days. Protein extraction and western blot were performed (**Figure 3-16**). GAPDH served as a loading control and CACO-2 as a positive control.

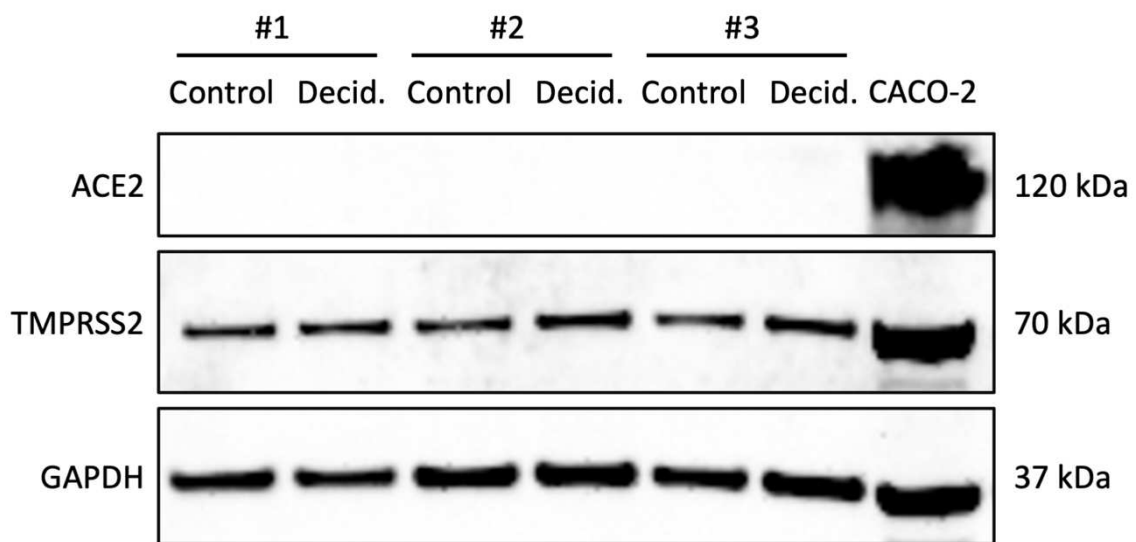


Figure 3-16: Protein Levels of ACE2 and TMPRSS2 in Endometrial Organoids. Different endometrial organoid lines (n = 3) were cultured embedded in BME and treated with 0.5 mM 8-bromo-cAMP and 1 μ M MPA for 6 days. The organoids were collected and lysed for protein extraction. Western blot was performed and the amount of ACE2 and TMPRSS2 was determined through normalization with GAPDH. CACO-2 served as a positive control.

No ACE2 was detected in any of the three organoid lines, neither in the control nor in the decidualized group. Bands for TMPRSS2 and GAPDH were obtained. The full blot is shown in **Supplementary Figure 8-7**.

3.8 Infection of Endometrial Organoids with SARS-CoV-2

Basal out organoids (n = 1) and apical out organoids (n = 1) were decidualized for 5 days prior to infection with SARS-CoV-2. Basal out organoids were infected with wildtype SARS-CoV-2 B.1 and apical out organoids were infected with wildtype SARS-CoV-2 B.1.617.2. Protein was extracted 48 h and 72 h post-infection of basal out and apical out organoids, respectively. Western blots were performed for SARS-CoV-2 nucleocapsid protein with actin as a loading control and infected CACO-2 cells as a positive control. While the actin signal was strong, no bands were observed for the SARS-CoV-2 nucleocapsid in basal out endometrial organoids with or without decidualization treatment (**Figure 3-17A**). In the apical out endometrial organoids, faint bands were visible for SARS-CoV-2 nucleocapsid (**Figure 3-17B**). The full blots are shown in **Supplementary Figure 8-8** and **Supplementary Figure 8-9**.

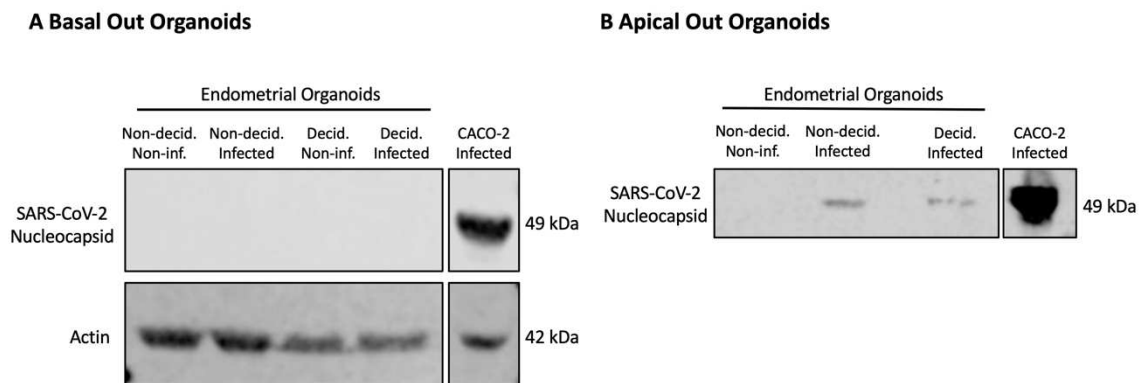


Figure 3-17: Infection of Endometrial Organoids with SARS-CoV-2. Endometrial organoids (n = 1) were cultured either in basal out or apical out polarity and treated with 0.5 mM 8-bromo-cAMP and 1 μ M MPA for 5 days. After 48 h of infection with SARS-CoV-2 B.1 (200930034 IU/ml, diluted 1:100), the protein was extracted from basal out organoids and a western blot was performed (**A**). Protein extraction and western blot of apical out organoids were performed after 72 h of infection with SARS-CoV-2 B.1.617.2 (648267898 IU/ml, diluted 1:100) (**B**). Actin was used as loading control and SARS-CoV-2 infected CACO-2 as positive control.

3.9 Infectibility of 2D Endometrial Cells with SARS-CoV-2

In order to test if SARS-CoV-2 can infect endometrial cells, a preliminary experiment using HESC and ISK cells cultured as monolayers was conducted.

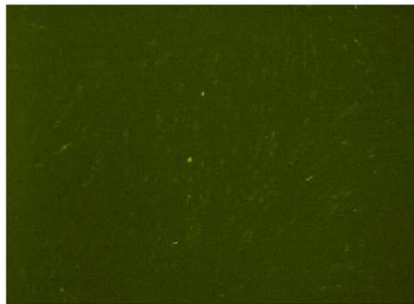
HESC and ISK monolayers were cultured with or without decidualization treatment prior to infection (n = 1). Cells were either infected with icSARS-CoV-2-mNG, a clone of SARS-CoV-2 exhibiting green fluorescence, or with wildtype SARS-CoV-2 B.1 from a clinical isolate.

For ISK, a strong fluorescent signal was observed in infected cells treated with decidualization medium, whereas no fluorescence was detected in non-infected ISK or any HESC samples (**Figure 3-18A, B**). A western blot of ISK and HESC without decidualization treatment after 72 h of infection with the wildtype virus showed no band for the SARS-CoV-2 nucleocapsid in contrast to the positive control (**Figure 3-18C**). In another western blot using ISK, bands were observed for the cells infected with both the icSARS-CoV-2-mNG and the wildtype virus after decidualization treatment (**Figure 3-18D**).

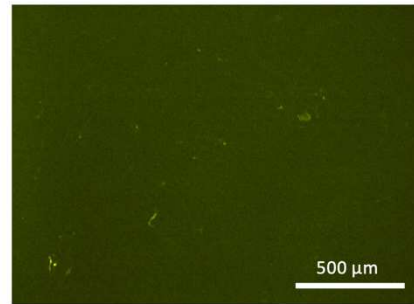
Full western blots can be seen in **Supplementary Figure 8-10**.

A HESC

Non-decidualized, non-infected

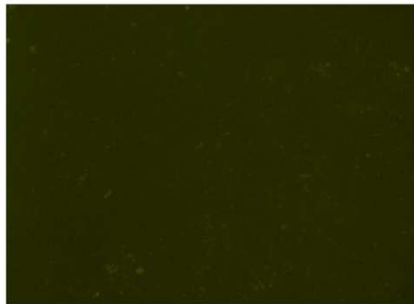


Decidualized, infected

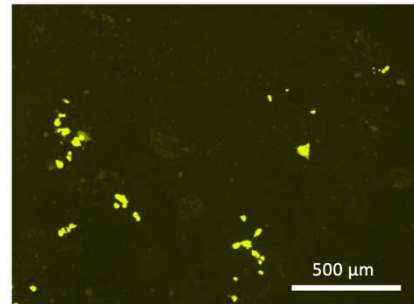


B ISK

Non-decidualized, non-infected



Decidualized, infected



C Non-decidualized 2D cells



D ISK Western Blot

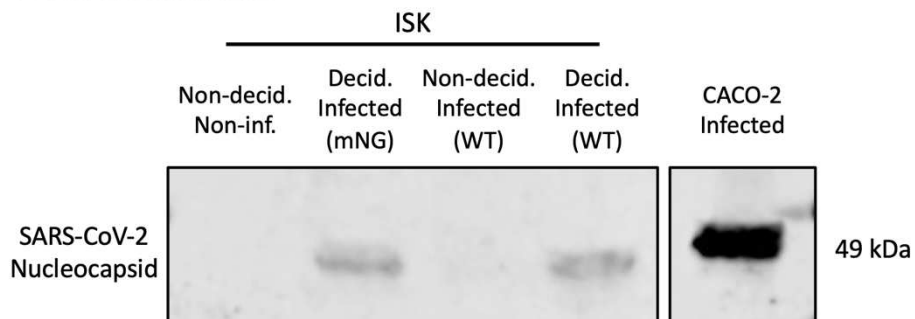


Figure 3-18: Infection of HESC and ISK with SARS-CoV-2. 2D HESC and ISK were cultured either with or without decidualization medium ($n = 1$). After infection with either icSARS-CoV-2-mNG (mNG, MOI = 10), a green-fluorescent clone of SARS-CoV-2, or with wildtype SARS-CoV-2 B.1 (WT, MOI = 40) from a clinical isolate, infection was monitored through fluorescence microscopy (A, B) and/or western blot (C, D). Infected CACO-2 served as positive control.

3.10 Infection of Endometrial Spheroids with SARS-CoV-2

Following preliminary experiments with monolayer cultures, infection of endometrial spheroids with SARS-CoV-2 was carried out. The experimental set-up is depicted in **Figure 3-19**. Infection was confirmed through immunostaining and western blot. Further, cytokine levels were measured in the supernatant. RNA-seq was performed and validated through qPCR.

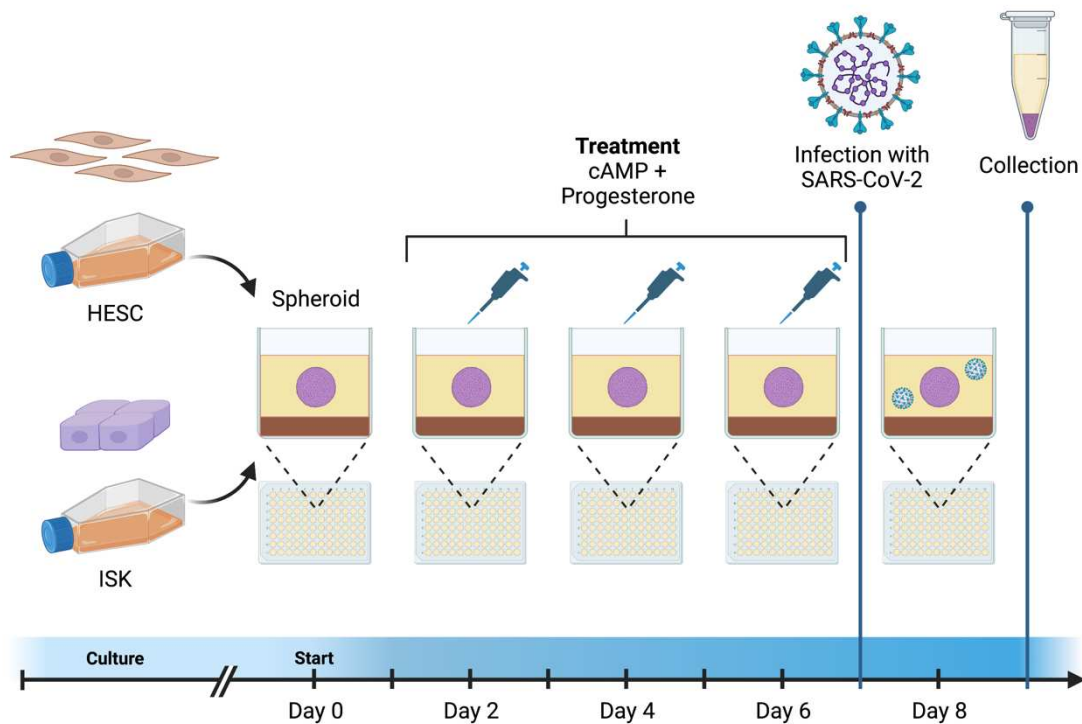


Figure 3-19: Experimental Set-Up for Infection of Endometrial Spheroids. HESC and ISK were cultured separately before being added to agarose-coated wells of a 96-well plate for spheroid formation. After 2 days, the spheroids were treated with 0.5 mM 8-bromo-cAMP and 1 μ M MPA, which was repeated every 48 h. On day 7, spheroids were infected with wildtype SARS-CoV-2 B.1.617.2 (Delta variant, 648267898 IU/ml, diluted 1:20) and 48 h post-infection, spheroids were collected for downstream analyses. Created with BioRender.com.

3.10.1 Immunostaining of Infected Endometrial Spheroids

After infection, spheroids (n = 1) were fixed, dehydrated and rehydrated, blocked and stained with primary antibodies against ACE2 and SARS-CoV-2 nucleocapsid. After incubation with the corresponding secondary antibodies, the spheroids were imaged through immunofluorescence microscopy (**Figure 3-20**).

All endometrial spheroids expressed ACE2 (green). SARS-CoV-2 nucleocapsid protein (red) was only present in infected endometrial spheroids. Additional images are shown in **Supplementary Figure 8-11**.

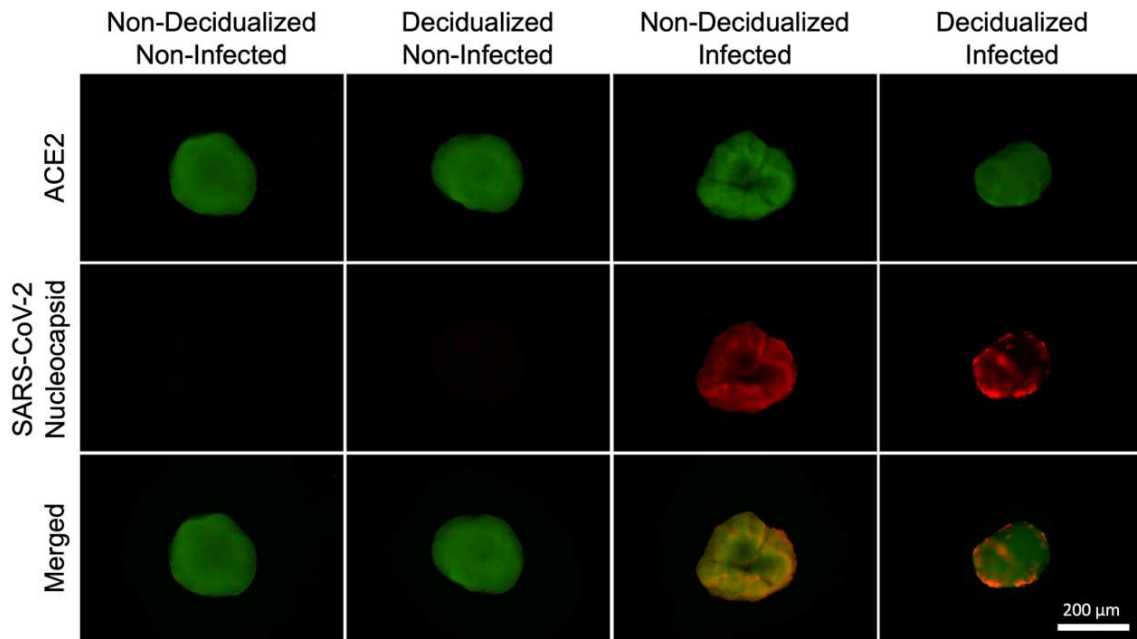


Figure 3-20: Immunostaining of Non-Infected and Infected Endometrial Spheroids. After 7 days in culture, decidualized and non-decidualized endometrial spheroids were either infected with wildtype SARS-CoV-2 B.1.617.2 (Delta variant, 648 267 898 IU/ml, diluted 1:20) or mock-infected ($n = 1$). 48 hours post-infection, endometrial spheroids were fixed and stained for ACE2 (green) and SARS-CoV-2 nucleocapsid protein (red). The scale bar is 200 μm . Images are representative of at least 5 spheroids per group.

3.10.2 Verification of Infection in Endometrial Spheroids through Western Blot

To further demonstrate successful infection with SARS-CoV-2, a western blot was performed for the detection of SARS-CoV-2 nucleocapsid protein ($n = 5$). GAPDH was used as an internal loading control (**Figure 3-21A**). SARS-CoV-2 nucleocapsid protein was detected in the infected non-decidualized and decidualized spheroids, but not in the non-infected samples.

To study the effect of decidualization in infected endometrial spheroids, band size and intensity of non-decidualized (defined as 1.0) and decidualized spheroids were compared (**Figure 3-21B**). The data was analyzed with an

unpaired two-tailed student's t-test, as no significant deviation from the normal distribution was observed. The amount of SARS-CoV-2 nucleocapsid protein was not significantly different between the infected non-decidualized and decidualized samples ($p = 0.666$). The full blot is presented in **Supplementary Figure 8-12**.

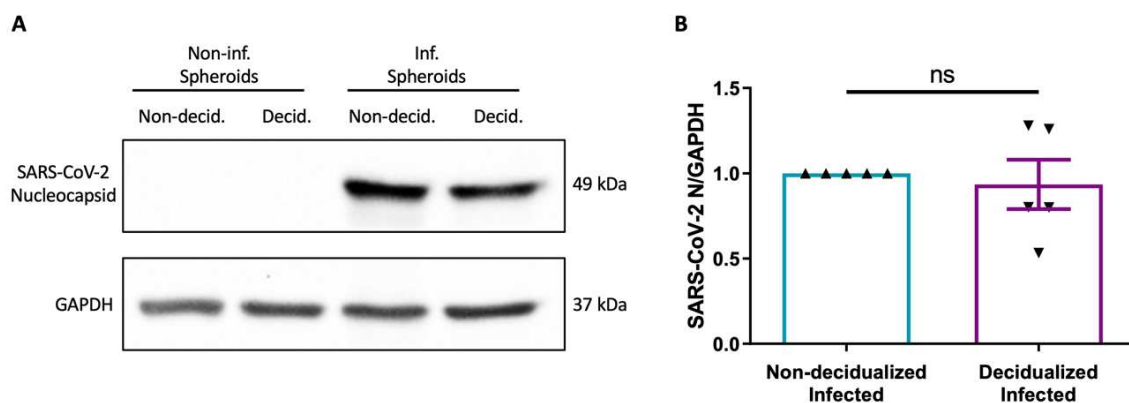


Figure 3-21: Detection of SARS-CoV-2 Nucleocapsid Protein in Infected and Non-Infected Endometrial Spheroids. Endometrial spheroids ($n = 5$) were cultured for 7 days and decidualized prior to infection with SARS-CoV-2 B.1.617.2 (Delta variant, 648 267 898 IU/ml, diluted 1:20). After 48 h of incubation, cells were lysed and protein was extracted. Western blot was performed for the detection of SARS-CoV-2 nucleocapsid protein (A). GAPDH was used as an internal loading control. SARS-CoV-2 nucleocapsid protein levels were compared between the infected non-decidualized and decidualized samples (B). An unpaired student's t-test was used for statistical analysis. Data is presented as the arithmetic mean and SEM. ns, non-significant.

3.10.3 Cytokine Levels in Endometrial Spheroids after Infection with SARS-CoV-2

To evaluate the inflammatory response elicited by SARS-CoV-2 infection in endometrial spheroids, cytokine levels were measured in the supernatant after 24 h and 48 h of infection ($n = 5$). Cytokine measurement was performed using the Human Inflammation Panel 1 (13-plex) assay and flow cytometry. Data was tested for normality and analyzed with ANOVA followed by Tukey's multiple comparisons test. Of the measured cytokines, two were detectable: MCP-1 and IL-8 (**Figure 3-22**).

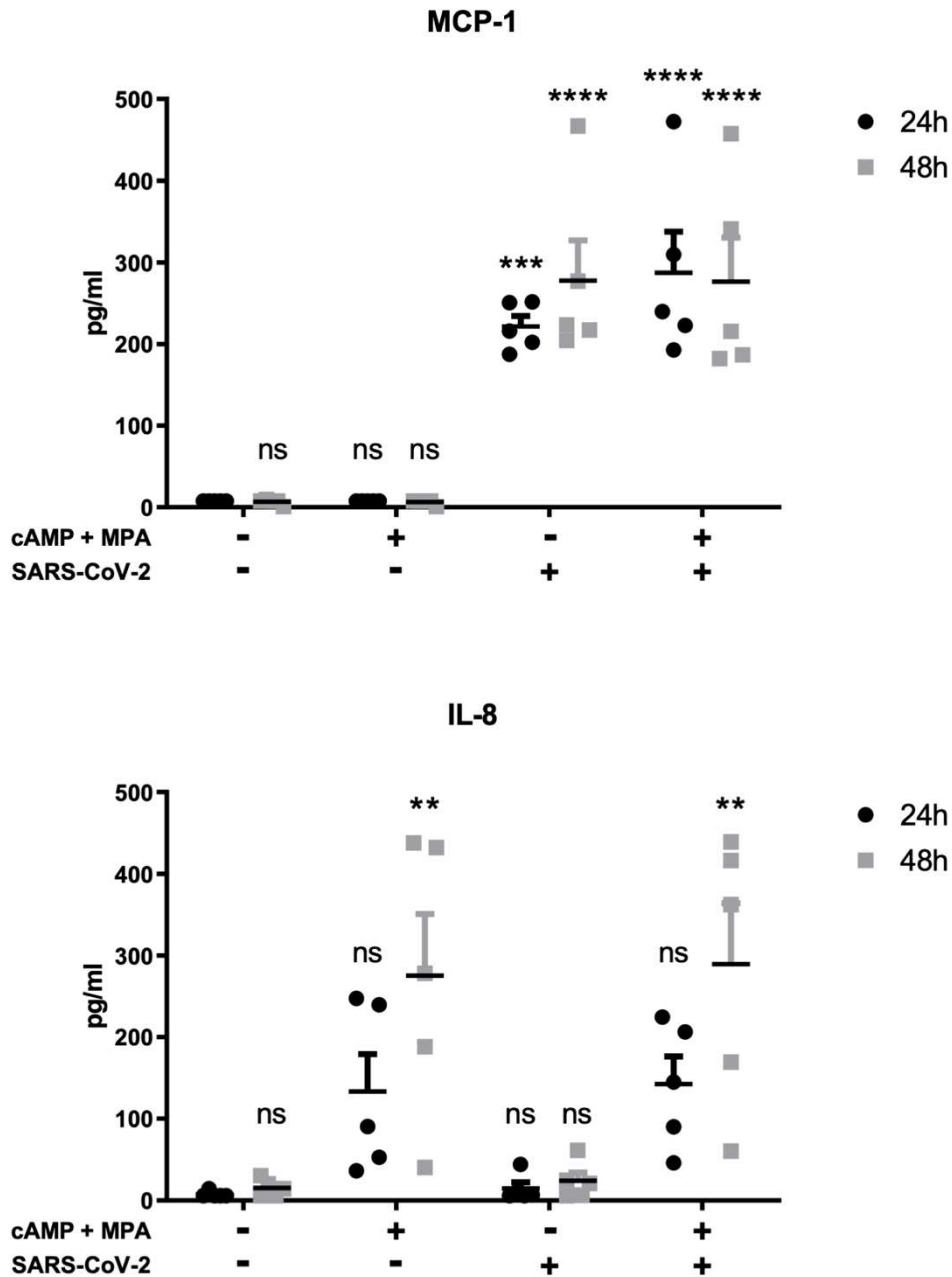


Figure 3-22: Cytokine Levels of Infected and Non-Infected Endometrial Spheroids. Endometrial spheroids ($n = 5$) were cultured for 7 days and decidualized for 5 days prior to infection with SARS-CoV-2 B.1.617.2 (648 267 898 IU/ml, diluted 1:20). Supernatant was collected 24 h and 48 h post-infection. ANOVA was used for statistical analysis. Data is presented as the arithmetic mean and SEM. The degree of statistical significance is shown in comparison to non-decidualized non-infected endometrial spheroids. $**p < 0.01$; $***p < 0.001$; $****p < 0.0001$; ns, non-significant.

MCP-1 levels were low in the non-infected samples. In the non-infected non-decidualized (SARS-CoV-2 -, cAMP + MPA -) spheroids, the mean MCP-1 amount was 7.75 pg/ml after 24 h and 6.69 pg/ml after 48 h. Mean MCP-1

levels in non-infected decidualized (SARS-CoV-2 -, cAMP + MPA +) spheroids were 7.75 pg/ml after 24 h and 6.35 pg/ml after 48 h.

MCP-1 increased significantly in the infected samples ($p < 0.001$) with 221.70 pg/ml in infected non-decidualized (SARS-CoV-2 +, cAMP + MPA -) samples after 24 h and 277.90 pg/ml after 48 h. Infected decidualized (SARS-CoV-2 +, cAMP + MPA +) spheroids had MCP-1 levels of 287.40 pg/ml 24 h post-infection and 276.60 pg/ml after 48 h. Regardless of infection status, no significant difference in the amount of MCP-1 was detected between non-decidualized and decidualized spheroids.

IL-8 was not significantly changed in infected compared to non-infected samples. The mean IL-8 amount of non-infected non-decidualized spheroids was 7.51 pg/ml after 24 h and 15.17 pg/ml after 48 h. 14.58 pg/ml of IL-8 was measured in infected non-decidualized samples at the 24 h timepoint and 23.82 pg/ml at 48 h.

In both non-infected and infected spheroids, a significant increase was seen in the supernatant from decidualized spheroids after 48 h compared to the non-decidualized ones ($p < 0.01$). After 24 h, mean IL-8 levels were 133.20 pg/ml in non-infected decidualized and 142.30 pg/ml in infected decidualized spheroids. The amount further increased at the 48 h timepoint to 275.40 pg/ml and 289.40 pg/ml, respectively.

3.10.4 RNA Sequencing of Infected Endometrial Spheroids

RNA-seq was performed to identify gene expression profiles in non-infected and infected as well as decidualized and non-decidualized endometrial spheroids ($n=3$). The sequencing generated an average read per sample of 23280406.17, with a unique mapping rate of 91.9% to the reference genome.

Differential gene expression (DEG) analysis was performed by pairwise comparison of the four experimental groups (**Table 3-1**). Genes with a $|\log_2 \text{fold change}| \geq 1.50$ and a Benjamini-Hochberg adjusted p -value < 0.05 were considered significantly differentially expressed. The effect of infection

resulted in 123 DEGs between non-infected and infected non-decidualized as well as 362 DEGs between non-infected and infected decidualized endometrial spheroids. Between non-decidualized and decidualized spheroids, the identification of 228 DEGs in non-infected samples and 295 DEGs in infected samples can be attributed to the effect of decidualization.

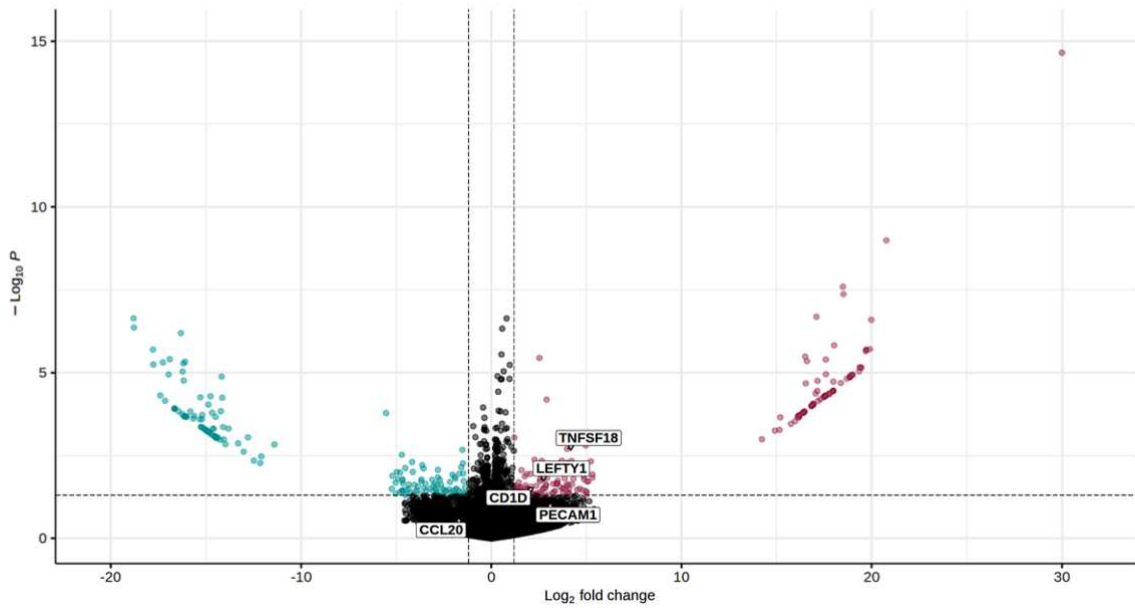
Table 3-1: Number of Differentially Expressed Genes. Pairwise comparisons of RNA-seq data from endometrial spheroids according to the fold change ($|\log_2FC| \geq 1.50$) and significance (adjusted p-value < 0.05) cut-offs.

Pairwise Comparison	Upregulated	Downregulated	Total
Non-decidualized Infected vs. Non-decidualized Non-infected	81	42	123
Decidualized Infected vs. Decidualized Non-infected	212	150	362
Decidualized Non-infected vs. Non-decidualized Non-infected	128	100	228
Decidualized Infected vs. Non-decidualized Infected	162	133	295

The DEGs are further visualized in volcano plots (**Figure 3-23**). The X-axis of the plot represents the \log_2 -fold change between the two groups and the Y-axis represents the negative logarithm (base 10) of the p-value. Significantly up- or downregulated genes are shown in purple or turquoise, respectively, and non-significantly changed genes are shown in black.

Several genes stood out with notably high \log_2 -fold changes and low p-values, suggesting a strong association between their expression and the treatment effect. In non-decidualized spheroids, infection led to increased expression of *TNFSF18* and *LEFTY1*. Interestingly, this effect was not observed in the decidualized samples, in which infection resulted in higher *NR4A3* and lower *C7* expression.

Non-dec Inf vs. Non-dec Non-inf



Dec Inf vs. Dec Non-inf

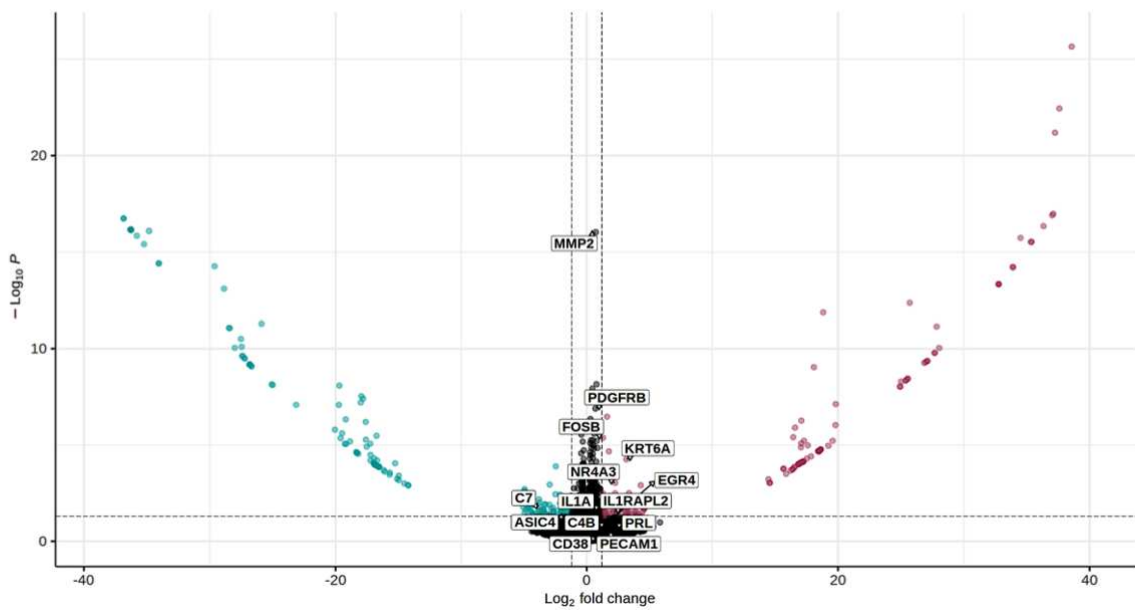
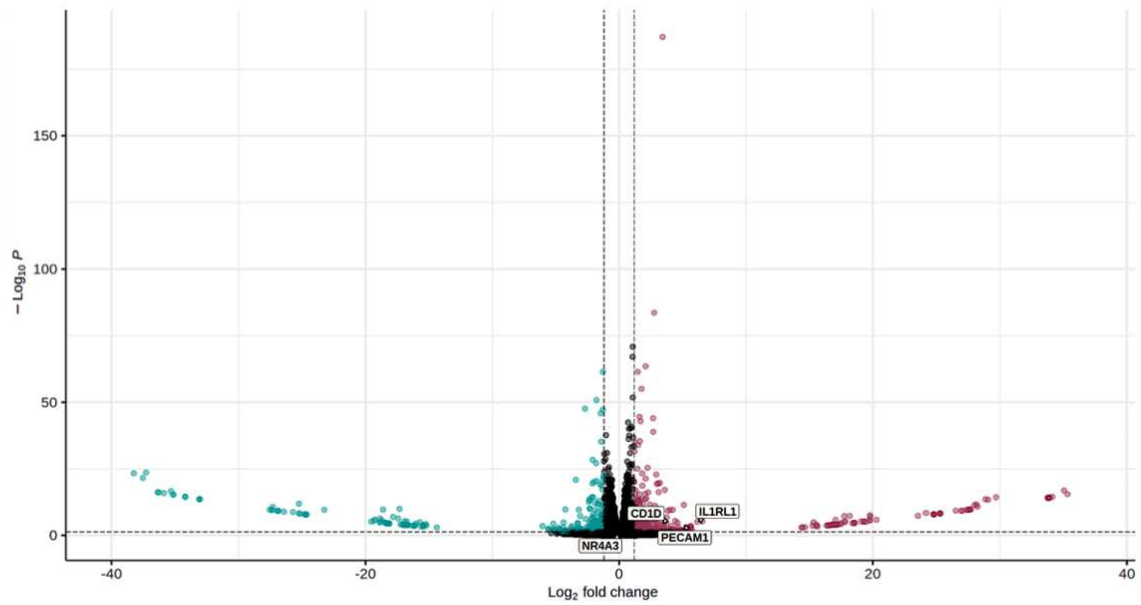


Figure 3-23: Volcano Plots of DEGs in Endometrial Spheroids Infected with SARS-CoV-2. Following decidualization treatment and infection with SARS-CoV-2 B.1.617.2 of endometrial spheroids ($n = 3$), RNA-seq was performed. Each data point represents an individual gene and DEGs are indicated by red dots ($|\log_2FC| \geq 1.5$, FDR-adjusted $p < 0.05$), with upregulated genes shown on the right side of the plot (purple dots) and downregulated genes on the left side (turquoise dots). Non-significant genes are shown as black dots. Example genes are labeled with names.

Dec Non-inf vs. Non-dec Non-inf



Dec Inf vs. Non-dec Inf

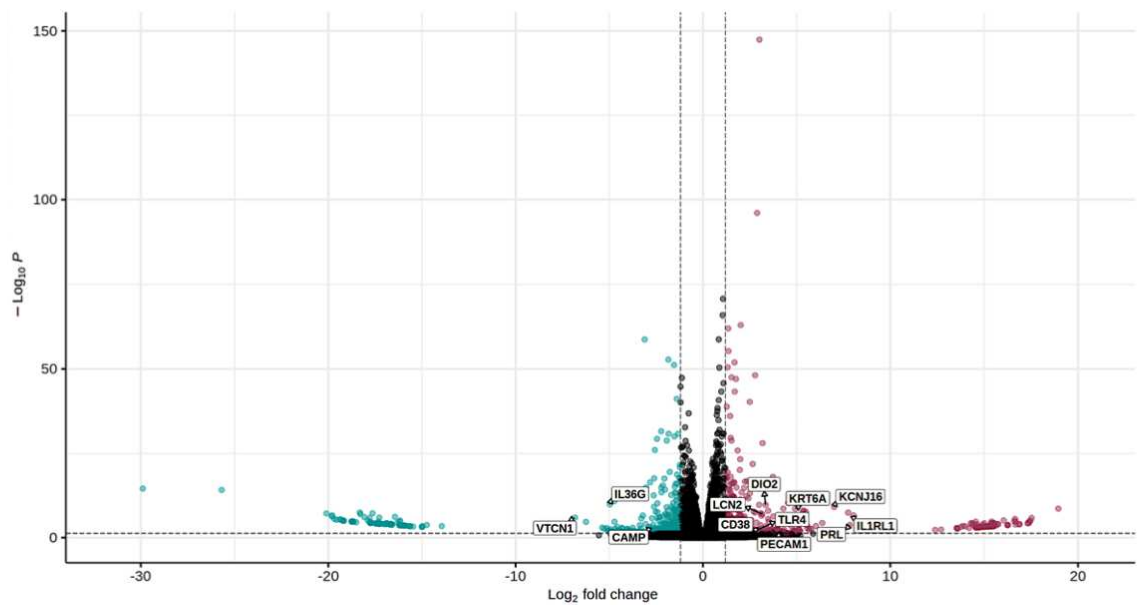


Figure 3-23: Volcano Plots of DEGs in Endometrial Spheroids Infected with SARS-CoV-2. Continued.

The effect of decidualization can be seen by an upregulation of *IL1RL1* and *PECAM1* in both non-infected and infected samples. Notably, *VTCN1* and *IL38G* were downregulated in decidualized infected spheroids but not in decidualized non-infected. These examples show that both infection and

decidualization impacted the gene expression profiles of the endometrial spheroids.

To analyze the variance in mRNA expression between the experimental groups, principal component analysis (PCA) was performed (**Figure 3-24**). The cumulative explained variance plot demonstrated that the first two principal components (PC1 and PC2) accounted for 37.7% of the total variance in the dataset. PC1 explained 24.9% of the variance and PC2 explained 12.8%. These two components were selected for further interpretation and visualization. The score plot based on PC1 and PC2 revealed distinct clustering of samples between non-decidualized and decidualized groups. The separation according to infection status is not as clear in the non-decidualized samples but more pronounced in decidualized spheroids.

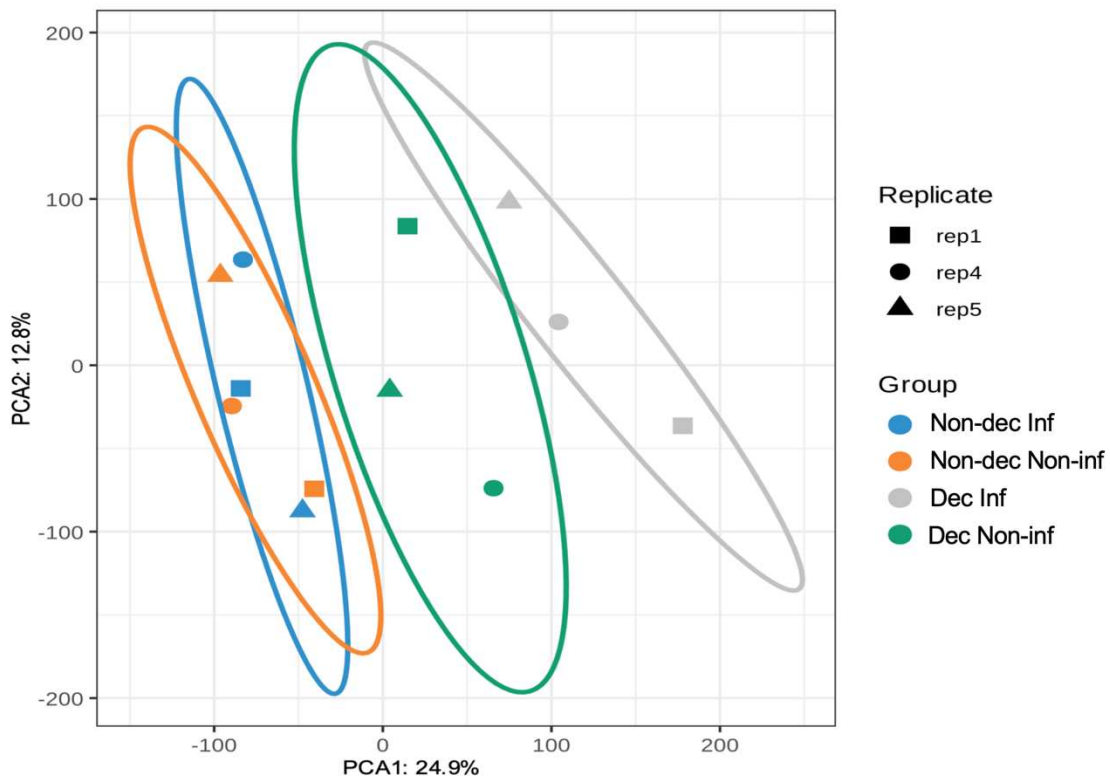


Figure 3-24: Principal Component Analysis of RNA-Seq Data from Endometrial Spheroids after Infection with SARS-CoV-2. Endometrial spheroids were decidualized and infected with SARS-CoV-2 B.1.617.2 ($n = 3$). RNA-seq was performed and the first two principal components were used for analysis. Axis percentages indicate variance contribution of the first two principal components. Biological replicates are represented as different symbols and experimental groups are shown in different colors.

Focusing on selected DEGs, the heat map (**Figure 3-25**) displays the expression patterns in pairwise comparisons of the experimental groups. Comparisons between each group provide insights into the specific gene expression changes associated with decidualization treatment (first and second column) and infection (third and fourth column).

A heat map with dendrograms can be seen in **Supplementary Figure 8-13**.

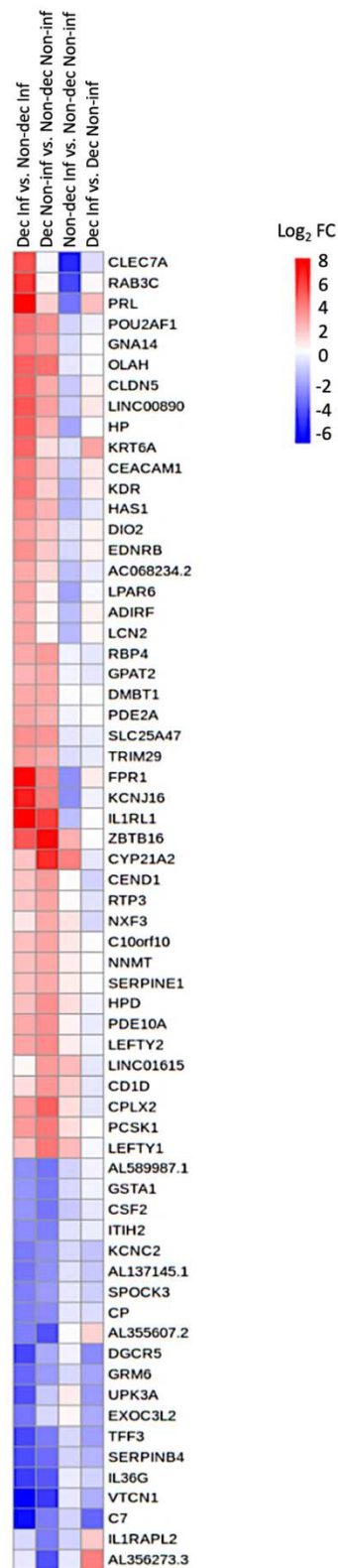


Figure 3-25: Heat Map Analysis of Gene Expression Profiles of Endometrial Spheroids after Infection with SARS-CoV-2. RNA-seq was performed on endometrial spheroids after decidualization treatment and infection with SARS-CoV-2 B.1.617.2 ($n = 3$). A subset of selected DEGs are displayed in this heat map with each row representing an individual gene and each column representing a pairwise comparison of two experimental groups. The color scale indicates the gene expression levels, with red indicating upregulation and blue indicating downregulation.

To gain insight into the biological processes and pathways associated with the DEGs, we performed gene ontology (GO) enrichment analysis and pathway annotation of the top 40 up- and downregulated genes using the Metascape database (**Figure 3-26**). GO analysis revealed that the upregulated genes in infected spheroids were significantly enriched in categories such as fan embryonic CTX brain myeloid or target genes of DNA topoisomerase 2-beta in non-decidualized or decidualized spheroids, respectively. The downregulated genes were enriched in categories related to immune response regardless of decidualization status.

In the non-infected samples, significantly enriched upregulated genes in decidualized spheroids were involved in carbohydrate metabolism, TGF- β signaling and inflammation. The downregulated genes also correlated with inflammatory regulation and the TNF signaling pathway. In infected samples, decidualization led to a significant enrichment of upregulated genes associated mainly with immune response and secretion, whereas the downregulated genes were significantly enriched in processes linked to cell and ECM structure.

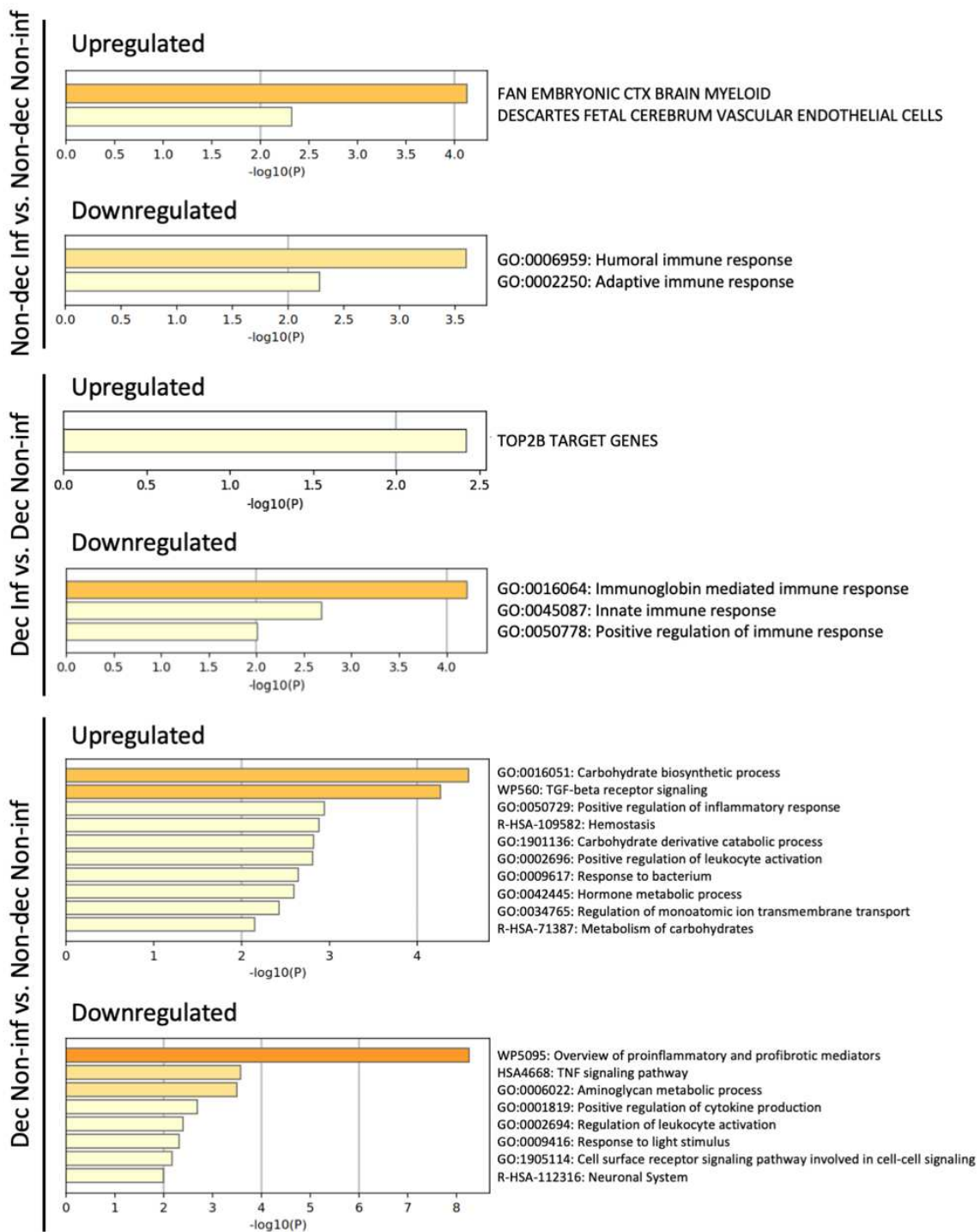


Figure 3-26: Gene Ontology Enrichment Analysis and Pathway Annotation of Endometrial Spheroids Infected with SARS-CoV-2. Endometrial spheroids were decidualized and infected with SARS-CoV-2 B.1.617.2 ($n = 3$). RNA-seq was performed and the data was compared to the Metascape database. Gene ontology enrichment analysis as well as pathway annotation were performed for up- and downregulated DEGs of pairwise group comparisons. Statistical significance is indicated by $-\log_{10}(p\text{-value})$ on the x-axis and by the shade of orange.

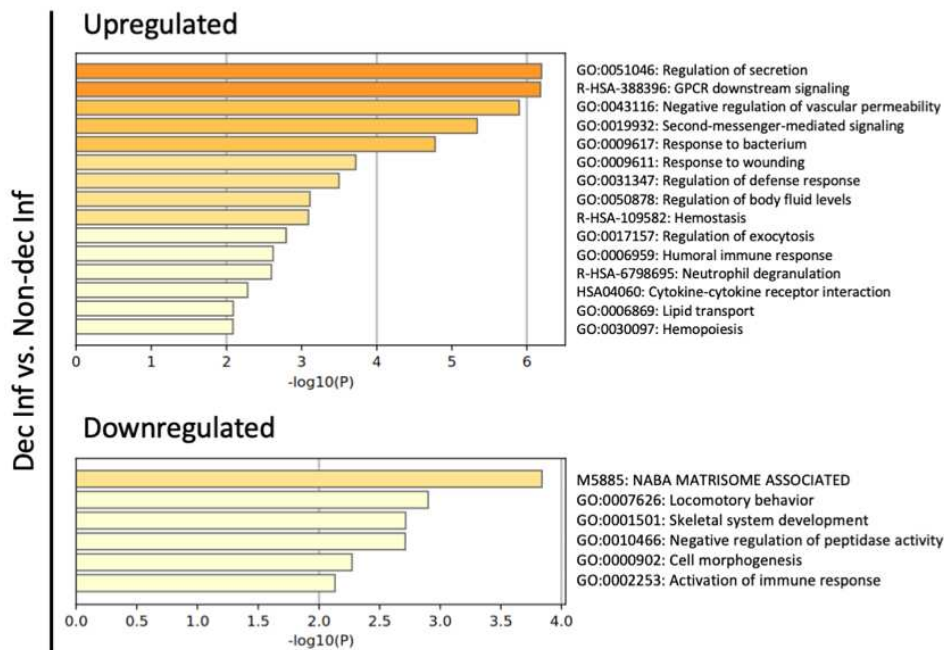


Figure 3-26: Gene Ontology Enrichment Analysis and Pathway Annotation of Endometrial Spheroids Infected with SARS-CoV-2. Continued.

3.10.5 Verification of RNA Sequencing Results of Infected Endometrial Spheroids through qPCR

To validate the RNA-seq results, qPCR was performed on a subset of selected DEGs (Figure 3-27). A new batch of endometrial spheroids (n = 5) was cultured, decidualization treated and infected as in previous experiments. qPCR was performed for *CCL20*, *CD38*, *LCN2*, *VTCN1*, *NR4A3*, *LEFTY1*, *IL1RL1* and *ACTB* as the reference gene. The qPCR results were analyzed using the $2^{-\Delta\Delta Ct}$ method and the value of the control group was defined as 1.0. Statistical significance was tested with unpaired student's t-tests.

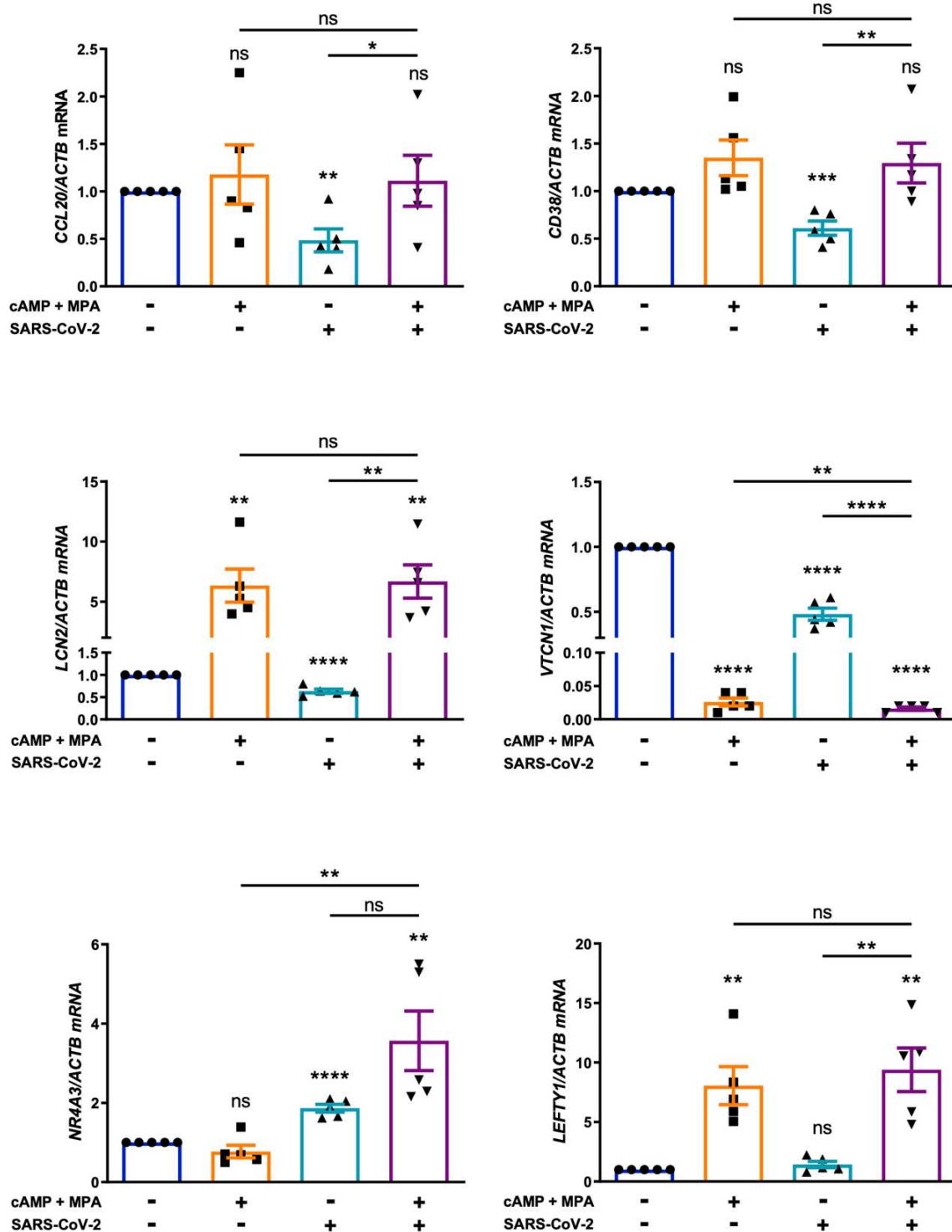


Figure 3-27: Validation of DEGs in SARS-CoV-2 Infected Endometrial Spheroids through qPCR. RNA-seq data was analyzed and up- or downregulated genes were chosen for verification. A new batch of endometrial spheroids ($n = 5$) was decidualized and infected with SARS-CoV-2 B.1.617.2 (648 267 898 IU/ml, diluted 1:20). RNA was extracted after 48 h of incubation and qPCR was performed with ACTB as reference gene. Unpaired student's *t*-tests were performed. Data is presented as the arithmetic mean and SEM. The degree of statistical significance is shown in comparison to non-decidualized non-infected endometrial spheroids, if not otherwise indicated by straight lines. * $p < 0.05$; ** $p < 0.01$; *** $p < 0.001$; **** $p < 0.0001$; ns, non-significant.

Three of the tested genes were downregulated upon SARS-CoV-2 infection only in non-decidualized endometrial spheroids: *CCL20* (0.48-fold \pm 0.12, $p = 0.003$), *CD38* (0.61-fold \pm 0.07, $p < 0.001$) and *LCN2* (0.63-fold \pm 0.04, $p < 0.001$). For *CCL20* and *CD38*, gene expression was also significantly higher in the decidualized infected compared to the non-decidualized infected samples (2.30-fold \pm 0.50, $p = 0.032$ and 1.96-fold \pm 0.21, $p = 0.002$, respectively). An upregulation of *LCN2* was observed in decidualized non-infected (6.34-fold \pm 1.38, $p = 0.005$) and decidualized infected (6.68-fold \pm 1.39, $p = 0.004$) spheroids.

In the RNA-seq data, the downregulation of *CCL20* upon infection in the non-decidualized samples was not statistically significant ($p_{\text{adj}} = 0.260$). However, in line with the qPCR results, *CCL20* was significantly higher in decidualized infected compared to non-decidualized infected spheroids ($\log_2\text{FC} = 3.39$, $p_{\text{adj}} = 0.036$). According to RNA-seq, *CD38* was significantly upregulated in decidualized infected compared to non-decidualized infected spheroids ($\log_2\text{FC} = 4.03$, $p_{\text{adj}} = 0.014$), similar to the qPCR results. Likewise, no significant change was found between non-infected and infected non-decidualized spheroids ($p_{\text{adj}} = 0.196$). For *LCN2*, infection in non-decidualized spheroids resulted in a downregulation, which did not meet the \log_2 fold change cut-off ($\log_2\text{FC} = -1.45$, $p_{\text{adj}} = 0.019$). As in the qPCR, RNA-seq data showed a significant upregulation of *LCN2* in decidualized infected versus non-decidualized infected spheroids ($\log_2\text{FC} = 3.17$, $p_{\text{adj}} < 0.001$) but no significant difference was found between decidualized and non-decidualized non-infected samples ($p_{\text{adj}} = 0.113$).

In *VTCN1*, a downregulatory effect was observed both through SARS-CoV-2 infection and decidualization. Thus, *VTCN1* was highest in the non-decidualized non-infected and lowest in the decidualized infected group (0.02-fold \pm 0.002, $p < 0.001$). Between the decidualized spheroids, *VTCN1* was decreased by a third (0.66-fold \pm 0.07, $p = 0.001$) through infection.

Similar effects were found in RNA-seq, such as downregulation through decidualization in non-infected ($\log_2\text{FC} = -5.20$, $p_{\text{adj}} < 0.001$) and infected

samples ($\log_2FC = -6.83$, $p_{adj} < 0.001$). The effect of infection led to a decrease of *VTCN1* in decidualized spheroids ($\log_2FC = -6.89$, $p_{adj} < 0.001$), but was not significant in non-decidualized spheroids ($p_{adj} = 0.946$).

An increase in *NR4A3* expression was found in the infected samples. The non-decidualized infected spheroids had 1.86-fold (± 0.10 , $p < 0.001$) and the decidualized infected 3.57-fold (± 0.75 , $p = 0.009$) higher *NR4A3* levels than the non-decidualized non-infected spheroids. These results match the RNA-seq data, in which decidualized infected spheroids expressed significantly more *NR4A3* than decidualized non-infected spheroids ($\log_2FC = 2.38$, $p_{adj} = 0.003$). RNA-seq also identified a significant change of *NR4A3* between decidualized infected and non-decidualized infected spheroids ($\log_2FC = 2.39$, $p_{adj} = 0.004$), which was not found in the qPCR data. The other RNA-seq group comparisons for *NR4A3* were non-significant.

While infection had no significant effect on *LEFTY1* levels, its expression was significantly higher in decidualized samples (8.06-fold ± 1.61 , $p = 0.002$ and 9.39-fold ± 1.83 , $p = 0.002$ in non-infected and infected, respectively). This pattern was also observed in RNA-seq, with an upregulation of *LEFTY1* in decidualized non-infected ($\log_2FC = 4.59$, $p_{adj} < 0.001$) compared to the non-decidualized samples.

In the qPCR, *IL1RL1* was below detection level in non-decidualized samples but detectable in decidualized spheroids (not shown in graphs). This result is consistent with the RNA-seq data, in which decidualized spheroids had significantly upregulated *IL1RL1* compared to non-decidualized in both non-infected ($\log_2FC = 6.16$, $p_{adj} < 0.001$) and infected samples ($\log_2FC = 8.03$, $p_{adj} < 0.001$).

Overall, the qPCR analysis supported the reliability of the RNA-seq results.

4 Discussion

The spread of SARS-CoV-2 resulted in a global pandemic of unprecedented scale. The effect of COVID-19 on pregnancy and, particularly, the question of *in utero* transmission are of utmost importance. During early pregnancy, the endometrium undergoes decidualization to allow embryo implantation. Together with the trophoblast, the decidua forms the placenta and therefore acts as a protective barrier against vertical transmission.

The objective of this thesis was to investigate if SARS-CoV-2 can infect the human endometrium and what effect SARS-CoV-2 infection has on endometrial cells. To this end, endometrial spheroids were established as a novel three-dimensional *in vitro* model and compared to endometrial monolayers as well as organoids. ACE2 and TMPRSS2, necessary for SARS-CoV-2 infection, were found in endometrial cells and their expression changed through decidualization. Our findings suggest that the human endometrium is susceptible to infection by SARS-CoV-2 and that an inflammatory response is elicited. Furthermore, a dysregulation of genes associated with the endometrial immune response was noted and the degree varied between decidualized and non-decidualized endometrial spheroids.

4.1 Endometrial Spheroids

4.1.1 Establishment and Optimization of Endometrial Spheroids

Spheroids are a three-dimensional cell culture model consisting of an aggregation of adherent cells (Lin and Chang, 2008). This process resembles the formation of tissues during embryonic development through self-assembly of cells (Laschke and Menger, 2017). To facilitate the formation of multicellular spheroids, adherent cells need to be prevented from attaching to the surface of the culture ware, for which several methods are available.

In our approach, both agarose-coated well plates and prefabricated ultra-low attachment well plates yielded comparable results. We chose this liquid-overlay technique because of its many advantages, including cost-efficiency,

accessibility of equipment, low shear stress, the possibility of large-scale spheroid production and the ability to sustain long-term spheroid cultures (Costa et al., 2018). However, a common drawback seen in spheroids cultured using the liquid-overlay technique is higher variability in size and shape compared to other methods like hanging-drop or microfabricated wells (Froehlich et al., 2016, Napolitano et al., 2007). As this irregularity in spheroid formation is mainly seen in spheroids cultured on flat surfaces, we optimized our protocol to use enough agarose gel to form a concave foundation in the wells (Costa et al., 2014, Gaskell et al., 2016). Further, we found that the formation of uniform and stable spheroids was improved by using a 96-well plate instead of a 48-well plate. This can be plausibly explained by the smaller well size which in turn leads to higher cell density when the same number of cells is initially seeded. Difficulties with creating uniform and size-controlled spheroids in large wells have also been described by others (Mirab et al., 2019).

In most organs, e.g., the liver or lungs, the specific morphology and physiology is mainly determined by the parenchyma. Hence, research on these organs is focused on epithelial cells only (Glicklis et al., 2004, Han et al., 2021). In contrast, stromal and epithelial cells are both vital for the characteristics of the endometrium (Gellersen and Brosens, 2014). Therefore, we chose to include both cell types in our spheroid model.

An immortalized, benign human endometrial stromal cell line and the Ishikawa cell line, a well-differentiated endometrial adenocarcinoma cell line, were used to represent endometrial stromal and epithelial cells. ISK cells are known to carry estrogen and progesterone receptors and are thus widely used as a model in reproductive biology (Nishida et al., 1985, Nishida, 2002).

An initial attempt to establish a spheroid model with a stromal cell core and epithelial cells on the surface by seeding HESC first and ISK cells the following day resulted in the formation of separate cell clusters. When both cell types were seeded at the same time, a single spheroid was assembled. This might be due to a limited time window for spheroid formation, which could also explain

our observation that already-formed spheroids could be transferred to regular well plates without attaching and losing their spherical shape.

The resulting spheroid is potentially more suitable to mimic the morphology of the endometrium as epithelial cells are not limited to the surface *in vivo*, but penetrate the stromal compartment (Gray et al., 2001). A high degree of cell-cell interaction between both cell types is also beneficial as it is known that mutual exchange between stromal and epithelial cells is crucial for healthy endometrial function (Pierro et al., 2001, Cunha et al., 2004).

To determine the optimal cell number and ratio of HESC to ISK cells, several criteria were considered. For the replication of *in vivo* histology, more stromal cells than epithelial cells were to be used (Kim et al., 2013, Decensi et al., 1996). Our data showed that a very low proportion of ISK cells yielded uneven, fragile and irregularly shaped spheroids. Analogous to large well sizes, small cell numbers resulted in inconsistent spheroid formation with higher variability and lower stability. However, there was an upper limit to the cell number too, since necrosis has been described in large spheroids (Groebe and Mueller-Klieser, 1996). Therefore, we settled on a 2:1 ratio of HESC to ISK and a total number of 9000 cells seeded per spheroid.

Previously described models include endometrial spheroids incorporating cells of bovine origin (Haeger et al., 2015), endometrial adenocarcinoma (epithelial) cells only (Buck et al., 2015), endometrial mesenchymal stem (stromal) cells only (Domnina et al., 2021) and primary cells from endometriotic lesions (Song et al., 2023). To the author's knowledge, the current study describes the first-ever spheroid model of the human endometrium derived from both epithelial and stromal cell lines.

4.1.2 Formation and Growth of Endometrial Spheroids

Spheroid formation relies on the self-assembly of cells without external cues and can be divided into three phases (Lin and Chang, 2008, Enmon et al., 2001): transient and fast aggregation of the initially single cells, followed by an

active strong cell-cell adhesion with compaction of the spheroid and finally a growth phase of the established spheroid. This process was also evident in our endometrial spheroids with single cells immediately after seeding, loose aggregation after six hours, beginning compaction after 1 day and growth of the established spheroid after day 2 (**Figure 4-1**).

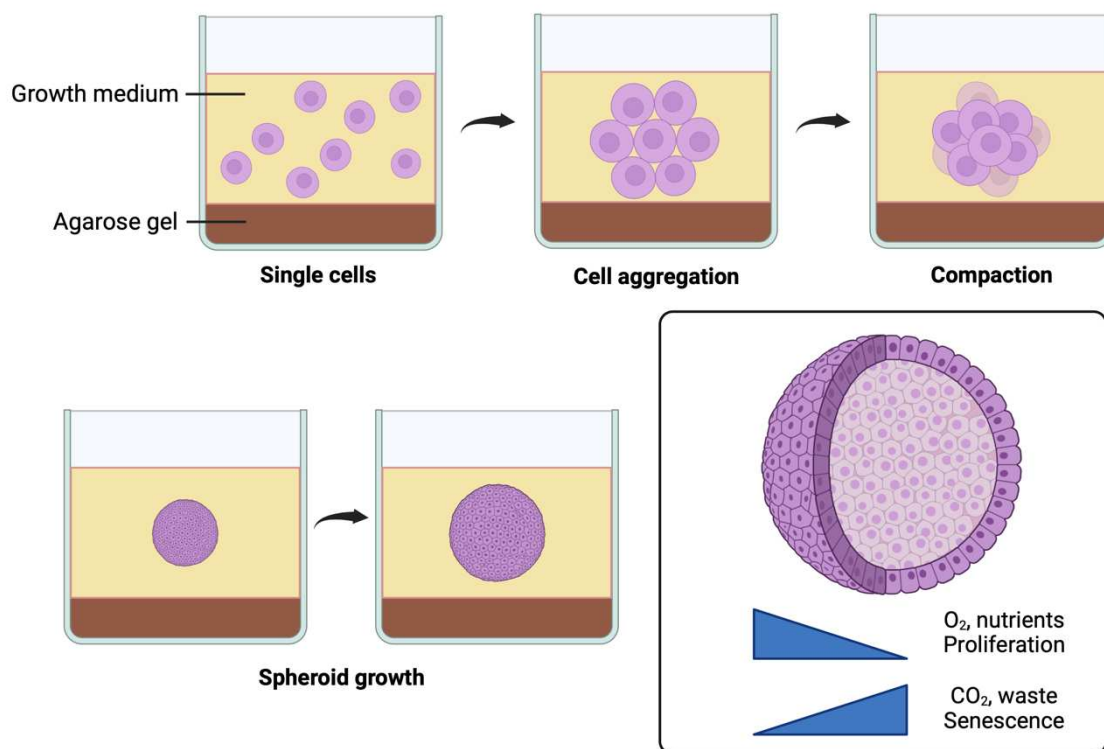


Figure 4-1: Spheroid Formation, Growth and Microenvironment. Medium containing cells in suspension is added to an agarose-coated well. At first, single cells loosely aggregate before compacting into spheroids, which continue to grow after formation. A gradient of oxygen, carbon dioxide, nutrients and waste products as well as varying values of pH and proliferation rates are distributed across the diameter of spheroids (insert). Created with BioRender.com.

This complex process of self-assembly is the result of an interplay of cell-cell and cell-ECM interactions (Lin et al., 2006). Cell adhesion molecules like integrins (e.g., integrin $\beta 1$, integrin $\alpha 5 \beta 1$) and cadherins (e.g., E-cadherin, N-cadherin, cadherin-6) play an important role in the aggregation of cells and compaction of spheroids (Lin et al., 2006, Robinson et al., 2004, Ivascu and Kubbies, 2007, Shimazui et al., 2004). It is noteworthy that diverse molecular

mechanisms are responsible for spheroid formation across different cell types and that some cells only form loose aggregates, unable to compact into spheroids (Ivascu and Kubbies, 2007, Gunay et al., 2020).

To monitor growth, we imaged the endometrial spheroids over 11 days and measured the area. We chose this quantity because two-dimensional images of three-dimensional spheroids did not allow for direct measurement of the volume. Since spheroids are not perfect geometric spheres, each measurement is subject to inherent uncertainties. If the diameter was to be used to represent the whole spheroid, an infinite number of diameters would be required to approximate the mean diameter. The perimeter, on the other hand, is subject to considerable deviations by surface effects, such as involutions and protrusions. Thus, the area was the most stable and most representative quantity for monitoring spheroid growth. We further calculated the diameter, which is an intuitive quantity as it is used widely in cell biology and can be easily compared with the scale bar, as well as the volume, which best describes the three-dimensional nature of the spheroids.

Comparing the growth of one type of spheroid to another can be problematic as variability exists in methods of culture and growth kinetics of each cell type (Costa et al., 2018, Froehlich et al., 2016). In one study using the MCF-7 cell line, derived from human breast adenocarcinoma, and an initial cell number of 8000 cells per well, the spheroid diameter after 6 days was 450-500 μm (Gong et al., 2015), which is slightly smaller than our observed diameter of around 540 μm (initial cell number of 9000 cells). Spheroids cultured from C3A cells, a hepatocarcinoma cell line, reached a diameter of almost 600 μm after 6 days at a starting cell number of only 2500 cells (Gaskell et al., 2016). These astounding differences in the extent of growth suggest that each spheroid model should be viewed as unique.

Nonetheless, certain features are shared by various spheroid models. The growth kinetics that we observed in our endometrial spheroids with a slight decrease in size on day 2, followed by a continuous increase in size, have already been described elsewhere (Gong et al., 2015). This is likely because of

spheroid compaction and increased density, which also results in a darker appearance in phase-contrast microscopy. Mainly cells located in the periphery of a spheroid seem to be responsible for spheroid growth through cell proliferation (Gaskell et al., 2016). The shape of spheroids tends to get more regular and spherical over time, which can also be seen in our spheroid cultures (Zanoni et al., 2020).

4.1.3 Viability of Endometrial Spheroids

Due to the lack of vasculature, the supply of nutrients and oxygen in spheroids depends on diffusion, hence, limiting spheroid size (Lin and Chang, 2008). Multiple studies have shown that a diffusion gradient exists with lower oxygen availability and waste product accumulation towards the spheroid center (Zanoni et al., 2020). With diffusion distance limited to approximately 200 μm for most molecules, it is estimated that a necrotic core is formed when spheroids exceed 400-600 μm in diameter (Groebe and Mueller-Klieser, 1996, Lin and Chang, 2008). This characteristic can be an advantage when modeling avascular tumor growth and drug penetration, but it poses a challenge for basic biological research (**Figure 4-1**).

To investigate the viability of cells within the endometrial spheroids, we stained live cells with calcein-AM and dead cells with ethidium homodimer-1. The two timepoints chosen represent spheroids after stable formation (day 2) and after the maximum period of culture time required for our experiments (day 10). Importantly, we observed no sign of cell death at both timepoints whereas spheroids treated with ethanol or DMSO were mostly not viable. Despite a spheroid diameter of around 700 μm after 10 days of culture, no necrotic core was visible.

These results are similar to what Gong et al. (2015) found in the aforementioned MCF-7 spheroids, which remained fully viable even 12 days after culture. It is noteworthy that spheroid diameter is not the only factor in the development of necrosis and that cell type and culture conditions influence the

depletion of oxygen and nutrients in a culture system (Groebe and Mueller-Klieser, 1996). For instance, the frequency of medium change significantly impacts the viability and growth of spheroids (McMillan et al., 2016). Thus, our selected cell number and culture conditions yielded spheroids, which remained viable over a period of time suitable for our purposes.

4.1.4 Epithelial and Stromal Cell Markers in Endometrial Spheroids

For the visualization of HESC and ISK cell distribution in the endometrial spheroids and to confirm the presence of both cell types, endometrial spheroids were stained for cytokeratin 7 and vimentin. Cytokeratins are water-insoluble proteins, which are located in the cytoplasm of almost all epithelial cells (Sun et al., 1983). Therefore, some members of this protein class are widely used as epithelial cell markers and cytokeratin 7 has been found in benign and malignant endometrial epithelial cells (Zhang et al., 2012, Chu et al., 2000). Vimentin, on the other hand, is an intermediate filament protein found in cells of mesenchymal origin, which includes stromal cells (Osborn, 1983, Ivaska et al., 2007). It can be inferred from our data that stromal and epithelial cells are both present and evenly distributed throughout the whole endometrial spheroid.

The protocol described by Weiswald et al. (2010) was used for immunostaining with minor modifications. Since spheroids are three-dimensional, multicellular structures, penetration of antibodies into the center is impeded and obtaining high-quality images can be challenging. To improve immunostaining outcome, each fixation, permeabilization and antibody staining step was prolonged and additional dehydration/rehydration steps were included (Weiswald et al., 2010). In total, immunostaining of the spheroids was a 6-day procedure compared to 2 days for 2D cells. Thus, immunostaining of spheroids is a much more labor- and time-intensive task.

4.2 Endometrial Organoids

4.2.1 Culture and Growth of Endometrial Organoids

Organoids are a 3D cell culture model derived from stem cells, which differentiate and self-organize into structures characteristic of the respective organ (Lancaster and Knoblich, 2014). For our experiments, we used endometrial epithelial organoid lines, which were kindly provided by Dr. André Koch (Research Centre for Women's Health, Tübingen University Hospital) and derived from healthy endometrial biopsies.

Single cells embedded in BME were visible on day 0, which then proliferated and formed cystic, gland-like structures over the following days. The separate organoids continued to grow and neighboring ones merged into even larger organoids while still maintaining a single lumen. This growth pattern closely mimics the *in vivo* development of endometrial glands and has been described in other endometrial organoid cultures too (Turco et al., 2017, Boretto et al., 2017, Brucker et al., 2022).

Some notable differences between the endometrial organoids and the newly established endometrial spheroids ought to be pointed out. Whereas the spheroids are assembled from fully differentiated, commercially available cell lines, organoids are developed from primary stem cells. Therefore, the formation of spheroids relies on aggregation of cells followed by growth through proliferation whereas organoids are established from stem cells, which are prompted to differentiate and proliferate by growth factors (Lin and Chang, 2008, Clevers, 2016).

The endometrial spheroids are comprised of stromal and epithelial cells, while most organoids, including the endometrial organoids utilized in this study, only contain epithelial cells (Wörsdörfer et al., 2020). To include mesoderm-derived stromal cells in a culture optimized to support the growth of epithelial cells, which are of endoderm or ectoderm origin, is challenging because of differing requirements regarding culture conditions (Wörsdörfer et al., 2020). Notwithstanding, several applications of co-cultures with organoids and stromal cells have been described, which proved to be beneficial for the viability and

maturation of the organoids (Koledova, 2017, Richards et al., 2019, Asai et al., 2017, Leeman et al., 2019).

4.2.2 Basal Out and Apical Out Polarity of Endometrial Organoids

Many organoids are traditionally embedded in BME and in basal out formation, meaning that the basolateral side of the cells faces toward the outside whereas the apical side faces the lumen of the organoids (Co et al., 2019). This is also true for endometrial organoids, as was shown by the staining of perlecan, a basement membrane specific protein (Brucker et al., 2022). This circumstance complicates studying interactions of pathogens with proteins located at the apical cell surface, including ACE2 (Rouaud et al., 2022).

Co et al. (2019) have shown that intestinal organoids, which were originally cultured in BME and of basal out polarity, could be transformed into apical out formation by removal of ECM proteins and transfer to suspension culture. However, when we followed their protocol of dissolving the BME with an EDTA solution, only a few organoids could be collected. Therefore, we switched to a commercially available organoid harvesting solution.

Organoids embedded in BME have a large, clear central lumen and a smooth outer and inner border. After culturing in suspension for 3 days, most organoids were transformed into apical out polarity with smaller size, higher density and a small, dark lumen. Staining of whole organoids and sections for ZO-1, associated with tight junctions, and β -catenin, associated with adherens junctions, showed a tendency for ZO-1 to be located on the outside whereas more β -catenin was found on the inside of apical out organoids. This distribution pattern was not observed in the basal out organoids. Similar changes in morphology have also been described in intestinal and lung organoids, which have been used for infection experiments with various bacteria and viruses, including SARS-CoV-2 (Co et al., 2019, Li et al., 2020c, Salahudeen et al., 2020). However, the differences that we observed were not as apparent as expected.

4.3 Decidualization and the Effect on ACE2 and TMPRSS2 in the Endometrium

4.3.1 Markers of Decidualization

Decidualization in the human endometrium occurs in the second half of the menstrual cycle, during the secretory phase and approximately 6 days after ovulation (Gellersen and Brosens, 2014). Strictly speaking, it only encompasses the stromal compartment as it is characterized by mesenchymal-epithelial transformation of stromal cells (Gellersen et al., 2007, Ng et al., 2020, Okada et al., 2018). This process is crucial for a successful pregnancy as it prepares the endometrium for implantation of the embryo and the subsequent formation of the maternal part of the placenta by the decidua (Gellersen and Brosens, 2014, Vento-Tormo et al., 2018).

As previously described, cotreatment with 8-bromo-cAMP and medroxyprogesterone 17-acetate (MPA) induces decidualization in endometrial stromal cells (Dunn et al., 2003, Brosens et al., 1999). In our experiment, we found that treatment of HESC led to an increase in RNA levels of prolactin, IGFBP-1 and 11 β -HSD1. In ISK cells, however, no significant increase in *IGFBP1* and *HSD11B1* was observed and surprisingly, *PRL* was decreased in ISK after decidualization treatment.

The endometrial spheroids, in which decidualization was induced, showed a significant increase in *IGFBP1* and *HSD11B1*, while *PRL* remained unchanged. In comparison to the effect in monolayer HESC, the fold change of *IGFBP1* and *HSD11B1* was much lower (1.7- and 3.0-fold in spheroids compared to 6.6×10^4 - and 5.4×10^2 -fold in HESC) and *PRL* was also significantly changed in HESC. Since the endometrial spheroids contain ISK cells, in which none of the decidualization markers were significantly upregulated after treatment, it was expected that the observed effect would be less than in HESC alone. Although ISK cells only make up a third of the cells in the spheroids, their proliferation rate and RNA content tend to be higher than those of HESC. Specifically, the RNA concentration of ISK cells was almost five times higher

despite being diluted in nearly twice the volume (50 μ l compared to 30 μ l for HESC).

Furthermore, culturing HESC and ISK together enables both cell types to interact with each other, which might also affect the response to decidualization treatment. Several studies have described that estrogen stimulates the proliferation of endometrial epithelial cells *in vivo*, but when cultured separately *in vitro*, response is poor (Inaba et al., 1988, Uchima et al., 1991, Pierro et al., 2001). However, culturing endometrial epithelial and stromal cells together restores *in vivo* characteristics, such as estrogen responsiveness of epithelial cells (Cooke et al., 1986, Inaba et al., 1988). Likewise, the antiproliferative effect of progesterone on the endometrial epithelium is mediated through crosstalk between epithelial and stromal cells (Kurita et al., 1998, Li et al., 2011b). Epithelial-stromal interactions also play a role in decidualization as paracrine signals from epithelial cells enhance stromal decidualization (Kim et al., 2006, Pawar et al., 2015). While endometrial spheroids are a valuable model for studying these crucial interactions, some HESC reactions might be concealed by the ISK cells.

It is well-known that decidualized stromal cells produce prolactin and that the amount of prolactin produced indicates the extent of decidual differentiation (Daly et al., 1983, Maslar and Riddick, 1979). Notably, expression of prolactin receptors in the endometrium varies throughout the menstrual cycle and the receptors are mainly present during the mid- and late-secretory phase as well as during early pregnancy (Jones et al., 1998). This temporal expression pattern coincides with prolactin production of endometrial stromal cells.

The role of prolactin for reproduction has not been conclusively explained yet, but a regulatory role in controlling trophoblast invasion, angiogenesis and immune defense has been suggested (Jabbour and Critchley, 2001). A study from Berkhout et al. (2020) showed that repeated implantation failure is associated with premature expression of prolactin in the endometrium. Prolactin receptors have also been found in epithelial glands, albeit to a lesser extent than in stromal cells (Jones et al., 1998, Tseng and Zhu, 1998). There is little

data available on the effect of prolactin on endometrial epithelial cells but it is known that low levels of prolactin promote the growth of endometrial epithelial cells whereas high levels have an inhibitory effect (Negami and Tominaga, 1991).

Insulin-like growth factor binding-protein 1 is another known marker for decidualization in endometrial stromal cells and our finding is consistent with evidence found in literature (Dunn et al., 2003). IGFBP-1 is vital in regulating proliferation and differentiation in the endometrium through inhibiting the function of insulin-like growth factor 1 and 2 (Rutanen, 1998). Although the exact mechanism is not known, IGFBP-1 is proposed to restrain trophoblast invasion (Giudice, 1997). In placentas of patients with preeclampsia, a condition associated with shallow implantation, IGFBP-1 expression is elevated (Li et al., 2022).

Two types of 11β -hydroxysteroid dehydrogenases exist and the expression of 11β -HSD1 is known to be induced by decidualization (Kuroda et al., 2013), which is supported by our results. During early pregnancy, 11β -HSD1 is predominantly found on the maternal side of the placenta, including decidual cells, whereas 11β -HSD2 is more abundant in the syncytium and decidual epithelium (Yang et al., 2016, Funghi et al., 2016). As regulator of glucocorticoid levels at the maternal-fetal interface, 11β -HSD is relevant in the pathogenesis of gestational diabetes, preeclampsia, intrauterine growth restriction and preterm birth (Konstantakou et al., 2017).

The availability of data regarding the effects of decidualization treatment on endometrial epithelial cells is limited, likely due to the predominant role of stromal cells in the decidualization process. However, in other mammals, such as rats, the epithelial cells might be the initiators of decidualization after attachment of the blastocyst (Leroy and Lejeune, 1981). Since our aim was to establish endometrial spheroids consisting of both endometrial stromal and epithelial cells, we chose to include ISK cells in our decidualization experiments. Thus, we did not expect a significant increase in decidualization markers in ISK cells after treatment, which is consistent with our findings on IGFBP-1 and

11 β -HSD1 RNA levels. The cause for the decrease of prolactin in ISK cells upon treatment with 8-bromo-cAMP and MPA can only be speculated. Braverman et al. (1984) described secretion of prolactin from decidual cells isolated during the second trimester, whereas prolactin release was undetectable in the epithelial cells. Several studies described an inhibitory effect of progesterone on endometrial epithelial cell proliferation (Kim et al., 2013, Pan et al., 2017, Yuan et al., 2019). Hence, progesterone is applied in the prevention and treatment of endometrial cancer (Derbyshire et al., 2021, Westin et al., 2021). Further, the inhibitory effect of progesterone on the growth of endometrial epithelial cells and the shift toward differentiation might support uterine receptivity (Yang et al., 2011, Gebril et al., 2020). This is in accordance with progesterone supplementation during early pregnancy to prevent miscarriage (Wu et al., 2021) and preterm birth (Norwitz and Caughey, 2011) as well as after *in vitro* fertilization (Proctor et al., 2006). The underlying mechanisms are not fully understood yet but improved endometrial blood flow (Ghosh et al., 2014), inhibition of the oxytocin receptor (Grazzini et al., 1998) and luteal phase support (Bulletti et al., 2022) have been proposed.

4.3.2 Effect of Decidualization on ACE2 and TMPRSS2 Levels

SARS-CoV-2 infection of host cells is dependent on key entry factors: the angiotensin-converting enzyme 2 (ACE2) as the receptor and the transmembrane protease serine 2 (TMPRSS2) for priming of the spike protein (Hoffmann et al., 2020). To verify the presence of ACE2 and TMPRSS2 in the endometrium and to study the effect of decidualization treatment on these very proteins, western blots were performed.

Our data shows that ACE2 and TMPRSS2 are present in endometrial cells. In monolayers, decidualization treatment results in increased levels of ACE2 protein in both stromal and epithelial cells, while TMPRSS2 levels remained unchanged. Similarly, a study by Chadchan et al. (2021) reported an increase in ACE2 RNA and protein levels in HESC after *in vitro* decidualization. They also showed an ACE2 increase in stromal cells in endometrial biopsies obtained in

the secretory phase compared to the proliferative phase. In contrast to our results, Chadchan et al. did not find a significant change in ACE2 expression in endometrial epithelial cells throughout the menstrual cycle. Notably, we found only a 1.3-fold increase in ACE2 protein levels in the ISK cells compared to 177.0-fold in the HESC.

Surprisingly, only faint bands were observed for ACE2 in control and decidualized spheroids while clearly detectable amounts of TMPRSS2 and GAPDH were found. Similar to the 2D endometrial cells, TMPRSS2 levels were not significantly changed through decidualization treatment in the endometrial spheroids. The low level of ACE2 in the spheroids is striking as ACE2 was present in ISK with and without decidualization treatment as well as in decidualized HESC. However, immunostaining was positive for ACE2 in all spheroids. One potential reason for this result is the localization of ACE2 on cells. ACE2 is mainly found on the cell surface with only little intracellular presence (Hamming et al., 2007). Importantly, ACE2 is expressed predominantly on the apical surface of cells, which has been described in the kidney, lung and several epithelial cells (Warner et al., 2005, Ren et al., 2006, Jia et al., 2006, Rouaud et al., 2022). Unlike in conventional monolayer cell culture, cell polarity comparable to *in vivo* tissues is retained in spheroids (de Dios-Figueroa et al., 2021, de Melo et al., 2021).

The surface area for the same number of cells is higher in monolayer compared to spheroid cultures. For each sample of a 2D culture one well of a 6-well plate (growth area of 9.5 cm²) compared to a surface area of 0.17 cm² per spheroid sample (surface area of 12 day 8 spheroids). Assuming that ACE2 is mainly expressed at the surface of the spheroids while GAPDH is present in each cell, this might explain the tremendous difference found in ACE2 protein levels in endometrial spheroids compared to 2D cells.

In three different endometrial organoid lines, western blot revealed no or below detection levels of ACE2, whereas strong bands were visible for TMPRSS2 and GAPDH. This result was found in organoids with and without decidualization treatment. Possibly, these findings might not be generalizable due to the small

sample size and low ACE2 levels could also be explained by the observations in spheroids described above. Notably, low levels of ACE2 do not rule out the possibility of SARS-CoV-2 infection as only small amounts of ACE2 RNA are expressed in the lungs, the main site of infection (Sun et al., 2021). Additionally, the presence of TMPRSS2 enhances the ability for viral entry via the few existing ACE2 receptors (Harrison et al., 2020, Shulla et al., 2011). However, RNA sequencing data also showed no ACE2 expression in the endometrial organoids (personal communication of Dr. A. Koch, 12.01.2022). Thus, endometrial organoids might not be a suitable model for studying SARS-CoV-2 infection.

Our findings are supported by the well-established fact that ACE2 is abundantly expressed in the placenta and most amply so during early pregnancy (Merrill et al., 2002, Levy et al., 2008, Neves et al., 2008, Marques et al., 2011, Bloise et al., 2021). Furthermore, ACE2 gene expression changes throughout the menstrual cycle with an increase in the secretory phase (Henarejos-Castillo et al., 2020, Vaz-Silva et al., 2009), which aligns with our observed increase in ACE2 through decidualization. However, another study did not find significant expression of ACE2 in either stromal or epithelial cells in any phase of the menstrual cycle (Vilella et al., 2021).

ACE2 has a regulatory function in the renin-angiotensin system (RAS) by counteracting vasoconstriction as well as retention of salt and water (Donoghue et al., 2000, Wang et al., 2020b). During early pregnancy, ACE2 also plays a role in implantation, spiral artery remodeling and angiogenesis (Weatherbee et al., 2020, Valdés et al., 2006, Morgan et al., 1998). Notably, drugs for the treatment of hypertension by antagonizing RAS (e.g., angiotensin converting enzyme inhibitors, angiotensin receptor blockers) are contraindicated during pregnancy and associated with teratogenicity and fetopathy (Bullo et al., 2012). Because the physiological function of ACE2 is similar to the effects of these drugs, it is worth noting that the risk of adverse pregnancy outcomes and congenital malformations is not increased when these antihypertensives are taken during the first trimester (Diav-Citrin et al., 2011, Bateman et al., 2017). Decreased blood pressure may lead to placental hypoperfusion, which is

particularly detrimental to fetal growth, primarily in late pregnancy. This explanation would also be consistent with the dynamics of *ACE2* during pregnancy described above.

The mechanism behind the upregulation of *ACE2* during decidualization and pregnancy is yet to be fully elucidated. In pneumocytes, *ACE2* gene expression is upregulated upon stimulation through interferons and the expression of *ACE2* correlated with that of *STAT1* (Ziegler et al., 2020). Additionally, an association between *ACE2* and genes of other JAK-STAT (Janus kinase – signal transducer and activator of transcription proteins) signaling pathway components was found, such as *JAK2*, *STAT2*, *STAT4* and *STAT5A* (Luo et al., 2021). Treatment with a JAK inhibitor diminished the activation of *ACE2* by interferons in kidney cells (Jankowski et al., 2021). Data from Hennighausen and Lee (2020) further support this explanation by showing that *ACE2* is upregulated in the mammary gland during pregnancy and lactation through activation of prolactin and *STAT5*.

The provided evidence from the literature along with the fact that both prolactin and prolactin receptors are present in the endometrium during decidualization might help to understand our finding that *ACE2* is upregulated through decidualization (Jones et al., 1998). Prolactin may promote the expression of its own receptor through an autocrine effect in the endometrium and decidua (Jikihara et al., 1996). Moreover, *STAT5* levels are increased during decidualization in endometrial stromal cells and components of the JAK/STAT pathway are phosphorylated after prolactin stimulation (Mak et al., 2002, Jabbour et al., 1998). We therefore hypothesize that *ACE2* expression in the endometrium is regulated through the JAK/STAT pathway (**Figure 4-2**).

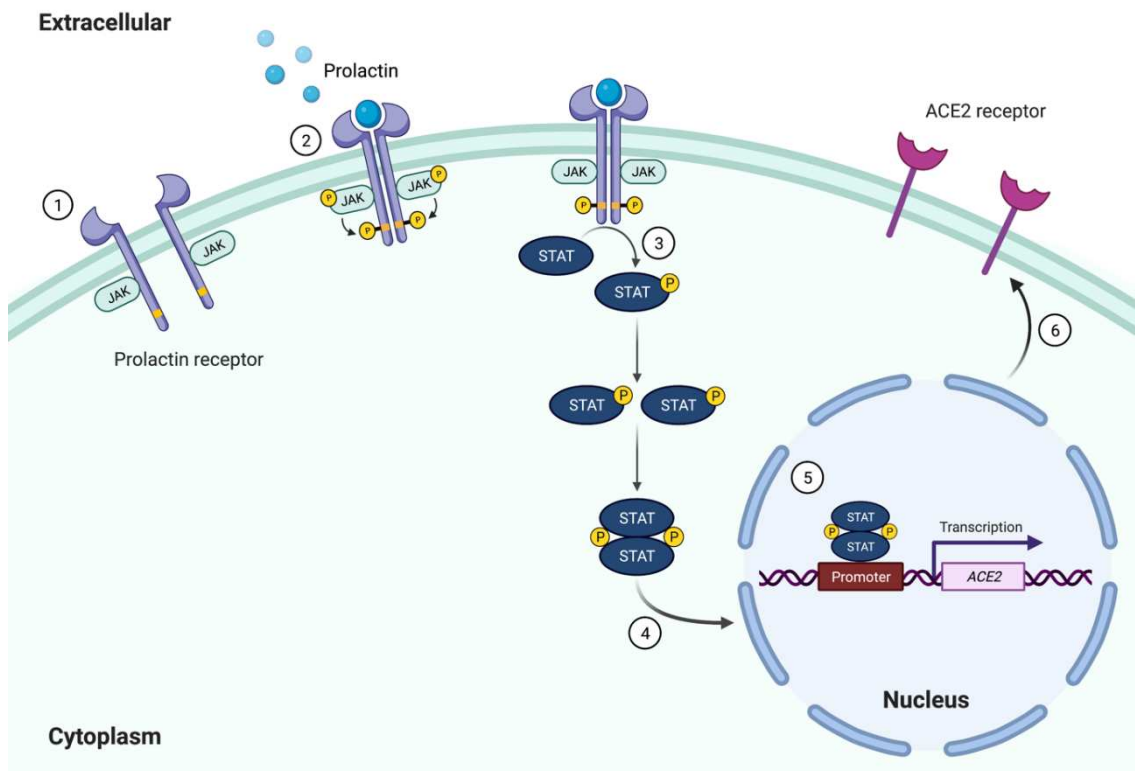


Figure 4-2: Hypothetical Pathway of ACE2 Upregulation during Decidualization. The prolactin receptor is associated with Janus kinases (JAKs) and is inactive (1). During decidualization, prolactin receptors are upregulated and prolactin is secreted by HESCs. After binding of prolactin, the receptor dimerizes and the JAKs phosphorylate tyrosine residues of the receptor (2). STAT proteins bind to the receptor, are phosphorylated and dimerized (3). The phosphorylated STAT dimers translocate into the cell nucleus (4) and induce transcription of the ACE2 gene (5). Thus, ACE2 expression increases (6). Created with BioRender.com.

Notably, transfection of endometrial stromal cells with siRNA targeting ACE2 was shown to result in impaired decidualization (Chadchan et al., 2021). This means that not only is ACE2 upregulated during decidualization, but it is also necessary for the physiological changes in morphology and expression of decidualization markers.

Regarding our findings on TMPRSS2 levels, the same study by Chadchan et al. (2021) showed compatible results, as no significant difference was observed neither in epithelial, nor in stromal cells between the proliferative and secretory endometrium. Stable TMPRSS2 gene expression throughout the menstrual cycle is also supported by Henarejos-Castillo et al. (2020).

4.4 SARS-CoV-2 Infection in the Endometrium

4.4.1 Susceptibility of Endometrial Monolayers and 3D Cultures to SARS-CoV-2

Prior to SARS-CoV-2 infection experiments with endometrial spheroids, a preliminary experiment using HESC and ISK cultured as monolayers was conducted to test for infectibility. Both fluorescence microscopy and western blot showed infection in ISK after treatment with MPA and 8-bromo-cAMP but not in HESC or non-decidualized ISK samples. However, this experiment was only intended as a preliminary assessment of infectibility. Due to the small sample size of $n = 1$, the data must be interpreted with caution. Repetition of the infection experiments involving non-decidualized and decidualized ISK revealed susceptibility to SARS-CoV-2 (unpublished data).

Subsequently, infection of decidualized- and non-decidualized endometrial spheroids was carried out. The first step was to verify the susceptibility of endometrial spheroids to SARS-CoV-2 infection. To this end, immunostaining and western blot were carried out for the detection of SARS-CoV-2 nucleocapsid protein. Both methods revealed the presence of SARS-CoV-2 nucleocapsid in infected but not in non-infected spheroids. Further, immunostaining was positive for ACE2 in all spheroids. Moreover, non-decidualized and decidualized spheroids were both susceptible to infection, in contrast to the results from 2D cells, and had comparable amounts of SARS-CoV-2 nucleocapsid protein.

Despite the lack of ACE2 expression, we attempted to infect endometrial organoids with SARS-CoV-2. Basal out and apical out organoids were compared, however, the methods used differed greatly. While the wildtype virus was used at a dilution of 1:100 in the basal out organoids, a 1:10 dilution of the delta variant was used in the apical out organoids. Furthermore, the time points varied with protein extraction 48 h post-infection in basal out and 72 h in apical out organoids. Due to limited time and resources, no further experiments were conducted using the endometrial organoids, resulting in a sample size of $n = 1$.

Hence, the results of the infection experiments with endometrial organoids remain inconclusive.

The main objective of this study was to identify the possibility of SARS-CoV-2 infection in the human endometrium and, thus, to shed light on the risk of vertical transmission. Mother-to-child transmission of pathogens can occur during pregnancy, labor or in the postnatal period (Arora et al., 2017). While it is well established that SARS-CoV-2 can be transmitted via respiratory droplets and close physical contact ante- and postnatal, data on *in utero* transmission remains inconclusive (Meyerowitz et al., 2021).

Several meta-analyses and systematic reviews have been conducted, which report no or few but questionable cases of vertical transmissions (Juan et al., 2020, Diriba et al., 2020, Wei et al., 2021, Di Toro et al., 2021, Barcelos et al., 2021, Musa et al., 2021, Allotey et al., 2022). Positive tests in neonates born to SARS-CoV-2 positive mothers cannot be taken as a sure sign of *in utero* transmission because the possibility of intrapartum or early postnatal infection is not excluded. Furthermore, IgM antibodies against SARS-CoV-2 were identified in newborns born to women with COVID-19 (Zeng et al., 2020, Dong et al., 2020). Due to their large size, IgM antibodies do not cross the placental barrier and their presence might indicate fetal infection *in utero* (Ben-Hur et al., 2005). However, these reports should be considered with caution as IgM testing is error-prone and inflammation can damage the placental barrier (Kimberlin and Stagno, 2020, Ben-Hur et al., 2005). Additionally, SARS-CoV-2 spike and nucleocapsid protein as well as RNA have been detected in placental tissues of women with COVID-19 (Facchetti et al., 2020, Hecht et al., 2020).

Case reports on suspected *in utero* transmission of SARS-CoV-2 exist. Five women tested positive for SARS-CoV-2 gave birth to neonates with symptoms of early-onset COVID-19, of which one died after 4 days, and a reported stillbirth (Allotey et al., 2022). Tests for SARS-CoV-2 were positive in the placenta, cord blood and fetal/neonatal organs at autopsy (Allotey et al., 2022). Notably, the cases mentioned were of women who tested positive during the third trimester of pregnancy or in the postnatal period and only little is known

about the effect of COVID-19 during early pregnancy. Valdespino-Vázquez et al. (2021) reported a miscarriage of a twin pregnancy during the first trimester and found SARS-CoV-2 protein and RNA as well as inflammatory damage in the placenta and fetal organs. Another case report by Shende et al. (2021) on an asymptomatic woman who tested positive at eight weeks of gestation showed that SARS-CoV-2 infection can persist in the placenta despite her throat swab being negative after five weeks. Not only were viral RNA and protein found in the placenta, amniotic fluid and fetal membranes, but the fetus also died of hydrops fetalis (Shende et al., 2021). While these reports shed light on the effects of COVID-19 during the first trimester, a blind window remains. As most pregnancies go unnoticed during very early pregnancy, studying the effects of SARS-CoV-2 on decidualization and implantation is challenging.

We show for the first time in an *in vitro* experiment that SARS-CoV-2 can infect the human endometrium, thus our results support the likelihood of vertical transmission. These findings may be somewhat limited by the lack of embryonic cells in our spheroid model. Further experiments are required to confirm our findings.

Infection by SARS-CoV-2 can lead to pregnancy complications through several mechanisms. By infecting the unborn, the virus can directly evoke early-onset COVID-19 in neonates causing fever and cough, but also more severe symptoms, such as respiratory distress or multi-organ failure, which require treatment in the ICU and are potentially lethal (Cui et al., 2021, Allotey et al., 2020). Furthermore, SARS-CoV-2 cell entry depends on interaction with ACE2 and subsequent endocytosis, which leads to downregulation of ACE2 and its catalytic activity (Ou et al., 2020, Verdecchia et al., 2020). The resulting ACE2 deficiency can dysregulate the maternal renin-angiotensin system and impair decidualization, placentation, uterine vascular remodeling as well as adequate blood flow (Azinheira Nobrega Cruz et al., 2021). Placentas of infected women also showed abnormal perfusion of fetal blood vessels and fetal vascular thrombosis (Pilarska et al., 2023). This notion is emphasized by the finding of increased disease severity in patients with comorbidities associated with ACE2

depletion, such as hypertension, heart failure and diabetes (Crackower et al., 2002, Patel et al., 2016, Shiota et al., 2010).

From these findings, the issue of how the endometrium or the placenta might be exposed to SARS-CoV-2 emerges. There are two conceivable ways: via the vagina and the cavum uteri (ascending infection from the apical side) or via the bloodstream (hematogenous infection from the basal side). This thought is reflected in our study of the polarity of the endometrial organoids in preparation for infection experiments.

Ascending infections during pregnancy have mostly been described for bacteria, such as *Chlamydia trachomatis* (Bagheri et al., 2018) and group B *streptococcus* (Brokaw et al., 2021). The herpes simplex virus (HSV) is also known to cause ascending infections, however, mother-to-child transmission is highest during delivery and intrauterine infection of the fetus is rare (Straface et al., 2012). Genital infection, a prerequisite for ascending infection of the mentioned pathogens, has repeatedly not been detected in SARS-CoV-2 (Qiu et al., 2020, Takmaz et al., 2021, Fenizia et al., 2021, Erdem et al., 2023). Similarly, vaginal delivery of SARS-CoV-2 infected women is not associated with a higher risk of intrapartum transmission (Ferrazzi et al., 2020, Rottenstreich et al., 2021). Hence, *in utero* transmission of ascending SARS-CoV-2 infection seems unlikely.

Most transplacental viral infections occur through the blood, including cytomegalovirus (CMV) (Périllaud-Dubois et al., 2021), hepatitis B and C (Wen et al., 2013, Pan et al., 2022), human immunodeficiency virus (HIV) (le Roux et al., 2019) and Zika virus (Pomar et al., 2021). These infections cause viremia, meaning viral presence in the blood, that can lead to the spread of the virus from the original site of infection to other organs. Several studies have described low rates of SARS-CoV-2 viremia and its association with disease severity and death (Li et al., 2021, Jacobs et al., 2022, Hagman et al., 2022). During pregnancy, SARS-CoV-2 viremia is linked to vertical transmission, placentitis and stillbirth (Vivanti et al., 2020, Mithal et al., 2022). It is therefore feasible, that transient viremia may lead to *in utero* infection of the fetus.

4.4.2 Cytokines in Endometrial Spheroids Infected with SARS-CoV-2

The “cytokine storm” plays a pivotal role in the pathophysiology of COVID-19 (Ragab et al., 2020). It is characterized by an excessive release of proinflammatory cytokines, which subsequently leads to organ damage (Chousterman et al., 2017). Therefore, we were interested in the pattern of cytokine secretion from endometrial spheroids with and without infection. Of the 13 assayed cytokines, MCP-1 and IL-8 were above detection level.

Levels of monocyte chemoattractant protein 1 (MCP-1) were significantly increased in all infected spheroid samples. MCP-1 is a proinflammatory chemotactic cytokine and promotes recruitment as well as infiltration of macrophages from bloodstream into tissue (Singh et al., 2021). MCP-1 was among the cytokines found to be elevated in plasma from COVID-19 patients with ICU admission compared to non-ICU patients (Huang et al., 2020). High levels of MCP-1 were also detected in bronchoalveolar lavage fluid and peripheral blood mononuclear cells of COVID-19 patients, which is consistent with the accumulation of macrophages found in lung autopsies (Xiong et al., 2020, Yao et al., 2021). Notably, MCP-1 not only attracts macrophages but also other inflammatory cells, such as T cells and NK cells (Carr et al., 1994, Allavena et al., 1994). MCP-1 is crucial in the defense against viral infections including influenza, EBV and HIV (Julkunen et al., 2000, Gaudreault et al., 2007, Eugenin et al., 2003). When MCP-1 was blocked and macrophage recruitment was impeded, alveolar damage caused by influenza was further aggravated, which highlights the protective function of MCP-1 (Narasaraju et al., 2010).

In addition to infections, MCP-1 is also involved in oxidative stress, insulin resistance, multiple sclerosis, tumor angiogenesis, rheumatoid arthritis and many other diseases (Deshmane et al., 2009, Singh et al., 2021). In the human endometrium, MCP-1 is found in endometrial epithelial, endothelial as well as decidual cells whereas its receptor CCR2 is present in the blastocyst (Caballero-Campo et al., 2002, Dimitriadis et al., 2005). Expression of endometrial MCP-1 fluctuates throughout the menstrual cycle with high premenstrual levels and low periovulatory levels, which is reflected in the

number of endometrial macrophages (Arici et al., 1999). These cyclic changes might be regulated by sex hormones, which is supported by the observation that estrogen inhibits MCP-1 expression in endometrial stromal cells (Arici et al., 1999). During early pregnancy, MCP-1 is highly expressed in the decidua and might play a role in regulating the immune system at the maternal-fetal interface by suppressing the cytotoxicity of NK cells (He et al., 2007, Xu et al., 2012). However, elevated levels of MCP-1 in the amniotic fluid and cervix are also associated with preterm birth with or without infection as well as with pregnancy loss (Esplin et al., 2005, Törnblom et al., 2005, Chaiworapongsa et al., 2002). These findings indicate that while critical for immune defense and balance during pregnancy, dysregulation of MCP-1 might have deleterious effects.

Another detected cytokine in our experiment, interleukin 8 (IL-8), was elevated in decidualized samples, particularly 48 h post-infection (day 7 of decidualization treatment). IL-8 is a cytokine that stimulates chemotaxis and phagocytosis mainly in neutrophils but also in macrophages (Teijeira et al., 2021, Beste et al., 2015). IL-8 is involved in mechanisms of both acute and chronic inflammation (Harada et al., 1994, Kienhorst et al., 2015). Hence, treatment with anti-IL-8 antibodies or IL-8 receptor blockers might be beneficial in ischemia, rheumatoid arthritis and breast cancer, among others (Villa et al., 2007, Morita et al., 2019, Alraouji and Aboussekhra, 2021). Concerning COVID-19, IL-8 is among the cytokines found to be elevated in patient plasma (Huang et al., 2020).

During pregnancy, IL-8 is present in fetal and maternal tissues (Saito et al., 1994). Throughout the menstrual cycle, IL-8 is increased in the mid- and late secretory phase compared to low levels during the proliferative and early secretory phase (Wolff et al., 2000). This is in accordance with the increase in IL-8 that we observed in the supernatant of decidualized endometrial spheroids, especially in the 48 h samples. The finding that progesterone upregulates immunoreactive levels of IL-8 in endometrial epithelial cells further supports this notion (Caballero-Campo et al., 2002). However, the number of leukocytes in the endometrium, which may be attracted by IL-8, is highest around the time of

menstruation after a drop in progesterone levels (Salamonsen and Lathbury, 2000).

Other cytokines frequently increased during SARS-CoV-2 infection, such as IL-6 or TNF, were measured in the endometrial spheroids but below detection level (Wang et al., 2020a). This discrepancy might exist because the overproduction of cytokines seen in COVID-19 originates mostly from immune cells (Song et al., 2020). Nonetheless, our results indicate a local inflammatory process in the endometrium during SARS-CoV-2 infection.

This finding is of utmost importance because not only the pathogen itself but also the inflammatory response it elicits can have harmful effects on the developing fetus (Adams Waldorf and McAdams, 2013). Intrauterine inflammation and elevated levels of proinflammatory cytokines can lead to preterm birth, fetal organ damage and spontaneous abortion (Esplin et al., 2005, Törnblom et al., 2005, Chaiworapongsa et al., 2002, Adams Waldorf and McAdams, 2013, Yockey and Iwasaki, 2018). Commonly described pathological placental abnormalities include the triad of histiocytic intervillitis, perivillous fibrin deposition and trophoblast necrosis, defined as “SARS-CoV-2 placentitis” by Watkins et al. (2021). Notably, only aspects of local inflammation were discussed and deleterious effects of systemic inflammation during pregnancy should also be taken into consideration (Calleja-Agius et al., 2011, Germain et al., 2007).

4.4.3 Changes in Gene Expression in Endometrial Spheroids Infected with SARS-CoV-2

To analyze the effect of SARS-CoV-2 infection and decidualization on the endometrial spheroids, we conducted RNA sequencing and identified differentially expressed genes, which were used for principal component analysis (PCA) and gene ontology (GO) enrichment analysis.

The effect of infection on gene expression can be observed by pairwise comparison of non-infected and infected spheroids whereas differential

expression between non-decidualized and decidualized spheroids indicates the effect of decidualization. As illustrated by the PCA, the four experimental groups form three distinct clusters. While non-decidualized non-infected and infected spheroids are grouped together, they are clearly separated from the decidualized non-infected as well as the decidualized infected spheroids. This pattern is also visualized in the heat map with dendrograms and explains, why the comparison between non-decidualized infected and non-decidualized non-infected samples yielded the lowest number of DEGs. These findings suggest that decidualization has a significant impact on the transcriptome and that SARS-CoV-2 significantly alters the gene expression signature, particularly in decidualized endometrial spheroids.

GO enrichment analysis and pathway annotation were employed to identify the molecular pathways and biological processes associated with decidualization and SARS-CoV-2 infection in the endometrium. Mainly, DEGs were found to be enriched in immune response, embryonic development and hematovascular function as well as cellular structure and carbohydrate metabolism.

Surprisingly, we observed enrichment for genes related to the immune system in both upregulated and downregulated DEGs caused by infection and/or decidualization. One possible interpretation of this seemingly contradictory finding is the complexity of the endometrial immune system, which is tightly regulated by numerous autocrine and paracrine factors. The DEGs were associated with the innate (e.g., inflammatory response, neutrophil activation) and adaptive (e.g., humoral immunity) immune system or both (e.g., leukocyte activation, cytokine production). While SARS-CoV-2 infection resulted in a downregulation of genes associated with immune response in the spheroids regardless of decidualization status, decidualization exhibited a dual effect on these DEGs. During pregnancy, the immune system is modulated to balance tolerance of the semi-allogenic conceptus and defense against pathogens (Thellin and Heinen, 2003). These changes not only occur on a systemic level but also in the endometrial microenvironment. The effect of SARS-CoV-2 infection and decidualization on the expression of individual genes associated with the immune system are discussed in detail below.

Further, an upregulation of DEGs associated with TGF- β signaling was found after decidualization in non-infected spheroids but not in infected spheroids. A study by Kim et al. (2006) illustrated the role of the transforming growth factor β in decidualization. Progesterone was shown to increase TGF- β 1 in endometrial epithelial cells, which in turn induced decidualization in endometrial stromal cells. Moreover, members of the TGF- β superfamily were identified in secretory phase endometrial cells and their inhibition resulted in impaired decidualization (Stoikos et al., 2008). In COVID-19, induction of TGF- β leads to chronic immune reaction and vascular leak (Ferreira-Gomes et al., 2021, Biering et al., 2022). Thus, dysregulation of TGF- β signaling by SARS-CoV-2 infection is a potential mechanism for reproductive failure.

Similarly, the TNF signaling pathway was downregulated in decidualized non-infected but not in decidualized infected spheroids. The tumor necrosis factor α is an inflammatory cytokine, which is expressed highly in the endometrium during the menstrual phase (Tabibzadeh et al., 1999). Elevated levels of TNF- α are linked to pregnancy complications including preeclampsia, gestational diabetes and recurrent pregnancy loss (Anim-Nyame et al., 2003, Xu et al., 2014, Li et al., 2016). TNF- α is increased in COVID-19 patients and associated with disease severity and mortality (Karki et al., 2021, Del Valle et al., 2020). High levels of TNF- α due to SARS-CoV-2 infection could therefore be harmful during pregnancy.

Enrichment of genes involved in embryonic development was found, including Fan embryonic CTX brain myeloid (Fan et al., 2018) and Descartes fetal cerebrum vascular endothelial cells (Cao et al., 2020), which were both upregulated in non-decidualized infected compared to non-decidualized non-infected spheroids. Further, downregulated DEGs in decidualized infected compared to non-decidualized infected spheroids were associated with skeletal system development. The relevance of the differential expression of genes associated with this category due to infection or decidualization in the endometrium needs to be validated by further studies.

Our analysis revealed enrichment of genes involved in hematovascular function. Negative regulation of vascular permeability and hemopoiesis were associated with upregulated DEGs in decidualized infected compared to non-decidualized infected spheroids. Normal endometrial vascular function is crucial for successful placentation and healthy pregnancy (Staff et al., 2022). Remodeling of uterine spiral arteries occurs during the secretory phase of the menstrual cycle and during early pregnancy (Robson et al., 2012), which supports our finding of differential expression due to decidualization. Our observation of the distinct effect of decidualization on non-infected and infected spheroids indicates a possible dysregulation of this complex process due to SARS-CoV-2 infection. This could explain the elevated risk of preeclampsia, a complication with abnormal placentation and maternal hypertension, in pregnant women infected with SARS-CoV-2 (Conde-Agudelo and Romero, 2022). The underlying pathogenesis might be linked to ACE2 depletion and RAS dysregulation caused by SARS-CoV-2 infection with subsequently impaired placentation, vascular remodeling and fetal perfusion (Azinheira Nobrega Cruz et al., 2021, Pilarska et al., 2023).

Further, decidualization increased the expression of genes associated with hemostasis in both non-infected and infected spheroids. This result is consistent with the increase in hemostatic proteins during decidualization, including tissue factor and plasminogen activator inhibitor type 1 (Christian et al., 2001, Schatz and Lockwood, 1993). The importance of hemostasis during pregnancy is highlighted by Lykke et al. (2010), who observed a higher risk for preterm birth, placental abruption and recurrent bleeding in women with first-trimester vaginal bleeding.

Several other enriched genes were identified in the decidualized spheroids, including those involved in cell morphology and ECM structure, secretion and exocytosis, lipid and carbohydrate metabolism as well as hormone regulation, response to wounding and immune response. Similar changes in transcriptomics during decidualization have been reported elsewhere (Giudice, 2004, Altmäe et al., 2017) and additional genes associated with cell cycle, vasoregulation and complement activation have been described. Hence, our

findings reflect the extensive morphologic, metabolic and endocrine remodeling of the endometrium during decidualization. Notably, the changes in gene expression evoked by decidualization differed between non-infected and infected spheroids. This might indicate a disruption of healthy decidualization by SARS-CoV-2, which could contribute to pregnancy complications, such as implantation failure, preeclampsia and fetal growth restriction (Zhou et al., 2019a, Gellersen et al., 2007). The clinical relevance of these distinct gene expression profiles ought to be validated in future studies.

To verify our RNA-seq results, qPCR was performed. Overall, the qPCR results matched the RNA-seq data and found similar effects of decidualization and/or infection on the tested genes. However, several genes were found to be significantly differentially expressed through qPCR, which were not identified through RNA-seq. This discrepancy could be attributed to a smaller sample size as well as the Benjamini-Hochberg adjustment of the p-value for multiple testing, resulting in a more conservative statistical threshold in RNA-seq.

While GO enrichment analysis and pathway annotation shed light on possible dysregulation of endometrial processes, the following section focuses on individual genes. In three of the tested genes (*CCL20*, *CD38* and *LCN2*) infection led to a downregulation in non-decidualized spheroids but not in the decidualized ones.

Chemokine (C-C motif) ligand 20 (*CCL20*) is a chemokine that stimulates lymphocytes as well as neutrophils to migrate towards the site of inflammation (Zhao et al., 2014, Kwantwi et al., 2021). An interesting feature of *CCL20* is its ability to promote both immunotolerance and inflammation by recruiting immunosuppressive as well as proinflammatory T cells (Comerford et al., 2010). In the context of infection, *CCL20* has direct antimicrobial and antiviral activity (Yang et al., 2003, Ghosh et al., 2009). Furthermore, *CCL20* also plays an important role in the immune system and lack of *CCL20* receptor *CCR6* results in an impaired humoral immune response against rotavirus infection (Cook et al., 2000). If *CCL20* is downregulated during infection with *Cryptosporidium parvum*, clearance of the parasite is impeded (Guesdon et al., 2015). In contrast

to our results, others reported high levels of CCL20 in the lungs during SARS-CoV-2 infection (Saris et al., 2021, Maxwell et al., 2021).

Regarding CCL20 in the endometrium, Park et al. (2019) described an upregulation in the porcine endometrium during early pregnancy, especially in glandular and luminal epithelial cells. In the ovary, a periovulatory induction of CCL20 is found, which correlates with progesterone production (Al-Alem et al., 2015). However, other studies suggest a lack of or even an inhibitory effect of progesterone on CCL20 in endometrial epithelial cells (Haddad and Wira, 2014, Mita et al., 2017). No data was found on the effect of decidualization or progesterone on CCL20 expression in stromal cells.

The second gene, which displayed a similar dynamic, encodes Cluster of Differentiation 38 (CD38), a transmembrane protein involved in the differentiation, activation and proliferation of T cells (Kar et al., 2020). In addition, it functions as an enzyme participating in the regulation of intracellular calcium levels and, thus, plays a vital role in various cell functions (De Flora et al., 2004). In infections, CD38 is a key component of innate and adaptive immune responses (Glaría and Valledor, 2020). Upregulation of CD38 is seen in bacterial and viral infections and leads to the activation of macrophages and dendritic cells (Matalonga et al., 2017, Schiavoni et al., 2018). Through calcium signaling, CD38 promotes the elimination of pathogens through phagocytosis (Kang et al., 2012). In CD38-deficient mice, higher susceptibility to bacterial infections was observed, which is consistent with the finding that respiratory infections are the most frequent adverse effect under treatment with daratumumab, an antibody targeting CD38 (Partida-Sánchez et al., 2001, Mateos et al., 2020). Strikingly, patients undergoing anti-CD38 immunotherapy had a higher risk of SARS-CoV-2 infection after vaccination due to impaired immune response (Henriquez et al., 2022).

Only little information is available on the role of CD38 in the endometrium. The number of CD38-positive granulated lymphocytes is increased in the late-secretory phase endometrium (Bulmer et al., 1991). During pregnancy, progesterone activates the immune system and levels of CD38 are increased

(Shah et al., 2018). No data on the association between CD38 and endometrial stromal or epithelial cells was found.

LCN2, which encodes for lipocalin 2 (*LCN2*), was also downregulated in the non-decidualized spheroids infected with SARS-CoV-2. *LCN2* is a glycoprotein and part of the innate immune system (Abella et al., 2015). Through sequestration of iron, *LCN2* inhibits iron-dependent growth of bacteria, thus, functioning as a bacteriostatic agent during acute bacteremia (Flo et al., 2004). Furthermore, *LCN2* has a regulatory role in cellular immunity by increasing the expression of tolerogenic HLA-G on T helper cells and by stimulating the expansion of T regulatory cells (La Manna et al., 2014). Proinflammatory cytokines IL-17 and TNF- α induce *LCN2* expression and *LCN2* deficiency is associated with lower inflammation, which makes it a potential therapeutic target in autoimmune diseases (Karlsen et al., 2010, Nam et al., 2014).

Unlike *CCL20* and *CD38*, *LCN2* was significantly upregulated in decidualized samples regardless of infection. This result is consistent with an increase in *LCN2* expression during early pregnancy (Haneda et al., 2017, Hayes et al., 2018). *LCN2* in the uterine fluid is also suggested to be a marker for endometrial receptivity (Kasvandik et al., 2019). Liu et al. (2016) showed that *LCN2* is increased during decidualization, which is controlled by progesterone. Regarding infections of the female reproductive tract, *LCN2* is involved in the inflammatory response induced by bacterial lipopolysaccharides and in *Chlamydia trachomatis* infection (Liu et al., 2016, Wan et al., 2014). Moreover, lower plasma levels of *LCN2* are found in preeclamptic patients compared to healthy pregnancies (Cemgil Arıkan et al., 2011).

We found a downregulation of several genes in the endometrial spheroids upon infection with SARS-CoV-2. *CCL20*, *CD38* and *LCN2* are all involved in inflammation and immune responses against pathogens. Downregulation of these protective factors is a potential way for SARS-CoV-2 to evade the immune system by impeding the innate immune response. Notably, SARS-CoV-2 infection differentially impacts decidualized and non-decidualized endometrial cells. As to why *CCL20*, *CD38* and *LCN2* are not downregulated in infected

spheroids after decidualization treatment, a possible explanation is that progesterone might counteract this effect. During the secretory phase of the menstrual cycle, an accumulation of macrophages, neutrophils and T cells as well as an increase of MCP-1 is found (Russell et al., 2013, Thiruchelvam et al., 2013, Hafner et al., 2013). Progesterone promotes an increase in multiple chemokines, molecules of the innate immune system, pattern recognition receptors and antimicrobial peptides, which play a key role in defense against infection (King and Critchley, 2010, Hafner et al., 2013, Wan et al., 2014). At the same time, progesterone modulates the immune system during pregnancy towards immunotolerance of the fetus by reducing inflammation and cytotoxicity of T cells (Shah et al., 2018).

We detected another gene, which was downregulated upon infection in the endometrial spheroids. *VTCN1* was highest in the control group as both decidualization and infection decreased its expression. The V-set domain-containing T-cell activation inhibitor 1, also known as B7-H4, is a negative regulator of T cell immunity and an immune checkpoint inhibitor (Zhang and Zheng, 2020). Thus, expression of *VTCN1* in numerous cancer types is associated with immune escape and poor prognosis (Janakiram et al., 2017). *VTCN1* modulates immune response to infection and deficiency slightly promotes T cell response and augments neutrophil growth (Suh et al., 2006, Zhu et al., 2009). Our result of *VTCN1* downregulation in SARS-CoV-2 infection is supported by the finding that infection with *Toxoplasma gondii* also has a decreasing effect (Sun et al., 2022). This downregulation might be a protective mechanism to promote a stronger immune response, mainly from the adaptive immune system.

The downregulation of *VTCN1* in the decidualized samples, that we observed, is supported by the finding that *VTCN1* expression is higher during the secretory phase of the menstrual cycle than in the proliferative phase (Qin et al., 2021). Furthermore, high concentrations of progesterone downregulate *VTCN1* expression (Young et al., 2017). During menstruation, which is induced by progesterone withdrawal, *VTCN1* was also described to be upregulated (Paiva et al., 2016). In the course of pregnancy, levels of soluble *VTCN1* change and

are highest during the second trimester (Mach et al., 2022). This implies a dynamic in regulatory T cell function, which is yet to be elucidated.

Among the tested genes, *NR4A3* was upregulated upon SARS-CoV-2 infection. It encodes for a nuclear receptor and functions as an intracellular transcription factor known as NR4A3 or NOR-1 (Martínez-González et al., 2021). Several stimuli are known to induce NR4A3, including mechanical stress, lipopolysaccharides, cytokines and oxidized lipids (Bandoh et al., 1997, Pei et al., 2005). NR4A3 is associated with proinflammatory effects, neutrophil activation and survival, mast cell activation and monocyte-derived dendritic cell differentiation (Ma et al., 2020, Prince et al., 2017, Lundquist et al., 2011, Boulet et al., 2019). However, NR4A3 can also limit inflammation, as described in the cardiovascular system (Bonta et al., 2006, Calvayrac et al., 2015, Jiang et al., 2019). The role of NR4A3 during infection is not well understood and varying results were found, namely, downregulation through *Mycobacterium tuberculosis* and Zika virus infection, but upregulation during *Streptococcus equi* infection (Saini et al., 2018, Alpuche-Lazcano et al., 2021, von Beek et al., 2019). Notably, Phelan et al. (2021) used transcriptional profiling to identify that loss of *NR4A3* shifted the transcriptomic profile towards an increase in interferon and viral response. Thus, upregulation of NR4A3 in SARS-CoV-2 infection might have implications on dampened immune response of the endometrium.

The role of NR4A3 in the endometrium was illustrated by a study from Jiang et al. (2016). They showed that NR4A3, along with other members of the NR4 receptor group, induces prolactin and IGFBP-1 expression in endometrial stromal cells during decidualization by targeting FOXO1A. With this in mind, it is not surprising that infected decidualized endometrial spheroids have a higher increase in NR4A3 than the infected non-decidualized. Interestingly, NR4A3 is also upregulated in decidual cells through IL-1 β , an embryonic factor that promotes implantation and full decidualization (Guzeloglu-Kayisli et al., 2015, Geisert et al., 2012).

In decidualized spheroids, *LEFTY1* was upregulated and infection did not significantly impact its expression. The left-right determination factor 1, also known as LEFTYB, is a member of the TGF- β superfamily and is important for left-right asymmetry determination during embryonic development (Zhang et al., 2020, Meno et al., 1998). In support of our finding, others described LEFTY1 to be upregulated during decidualization and after progesterone treatment (Li et al., 2014, Fei et al., 2017). However, in mice, LEFTY1 is highest during the proestrus phase, when progesterone levels are low, but is also increased during early pregnancy (Tang et al., 2005). Interestingly, low expression of LEFTY1 in placental villous tissue is linked to unexplained abortion, whereas overexpression inhibits decidualization and secretion of prolactin and IGFBP-1 (Xue et al., 2017, Li et al., 2014).

Finally, we observed an upregulation of *IL1RL1*, which encodes for Interleukin 1 receptor-like 1 (also known as ST2) due to decidualization. IL-33, the ligand for IL1RL1, is released after cell or tissue damage and this signaling pathway is involved in immunity, inflammation, allergic reactions, viral infection and cancer (Cayrol and Girard, 2022). Similar to our findings, Granne et al. (2011) described an increase in soluble IL1RL1 in the third trimester of normal pregnancies and placental secretion of the receptor. Importantly, dysregulation of the IL-33/IL1RL1 pathway is associated with recurrent spontaneous abortion (Zhao et al., 2021, Salker et al., 2012), miscarriage (Kaitu'u-Lino et al., 2012) and preeclampsia (Granne et al., 2011).

Taken together, we found that SARS-CoV-2 infection caused downregulation in four genes (*CCL20*, *CD38*, *LCN2* and *VTCN1*) and upregulation in one gene (*NR4A3*) in the endometrial spheroids. Notably, gene expression was altered to varying degrees between non-decidualized and decidualized endometrial spheroids. *LEFTY1* and *IL1RL1* were not significantly affected by infection but increased through decidualization.

Pregnancy requires a well-calibrated balance between immunotolerance of the conceptus and defense against pathogens (Thellin and Heinen, 2003). During the first trimester, the endometrium presents a proinflammatory setting and the

immune system shifts towards innate immune responses (Cornish et al., 2020). The innate immune system is the first line of defense when pathogens invade the body; it comprises anatomical barriers (e.g., skin, mucosa), immune cells (macrophages, dendritic cells, granulocytes and natural killer cells) and the complement system (McComb et al., 2019). By binding of pathogen-associated molecular patterns (PAMPS), immune cells are activated and elicit an inflammatory response as well as activation of the adaptive immune system (McComb et al., 2019). In the context of viral infection, the innate immune system plays a key role in inhibiting viral replication, eliminating the virus and restricting widespread disease (Cornish et al., 2020).

Our results imply a downregulation in several genes associated with the innate immune system after SARS-CoV-2 infection. CCL20 has direct antimicrobial and antiviral activity as well as chemotactic functions in the migration of lymphocytes and neutrophils (Yang et al., 2003, Ghosh et al., 2009, Zhao et al., 2014, Kwantwi et al., 2021). An important role of CD38 is seen in the activation of macrophages and dendritic cells as well as in the elimination of pathogens through phagocytosis (Matalonga et al., 2017, Schiavoni et al., 2018, Kang et al., 2012). LCN2 functions as a bacteriostatic agent during acute bacteremia and promotes inflammation (Flo et al., 2004, Nam et al., 2014). Furthermore, NR4A3 was upregulated, which may lead to reduced effectiveness in viral response (Phelan et al., 2021). Dysregulation in these components could be a novel way for SARS-CoV-2 to evade the innate immune system.

In contrast, VTCN1 expression was lower in infected spheroids, which could promote T cell response and might be a protective mechanism (Zhang and Zheng, 2020). Downregulation of VTCN1 causes heightened activation of the adaptive immune system, which might lead to tissue damage, as seen in autoimmune diseases (e.g., diabetes, nephritis, Sjögren's syndrome) (Kamimura et al., 2009, Wei et al., 2011, Wang et al., 2011, Pawar et al., 2015, Zheng et al., 2020). Thus, VTCN1 can be a double-edged sword and its role in viral immune response should be further explored.

SARS-CoV-2 is known to impair innate immune response by inhibiting early type 1 interferon response, which allows unimpeded viral replication and spread (Brodin, 2021, Arunachalam et al., 2020). To cope with increasing viral load and tissue damage, the immune system subsequently reacts with hyperinflammation, which might lead to the cytokine storm observed in severe COVID-19 (Lowery et al., 2021, Brodin, 2021). This might partially explain better COVID-19 outcomes in female patients, who are known to mount faster and stronger immune responses during infections (Zhou et al., 2020a, Klein and Flanagan, 2016). Toll-like receptor 7, which is encoded on the X-chromosome and known to escape gene silencing, recognizes single-strand viral RNA and triggers a type 1 interferon response (Diebold et al., 2004, Souyris et al., 2018, Khanmohammadi and Rezaei, 2021). Our results shed light on potential mechanisms of impaired innate immune response by SARS-CoV-2 in the human endometrium. Interestingly, this pattern of dysregulation was less pronounced in the decidualized spheroids. While it has been described that therapy targeting CD38 results in a higher risk of SARS-CoV-2 infection despite vaccination (Henriquez et al., 2022), the effects of differential CCL20, LCN2 and NR4A3 expression have not been described yet in the context of COVID-19.

4.5 Conclusion and Outlook

This study aimed to analyze the effect of SARS-CoV-2 infection in the human endometrium. It was shown that endometrial cells express the key entry factors of SARS-CoV-2 ACE2 and TMPRSS2 and that decidualization results in an increase of ACE2. A novel, three-dimensional spheroid model of the human endometrium was established and characterized. In addition, human endometrial organoids were cultured and an apical out assay was conducted. In contrast to endometrial monolayer and spheroid cultures, the organoids did not express ACE2 and infection experiments with SARS-CoV-2 remained inconclusive. SARS-CoV-2 infects both non-decidualized and decidualized endometrial spheroids. Upon infection, an inflammatory response is elicited with a significant increase in MCP-1 levels. The cytokine IL-8 was upregulated in

decidualized spheroids. Further, SARS-CoV-2 infection affects the gene expression to varying degrees between non-decidualized and decidualized endometrial spheroids. Enrichment of DEGs related to the immune system, hematovascular function as well as different aspects of decidualization were observed. Genes associated with the innate immune system (*CCL20*, *CD38*, *LCN2* and *NR4A3*) were dysregulated as a potential mechanism for immune evasion of SARS-CoV-2. An upregulation in *VTCN1*, associated mainly with the adaptive immune system, was found. In summary, SARS-CoV-2 infection can occur in the human endometrium, leading to a plethora of possibly harmful effects on pregnancy (**Figure 4-3**).

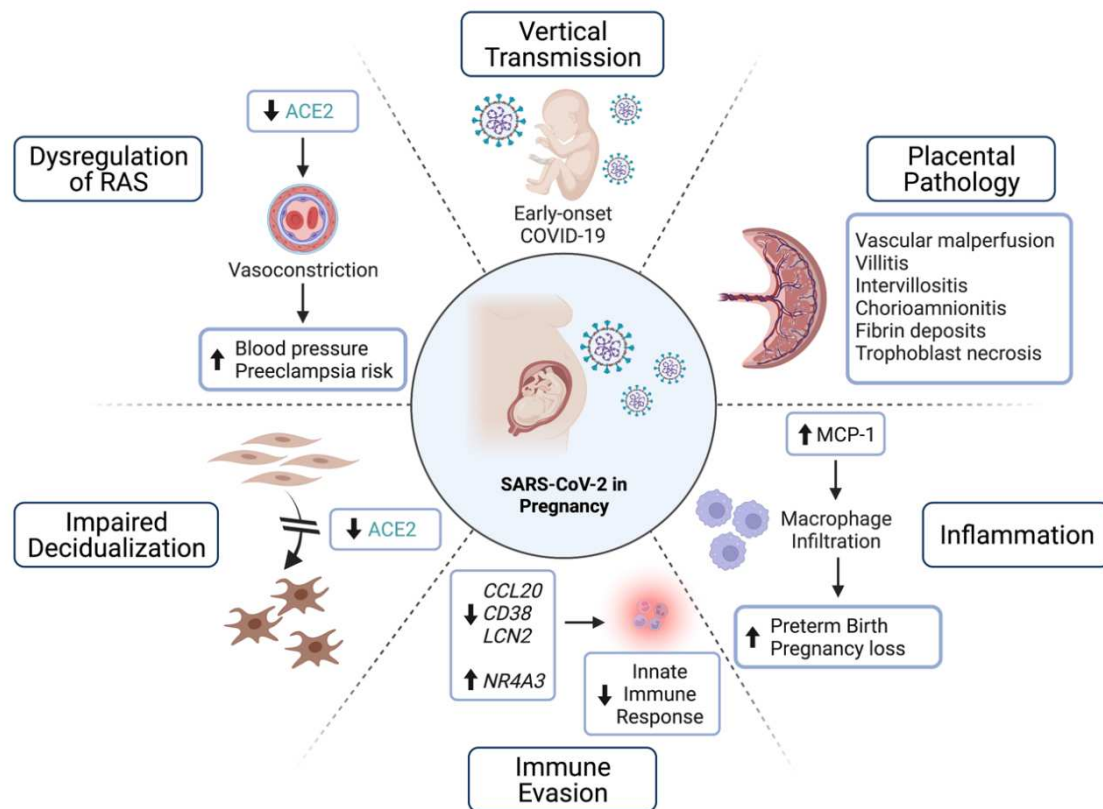


Figure 4-3: Potential Harmful Effects of SARS-CoV-2 Infection during Pregnancy. SARS-CoV-2 can directly infect the unborn, leading to early-onset COVID-19. Infection can also cause downregulation of ACE2, which can result in a dysregulation of maternal RAS as well as impairing decidualization of endometrial stromal cells. Furthermore, COVID-19 has been associated with placental pathology, which may impact the nutrient supply and growth of the fetus. MCP-1 is upregulated in the endometrium after infection, potentially promoting infiltration of macrophages and inflammation, thus, increasing the risk for preterm birth and pregnancy loss. Several genes associated with the innate immune system are dysregulated after SARS-CoV-2 infection, which might be a novel mechanism of immune evasion. Created with BioRender.com.

As we have shown, ACE2 increases during decidualization. Further research is needed to fully understand its role in the endometrium and during pregnancy. A possible regulatory role of the JAK/STAT pathway for ACE2 expression in the endometrium was proposed, which needs to be investigated by future studies. While it is known that knockdown of ACE2 results in deficient decidualization, its exact function remains to be elucidated.

While endometrial stromal cell decidualization has been studied extensively, only little is known about the effect of progesterone and cAMP on endometrial epithelial cells. We found a downregulation of prolactin after treatment, the physiological meaning of which needs to be clarified in further studies. The endometrial spheroid model is a useful tool for exploring the interaction between epithelial and stromal cells in the context of physiology and pathology.

A major limitation of our results is the absence of embryonic tissue in our model. Future advancements of the endometrial spheroids could include coculturing with embryonic cells or spheroids. This would mimic the maternal-fetal interface more closely and allow interactions of higher complexity.

To develop a deeper understanding of the mechanisms of SARS-CoV-2 vertical transmission and to further validate endometrial spheroids as an *in vitro* model, future research could compare our findings with the effect of pathogens known to be vertically transmitted.

Additionally, additional studies are required to examine the clinical relevance of the cytokines and dysregulated genes that we described in the human endometrium infected by SARS-CoV-2. Whilst many reports on COVID-19 during the third trimester exist, more data on its effect during early pregnancy and around the time of conception is required. Further research is urgently needed to provide adequate health care and evidence-based treatments for pregnant women.

5 Abstract

The global outbreak of COVID-19 caused by SARS-CoV-2 has posed unprecedented challenges to public health. SARS-CoV-2 infection during pregnancy has been associated with an elevated risk of preterm birth and miscarriage, while the potential for intrauterine transmission remains uncertain. The primary objectives of this thesis are to confirm the presence of key SARS-CoV-2 entry factors in the endometrium and to investigate the impact of decidualization on their expression. Further, it seeks to establish 3D spheroids as a novel *in vitro* model of the endometrium to determine the susceptibility of endometrial cells to SARS-CoV-2 and to assess the endometrial pathophysiology of SARS-CoV-2 infection on a molecular level.

The liquid-overlay technique was employed to establish 3D endometrial spheroids using human endometrial stromal cells and the Ishikawa cell line. Endometrial organoids, derived from primary stem cells of endometrial biopsies, were cultured and compared to the spheroids. Decidualization was induced with 8-bromo-cAMP and medroxyprogesterone to mimic *in vivo* conditions during pregnancy. The expression of decidualization markers (*PRL*, *IGFBP1* and *HSD11B1*) as well as SARS-CoV-2 entry factors (*ACE2* and *TMPRSS2*) were assessed with qPCR and western blotting. Infection experiments involving a recombinant virus strand expressing mNeonGreen and authentic SARS-CoV-2 were conducted, followed by cytokine assays and RNA sequencing to evaluate the host response to viral invasion.

Our study revealed the presence of *ACE2* and *TMPRSS2* in endometrial cells as well as an increased expression of the former following decidualization. A novel endometrial spheroid model was successfully established. Susceptibility to SARS-CoV-2 infection was demonstrated with ensuing inflammation and dysregulation of genes associated with immune response, hematovascular and cellular functions. Changes in gene expression varied between non-decidualized and decidualized spheroids and genes associated with the innate immune system (*CCL20*, *CD38*, *LCN2* and *NR4A3*) were dysregulated, constituting a potential mechanism for immune evasion of SARS-CoV-2.

These findings offer valuable insights into the possibility of vertical transmission of SARS-CoV-2 during pregnancy, closely aligning with the originally defined objectives. The endometrial spheroids provide a novel platform for studying viral interactions, which require further validation in studies using pathogens with known vertical transmission. Understanding the molecular mechanisms involved holds implications for the development of preventive and therapeutic interventions for pregnant patients with COVID-19.

6 Zusammenfassung

Der globale Ausbruch von COVID-19, verursacht durch SARS-CoV-2, stellt eine beispiellose Herausforderung für die öffentliche Gesundheit dar. Eine Infektion mit SARS-CoV-2 während der Schwangerschaft wurde mit einem erhöhten Risiko für Früh- und Fehlgeburten in Verbindung gebracht, während die Möglichkeit einer intrauterinen Übertragung noch ungeklärt ist. Die Ziele dieser Arbeit sind die Bestätigung des Vorkommens der Eintrittsfaktoren für SARS-CoV-2 im Endometrium und die Untersuchung des Einflusses der Dezidualisierung auf deren Expression. Zudem soll ein neuartiges *in vitro*-Modell des Endometriums in Form von 3D-Sphäroiden etabliert werden, um die Anfälligkeit von Endometriumzellen für SARS-CoV-2 zu bestimmen und die pathophysiologischen Auswirkungen einer endometrialen SARS-CoV-2-Infektion auf molekularer Ebene zu evaluieren.

Die Liquid-Overlay-Technik wurde verwendet, um 3D-Sphäroide des Endometriums aus humanen endometrialen Stromazellen und der Ishikawa-Zelllinie zu generieren. Endometriale Organoide, aus primären Stammzellen von Endometriumbiopsien, wurden kultiviert und mit den Sphäroiden verglichen. Die Dezidualisierung wurde mittels 8-Bromo-cAMP und Medroxyprogesteron induziert, um die *in vivo*-Bedingungen während der Schwangerschaft zu simulieren. Die Expression von Dezidualisierungsmarkern (*PRL*, *IGFBP1* und *HSD11B1*) sowie SARS-CoV-2-Eintrittsfaktoren (*ACE2* und *TMPRSS2*) wurde mittels qPCR und Western Blot analysiert. Infektionsexperimente mit einem rekombinanten Virusstamm, der mNeonGreen exprimiert, sowie mit authentischen SARS-CoV-2-Viren wurden durchgeführt. Mittels Zytokin-Assays und RNA-Sequenzierung wurde die Reaktion der Wirtszelle auf die virale Invasion untersucht.

Unsere Studie zeigte die Anwesenheit von *ACE2* und *TMPRSS2* in Endometriumzellen sowie eine erhöhte Expression von *ACE2* nach Dezidualisierung. Ein neues endometriales Sphäroidmodell wurde erfolgreich etabliert. Die Anfälligkeit für eine SARS-CoV-2-Infektion wurde nachgewiesen. Diese geht mit einer Entzündungsreaktion und Dysregulation von Genen einher,

die mit der Immunantwort, hämatovaskulären und zellulären Funktionen assoziiert sind. Die Veränderungen in der Genexpression variierten zwischen nicht-dezidualisierten und dezidualisierten Sphäroiden und Gene, die mit dem angeborenen Immunsystem assoziiert sind (*CCL20*, *CD38*, *LCN2* und *NR4A3*), waren dysreguliert. Dies ist ein potenzieller Mechanismus für die Immunevasion von SARS-CoV-2.

Diese Ergebnisse liefern bedeutende Erkenntnisse zur Möglichkeit der vertikalen Übertragung von SARS-CoV-2 während der Schwangerschaft und erfüllen somit die anfänglich definierten Ziele. Endometriale Sphäroide stellen ein innovatives Modell für die Erforschung viraler Interaktionen dar und sollten in Studien mit bekannten vertikal übertragbaren Erregern weiter validiert werden. Das Verständnis dieser molekularen Mechanismen ist von zentraler Bedeutung für die Entwicklung präventiver und therapeutischer Interventionen für schwangere Patientinnen mit COVID-19.

7 Bibliography

- ABELLA, V., SCOTECE, M., CONDE, J., GÓMEZ, R., LOIS, A., PINO, J., GÓMEZ-REINO, J. J., LAGO, F., MOBASHERI, A. & GUALILLO, O. 2015. The potential of lipocalin-2/NGAL as biomarker for inflammatory and metabolic diseases. *Biomarkers*, 20, 565-571.
- ACHACHE, H. & REVEL, A. 2006. Endometrial receptivity markers, the journey to successful embryo implantation. *Hum Reprod Update*, 12, 731-46.
- ADAM, M. P., POLIFKA, J. E. & FRIEDMAN, J. M. 2011. Evolving knowledge of the teratogenicity of medications in human pregnancy. *Am J Med Genet C Semin Med Genet*, 157c, 175-82.
- ADAMS WALDORF, K. M. & MCADAMS, R. M. 2013. Influence of infection during pregnancy on fetal development. *Reproduction*, 146, R151-62.
- ADHIKARI, E. H., MACDONALD, L., SORELLE, J. A., MORSE, J., PRUSZYNSKI, J. & SPONG, C. Y. 2022a. COVID-19 Cases and Disease Severity in Pregnancy and Neonatal Positivity Associated With Delta (B.1.617.2) and Omicron (B.1.1.529) Variant Predominance. *Jama*, 327, 1500-1502.
- ADHIKARI, E. H., SORELLE, J. A., MCINTIRE, D. D. & SPONG, C. Y. 2022b. Increasing severity of COVID-19 in pregnancy with Delta (B.1.617.2) variant surge. *Am J Obstet Gynecol*, 226, 149-151.
- ADIL, M. T., RAHMAN, R., WHITELAW, D., JAIN, V., AL-TAAN, O., RASHID, F., MUNASINGHE, A. & JAMBULINGAM, P. 2021. SARS-CoV-2 and the pandemic of COVID-19. *Postgrad Med J*, 97, 110-116.
- AL-ALEM, L., PUTTABYATAPPA, M., ROSEWELL, K., BRÄNNSTRÖM, M., AKIN, J., BOLDT, J., MUSE, K. & CURRY, T. E., JR. 2015. Chemokine Ligand 20: A Signal for Leukocyte Recruitment During Human Ovulation? *Endocrinology*, 156, 3358-3369.
- ALLAVENA, P., BIANCHI, G., ZHOU, D., VAN DAMME, J., JÍLEK, P., SOZZANI, S. & MANTOVANI, A. 1994. Induction of natural killer cell migration by monocyte chemotactic protein-1, -2 and -3. *Eur J Immunol*, 24, 3233-6.
- ALLOTEY, J., CHATTERJEE, S., KEW, T., GAETANO, A., STALLINGS, E., FERNÁNDEZ-GARCÍA, S., YAP, M., SHEIKH, J., LAWSON, H., COOMAR, D., DIXIT, A., ZHOU, D., BALAJI, R., LITTMODEN, M., KING, Y., DEBENHAM, L., LLAVALL, A. C., ANSARI, K., SANDHU, G., BANJOKO, A., WALKER, K., O'DONOGHUE, K., VAN WELY, M., VAN LEEUWEN, E., KOSTOVA, E., KUNST, H., KHALIL, A., BRIZUELA, V., BROUTET, N., KARA, E., KIM, C. R., THORSON, A., OLADAPO, O. T., ZAMORA, J., BONET, M., MOFENSON, L. & THANGARATINAM, S. 2022. SARS-CoV-2 positivity in offspring and timing of mother-to-child transmission: living systematic review and meta-analysis. *Bmj*, 376, e067696.
- ALLOTEY, J., STALLINGS, E., BONET, M., YAP, M., CHATTERJEE, S., KEW, T., DEBENHAM, L., LLAVALL, A. C., DIXIT, A., ZHOU, D., BALAJI, R., LEE, S. I., QIU, X., YUAN, M., COOMAR, D., SHEIKH, J., LAWSON, H., ANSARI, K., VAN WELY, M., VAN LEEUWEN, E., KOSTOVA, E., KUNST, H., KHALIL, A., TIBERI, S., BRIZUELA, V., BROUTET, N.,

- KARA, E., KIM, C. R., THORSON, A., ESCURIET, R., OLADAPO, O. T., MOFENSON, L., ZAMORA, J. & THANGARATINAM, S. 2020. Clinical manifestations, risk factors, and maternal and perinatal outcomes of coronavirus disease 2019 in pregnancy: living systematic review and meta-analysis. *BMJ*, 370, m3320.
- ALPUCHE-LAZCANO, S. P., SALIBA, J., COSTA, V. V., CAMPOLINA-SILVA, G. H., MARIM, F. M., RIBEIRO, L. S., BLANK, V., MOULAND, A. J., TEIXEIRA, M. M. & GATIGNOL, A. 2021. Profound downregulation of neural transcription factor Npas4 and Nr4a family in fetal mice neurons infected with Zika virus. *PLOS Neglected Tropical Diseases*, 15, e0009425.
- ALRAOUJI, N. N. & ABOUSSEKHRA, A. 2021. Tocilizumab inhibits IL-8 and the proangiogenic potential of triple negative breast cancer cells. *Mol Carcinog*, 60, 51-59.
- ALTMÄE, S., KOEL, M., VÕSA, U., ADLER, P., SUHORUTŠENKO, M., LAISK-PODAR, T., KUKUSHKINA, V., SAARE, M., VELTHUT-MEIKAS, A., KRJUTŠKOV, K., AGHAJANOVA, L., LALITKUMAR, P. G., GEMZELL-DANIELSSON, K., GIUDICE, L., SIMÓN, C. & SALUMETS, A. 2017. Meta-signature of human endometrial receptivity: a meta-analysis and validation study of transcriptomic biomarkers. *Sci Rep*, 7, 10077.
- ANDERSEN, M. L. & WINTER, L. M. F. 2019. Animal models in biological and biomedical research - experimental and ethical concerns. *An Acad Bras Cienc*, 91, e20170238.
- ANIM-NYAME, N., GAMBLE, J., SOORANNA, S. R., JOHNSON, M. R. & STEER, P. J. 2003. Microvascular permeability is related to circulating levels of tumour necrosis factor- α in pre-eclampsia. *Cardiovascular Research*, 58, 162-169.
- ARCURI, F., MONDER, C., LOCKWOOD, C. J. & SCHATZ, F. 1996. Expression of 11 beta-hydroxysteroid dehydrogenase during decidualization of human endometrial stromal cells. *Endocrinology*, 137, 595-600.
- ARICI, A., SENTURK, L. M., SELI, E., BAHTIYAR, M. O. & KIM, G. 1999. Regulation of Monocyte Chemotactic Protein-1 Expression in Human Endometrial Stromal Cells by Estrogen and Progesterone1. *Biology of Reproduction*, 61, 85-90.
- ARORA, M. & LAKSHMI, R. 2021. Vaccines - safety in pregnancy. *Best Pract Res Clin Obstet Gynaecol*, 76, 23-40.
- ARORA, N., SADOVSKY, Y., DERMODY, T. S. & COYNE, C. B. 2017. Microbial Vertical Transmission during Human Pregnancy. *Cell Host Microbe*, 21, 561-567.
- ARUNACHALAM, P. S., WIMMERS, F., MOK, C. K. P., PERERA, R., SCOTT, M., HAGAN, T., SIGAL, N., FENG, Y., BRISTOW, L., TAK-YIN TSANG, O., WAGH, D., COLLIER, J., PELLEGRINI, K. L., KAZMIN, D., ALAAEDDINE, G., LEUNG, W. S., CHAN, J. M. C., CHIK, T. S. H., CHOI, C. Y. C., HUERTA, C., PAINE MCCULLOUGH, M., LV, H., ANDERSON, E., EDUPUGANTI, S., UPADHYAY, A. A., BOSINGER, S. E., MAECKER, H. T., KHATRI, P., ROUPHAEL, N., PEIRIS, M. & PULENDRAN, B. 2020. Systems biological assessment of immunity to

- mild versus severe COVID-19 infection in humans. *Science*, 369, 1210-1220.
- ASAI, A., AIHARA, E., WATSON, C., MOURYA, R., MIZUOCHI, T., SHIVAKUMAR, P., PHELAN, K., MAYHEW, C., HELMRATH, M., TAKEBE, T., WELLS, J. & BEZERRA, J. A. 2017. Paracrine signals regulate human liver organoid maturation from induced pluripotent stem cells. *Development*, 144, 1056-1064.
- AZINHEIRA NOBREGA CRUZ, N., STOLL, D., CASARINI, D. E. & BERTAGNOLLI, M. 2021. Role of ACE2 in pregnancy and potential implications for COVID-19 susceptibility. *Clin Sci (Lond)*, 135, 1805-1824.
- BAGGEN, J., VANSTREELS, E., JANSEN, S. & DAELEMANS, D. 2021. Cellular host factors for SARS-CoV-2 infection. *Nat Microbiol*, 6, 1219-1232.
- BAGHERI, S., ROGHANIAN, R., GOLBANG, N., GOLBANG, P. & NASR ESFAHANI, M. H. 2018. Molecular Evidence of Chlamydia trachomatis Infection and Its Relation to Miscarriage. *Int J Fertil Steril*, 12, 152-156.
- BAMFO, J. E. A. K., KAMETAS, N. A., NICOLAIDES, K. H. & CHAMBERS, J. B. 2007. Maternal left ventricular diastolic and systolic long-axis function during normal pregnancy. *European Journal of Echocardiography*, 8, 360-368.
- BANDOH, S., TSUKADA, T., MARUYAMA, K., OHKURA, N. & YAMAGUCHI, K. 1997. Mechanical agitation induces gene expression of NOR-1 and its closely related orphan nuclear receptors in leukemic cell lines. *Leukemia*, 11, 1453-8.
- BAPTISTA, L. S., KRONEMBERGER, G. S., SILVA, K. R. & GRANJEIRO, J. M. 2018. Spheroids of stem cells as endochondral templates for improved bone engineering. *Front Biosci (Landmark Ed)*, 23, 1969-1986.
- BARCELOS, I., PENNA, I. A. A., SOLIGO, A. G., COSTA, Z. B. & MARTINS, W. P. 2021. Vertical Transmission of SARS-CoV-2: A Systematic Review. *Rev Bras Ginecol Obstet*, 43, 207-215.
- BASILE, K., ROCKETT, R. J., MCPHIE, K., FENNELL, M., JOHNSON-MACKINNON, J., AGIUS, J. E., FONG, W., RAHMAN, H., KO, D., DONAVAN, L., HUESTON, L., LAM, C., ARNOTT, A., CHEN, S. C., MADDOCKS, S., O'SULLIVAN, M. V., DWYER, D. E., SINTCHENKO, V. & KOK, J. 2022. Improved Neutralisation of the SARS-CoV-2 Omicron Variant following a Booster Dose of Pfizer-BioNTech (BNT162b2) COVID-19 Vaccine. *Viruses*, 14.
- BATEMAN, B. T., PATORNO, E., DESAI, R. J., SEELY, E. W., MOGUN, H., DEJENE, S. Z., FISCHER, M. A., FRIEDMAN, A. M., HERNANDEZ-DIAZ, S. & HUYBRECHTS, K. F. 2017. Angiotensin-Converting Enzyme Inhibitors and the Risk of Congenital Malformations. *Obstet Gynecol*, 129, 174-184.
- BÉDARD, P., GAUVIN, S., FERLAND, K., CANEPARO, C., PELLERIN, È., CHABAUD, S. & BOLDUC, S. 2020. Innovative Human Three-Dimensional Tissue-Engineered Models as an Alternative to Animal Testing. *Bioengineering (Basel)*, 7.

- BELL, C. C., HENDRIKS, D. F., MORO, S. M., ELLIS, E., WALSH, J., RENBLOM, A., FREDRIKSSON PUIGVERT, L., DANKERS, A. C., JACOBS, F., SNOEYS, J., SISON-YOUNG, R. L., JENKINS, R. E., NORDLING, Å., MKRTCHIAN, S., PARK, B. K., KITTERINGHAM, N. R., GOLDRING, C. E., LAUSCHKE, V. M. & INGELMAN-SUNDBERG, M. 2016. Characterization of primary human hepatocyte spheroids as a model system for drug-induced liver injury, liver function and disease. *Sci Rep*, 6, 25187.
- BEN-HUR, H., GUREVICH, P., ELHAYANY, A., AVINOACH, I., SCHNEIDER, D. F. & ZUSMAN, I. 2005. Transport of maternal immunoglobulins through the human placental barrier in normal pregnancy and during inflammation. *Int J Mol Med*, 16, 401-7.
- BENTIN-LEY, U., PEDERSEN, B., LINDENBERG, S., LARSEN, J. F., HAMBERGER, L. & HORN, T. 1994. Isolation and culture of human endometrial cells in a three-dimensional culture system. *J Reprod Fertil*, 101, 327-32.
- BERKHOUT, R. P., LAMBALK, C. B., REPPING, S., HAMER, G. & MASTENBROEK, S. 2020. Premature expression of the decidualization marker prolactin is associated with repeated implantation failure. *Gynecol Endocrinol*, 36, 360-364.
- BESTE, M. T., LOMAKINA, E. B., HAMMER, D. A. & WAUGH, R. E. 2015. Immobilized IL-8 Triggers Phagocytosis and Dynamic Changes in Membrane Microtopology in Human Neutrophils. *Ann Biomed Eng*, 43, 2207-19.
- BIERING, S. B., GOMES DE SOUSA, F. T., TJANG, L. V., PAHMEIER, F., ZHU, C., RUAN, R., BLANC, S. F., PATEL, T. S., WORTHINGTON, C. M., GLASNER, D. R., CASTILLO-ROJAS, B., SERVELLITA, V., LO, N. T. N., WONG, M. P., WARNES, C. M., SANDOVAL, D. R., CLAUSEN, T. M., SANTOS, Y. A., FOX, D. M., ORTEGA, V., NÄÄR, A. M., BARIC, R. S., STANLEY, S. A., AGUILAR, H. C., ESKO, J. D., CHIU, C. Y., PAK, J. E., BEATTY, P. R. & HARRIS, E. 2022. SARS-CoV-2 Spike triggers barrier dysfunction and vascular leak via integrins and TGF- β signaling. *Nat Commun*, 13, 7630.
- BINDOM, S. M. & LAZARTIGUES, E. 2009. The sweeter side of ACE2: physiological evidence for a role in diabetes. *Mol Cell Endocrinol*, 302, 193-202.
- BIROL ILTER, P., PRASAD, S., MUTLU, M., TEKIN, A., O'BRIEN, P., VON DADELSZEN, P., MAGEE, L., TEKIN, S., TUG, N. & KALAFAT, E. 2022. Maternal and perinatal outcomes of SARS-CoV-2 infection in unvaccinated pregnancies during Delta and Omicron waves. *Ultrasound in Obstetrics & Gynecology*.
- BISSELL, M. J., RADISKY, D. C., RIZKI, A., WEAVER, V. M. & PETERSEN, O. W. 2002. The organizing principle: microenvironmental influences in the normal and malignant breast. *Differentiation*, 70, 537-46.
- BLANCO-MELO, D., NILSSON-PAYANT, B. E., LIU, W. C., UHL, S., HOAGLAND, D., MØLLER, R., JORDAN, T. X., OISHI, K., PANIS, M., SACHS, D., WANG, T. T., SCHWARTZ, R. E., LIM, J. K., ALBRECHT,

- R. A. & TENOEVER, B. R. 2020. Imbalanced Host Response to SARS-CoV-2 Drives Development of COVID-19. *Cell*, 181, 1036-1045.e9.
- BLOISE, E., ZHANG, J., NAKPU, J., HAMADA, H., DUNK, C. E., LI, S., IMPERIO, G. E., NADEEM, L., KIBSCHULL, M., LYE, P., MATTHEWS, S. G. & LYE, S. J. 2021. Expression of severe acute respiratory syndrome coronavirus 2 cell entry genes, angiotensin-converting enzyme 2 and transmembrane protease serine 2, in the placenta across gestation and at the maternal-fetal interface in pregnancies complicated by preterm birth or preeclampsia. *Am J Obstet Gynecol*, 224, 298.e1-298.e8.
- BONNEY, E. A. 2017. Alternative theories: Pregnancy and immune tolerance. *J Reprod Immunol*, 123, 65-71.
- BONTA, P. I., TIEL, C. M. V., VOS, M., POLS, T. W. H., THIENEN, J. V. V., FERREIRA, V., ARKENBOUT, E. K., SEPPEN, J., SPEK, C. A., POLL, T. V. D., PANNEKOEK, H. & VRIES, C. J. M. D. 2006. Nuclear Receptors Nur77, Nurr1, and NOR-1 Expressed in Atherosclerotic Lesion Macrophages Reduce Lipid Loading and Inflammatory Responses. *Arteriosclerosis, Thrombosis, and Vascular Biology*, 26, 2288-2288.
- BORETTO, M., COX, B., NOBEN, M., HENDRIKS, N., FASSBENDER, A., ROOSE, H., AMANT, F., TIMMERMAN, D., TOMASSETTI, C., VANHIE, A., MEULEMAN, C., FERRANTE, M. & VANKELECOM, H. 2017. Development of organoids from mouse and human endometrium showing endometrial epithelium physiology and long-term expandability. *Development*, 144, 1775-1786.
- BOULET, S., DAUDELIN, J.-F., ODAGIU, L., PELLETIER, A.-N., YUN, T. J., LESAGE, S., CHEONG, C. & LABRECQUE, N. 2019. The orphan nuclear receptor NR4A3 controls the differentiation of monocyte-derived dendritic cells following microbial stimulation. *Proceedings of the National Academy of Sciences*, 116, 15150-15159.
- BRAR, A. K., FRANK, G. R., KESSLER, C. A., CEDARS, M. I. & HANDWERGER, S. 1997. Progesterone-dependent decidualization of the human endometrium is mediated by cAMP. *Endocrine*, 6, 301-7.
- BRAVERMAN, M. B., BAGNI, A., DE ZIEGLER, D., DEN, T. & GURPIDE, E. 1984. Isolation of prolactin-producing cells from first and second trimester decidua. *J Clin Endocrinol Metab*, 58, 521-5.
- BRIGHTON, P. J., MARUYAMA, Y., FISHWICK, K., VRLJICAK, P., TEWARY, S., FUJIHARA, R., MUTER, J., LUCAS, E. S., YAMADA, T., WOODS, L., LUCCIOLA, R., HOU LEE, Y., TAKEDA, S., OTT, S., HEMBERGER, M., QUENBY, S. & BROSENS, J. J. 2017. Clearance of senescent decidual cells by uterine natural killer cells in cycling human endometrium. *Elife*, 6.
- BRODIN, P. 2021. Immune determinants of COVID-19 disease presentation and severity. *Nature Medicine*, 27, 28-33.
- BROKAW, A., FURUTA, A., DACANAY, M., RAJAGOPAL, L. & ADAMS WALDORF, K. M. 2021. Bacterial and Host Determinants of Group B Streptococcal Vaginal Colonization and Ascending Infection in Pregnancy. *Front Cell Infect Microbiol*, 11, 720789.
- BROSENS, J. J., HAYASHI, N. & WHITE, J. O. 1999. Progesterone receptor regulates decidual prolactin expression in differentiating human endometrial stromal cells. *Endocrinology*, 140, 4809-20.

- BROSENS, J. J., PARKER, M. G., MCINDOE, A., PIJNENBORG, R. & BROSENS, I. A. 2009. A role for menstruation in preconditioning the uterus for successful pregnancy. *Am J Obstet Gynecol*, 200, 615.e1-6.
- BROSENS, J. J., PIJNENBORG, R. & BROSENS, I. A. 2002. The myometrial junctional zone spiral arteries in normal and abnormal pregnancies: a review of the literature. *Am J Obstet Gynecol*, 187, 1416-23.
- BROSENS, J. J., SALKER, M. S., TEKLENBURG, G., NAUTIYAL, J., SALTER, S., LUCAS, E. S., STEEL, J. H., CHRISTIAN, M., CHAN, Y. W., BOOMSMA, C. M., MOORE, J. D., HARTSHORNE, G. M., SUĆUROVIĆ, S., MULAC-JERICEVIC, B., HEIJNEN, C. J., QUENBY, S., KOERKAMP, M. J., HOLSTEGE, F. C., SHMYGOL, A. & MACKLON, N. S. 2014. Uterine selection of human embryos at implantation. *Sci Rep*, 4, 3894.
- BRUCKER, S. Y., HENTRICH, T., SCHULZE-HENTRICH, J. M., PIETZSCH, M., WAJNGARTEN, N., SINGH, A. R., RALL, K. & KOCH, A. 2022. Endometrial organoids derived from Mayer–Rokitansky–Küster–Hauser syndrome patients provide insights into disease-causing pathways. *Disease Models & Mechanisms*, 15.
- BUCK, V. U., GELLERSEN, B., LEUBE, R. E. & CLASSEN-LINKE, I. 2015. Interaction of human trophoblast cells with gland-like endometrial spheroids: a model system for trophoblast invasion. *Human Reproduction*, 30, 906-916.
- BULLETTI, C., BULLETTI, F. M., SCIORIO, R. & GUIDO, M. 2022. Progesterone: The Key Factor of the Beginning of Life. *Int J Mol Sci*, 23.
- BULLO, M., TSCHUMI, S., BUCHER, B. S., BIANCHETTI, M. G. & SIMONETTI, G. D. 2012. Pregnancy Outcome Following Exposure to Angiotensin-Converting Enzyme Inhibitors or Angiotensin Receptor Antagonists. *Hypertension*, 60, 444-450.
- BULMER, J. N., MORRISON, L., LONGFELLOW, M., RITSON, A. & PACE, D. 1991. Granulated lymphocytes in human endometrium: histochemical and immunohistochemical studies. *Human Reproduction*, 6, 791-798.
- BULMER, J. N., WILLIAMS, P. J. & LASH, G. E. 2010. Immune cells in the placental bed. *Int J Dev Biol*, 54, 281-94.
- CABALLERO-CAMPO, P., DOMÍNGUEZ, F., COLOMA, J., MESEGUER, M., REMOHÍ, J., PELLICER, A. & SIMÓN, C. 2002. Hormonal and embryonic regulation of chemokines IL-8, MCP-1 and RANTES in the human endometrium during the window of implantation. *Molecular Human Reproduction*, 8, 375-384.
- CALLEJA-AGIUS, J., JAUNIAUX, E., PIZZEY, A. R. & MUTTUKRISHNA, S. 2011. Investigation of systemic inflammatory response in first trimester pregnancy failure. *Human Reproduction*, 27, 349-357.
- CALVAYRAC, O., RODRÍGUEZ-CALVO, R., MARTÍ-PAMIES, I., ALONSO, J., FERRÁN, B., AGUILÓ, S., CRESPO, J., RODRÍGUEZ-SINOVAS, A., RODRÍGUEZ, C. & MARTÍNEZ-GONZÁLEZ, J. 2015. NOR-1 modulates the inflammatory response of vascular smooth muscle cells by preventing NFκB activation. *Journal of Molecular and Cellular Cardiology*, 80, 34-44.

- CAO, J., O'DAY, D. R., PLINER, H. A., KINGSLEY, P. D., DENG, M., DAZA, R. M., ZAGER, M. A., ALDINGER, K. A., BLECHER-GONEN, R., ZHANG, F., SPIELMANN, M., PALIS, J., DOHERTY, D., STEEMERS, F. J., GLASS, I. A., TRAPNELL, C. & SHENDURE, J. 2020. A human cell atlas of fetal gene expression. *Science*, 370.
- CAPOBIANCO, G., SADERI, L., ALIBERTI, S., MONDONI, M., PIANA, A., DESSOLE, F., DESSOLE, M., CHERCHI, P. L., DESSOLE, S. & SOTGIU, G. 2020. COVID-19 in pregnant women: A systematic review and meta-analysis. *Eur J Obstet Gynecol Reprod Biol*, 252, 543-558.
- CARFÌ, A., BERNABEI, R. & LANDI, F. 2020. Persistent Symptoms in Patients After Acute COVID-19. *Jama*, 324, 603-605.
- CARR, M. W., ROTH, S. J., LUTHER, E., ROSE, S. S. & SPRINGER, T. A. 1994. Monocyte chemoattractant protein 1 acts as a T-lymphocyte chemoattractant. *Proceedings of the National Academy of Sciences*, 91, 3652-3656.
- CAYROL, C. & GIRARD, J. P. 2022. Interleukin-33 (IL-33): A critical review of its biology and the mechanisms involved in its release as a potent extracellular cytokine. *Cytokine*, 156, 155891.
- CEMGIL ARIKAN, D., OZKAYA, M., ADALI, E., KILINC, M., COSKUN, A., OZER, A. & BILGE, F. 2011. Plasma lipocalin-2 levels in pregnant women with pre-eclampsia, and their relation with severity of disease. *The Journal of Maternal-Fetal & Neonatal Medicine*, 24, 291-296.
- CEVIK, M., BAMFORD, C. G. G. & HO, A. 2020. COVID-19 pandemic-a focused review for clinicians. *Clin Microbiol Infect*, 26, 842-847.
- CHA, J., SUN, X. & DEY, S. K. 2012. Mechanisms of implantation: strategies for successful pregnancy. *Nat Med*, 18, 1754-67.
- CHADCHAN, S. B., POPLI, P., MAURYA, V. K. & KOMMAGANI, R. 2021. The SARS-CoV-2 receptor, angiotensin-converting enzyme 2, is required for human endometrial stromal cell decidualization†. *Biol Reprod*, 104, 336-343.
- CHAIWORAPONGSA, T., ROMERO, R., TOLOSA, J. E., YOSHIMATSU, J., ESPINOZA, J., KIM, Y. M., KIM, J. C., BUJOLD, E., KALACHE, K. & EDWIN, S. 2002. Elevated monocyte chemotactic protein-1 in amniotic fluid is a risk factor for pregnancy loss. *The Journal of Maternal-Fetal & Neonatal Medicine*, 12, 159-164.
- CHAPMAN, A. B., ABRAHAM, W. T., ZAMUDIO, S., COFFIN, C., MEROUANI, A., YOUNG, D., JOHNSON, A., OSORIO, F., GOLDBERG, C., MOORE, L. G., DAHMS, T. & SCHRIER, R. W. 1998. Temporal relationships between hormonal and hemodynamic changes in early human pregnancy. *Kidney Int*, 54, 2056-63.
- CHARUTA, A., SMUNIEWSKA, M., WOŹNIAK, Z. & PAZIEWSKA, A. 2023. Effect of COVID-19 on Pregnancy and Neonate's Vital Parameters: A Systematic Review. *J Pregnancy*, 2023, 3015072.
- CHATTERJEE, S., BHATTACHARYA, M., NAG, S., DHAMA, K. & CHAKRABORTY, C. 2023. A Detailed Overview of SARS-CoV-2 Omicron: Its Sub-Variants, Mutations and Pathophysiology, Clinical Characteristics, Immunological Landscape, Immune Escape, and Therapies. *Viruses*, 15.

- CHEN, K. G., PARK, K. & SPENCE, J. R. 2021. Studying SARS-CoV-2 infectivity and therapeutic responses with complex organoids. *Nature Cell Biology*, 23, 822-833.
- CHEN, W., YUAN, P., YANG, M., YAN, Z., KONG, S., YAN, J., LIU, X., CHEN, Y., QIAO, J. & YAN, L. 2020. SARS-CoV-2 Entry Factors: ACE2 and TMPRSS2 Are Expressed in Peri-Implantation Embryos and the Maternal-Fetal Interface. *Engineering (Beijing)*, 6, 1162-1169.
- CHIEN, E. J., LIAO, C. F., CHANG, C. P., PU, H. F., LU, L. M., SHIE, M. C., HSIEH, D. J. & HSU, M. T. 2007. The non-genomic effects on Na⁺/H⁺-exchange 1 by progesterone and 20alpha-hydroxyprogesterone in human T cells. *J Cell Physiol*, 211, 544-50.
- CHOUSTERMAN, B. G., SWIRSKI, F. K. & WEBER, G. F. 2017. Cytokine storm and sepsis disease pathogenesis. *Semin Immunopathol*, 39, 517-528.
- CHRISTIAN, M., MARANGOS, P., MAK, I., MCVEY, J., BARKER, F., WHITE, J. & BROSENS, J. J. 2001. Interferon-gamma modulates prolactin and tissue factor expression in differentiating human endometrial stromal cells. *Endocrinology*, 142, 3142-51.
- CHU, P., WU, E. & WEISS, L. M. 2000. Cytokeratin 7 and Cytokeratin 20 Expression in Epithelial Neoplasms: A Survey of 435 Cases. *Modern Pathology*, 13, 962-972.
- CLANCY, K. B. 2009. Reproductive ecology and the endometrium: physiology, variation, and new directions. *Am J Phys Anthropol*, 140 Suppl 49, 137-54.
- CLEVERS, H. 2016. Modeling Development and Disease with Organoids. *Cell*, 165, 1586-1597.
- CLEVERS, H. C. 2019. Organoids: Avatars for Personalized Medicine. *Keio J Med*, 68, 95.
- CO, J. Y., MARGALEF-CATALÀ, M., LI, X., MAH, A. T., KUO, C. J., MONACK, D. M. & AMIEVA, M. R. 2019. Controlling Epithelial Polarity: A Human Enteroid Model for Host-Pathogen Interactions. *Cell reports*, 26, 2509-2520.e4.
- COLLINS, M. K., TAY, C. S. & ERLEBACHER, A. 2009. Dendritic cell entrapment within the pregnant uterus inhibits immune surveillance of the maternal/fetal interface in mice. *J Clin Invest*, 119, 2062-73.
- COMERFORD, I., BUNTING, M., FENIX, K., HAYLOCK-JACOBS, S., LITCHFIELD, W., HARATA-LEE, Y., TURVEY, M., BRAZZATTI, J., GREGOR, C., NGUYEN, P., KARA, E. & MCCOLL, S. R. 2010. An immune paradox: how can the same chemokine axis regulate both immune tolerance and activation?: CCR6/CCL20: a chemokine axis balancing immunological tolerance and inflammation in autoimmune disease. *Bioessays*, 32, 1067-76.
- CONDE-AGUDELO, A. & ROMERO, R. 2022. SARS-CoV-2 infection during pregnancy and risk of preeclampsia: a systematic review and meta-analysis. *Am J Obstet Gynecol*, 226, 68-89.e3.
- COOK, D. N., PROSSER, D. M., FORSTER, R., ZHANG, J., KUKLIN, N. A., ABBONDANZO, S. J., NIU, X.-D., CHEN, S.-C., MANFRA, D. J., WIEKOWSKI, M. T., SULLIVAN, L. M., SMITH, S. R., GREENBERG, H.

- B., NARULA, S. K., LIPP, M. & LIRA, S. A. 2000. CCR6 Mediates Dendritic Cell Localization, Lymphocyte Homeostasis, and Immune Responses in Mucosal Tissue. *Immunity*, 12, 495-503.
- COOKE, P. S., UCHIMA, F. D., FUJII, D. K., BERN, H. A. & CUNHA, G. R. 1986. Restoration of normal morphology and estrogen responsiveness in cultured vaginal and uterine epithelia transplanted with stroma. *Proceedings of the National Academy of Sciences*, 83, 2109-2113.
- CORNISH, E. F., FILIPOVIC, I., ÅSENIUS, F., WILLIAMS, D. J. & MCDONNELL, T. 2020. Innate Immune Responses to Acute Viral Infection During Pregnancy. *Frontiers in immunology*, 11, 572567-572567.
- COSTA, E. C., DE MELO-DIOGO, D., MOREIRA, A. F., CARVALHO, M. P. & CORREIA, I. J. 2018. Spheroids Formation on Non-Adhesive Surfaces by Liquid Overlay Technique: Considerations and Practical Approaches. *Biotechnol J*, 13.
- COSTA, E. C., GASPAR, V. M., COUTINHO, P. & CORREIA, I. J. 2014. Optimization of liquid overlay technique to formulate heterogenic 3D co-cultures models. *Biotechnol Bioeng*, 111, 1672-85.
- COSTA, M. A. 2016. The endocrine function of human placenta: an overview. *Reprod Biomed Online*, 32, 14-43.
- CRACKOWER, M. A., SARAO, R., OUDIT, G. Y., YAGIL, C., KOZIERADZKI, I., SCANGA, S. E., OLIVEIRA-DOS-SANTOS, A. J., DA COSTA, J., ZHANG, L., PEI, Y., SCHOLEY, J., FERRARIO, C. M., MANOUKIAN, A. S., CHAPPELL, M. C., BACKX, P. H., YAGIL, Y. & PENNINGER, J. M. 2002. Angiotensin-converting enzyme 2 is an essential regulator of heart function. *Nature*, 417, 822-8.
- CRITCHLEY, H. O. D., MAYBIN, J. A., ARMSTRONG, G. M. & WILLIAMS, A. R. W. 2020. Physiology of the Endometrium and Regulation of Menstruation. *Physiol Rev*, 100, 1149-1179.
- CUI, X., ZHAO, Z., ZHANG, T., GUO, W., GUO, W., ZHENG, J., ZHANG, J., DONG, C., NA, R., ZHENG, L., LI, W., LIU, Z., MA, J., WANG, J., HE, S., XU, Y., SI, P., SHEN, Y. & CAI, C. 2021. A systematic review and meta-analysis of children with coronavirus disease 2019 (COVID-19). *J Med Virol*, 93, 1057-1069.
- CUNHA, G. R., COOKE, P. S. & KURITA, T. 2004. Role of stromal-epithelial interactions in hormonal responses. *Archives of Histology and Cytology*, 67, 417-434.
- DALY, D. C., MASLAR, I. A. & RIDDICK, D. H. 1983. Prolactin production during in vitro decidualization of proliferative endometrium. *American Journal of Obstetrics and Gynecology*, 145, 672-678.
- DAMIANI, F., MAKIEVA, S., RINALDI, S. F., HUA, L., MARCOLONGO, P., PETRAGLIA, F. & NORMAN, J. E. 2017. 11 β -hydroxysteroid dehydrogenase type 1 and pregnancy: Role in the timing of labour onset and in myometrial contraction. *Mol Cell Endocrinol*, 447, 79-86.
- DE DIOS-FIGUEROA, G. T., AGUILERA-MARQUEZ, J. D. R., CAMACHO-VILLEGAS, T. A. & LUGO-FABRES, P. H. 2021. 3D Cell Culture Models in COVID-19 Times: A Review of 3D Technologies to Understand and Accelerate Therapeutic Drug Discovery. *Biomedicines*, 9.

- DE FLORA, A., ZOCCHI, E., GUIDA, L., FRANCO, L. & BRUZZONE, S. 2004. Autocrine and paracrine calcium signaling by the CD38/NAD⁺/cyclic ADP-ribose system. *Ann N Y Acad Sci*, 1028, 176-91.
- DE HAAN, C. A., VENNEMA, H. & ROTTIER, P. J. 2000. Assembly of the coronavirus envelope: homotypic interactions between the M proteins. *J Virol*, 74, 4967-78.
- DE MELO, B. A. G., BENINCASA, J. C., CRUZ, E. M., MARICATO, J. T. & PORCIONATTO, M. A. 2021. 3D culture models to study SARS-CoV-2 infectivity and antiviral candidates: From spheroids to bioprinting. *Biomed J*, 44, 31-42.
- DE ZIEGLER, D., FANCHIN, R., DE MOUSTIER, B. & BULLETTI, C. 1998. The hormonal control of endometrial receptivity: estrogen (E2) and progesterone. *J Reprod Immunol*, 39, 149-66.
- DECENSI, A., FONTANA, V., BRUNO, S., GUSTAVINO, C., GATTESCHI, B. & COSTA, A. 1996. Effect of tamoxifen on endometrial proliferation. *Journal of Clinical Oncology*, 14, 434-440.
- DEL VALLE, D. M., KIM-SCHULZE, S., HUANG, H. H., BECKMANN, N. D., NIRENBERG, S., WANG, B., LAVIN, Y., SWARTZ, T. H., MADDURI, D., STOCK, A., MARRON, T. U., XIE, H., PATEL, M., TUBALLES, K., VAN OEKELLEN, O., RAHMAN, A., KOVATCH, P., ABERG, J. A., SCHADT, E., JAGANNATH, S., MAZUMDAR, M., CHARNEY, A. W., FIRPO-BETANCOURT, A., MENDU, D. R., JHANG, J., REICH, D., SIGEL, K., CORDON-CARDO, C., FELDMANN, M., PAREKH, S., MERAD, M. & GNJATIC, S. 2020. An inflammatory cytokine signature predicts COVID-19 severity and survival. *Nat Med*, 26, 1636-1643.
- DEMETRIUS, L. 2006. Aging in mouse and human systems: a comparative study. *Ann N Y Acad Sci*, 1067, 66-82.
- DERBYSHIRE, A. E., ALLEN, J. L., GITTINS, M., LAKHIANI, B., BOLTON, J., SHAW, J., PEMBERTON, P. W., NEEDHAM, M., MACKINTOSH, M. L., EDMONDSON, R. J., KITCHENER, H. C. & CROSBIE, E. J. 2021. Progesterone Therapy for Endometrial Cancer Prevention in Obese Women (PROTEC) Trial: A Feasibility Study. *Cancer Prev Res (Phila)*, 14, 263-274.
- DESHMANE, S. L., KREMLEV, S., AMINI, S. & SAWAYA, B. E. 2009. Monocyte chemoattractant protein-1 (MCP-1): an overview. *Journal of interferon & cytokine research : the official journal of the International Society for Interferon and Cytokine Research*, 29, 313-326.
- DEVROE, S., VAN DE VELDE, M. & REX, S. 2015. General anesthesia for caesarean section. *Curr Opin Anaesthesiol*, 28, 240-6.
- DI TORO, F., GJOKA, M., DI LORENZO, G., DE SANTO, D., DE SETA, F., MASO, G., RISSO, F. M., ROMANO, F., WIESENFELD, U., LEVI-D'ANCONA, R., RONFANI, L. & RICCI, G. 2021. Impact of COVID-19 on maternal and neonatal outcomes: a systematic review and meta-analysis. *Clin Microbiol Infect*, 27, 36-46.
- DI AV-CITRIN, O., SHECHTMAN, S., HALBERSTADT, Y., FINKEL-PEKARSKY, V., WAJNBERG, R., ARNON, J., DI GIANANTONIO, E., CLEMENTI, M. & ORNOY, A. 2011. Pregnancy outcome after in utero exposure to

- angiotensin converting enzyme inhibitors or angiotensin receptor blockers. *Reprod Toxicol*, 31, 540-5.
- DIEBOLD, S. S., KAISHO, T., HEMMI, H., AKIRA, S. & REIS E SOUSA, C. 2004. Innate antiviral responses by means of TLR7-mediated recognition of single-stranded RNA. *Science*, 303, 1529-31.
- DIMITRIADIS, E., WHITE, C. A., JONES, R. L. & SALAMONSEN, L. A. 2005. Cytokines, chemokines and growth factors in endometrium related to implantation. *Human Reproduction Update*, 11, 613-630.
- DIRIBA, K., AWULACHEW, E. & GETU, E. 2020. The effect of coronavirus infection (SARS-CoV-2, MERS-CoV, and SARS-CoV) during pregnancy and the possibility of vertical maternal-fetal transmission: a systematic review and meta-analysis. *Eur J Med Res*, 25, 39.
- DOMINGUEZ, F., GALAN, A., MARTIN, J. J., REMOHI, J., PELLICER, A. & SIMÓN, C. 2003. Hormonal and embryonic regulation of chemokine receptors CXCR1, CXCR4, CCR5 and CCR2B in the human endometrium and the human blastocyst. *Mol Hum Reprod*, 9, 189-98.
- DOMÍNGUEZ, F., SIMÓN, C., QUIÑONERO, A., RAMÍREZ, M., GONZÁLEZ-MUÑOZ, E., BURGHARDT, H., CERVERO, A., MARTÍNEZ, S., PELLICER, A., PALACÍN, M., SÁNCHEZ-MADRID, F. & YÁÑEZ-MÓ, M. 2010. Human endometrial CD98 is essential for blastocyst adhesion. *PLoS One*, 5, e13380.
- DOMNINA, A., ALEKSEENKO, L., KOZHUKHAROVA, I., LYUBLINSKAYA, O., SHOROKHOVA, M., ZENIN, V., FRIDLANSKAYA, I. & NIKOLSKY, N. 2021. Generation of Therapeutically Potent Spheroids from Human Endometrial Mesenchymal Stem/Stromal Cells. *Journal of Personalized Medicine*, 11, 466.
- DONG, L., TIAN, J., HE, S., ZHU, C., WANG, J., LIU, C. & YANG, J. 2020. Possible Vertical Transmission of SARS-CoV-2 From an Infected Mother to Her Newborn. *Jama*, 323, 1846-1848.
- DONOGHUE, M., HSIEH, F., BARONAS, E., GODBOUT, K., GOSSELIN, M., STAGLIANO, N., DONOVAN, M., WOOLF, B., ROBISON, K., JEYASEELAN, R., BREITBART, R. E. & ACTON, S. 2000. A novel angiotensin-converting enzyme-related carboxypeptidase (ACE2) converts angiotensin I to angiotensin 1-9. *Circ Res*, 87, E1-9.
- DRAKE, J. W., CHARLESWORTH, B., CHARLESWORTH, D. & CROW, J. F. 1998. Rates of spontaneous mutation. *Genetics*, 148, 1667-86.
- DUNN, C. L., KELLY, R. W. & CRITCHLEY, H. O. D. 2003. Decidualization of the human endometrial stromal cell: an enigmatic transformation. *Reproductive BioMedicine Online*, 7, 151-161.
- DUVAL, K., GROVER, H., HAN, L. H., MOU, Y., PEGORARO, A. F., FREDBERG, J. & CHEN, Z. 2017. Modeling Physiological Events in 2D vs. 3D Cell Culture. *Physiology (Bethesda)*, 32, 266-277.
- ECDC. 2023a. *Changes to list of SARS-CoV-2 variants of concern, variants of interest, and variants under monitoring* [Online]. Available: <https://www.ecdc.europa.eu/sites/default/files/documents/20230727%20Variants%20page%20changelog.pdf> [Accessed November 22 2023].

- ECDC. 2023b. SARS-CoV-2 variants of concern as of 17 November 2023 [Online]. Available: <https://www.ecdc.europa.eu/en/covid-19/variants-concern> [Accessed November 22 2023].
- EDMONDSON, R., BROGLIE, J. J., ADCOCK, A. F. & YANG, L. 2014. Three-dimensional cell culture systems and their applications in drug discovery and cell-based biosensors. *Assay Drug Dev Technol*, 12, 207-18.
- EIRAKU, M., TAKATA, N., ISHIBASHI, H., KAWADA, M., SAKAKURA, E., OKUDA, S., SEKIGUCHI, K., ADACHI, T. & SASAI, Y. 2011. Self-organizing optic-cup morphogenesis in three-dimensional culture. *Nature*, 472, 51-6.
- EMERA, D., ROMERO, R. & WAGNER, G. 2012. The evolution of menstruation: a new model for genetic assimilation: explaining molecular origins of maternal responses to fetal invasiveness. *Bioessays*, 34, 26-35.
- ENMON, R. M., JR., O'CONNOR, K. C., LACKS, D. J., SCHWARTZ, D. K. & DOTSON, R. S. 2001. Dynamics of spheroid self-assembly in liquid-overlay culture of DU 145 human prostate cancer cells. *Biotechnol Bioeng*, 72, 579-91.
- ERDEM, D., KAYAASLAN, B., CAKIR, E. Y., DINC, B., ASILTURK, D., KIRCA, F., SEGMENT, F., TURAN, I. O. & GUNER, R. 2023. Investigation of SARS-CoV-2 using RT-PCR in vaginal swab samples of female patients with a diagnosis of severe COVID-19. *Taiwan J Obstet Gynecol*, 62, 270-274.
- ERLEBACHER, A. 2013. Immunology of the maternal-fetal interface. *Annu Rev Immunol*, 31, 387-411.
- ESPLIN, M. S., ROMERO, R., CHAIWORAPONGSA, T., KIM, Y. M., EDWIN, S., GOMEZ, R., MAZOR, M. & ADASHI, E. Y. 2005. Monocyte chemotactic protein-1 is increased in the amniotic fluid of women who deliver preterm in the presence or absence of intra-amniotic infection. *The Journal of Maternal-Fetal & Neonatal Medicine*, 17, 365-373.
- EUGENIN, E. A., D'AVERSA, T. G., LOPEZ, L., CALDERON, T. M. & BERMAN, J. W. 2003. MCP-1 (CCL2) protects human neurons and astrocytes from NMDA or HIV-tat-induced apoptosis. *J Neurochem*, 85, 1299-311.
- EVERS, J. L. 2002. Female subfertility. *Lancet*, 360, 151-9.
- FACCHETTI, F., BUGATTI, M., DRERA, E., TRIPODO, C., SARTORI, E., CANCELILA, V., PAPACCIO, M., CASTELLANI, R., CASOLA, S., BONIOTTI, M. B., CAVADINI, P. & LAVAZZA, A. 2020. SARS-CoV2 vertical transmission with adverse effects on the newborn revealed through integrated immunohistochemical, electron microscopy and molecular analyses of Placenta. *EBioMedicine*, 59, 102951.
- FAN, X., DONG, J., ZHONG, S., WEI, Y., WU, Q., YAN, L., YONG, J., SUN, L., WANG, X., ZHAO, Y., WANG, W., YAN, J., WANG, X., QIAO, J. & TANG, F. 2018. Spatial transcriptomic survey of human embryonic cerebral cortex by single-cell RNA-seq analysis. *Cell Res*, 28, 730-745.
- FATEHULLAH, A., TAN, S. H. & BARKER, N. 2016. Organoids as an in vitro model of human development and disease. *Nat Cell Biol*, 18, 246-54.

- FEI, W., KIJIMA, D., HASHIMOTO, M., HASHIMURA, M., OGURI, Y., KAJITA, S., MATSUMOTO, T., YOKOI, A. & SAEGUSA, M. 2017. A functional role of LEFTY during progesterone therapy for endometrial carcinoma. *Cell Communication and Signaling*, 15, 56.
- FELSENSTEIN, S., HERBERT, J. A., MCNAMARA, P. S. & HEDRICH, C. M. 2020. COVID-19: Immunology and treatment options. *Clin Immunol*, 215, 108448.
- FENIZIA, C., SAULLE, I., DI GIMINIANI, M., VANETTI, C., TRABATTONI, D., PARISI, F., BIASIN, M. & SAVASI, V. 2021. Unlikely SARS-CoV-2 Transmission During Vaginal Delivery. *Reprod Sci*, 28, 2939-2941.
- FERRAZZI, E., FRIGERIO, L., SAVASI, V., VERGANI, P., PREFUMO, F., BARRESI, S., BIANCHI, S., CIRIELLO, E., FACCHINETTI, F., GERVASI, M. T., IURLARO, E., KUSTERMANN, A., MANGILI, G., MOSCA, F., PATANÈ, L., SPAZZINI, D., SPINILLO, A., TROJANO, G., VIGNALI, M., VILLA, A., ZUCCOTTI, G. V., PARAZZINI, F. & CETIN, I. 2020. Vaginal delivery in SARS-CoV-2-infected pregnant women in Northern Italy: a retrospective analysis. *Bjog*, 127, 1116-1121.
- FERREIRA-GOMES, M., KRUGLOV, A., DUREK, P., HEINRICH, F., TIZIAN, C., HEINZ, G. A., PASCUAL-REGUANT, A., DU, W., MOTHES, R., FAN, C., FRISCHBUTTER, S., HABENICHT, K., BUDZINSKI, L., NINNEMANN, J., JANI, P. K., GUERRA, G. M., LEHMANN, K., MATZ, M., OSTENDORF, L., HEIBERGER, L., CHANG, H.-D., BAUHERR, S., MAURER, M., SCHÖNRICH, G., RAFTERY, M., KALLINICH, T., MALL, M. A., ANGERMAIR, S., TRESKATSCH, S., DÖRNER, T., CORMAN, V. M., DIEFENBACH, A., VOLK, H.-D., ELEZKURTAJ, S., WINKLER, T. H., DONG, J., HAUSER, A. E., RADBRUCH, H., WITKOWSKI, M., MELCHERS, F., RADBRUCH, A. & MASHREGHI, M.-F. 2021. SARS-CoV-2 in severe COVID-19 induces a TGF- β -dominated chronic immune response that does not target itself. *Nature Communications*, 12, 1961.
- FLO, T. H., SMITH, K. D., SATO, S., RODRIGUEZ, D. J., HOLMES, M. A., STRONG, R. K., AKIRA, S. & ADEREM, A. 2004. Lipocalin 2 mediates an innate immune response to bacterial infection by sequestering iron. *Nature*, 432, 917-921.
- FRIEDRICH, J., SEIDEL, C., EBNER, R. & KUNZ-SCHUGHART, L. A. 2009. Spheroid-based drug screen: considerations and practical approach. *Nat Protoc*, 4, 309-24.
- FROEHLICH, K., HAEGER, J. D., HEGER, J., PASTUSCHEK, J., PHOTINI, S. M., YAN, Y., LUPP, A., PFARRER, C., MROWKA, R., SCHLEUSSNE, E., MARKERT, U. R. & SCHMIDT, A. 2016. Generation of Multicellular Breast Cancer Tumor Spheroids: Comparison of Different Protocols. *J Mammary Gland Biol Neoplasia*, 21, 89-98.
- FROHN, C., FRICKE, L., PUCHTA, J. C. & KIRCHNER, H. 2001. The effect of HLA-C matching on acute renal transplant rejection. *Nephrology Dialysis Transplantation*, 16, 355-360.
- FUJII, M., MATANO, M., TOSHIMITSU, K., TAKANO, A., MIKAMI, Y., NISHIKORI, S., SUGIMOTO, S. & SATO, T. 2018. Human Intestinal Organoids Maintain Self-Renewal Capacity and Cellular Diversity in Niche-Inspired Culture Condition. *Cell Stem Cell*, 23, 787-793.e6.

- FUNGHI, L., DAMIANI, F., YEN, C. F., LEE, C. L., LOMBARDI, A., SCHATZ, F., LOCKWOOD, C. J., MARCOLONGO, P., PETRAGLIA, F. & ARCURI, F. 2016. Expression and regulation of 11 β -hydroxysteroid dehydrogenase type 1 in first trimester human decidua cells: Implication in preeclampsia. *Mol Cell Endocrinol*, 437, 163-170.
- FYHRQUIST, F. & SAIJONMAA, O. 2008. Renin-angiotensin system revisited. *Journal of Internal Medicine*, 264, 224-236.
- GALE, C., QUIGLEY, M. A., PLACZEK, A., KNIGHT, M., LADHANI, S., DRAPER, E. S., SHARKEY, D., DOHERTY, C., MACTIER, H. & KURINCZUK, J. J. 2021. Characteristics and outcomes of neonatal SARS-CoV-2 infection in the UK: a prospective national cohort study using active surveillance. *Lancet Child Adolesc Health*, 5, 113-121.
- GASKELL, H., SHARMA, P., COLLEY, H. E., MURDOCH, C., WILLIAMS, D. P. & WEBB, S. D. 2016. Characterization of a functional C3A liver spheroid model. *Toxicology Research*, 5, 1053-1065.
- GAUDREAU, E., FIOLO, S., OLIVIER, M. & GOSSELIN, J. 2007. Epstein-Barr Virus Induces MCP-1 Secretion by Human Monocytes via TLR2. *Journal of Virology*, 81, 8016-8024.
- GEBRIL, M., HIROTA, Y., AIKAWA, S., FUKUI, Y., KAKU, T., MATSUO, M., HIRATA, T., AKAEDA, S., HIRAOKA, T., SHIMIZU-HIROTA, R., TAKEDA, N., TAHA, T., BALAH, O. A., ELNOURY, M. A. H., FUJII, T. & OSUGA, Y. 2020. Uterine Epithelial Progesterone Receptor Governs Uterine Receptivity Through Epithelial Cell Differentiation. *Endocrinology*, 161.
- GEISERT, R., FAZLEABAS, A., LUCY, M. & MATHEW, D. 2012. Interaction of the conceptus and endometrium to establish pregnancy in mammals: role of interleukin 1 β . *Cell Tissue Res*, 349, 825-38.
- GELLERSEN, B., BROSENS, I. A. & BROSENS, J. J. 2007. Decidualization of the human endometrium: mechanisms, functions, and clinical perspectives. *Semin Reprod Med*, 25, 445-53.
- GELLERSEN, B. & BROSENS, J. 2003. Cyclic AMP and progesterone receptor cross-talk in human endometrium: a decidualizing affair. *J Endocrinol*, 178, 357-72.
- GELLERSEN, B. & BROSENS, J. J. 2014. Cyclic decidualization of the human endometrium in reproductive health and failure. *Endocr Rev*, 35, 851-905.
- GERMAIN, S. J., SACKS, G. P., SOORANA, S. R., SARGENT, I. L. & REDMAN, C. W. 2007. Systemic Inflammatory Priming in Normal Pregnancy and Preeclampsia: The Role of Circulating Syncytiotrophoblast Microparticles. *The Journal of Immunology*, 178, 5949-5956.
- GHEBLAWI, M., WANG, K., VIVEIROS, A., NGUYEN, Q., ZHONG, J. C., TURNER, A. J., RAIZADA, M. K., GRANT, M. B. & OUDIT, G. Y. 2020. Angiotensin-Converting Enzyme 2: SARS-CoV-2 Receptor and Regulator of the Renin-Angiotensin System: Celebrating the 20th Anniversary of the Discovery of ACE2. *Circ Res*, 126, 1456-1474.

- GHOSH, M., SHEN, Z., SCHAEFER, T. M., FAHEY, J. V., GUPTA, P. & WIRA, C. R. 2009. CCL20/MIP3alpha is a novel anti-HIV-1 molecule of the human female reproductive tract. *Am J Reprod Immunol*, 62, 60-71.
- GHOSH, S., CHATTOPADHYAY, R., GOSWAMI, S., CHAUDHURY, K., CHAKRAVARTY, B. & GANESH, A. 2014. Assessment of sub-endometrial blood flow parameters following dydrogesterone and micronized vaginal progesterone administration in women with idiopathic recurrent miscarriage: a pilot study. *J Obstet Gynaecol Res*, 40, 1871-6.
- GIUDICE, L. C. 1997. Multifaceted Roles for IGFBP-1 in Human Endometrium during Implantation and Pregnancy. *Annals of the New York Academy of Sciences*, 828, 146-156.
- GIUDICE, L. C. 2004. Microarray expression profiling reveals candidate genes for human uterine receptivity. *Am J Pharmacogenomics*, 4, 299-312.
- GLARÍA, E. & VALLEDOR, A. F. 2020. Roles of CD38 in the Immune Response to Infection. *Cells*, 9, 228.
- GLICKLIS, R., MERCHUK, J. C. & COHEN, S. 2004. Modeling mass transfer in hepatocyte spheroids via cell viability, spheroid size, and hepatocellular functions. *Biotechnol Bioeng*, 86, 672-80.
- GONCU AYHAN, S., OLUKLU, D., ATALAY, A., MENEKSE BESER, D., TANACAN, A., MORALOGU TEKIN, O. & SAHIN, D. 2021. COVID-19 vaccine acceptance in pregnant women. *Int J Gynaecol Obstet*, 154, 291-296.
- GONG, X., LIN, C., CHENG, J., SU, J., ZHAO, H., LIU, T., WEN, X. & ZHAO, P. 2015. Generation of Multicellular Tumor Spheroids with Microwell-Based Agarose Scaffolds for Drug Testing. *PLOS ONE*, 10, e0130348.
- GRAEPEL, K. W., LU, X., CASE, J. B., SEXTON, N. R., SMITH, E. C. & DENISON, M. R. 2017. Proofreading-Deficient Coronaviruses Adapt for Increased Fitness over Long-Term Passage without Reversion of Exoribonuclease-Inactivating Mutations. *mBio*, 8.
- GRANNE, I., SOUTHCOMBE, J. H., SNIDER, J. V., TANNETTA, D. S., CHILD, T., REDMAN, C. W. & SARGENT, I. L. 2011. ST2 and IL-33 in pregnancy and pre-eclampsia. *PLoS One*, 6, e24463.
- GRAVANIS, A., STOURNARAS, C. & MARGIORIS, A. N. 1999. Paracrinology of endometrial neuropeptides: corticotropin-releasing hormone and opioids. *Semin Reprod Endocrinol*, 17, 29-38.
- GRAY, C. A., BARTOL, F. F., TARLETON, B. J., WILEY, A. A., JOHNSON, G. A., BAZER, F. W. & SPENCER, T. E. 2001. Developmental Biology of Uterine Glands1. *Biology of Reproduction*, 65, 1311-1323.
- GRAZZINI, E., GUILLON, G., MOUILLAC, B. & ZINGG, H. H. 1998. Inhibition of oxytocin receptor function by direct binding of progesterone. *Nature*, 392, 509-12.
- GREWAL, S., CARVER, J., RIDLEY, A. J. & MARDON, H. J. 2010. Human endometrial stromal cell rho GTPases have opposing roles in regulating focal adhesion turnover and embryo invasion in vitro. *Biol Reprod*, 83, 75-82.
- GREWAL, S., CARVER, J. G., RIDLEY, A. J. & MARDON, H. J. 2008. Implantation of the human embryo requires Rac1-dependent endometrial stromal cell migration. *Proc Natl Acad Sci U S A*, 105, 16189-94.

- GRIFFITH, L. G. & SWARTZ, M. A. 2006. Capturing complex 3D tissue physiology in vitro. *Nat Rev Mol Cell Biol*, 7, 211-24.
- GRINDHEIM, G., ESTENSEN, M.-E., LANGESAETER, E., ROSSELAND, L. A. & TOSKA, K. 2012. Changes in blood pressure during healthy pregnancy: a longitudinal cohort study. *Journal of Hypertension*, 30, 342-350.
- GROEBE, K. & MUELLER-KLIESER, W. 1996. On the relation between size of necrosis and diameter of tumor spheroids. *International journal of radiation oncology, biology, physics*, 34, 395-401.
- GUAN, W. J., NI, Z. Y., HU, Y., LIANG, W. H., OU, C. Q., HE, J. X., LIU, L., SHAN, H., LEI, C. L., HUI, D. S. C., DU, B., LI, L. J., ZENG, G., YUEN, K. Y., CHEN, R. C., TANG, C. L., WANG, T., CHEN, P. Y., XIANG, J., LI, S. Y., WANG, J. L., LIANG, Z. J., PENG, Y. X., WEI, L., LIU, Y., HU, Y. H., PENG, P., WANG, J. M., LIU, J. Y., CHEN, Z., LI, G., ZHENG, Z. J., QIU, S. Q., LUO, J., YE, C. J., ZHU, S. Y. & ZHONG, N. S. 2020. Clinical Characteristics of Coronavirus Disease 2019 in China. *N Engl J Med*, 382, 1708-1720.
- GUESDON, W., AURAY, G., PEZIER, T., BUSSIÈRE, F. I., DROUET, F., LE VERN, Y., MARQUIS, M., POTIRON, L., RABOT, S., BRUNEAU, A., WERTS, C., LAURENT, F. & LACROIX-LAMANDÉ, S. 2015. CCL20 Displays Antimicrobial Activity Against *Cryptosporidium parvum*, but Its Expression Is Reduced During Infection in the Intestine of Neonatal Mice. *The Journal of Infectious Diseases*, 212, 1332-1340.
- GUNAY, G., KIRIT, H. A., KAMATAR, A., BAGHDASARYAN, O., HAMSICI, S. & ACAR, H. 2020. The effects of size and shape of the ovarian cancer spheroids on the drug resistance and migration. *Gynecologic Oncology*, 159, 563-572.
- GUZELOGLU-KAYISLI, O., KAYISLI, U. A., SEMERCI, N., BASAR, M., BUCHWALDER, L. F., BUHIMSCHI, C. S., BUHIMSCHI, I. A., ARCURI, F., LARSEN, K., HUANG, J. S., SCHATZ, F. & LOCKWOOD, C. J. 2015. Mechanisms of chorioamnionitis-associated preterm birth: interleukin-1 β inhibits progesterone receptor expression in decidual cells. *J Pathol*, 237, 423-34.
- HACKAM, D. G. & REDELMEIER, D. A. 2006. Translation of Research Evidence From Animals to Humans. *JAMA*, 296, 1727-1732.
- HACKENTHAL, E., PAUL, M., GANTEN, D. & TAUGNER, R. 1990. Morphology, physiology, and molecular biology of renin secretion. *Physiological Reviews*, 70, 1067-1116.
- HADDAD, S. N. & WIRA, C. R. 2014. Estradiol regulation of constitutive and keratinocyte growth factor-induced CCL20 and CXCL1 secretion by mouse uterine epithelial cells. *Am J Reprod Immunol*, 72, 34-44.
- HAEGER, J. D., HAMBRUCH, N., DANTZER, V., HOELKER, M., SCHELLANDER, K., KLISCH, K. & PFARRER, C. 2015. Changes in endometrial ezrin and cytokeratin 18 expression during bovine implantation and in caruncular endometrial spheroids in vitro. *Placenta*, 36, 821-831.

- HAFNER, L. M., CUNNINGHAM, K. & BEAGLEY, K. W. 2013. Ovarian steroid hormones: effects on immune responses and Chlamydia trachomatis infections of the female genital tract. *Mucosal Immunol*, 6, 859-75.
- HAGEMANN, A., NIELSEN, A. H. & POULSEN, K. 1994. The uteroplacental renin-angiotensin system: a review. *Exp Clin Endocrinol*, 102, 252-61.
- HAGMAN, K., HEDENSTIERNA, M., RUDLING, J., GILLE-JOHNSON, P., HAMMAS, B., GRABBE, M., JAKOBSSON, J., DILLNER, J. & URSING, J. 2022. Duration of SARS-CoV-2 viremia and its correlation to mortality and inflammatory parameters in patients hospitalized for COVID-19: a cohort study. *Diagnostic Microbiology and Infectious Disease*, 102, 115595.
- HALPIN, S. J., MCIVOR, C., WHYATT, G., ADAMS, A., HARVEY, O., MCLEAN, L., WALSHAW, C., KEMP, S., CORRADO, J., SINGH, R., COLLINS, T., O'CONNOR, R. J. & SIVAN, M. 2021. Postdischarge symptoms and rehabilitation needs in survivors of COVID-19 infection: A cross-sectional evaluation. *J Med Virol*, 93, 1013-1022.
- HAMMING, I., COOPER, M. E., HAAGMANS, B. L., HOOPER, N. M., KORSTANJE, R., OSTERHAUS, A. D., TIMENS, W., TURNER, A. J., NAVIS, G. & VAN GOOR, H. 2007. The emerging role of ACE2 in physiology and disease. *J Pathol*, 212, 1-11.
- HAMMING, I., TIMENS, W., BULTHUIS, M. L., LELY, A. T., NAVIS, G. & VAN GOOR, H. 2004. Tissue distribution of ACE2 protein, the functional receptor for SARS coronavirus. A first step in understanding SARS pathogenesis. *J Pathol*, 203, 631-7.
- HAN, Y., DUAN, X., YANG, L., NILSSON-PAYANT, B. E., WANG, P., DUAN, F., TANG, X., YARON, T. M., ZHANG, T., UHL, S., BRAM, Y., RICHARDSON, C., ZHU, J., ZHAO, Z., REDMOND, D., HOUGHTON, S., NGUYEN, D. T., XU, D., WANG, X., JESSURUN, J., BORCZUK, A., HUANG, Y., JOHNSON, J. L., LIU, Y., XIANG, J., WANG, H., CANTLEY, L. C., TENOEVER, B. R., HO, D. D., PAN, F. C., EVANS, T., CHEN, H. J., SCHWARTZ, R. E. & CHEN, S. 2021. Identification of SARS-CoV-2 inhibitors using lung and colonic organoids. *Nature*, 589, 270-275.
- HANEDA, S., NAGAOKA, K., NAMBO, Y., KIKUCHI, M., NAKANO, Y., LI, J., MATSUI, M., MIYAKE, Y.-I. & IMAKAWA, K. 2017. Expression of uterine lipocalin 2 and its receptor during early- to mid-pregnancy period in mares. *Journal of Reproduction and Development*, 63, 127-133.
- HARADA, A., SEKIDO, N., AKAHOSHI, T., WADA, T., MUKAIDA, N. & MATSUSHIMA, K. 1994. Essential involvement of interleukin-8 (IL-8) in acute inflammation. *J Leukoc Biol*, 56, 559-64.
- HARRISON, A. G., LIN, T. & WANG, P. 2020. Mechanisms of SARS-CoV-2 Transmission and Pathogenesis. *Trends in immunology*, 41, 1100-1115.
- HAYES, M., QUINN, B., LILLIE, B., CÔTÉ, O., BIENZLE, D., WAELCHLI, R. & BETTERIDGE, K. 2018. Changes in various endometrial proteins during cloprostenol-induced failure of early pregnancy in mares. *Animal Reproduction (AR)*, 9, 723-741.
- HE, Y.-Y., DU, M.-R., GUO, P.-F., HE, X.-J., ZHOU, W.-H., ZHU, X.-Y. & LI, D.-J. 2007. Regulation of C-C motif chemokine ligand 2 and its receptor in

- human decidual stromal cells by pregnancy-associated hormones in early gestation. *Human Reproduction*, 22, 2733-2742.
- HECHT, J. L., QUADE, B., DESHPANDE, V., MINO-KENUDSON, M., TING, D. T., DESAI, N., DYGULSKA, B., HEYMAN, T., SALAFIA, C., SHEN, D., BATES, S. V. & ROBERTS, D. J. 2020. SARS-CoV-2 can infect the placenta and is not associated with specific placental histopathology: a series of 19 placentas from COVID-19-positive mothers. *Mod Pathol*, 33, 2092-2103.
- HEISS, M., HELLSTRÖM, M., KALÉN, M., MAY, T., WEBER, H., HECKER, M., AUGUSTIN, H. G. & KORFF, T. 2015. Endothelial cell spheroids as a versatile tool to study angiogenesis in vitro. *Faseb j*, 29, 3076-84.
- HEIT, J. A., KOBBERVIG, C. E., JAMES, A. H., PETTERSON, T. M., BAILEY, K. R. & MELTON, L. J., 3RD 2005. Trends in the incidence of venous thromboembolism during pregnancy or postpartum: a 30-year population-based study. *Ann Intern Med*, 143, 697-706.
- HENAREJOS-CASTILLO, I., SEBASTIAN-LEON, P., DEVESA-PEIRO, A., PELLICER, A. & DIAZ-GIMENO, P. 2020. SARS-CoV-2 infection risk assessment in the endometrium: viral infection-related gene expression across the menstrual cycle. *Fertil Steril*, 114, 223-232.
- HENNIGHAUSEN, L. & LEE, H. K. 2020. Activation of the SARS-CoV-2 Receptor Ace2 through JAK/STAT-Dependent Enhancers during Pregnancy. *Cell Rep*, 32, 108199.
- HENRIQUEZ, S., ZERBIT, J., BRUEL, T., OUEDRANI, A., PLANAS, D., DESCHAMPS, P., STAROPOLI, I., HADJADJ, J., VARET, B., ERMAK, N., BOUSCARY, D., WILLEMS, L., FOUQUET, G., DECROOCCQ, J., FRANCHI, P., DEAU-FISCHER, B., TERRIER, B., TAMBURINI, J., CHATENOU, L., SCHWARTZ, O. & VIGNON, M. 2022. Anti-CD38 therapy impairs SARS-CoV-2 vaccine response against alpha and delta variants in patients with multiple myeloma. *Blood*, 139, 942-946.
- HERR, D., BEKES, I. & WULFF, C. 2013. Local Renin-Angiotensin system in the reproductive system. *Front Endocrinol (Lausanne)*, 4, 150.
- HIERWEGER, A. M., ENGLER, J. B., FRIESE, M. A., REICHARDT, H. M., LYDON, J., DEMAYO, F., MITTRÜCKER, H. W. & ARCK, P. C. 2019. Progesterone modulates the T-cell response via glucocorticoid receptor-dependent pathways. *Am J Reprod Immunol*, 81, e13084.
- HOFFMANN, M., KLEINE-WEBER, H., SCHROEDER, S., KRÜGER, N., HERRLER, T., ERICHSEN, S., SCHIERGENS, T. S., HERRLER, G., WU, N. H., NITSCHKE, A., MÜLLER, M. A., DROSTEN, C. & PÖHLMANN, S. 2020. SARS-CoV-2 Cell Entry Depends on ACE2 and TMPRSS2 and Is Blocked by a Clinically Proven Protease Inhibitor. *Cell*, 181, 271-280.e8.
- HOLMBERG, J. C., HADDAD, S., WÜNSCHE, V., YANG, Y., ALDO, P. B., GNAINSKY, Y., GRANOT, I., DEKEL, N. & MOR, G. 2012. An in vitro model for the study of human implantation. *Am J Reprod Immunol*, 67, 169-78.
- HU, B., GUO, H., ZHOU, P. & SHI, Z. L. 2021. Characteristics of SARS-CoV-2 and COVID-19. *Nat Rev Microbiol*, 19, 141-154.

- HUANG, C., WANG, Y., LI, X., REN, L., ZHAO, J., HU, Y., ZHANG, L., FAN, G., XU, J., GU, X., CHENG, Z., YU, T., XIA, J., WEI, Y., WU, W., XIE, X., YIN, W., LI, H., LIU, M., XIAO, Y., GAO, H., GUO, L., XIE, J., WANG, G., JIANG, R., GAO, Z., JIN, Q., WANG, J. & CAO, B. 2020. Clinical features of patients infected with 2019 novel coronavirus in Wuhan, China. *Lancet*, 395, 497-506.
- HUGHES, B. L. & GYAMFI-BANNERMAN, C. 2016. Diagnosis and antenatal management of congenital cytomegalovirus infection. *Am J Obstet Gynecol*, 214, B5-b11.
- INABA, T., WIEST, W. G., STRICKLER, R. C. & MORI, J. 1988. Augmentation of the Response of Mouse Uterine Epithelial Cells to Estradiol by Uterine Stroma. *Endocrinology*, 123, 1253-1258.
- IRANI, R. A. & XIA, Y. 2008. The functional role of the renin-angiotensin system in pregnancy and preeclampsia. *Placenta*, 29, 763-71.
- IRANI, R. A. & XIA, Y. 2011. Renin angiotensin signaling in normal pregnancy and preeclampsia. *Semin Nephrol*, 31, 47-58.
- IVASCU, A. & KUBBIES, M. 2007. Diversity of cell-mediated adhesions in breast cancer spheroids. *Int J Oncol*, 31, 1403-13.
- IVASKA, J., PALLARI, H.-M., NEVO, J. & ERIKSSON, J. E. 2007. Novel functions of vimentin in cell adhesion, migration, and signaling. *Experimental Cell Research*, 313, 2050-2062.
- JABBOUR, H. N. & CRITCHLEY, H. O. 2001. Potential roles of decidual prolactin in early pregnancy. *Reproduction*, 121, 197-205.
- JABBOUR, H. N., CRITCHLEY, H. O. & BODDY, S. C. 1998. Expression of functional prolactin receptors in nonpregnant human endometrium: janus kinase-2, signal transducer and activator of transcription-1 (STAT1), and STAT5 proteins are phosphorylated after stimulation with prolactin. *J Clin Endocrinol Metab*, 83, 2545-53.
- JACOBS, J. L., BAIN, W., NAQVI, A., STAINES, B., CASTANHA, P. M. S., YANG, H., BOLTZ, V. F., BARRATT-BOYES, S., MARQUES, E. T. A., MITCHELL, S. L., METHÉ, B., OLONISAKIN, T. F., HAIDAR, G., BURKE, T. W., PETZOLD, E., DENNY, T., WOODS, C. W., MCVERRY, B. J., LEE, J. S., WATKINS, S. C., ST CROIX, C. M., MORRIS, A., KEARNEY, M. F., LADINSKY, M. S., BJORKMAN, P. J., KITSIOS, G. D. & MELLORS, J. W. 2022. Severe Acute Respiratory Syndrome Coronavirus 2 Viremia Is Associated With Coronavirus Disease 2019 Severity and Predicts Clinical Outcomes. *Clin Infect Dis*, 74, 1525-1533.
- JANAKIRAM, M., SHAH, U. A., LIU, W., ZHAO, A., SCHOENBERG, M. P. & ZANG, X. 2017. The third group of the B7-CD28 immune checkpoint family: HHLA2, TMIGD2, B7x, and B7-H3. *Immunol Rev*, 276, 26-39.
- JANKOWSKI, J., LEE, H. K., WILFLINGSIEDER, J. & HENNIGHAUSEN, L. 2021. JAK inhibitors dampen activation of interferon-activated transcriptomes and the SARS-CoV-2 receptor ACE2 in human renal proximal tubules. *iScience*, 24, 102928.
- JASSAT, W., ABDOL KARIM, S. S., MUDARA, C., WELCH, R., OZOUGWU, L., GROOME, M. J., GOVENDER, N., VON GOTTBURG, A., WOLTER, N., WOLMARANS, M., ROUSSEAU, P., BLUMBERG, L. & COHEN, C. 2022. Clinical severity of COVID-19 in patients admitted to hospital

- during the omicron wave in South Africa: a retrospective observational study. *Lancet Glob Health*.
- JENSEN, C. & TENG, Y. 2020. Is It Time to Start Transitioning From 2D to 3D Cell Culture? *Front Mol Biosci*, 7, 33.
- JENSEN, M. E., ROBIJN, A. L., GIBSON, P. G., OLDMEADOW, C. & MURPHY, V. E. 2021. Longitudinal Analysis of Lung Function in Pregnant Women with and without Asthma. *J Allergy Clin Immunol Pract*, 9, 1578-1585.e3.
- JIA, H. P., LOOK, D. C., HICKEY, M., SHI, L., PEWE, L., NETLAND, J., FARZAN, M., WOHLFORD-LENANE, C., PERLMAN, S. & MCCRAY, P. B., JR. 2006. Infection of human airway epithelia by SARS coronavirus is associated with ACE2 expression and localization. *Adv Exp Med Biol*, 581, 479-84.
- JIANG, Y., FENG, Y.-P., TANG, L.-X., YAN, Y.-L. & BAI, J.-W. 2019. The protective role of NR4A3 in acute myocardial infarction by suppressing inflammatory responses via JAK2-STAT3/NF- κ B pathway. *Biochemical and Biophysical Research Communications*, 517, 697-702.
- JIANG, Y., JIANG, R., CHENG, X., ZHANG, Q., HU, Y., ZHANG, H., CAO, Y., ZHANG, M., WANG, J., DING, L., DIAO, Z., SUN, H. & YAN, G. 2016. Decreased expression of NR4A nuclear receptors in adenomyosis impairs endometrial decidualization. *Molecular Human Reproduction*, 22, 655-668.
- JIKIHARA, H., KESSLER, C. A., CEDARS, M. I. & BRAR, A. K. 1996. Up-regulation of the human prolactin receptor in the endometrium. *Endocrine*, 5, 157-62.
- JONES, R. L., CRITCHLEY, H. O. D., BROOKS, J., JABBOUR, H. N. & MCNEILLY, A. S. 1998. Localization and Temporal Expression of Prolactin Receptor in Human Endometrium. *The Journal of Clinical Endocrinology & Metabolism*, 83, 258-262.
- JUAN, J., GIL, M. M., RONG, Z., ZHANG, Y., YANG, H. & POON, L. C. 2020. Effect of coronavirus disease 2019 (COVID-19) on maternal, perinatal and neonatal outcome: systematic review. *Ultrasound Obstet Gynecol*, 56, 15-27.
- JULKUNEN, I., MELÉN, K., NYQVIST, M., PIRHONEN, J., SARENEVA, T. & MATIKAINEN, S. 2000. Inflammatory responses in influenza A virus infection. *Vaccine*, 19, S32-S37.
- KAITU'U-LINO, T. J., TUOHEY, L. & TONG, S. 2012. Maternal serum interleukin-33 and soluble ST2 across early pregnancy, and their association with miscarriage. *J Reprod Immunol*, 95, 46-9.
- KAMIMURA, Y., KOBORI, H., PIAO, J., HASHIGUCHI, M., MATSUMOTO, K., HIROSE, S. & AZUMA, M. 2009. Possible involvement of soluble B7-H4 in T cell-mediated inflammatory immune responses. *Biochem Biophys Res Commun*, 389, 349-53.
- KANG, J., PARK, K.-H., KIM, J.-J., JO, E.-K., HAN, M.-K. & KIM, U.-H. 2012. The Role of CD38 in Fc γ Receptor (Fc γ)-mediated Phagocytosis in Murine Macrophages. *Journal of Biological Chemistry*, 287, 14502-14514.

- KAR, A., MEHROTRA, S. & CHATTERJEE, S. 2020. CD38: T Cell Immuno-Metabolic Modulator. *Cells*, 9, 1716.
- KARIMI-ZARCHI, M., NEAMATZADEH, H., DASTGHEIB, S. A., ABBASI, H., MIRJALILI, S. R., BEHFOROZ, A., FERDOSIAN, F. & BAHRAMI, R. 2020. Vertical Transmission of Coronavirus Disease 19 (COVID-19) from Infected Pregnant Mothers to Neonates: A Review. *Fetal Pediatr Pathol*, 39, 246-250.
- KARKI, R., SHARMA, B. R., TULADHAR, S., WILLIAMS, E. P., ZALDUONDO, L., SAMIR, P., ZHENG, M., SUNDARAM, B., BANOTH, B., MALIREDDI, R. K. S., SCHREINER, P., NEALE, G., VOGEL, P., WEBBY, R., JONSSON, C. B. & KANNEGANTI, T. D. 2021. Synergism of TNF- α and IFN- γ Triggers Inflammatory Cell Death, Tissue Damage, and Mortality in SARS-CoV-2 Infection and Cytokine Shock Syndromes. *Cell*, 184, 149-168.e17.
- KARLSEN, J. R., BORREGAARD, N. & COWLAND, J. B. 2010. Induction of neutrophil gelatinase-associated lipocalin expression by co-stimulation with interleukin-17 and tumor necrosis factor-alpha is controlled by I κ B-zeta but neither by C/EBP-beta nor C/EBP-delta. *J Biol Chem*, 285, 14088-100.
- KASVANDIK, S., SAARMA, M., KAART, T., ROODA, I., VELTHUT-MEIKAS, A., EHRENBERG, A., GEMZELL, K., LALITKUMAR, P. G., SALUMETS, A. & PETERS, M. 2019. Uterine Fluid Proteins for Minimally Invasive Assessment of Endometrial Receptivity. *The Journal of Clinical Endocrinology & Metabolism*, 105, 219-230.
- KEAM, S., MEGAWATI, D., PATEL, S. K., TIWARI, R., DHAMA, K. & HARAPAN, H. 2020. Immunopathology and immunotherapeutic strategies in severe acute respiratory syndrome coronavirus 2 infection. *Rev Med Virol*, 30, e2123.
- KHANMOHAMMADI, S. & REZAEI, N. 2021. Role of Toll-like receptors in the pathogenesis of COVID-19. *J Med Virol*, 93, 2735-2739.
- KIENHORST, L. B., VAN LOCHEM, E., KIEVIT, W., DALBETH, N., MERRIMAN, M. E., PHIPPS-GREEN, A., LOOF, A., VAN HEERDE, W., VERMEULEN, S., STAMP, L. K., VAN KOOLWIJK, E., DE GRAAF, J., HOLZINGER, D., ROTH, J., JANSSENS, H. J., MERRIMAN, T. R., BROEN, J. C., JANSSEN, M. & RADSTAKE, T. R. 2015. Gout Is a Chronic Inflammatory Disease in Which High Levels of Interleukin-8 (CXCL8), Myeloid-Related Protein 8/Myeloid-Related Protein 14 Complex, and an Altered Proteome Are Associated With Diabetes Mellitus and Cardiovascular Disease. *Arthritis Rheumatol*, 67, 3303-13.
- KIM, J., KOO, B. K. & KNOBLICH, J. A. 2020. Human organoids: model systems for human biology and medicine. *Nat Rev Mol Cell Biol*, 21, 571-584.
- KIM, J. J., KURITA, T. & BULUN, S. E. 2013. Progesterone Action in Endometrial Cancer, Endometriosis, Uterine Fibroids, and Breast Cancer. *Endocrine Reviews*, 34, 130-162.
- KIM, M. R., PARK, D. W., LEE, J. H., CHOI, D. S., HWANG, K. J., RYU, H. S. & MIN, C. K. 2006. Progesterone-dependent release of transforming growth factor-beta1 from epithelial cells enhances the endometrial

- decidualization by turning on the Smad signalling in stromal cells. *Molecular Human Reproduction*, 11, 801-808.
- KIMBER, S. J. 2000. Molecular interactions at the maternal-embryonic interface during the early phase of implantation. *Semin Reprod Med*, 18, 237-53.
- KIMBERLIN, D. W. & STAGNO, S. 2020. Can SARS-CoV-2 Infection Be Acquired In Utero?: More Definitive Evidence Is Needed. *Jama*, 323, 1788-1789.
- KIMURA, H., SAKAI, Y. & FUJII, T. 2018. Organ/body-on-a-chip based on microfluidic technology for drug discovery. *Drug Metab Pharmacokinet*, 33, 43-48.
- KING, A. E. & CRITCHLEY, H. O. D. 2010. Oestrogen and progesterone regulation of inflammatory processes in the human endometrium. *The Journal of Steroid Biochemistry and Molecular Biology*, 120, 116-126.
- KLEIN, S. L. & FLANAGAN, K. L. 2016. Sex differences in immune responses. *Nat Rev Immunol*, 16, 626-38.
- KLEINMAN, H. K., PHILP, D. & HOFFMAN, M. P. 2003. Role of the extracellular matrix in morphogenesis. *Curr Opin Biotechnol*, 14, 526-32.
- KOHLHEPP, L. M., HOLLERICH, G., VO, L., HOFMANN-KIEFER, K., REHM, M., LOUWEN, F., ZACHAROWSKI, K. & WEBER, C. F. 2018. [Physiological changes during pregnancy]. *Anaesthesist*, 67, 383-396.
- KOLEDOVA, Z. 2017. 3D Coculture of Mammary Organoids with Fibrospheres: A Model for Studying Epithelial–Stromal Interactions During Mammary Branching Morphogenesis. In: KOLEDOVA, Z. (ed.) *3D Cell Culture: Methods and Protocols*. New York, NY: Springer New York.
- KONSTANTAKOU, P., MASTORAKOS, G., VRACHNIS, N., TOMLINSON, J. W. & VALSAMAKIS, G. 2017. Dysregulation of 11beta-hydroxysteroid dehydrogenases: implications during pregnancy and beyond. *J Matern Fetal Neonatal Med*, 30, 284-293.
- KOOT, Y. E., TEKLENBURG, G., SALKER, M. S., BROSENS, J. J. & MACKLON, N. S. 2012. Molecular aspects of implantation failure. *Biochim Biophys Acta*, 1822, 1943-50.
- KUHN, N., KLINGER, B., UHLITZ, F., SIEBER, A., RIVERA, M., KLOTZ-NOACK, K., FICHTNER, I., HOFFMANN, J., BLÜTHGEN, N., FALK, C., SERS, C. & SCHÄFER, R. 2021. Mutation-specific effects of NRAS oncogenes in colorectal cancer cells. *Advances in Biological Regulation*, 79, 100778.
- KUMAR, S. V., ER, P. X., LAWLOR, K. T., MOTAZEDIAN, A., SCURR, M., GHOBRIAL, I., COMBES, A. N., ZAPPIA, L., OSHLACK, A., STANLEY, E. G. & LITTLE, M. H. 2019. Kidney micro-organoids in suspension culture as a scalable source of human pluripotent stem cell-derived kidney cells. *Development*, 146.
- KURITA, T., YOUNG, P., BRODY, J. R., LYDON, J. P., O'MALLEY, B. W. & CUNHA, G. R. 1998. Stromal progesterone receptors mediate the inhibitory effects of progesterone on estrogen-induced uterine epithelial cell deoxyribonucleic acid synthesis. *Endocrinology*, 139, 4708-13.
- KURODA, K., VENKATAKRISHNAN, R., SALKER, M. S., LUCAS, E. S., SHAHEEN, F., KURODA, M., BLANKS, A., CHRISTIAN, M., QUENBY, S. & BROSENS, J. J. 2013. Induction of 11β-HSD 1 and activation of

- distinct mineralocorticoid receptor- and glucocorticoid receptor-dependent gene networks in decidualizing human endometrial stromal cells. *Mol Endocrinol*, 27, 192-202.
- KWANTWI, L. B., WANG, S., ZHANG, W., PENG, W., CAI, Z., SHENG, Y., XIAO, H., WANG, X. & WU, Q. 2021. Tumor-associated neutrophils activated by tumor-derived CCL20 (C-C motif chemokine ligand 20) promote T cell immunosuppression via programmed death-ligand 1 (PD-L1) in breast cancer. *Bioengineered*, 12, 6996-7006.
- KYFFIN, J. A., COX, C. R., LEEDALE, J., COLLEY, H. E., MURDOCH, C., MISTRY, P., WEBB, S. D. & SHARMA, P. 2019. Preparation of Primary Rat Hepatocyte Spheroids Utilizing the Liquid-Overlay Technique. *Curr Protoc Toxicol*, 81, e87.
- LA MANNA, G., GHINATTI, G., TAZZARI, P. L., ALVIANO, F., RICCI, F., CAPELLI, I., CUNA, V., TODESCHINI, P., BRUNOCILLA, E., PAGLIARO, P., BONSI, L. & STEFONI, S. 2014. Neutrophil Gelatinase-Associated Lipocalin Increases HLA-G+/FoxP3+ T-Regulatory Cell Population in an In Vitro Model of PBMC. *PLOS ONE*, 9, e89497.
- LAI, C. C., KO, W. C., LEE, P. I., JEAN, S. S. & HSUEH, P. R. 2020. Extra-respiratory manifestations of COVID-19. *Int J Antimicrob Agents*, 56, 106024.
- LAMONT, R. F., SOBEL, J. D., VAISBUCH, E., KUSANOVIC, J. P., MAZAKITTOVI, S., KIM, S. K., ULDBJERG, N. & ROMERO, R. 2011. Parvovirus B19 infection in human pregnancy. *Bjog*, 118, 175-86.
- LANCASTER, M. A. & KNOBLICH, J. A. 2014. Organogenesis in a dish: modeling development and disease using organoid technologies. *Science*, 345, 1247125.
- LASCHKE, M. W. & MENGER, M. D. 2017. Life is 3D: Boosting Spheroid Function for Tissue Engineering. *Trends in Biotechnology*, 35, 133-144.
- LAUER, S. A., GRANTZ, K. H., BI, Q., JONES, F. K., ZHENG, Q., MEREDITH, H. R., AZMAN, A. S., REICH, N. G. & LESSLER, J. 2020. The Incubation Period of Coronavirus Disease 2019 (COVID-19) From Publicly Reported Confirmed Cases: Estimation and Application. *Ann Intern Med*, 172, 577-582.
- LE ROUX, S. M., DONALD, K. A., KROON, M., PHILLIPS, T. K., LESOSKY, M., ESTERHUYSE, L., ZERBE, A., BRITAIN, K., ABRAMS, E. J. & MYER, L. 2019. HIV Viremia During Pregnancy and Neurodevelopment of HIV-Exposed Uninfected Children in the Context of Universal Antiretroviral Therapy and Breastfeeding: A Prospective Study. *Pediatr Infect Dis J*, 38, 70-75.
- LEE, S. Y., CHIEN, D. K., HUANG, C. H., SHIH, S. C., LEE, W. C. & CHANG, W. H. 2017. Dyspnea in pregnancy. *Taiwan J Obstet Gynecol*, 56, 432-436.
- LEEMAN, K. T., PESSINA, P., LEE, J. H. & KIM, C. F. 2019. Mesenchymal Stem Cells Increase Alveolar Differentiation in Lung Progenitor Organoid Cultures. *Sci Rep*, 9, 6479.
- LEROY, F. & LEJEUNE, B. 1981. The Uterine Epithelium as a Transducer for the Triggering of Decidualization in the Rat. *In: GLASSER, S. R. &*

- BULLOCK, D. W. (eds.) *Cellular and Molecular Aspects of Implantation*. Boston, MA: Springer US.
- LEVY, A., YAGIL, Y., BURSZTYN, M., BARKALIFA, R., SCHARF, S. & YAGIL, C. 2008. ACE2 expression and activity are enhanced during pregnancy. *Am J Physiol Regul Integr Comp Physiol*, 295, R1953-61.
- LI, H., LI, H., BAI, L. & YU, H. 2014. Lefty inhibits in vitro decidualization by regulating P57 and cyclin D1 expressions. *Cell Biochem Funct*, 32, 657-64.
- LI, H.-H., XU, X.-H., TONG, J., ZHANG, K.-Y., ZHANG, C. & CHEN, Z.-J. 2016. Association of TNF- α genetic polymorphisms with recurrent pregnancy loss risk: a systematic review and meta-analysis. *Reproductive Biology and Endocrinology*, 14, 6.
- LI, M., CHEN, L., ZHANG, J., XIONG, C. & LI, X. 2020a. The SARS-CoV-2 receptor ACE2 expression of maternal-fetal interface and fetal organs by single-cell transcriptome study. *PLoS One*, 15, e0230295.
- LI, M. Y., LI, L., ZHANG, Y. & WANG, X. S. 2020b. Expression of the SARS-CoV-2 cell receptor gene ACE2 in a wide variety of human tissues. *Infect Dis Poverty*, 9, 45.
- LI, Q., CHEN, C., KAPADIA, A., ZHOU, Q., HARPER, M. K., SCHAACK, J. & LABARBERA, D. V. 2011a. 3D models of epithelial-mesenchymal transition in breast cancer metastasis: high-throughput screening assay development, validation, and pilot screen. *J Biomol Screen*, 16, 141-54.
- LI, Q., KANNAN, A., DEMAYO, F. J., LYDON, J. P., COOKE, P. S., YAMAGISHI, H., SRIVASTAVA, D., BAGCHI, M. K. & BAGCHI, I. C. 2011b. The antiproliferative action of progesterone in uterine epithelium is mediated by Hand2. *Science*, 331, 912-6.
- LI, W., MOORE, M. J., VASILIEVA, N., SUI, J., WONG, S. K., BERNE, M. A., SOMASUNDARAN, M., SULLIVAN, J. L., LUZURIAGA, K., GREENOUGH, T. C., CHOE, H. & FARZAN, M. 2003. Angiotensin-converting enzyme 2 is a functional receptor for the SARS coronavirus. *Nature*, 426, 450-4.
- LI, X., LI, C., WANG, Y., CAI, J., ZHAO, L., SU, Z. & YE, H. 2022. IGFBP1 inhibits the invasion, migration, and apoptosis of HTR-8/SVneo trophoblast cells in preeclampsia. *Hypertens Pregnancy*, 41, 53-63.
- LI, X. F. & AHMED, A. 1996. Dual role of angiotensin II in the human endometrium. *Hum Reprod*, 11 Suppl 2, 95-108.
- LI, Y., SCHNEIDER, A. M., MEHTA, A., SADE-FELDMAN, M., KAYS, K. R., GENTILI, M., CHARLAND, N. C., GONYE, A. L., GUSHTEROVA, I., KHANNA, H. K., LASALLE, T. J., LAVIN-PARSONS, K. M., LILLEY, B. M., LODENSTEIN, C. L., MANAKONGTREECHEEP, K., MARGOLIN, J. D., MCKAIG, B. N., PARRY, B. A., ROJAS-LOPEZ, M., RUSSO, B. C., SHARMA, N., TANTIVIT, J., THOMAS, M. F., REGAN, J., FLYNN, J. P., VILLANI, A. C., HACOEN, N., GOLDBERG, M. B., FILBIN, M. R. & LI, J. Z. 2021. SARS-CoV-2 viremia is associated with distinct proteomic pathways and predicts COVID-19 outcomes. *J Clin Invest*, 131.
- LI, Y., YANG, N., CHEN, J., HUANG, X., ZHANG, N., YANG, S., LIU, G. & LIU, G. 2020c. Next-Generation Porcine Intestinal Organoids: an Apical-Out

- Organoid Model for Swine Enteric Virus Infection and Immune Response Investigations. *Journal of virology*, 94, e01006-20.
- LIN, H. X., FENG, Y., WONG, G., WANG, L., LI, B., ZHAO, X., LI, Y., SMAILL, F. & ZHANG, C. 2008. Identification of residues in the receptor-binding domain (RBD) of the spike protein of human coronavirus NL63 that are critical for the RBD-ACE2 receptor interaction. *J Gen Virol*, 89, 1015-1024.
- LIN, R. Z. & CHANG, H. Y. 2008. Recent advances in three-dimensional multicellular spheroid culture for biomedical research. *Biotechnol J*, 3, 1172-84.
- LIN, R. Z., CHOU, L. F., CHIEN, C. C. & CHANG, H. Y. 2006. Dynamic analysis of hepatoma spheroid formation: roles of E-cadherin and beta1-integrin. *Cell Tissue Res*, 324, 411-22.
- LIU, A., RAJA XAVIER, J., SINGH, Y., BRUCKER, S. Y. & SALKER, M. S. 2022. Molecular and Physiological Aspects of SARS-CoV-2 Infection in Women and Pregnancy. *Frontiers in Global Women's Health*, 3.
- LIU, X., LIU, C., LIU, G., LUO, W. & XIA, N. 2020. COVID-19: Progress in diagnostics, therapy and vaccination. *Theranostics*, 10, 7821-7835.
- LIU, Y. & ROCKLÖV, J. 2021. The reproductive number of the Delta variant of SARS-CoV-2 is far higher compared to the ancestral SARS-CoV-2 virus. *Journal of Travel Medicine*, 28.
- LIU, Y. & ROCKLÖV, J. 2022. The effective reproduction number for the omicron SARS-CoV-2 variant of concern is several times higher than Delta. *J Travel Med*.
- LIU, Y. F., DENG, W. B., LI, S. Y., YAO, M. N., LIU, J., DOU, H. T., ZHAO, M. L., YANG, Z. M. & LIANG, X. H. 2016. Progesterone induces the expression of lipocalin-2 through Akt-c-Myc pathway during mouse decidualization. *FEBS Lett*, 590, 2594-602.
- LOWERY, S. A., SARIOL, A. & PERLMAN, S. 2021. Innate immune and inflammatory responses to SARS-CoV-2: Implications for COVID-19. *Cell Host Microbe*, 29, 1052-1062.
- LU, R., ZHAO, X., LI, J., NIU, P., YANG, B., WU, H., WANG, W., SONG, H., HUANG, B., ZHU, N., BI, Y., MA, X., ZHAN, F., WANG, L., HU, T., ZHOU, H., HU, Z., ZHOU, W., ZHAO, L., CHEN, J., MENG, Y., WANG, J., LIN, Y., YUAN, J., XIE, Z., MA, J., LIU, W. J., WANG, D., XU, W., HOLMES, E. C., GAO, G. F., WU, G., CHEN, W., SHI, W. & TAN, W. 2020. Genomic characterisation and epidemiology of 2019 novel coronavirus: implications for virus origins and receptor binding. *Lancet*, 395, 565-574.
- LUNDEQUIST, A., CALOUNOVA, G., WENSMAN, H., RÖNNBERG, E. & PEJLER, G. 2011. Differential regulation of Nr4a subfamily nuclear receptors following mast cell activation. *Molecular Immunology*, 48, 1753-1761.
- LUO, J., LU, S., YU, M., ZHU, L., ZHU, C., LI, C., FANG, J., ZHU, X. & WANG, X. 2021. The potential involvement of JAK-STAT signaling pathway in the COVID-19 infection assisted by ACE2. *Gene*, 768, 145325.
- LUXI, N., GIOVANAZZI, A., CAPUANO, A., CRISAFULLI, S., CUTRONEO, P. M., FANTINI, M. P., FERRAJOLO, C., MORETTI, U., POLUZZI, E.,

- RASCHI, E., RAVALDI, C., RENO, C., TUCCORI, M., VANNACCI, A., ZANONI, G. & TRIFIRÒ, G. 2021. COVID-19 Vaccination in Pregnancy, Paediatrics, Immunocompromised Patients, and Persons with History of Allergy or Prior SARS-CoV-2 Infection: Overview of Current Recommendations and Pre- and Post-Marketing Evidence for Vaccine Efficacy and Safety. *Drug Saf*, 44, 1247-1269.
- LYKKE, J. A., DIDERIKSEN, K. L., LIDEGAARD, Ø. & LANGHOFF-ROOS, J. 2010. First-trimester vaginal bleeding and complications later in pregnancy. *Obstet Gynecol*, 115, 935-944.
- MA, C., PENG, Y., LI, H. & CHEN, W. 2021. Organ-on-a-Chip: A New Paradigm for Drug Development. *Trends Pharmacol Sci*, 42, 119-133.
- MA, C., WU, L., SONG, L., HE, Y., ADEL ABDO MOQBEL, S., YAN, S., SHENG, K., WU, H., RAN, J. & WU, L. 2020. The pro-inflammatory effect of NR4A3 in osteoarthritis. *J Cell Mol Med*, 24, 930-940.
- MACH, P., KÖNINGER, A., REISCH, B., KIMMIG, R. & GELLHAUS, A. 2022. Soluble PD-L1 and B7-H4 serum levels during the course of physiological pregnancy. *Am J Reprod Immunol*, 87, e13519.
- MAGADUM, A. & KISHORE, R. 2020. Cardiovascular Manifestations of COVID-19 Infection. *Cells*, 9.
- MAK, I. Y., BROSENS, J. J., CHRISTIAN, M., HILLS, F. A., CHAMLEY, L., REGAN, L. & WHITE, J. O. 2002. Regulated expression of signal transducer and activator of transcription, Stat5, and its enhancement of PRL expression in human endometrial stromal cells in vitro. *J Clin Endocrinol Metab*, 87, 2581-8.
- MANDRYCKY, C., WANG, Z., KIM, K. & KIM, D. H. 2016. 3D bioprinting for engineering complex tissues. *Biotechnol Adv*, 34, 422-434.
- MAO, R., QIU, Y., HE, J. S., TAN, J. Y., LI, X. H., LIANG, J., SHEN, J., ZHU, L. R., CHEN, Y., IACUCCI, M., NG, S. C., GHOSH, S. & CHEN, M. H. 2020. Manifestations and prognosis of gastrointestinal and liver involvement in patients with COVID-19: a systematic review and meta-analysis. *Lancet Gastroenterol Hepatol*, 5, 667-678.
- MARCINIAK, B., PATRO-MAŁYSZA, J., PONIEDZIAŁEK-CZAJKOWSKA, E., KIMBER-TROJNAR, Z., LESZCZYŃSKA-GORZELAK, B. & OLESZCZUK, J. 2011. Glucocorticoids in pregnancy. *Curr Pharm Biotechnol*, 12, 750-7.
- MARONGE, L. & BOGOD, D. 2018. Complications in obstetric anaesthesia. *Anaesthesia*, 73 Suppl 1, 61-66.
- MARQUES, F. Z., PRINGLE, K. G., CONQUEST, A., HIRST, J. J., MARKUS, M. A., SARRIS, M., ZAKAR, T., MORRIS, B. J. & LUMBERS, E. R. 2011. Molecular characterization of renin-angiotensin system components in human intrauterine tissues and fetal membranes from vaginal delivery and cesarean section. *Placenta*, 32, 214-21.
- MARTÍNEZ-GONZÁLEZ, J., CAÑES, L., ALONSO, J., BALLESTER-SERVERA, C., RODRÍGUEZ-SINOVAS, A., CORRALES, I. & RODRÍGUEZ, C. 2021. NR4A3: A Key Nuclear Receptor in Vascular Biology, Cardiovascular Remodeling, and Beyond. *Int J Mol Sci*, 22.

- MASLAR, I. A. & RIDDICK, D. H. 1979. Prolactin production by human endometrium during the normal menstrual cycle. *American Journal of Obstetrics and Gynecology*, 135, 751-754.
- MATALONGA, J., GLARIA, E., BRESQUE, M., ESCANDE, C., CARBÓ, J. M., KIEFER, K., VICENTE, R., LEÓN, T. E., BECEIRO, S., PASCUAL-GARCÍA, M., SERRET, J., SANJURJO, L., MORÓN-ROS, S., RIERA, A., PAYTUBI, S., JUAREZ, A., SOTILLO, F., LINDBOM, L., CAELLES, C., SARRIAS, M.-R., SANCHO, J., CASTRILLO, A., CHINI, E. N. & VALLEDOR, A. F. 2017. The Nuclear Receptor LXR Limits Bacterial Infection of Host Macrophages through a Mechanism that Impacts Cellular NAD Metabolism. *Cell Reports*, 18, 1241-1255.
- MATEOS, M.-V., CAVO, M., BLADE, J., DIMOPOULOS, M. A., SUZUKI, K., JAKUBOWIAK, A., KNOP, S., DOYEN, C., LUCIO, P., NAGY, Z., POUR, L., COOK, M., GROSICKI, S., CREPALDI, A., LIBERATI, A. M., CAMPBELL, P., SHELEKHOVA, T., YOON, S.-S., IOSAVA, G., FUJISAKI, T., GARG, M., KREVVATA, M., CHEN, Y., WANG, J., KUDVA, A., UKROPEC, J., WROBLEWSKI, S., QI, M., KOBOS, R. & SAN-MIGUEL, J. 2020. Overall survival with daratumumab, bortezomib, melphalan, and prednisone in newly diagnosed multiple myeloma (ALCYONE): a randomised, open-label, phase 3 trial. *The Lancet*, 395, 132-141.
- MAXWELL, A. J., DING, J., YOU, Y., DONG, Z., CHEHADE, H., ALVERO, A., MOR, Y., DRAGHICI, S. & MOR, G. 2021. Identification of key signaling pathways induced by SARS-CoV2 that underlie thrombosis and vascular injury in COVID-19 patients. *J Leukoc Biol*, 109, 35-47.
- MCALOON, C., COLLINS, Á., HUNT, K., BARBER, A., BYRNE, A. W., BUTLER, F., CASEY, M., GRIFFIN, J., LANE, E., MCEVOY, D., WALL, P., GREEN, M., O'GRADY, L. & MORE, S. J. 2020. Incubation period of COVID-19: a rapid systematic review and meta-analysis of observational research. *BMJ Open*, 10, e039652.
- MCCOMB, S., THIRIOT, A., AKACHE, B., KRISHNAN, L. & STARK, F. 2019. Introduction to the Immune System. *Methods Mol Biol*, 2024, 1-24.
- MCDONALD, S. E., HENDERSON, T. A., GOMEZ-SANCHEZ, C. E., CRITCHLEY, H. O. & MASON, J. I. 2006. 11Beta-hydroxysteroid dehydrogenases in human endometrium. *Mol Cell Endocrinol*, 248, 72-8.
- MCMILLAN, K. S., MCCLUSKEY, A. G., SORENSEN, A., BOYD, M. & ZAGNONI, M. 2016. Emulsion technologies for multicellular tumour spheroid radiation assays. *Analyst*, 141, 100-110.
- MELENOTTE, C., SILVIN, A., GOUBET, A. G., LAHMAR, I., DUBUISSON, A., ZUMLA, A., RAOULT, D., MERAD, M., GACHOT, B., HÉNON, C., SOLARY, E., FONTENAY, M., ANDRÉ, F., MAEURER, M., IPPOLITO, G., PIACENTINI, M., WANG, F. S., GINHOUX, F., MARABELLE, A., KROEMER, G., DEROSA, L. & ZITVOGEL, L. 2020. Immune responses during COVID-19 infection. *Oncoimmunology*, 9, 1807836.
- MENO, C., SHIMONO, A., SAIJOH, Y., YASHIRO, K., MOCHIDA, K., OHISHI, S., NOJI, S., KONDOH, H. & HAMADA, H. 1998. lefty-1 is required for left-right determination as a regulator of lefty-2 and nodal. *Cell*, 94, 287-97.

- MERRILL, D. C., KAROLY, M., CHEN, K., FERRARIO, C. M. & BROSNIHAN, K. B. 2002. Angiotensin-(1-7) in normal and preeclamptic pregnancy. *Endocrine*, 18, 239-45.
- MEYEROWITZ, E. A., RICHTERMAN, A., GANDHI, R. T. & SAX, P. E. 2021. Transmission of SARS-CoV-2: A Review of Viral, Host, and Environmental Factors. *Annals of internal medicine*, 174, 69-79.
- MINSKAIA, E., HERTZIG, T., GORBALENYA, A. E., CAMPANACCI, V., CABBILLAU, C., CANARD, B. & ZIEBUHR, J. 2006. Discovery of an RNA virus 3'->5' exoribonuclease that is critically involved in coronavirus RNA synthesis. *Proc Natl Acad Sci U S A*, 103, 5108-13.
- MIRAB, F., KANG, Y. J. & MAJD, S. 2019. Preparation and characterization of size-controlled glioma spheroids using agarose hydrogel microwells. *PLOS ONE*, 14, e0211078.
- MISTRY, P., BARMANIA, F., MELLET, J., PETA, K., STRYDOM, A., VILJOEN, I. M., JAMES, W., GORDON, S. & PEPPER, M. S. 2021. SARS-CoV-2 Variants, Vaccines, and Host Immunity. *Front Immunol*, 12, 809244.
- MITA, S., NAKAKUKI, M., ICHIOKA, M., SHIMIZU, Y., HASHIBA, M., MIYAZAKI, H. & KYO, S. 2017. Dienogest inhibits C-C motif chemokine ligand 20 expression in human endometriotic epithelial cells. *European Journal of Obstetrics & Gynecology and Reproductive Biology*, 214, 65-70.
- MITCHELL, A. A., GILBOA, S. M., WERLER, M. M., KELLEY, K. E., LOUIK, C., HERNÁNDEZ-DÍAZ, S. & NATIONAL BIRTH DEFECTS PREVENTION, S. 2011. Medication use during pregnancy, with particular focus on prescription drugs: 1976-2008. *American journal of obstetrics and gynecology*, 205, 51.e1-51.e518.
- MITHAL, L. B., OTERO, S., SIMONS, L. M., HULTQUIST, J. F., MILLER, E. S., OZER, E. A., SHANES, E. D. & GOLDSTEIN, J. A. 2022. Low-level SARS-CoV-2 viremia coincident with COVID placentitis and stillbirth. *Placenta*, 121, 79-81.
- MORGAN, T., CRAVEN, C. & WARD, K. 1998. Human spiral artery renin-angiotensin system. *Hypertension*, 32, 683-7.
- MORITA, T., SHIMA, Y., FUJIMOTO, K., TSUBOI, H., SAEKI, Y., NARAZAKI, M., OGATA, A. & KUMANOGOH, A. 2019. Anti-receptor activator of nuclear factor κ B ligand antibody treatment increases osteoclastogenesis-promoting IL-8 in patients with rheumatoid arthritis. *Int Immunol*, 31, 277-285.
- MORNIROLI, D., VIZZARI, G., TOSI, M., TREGLIA, G., CORSELLO, A., MARCHISIO, P., MOSCA, F., AGOSTONI, C., GIANNÌ, M. L., MILANI, G. P. & PUGNI, L. 2023. Mother-to-child transmission of SARS-CoV-2 infection in high-income countries: a systematic review and meta-analysis of prospective observational studies. *Sci Rep*, 13, 8813.
- MOUZON, S. H. & LASSANCE, L. 2015. Endocrine and metabolic adaptations to pregnancy; impact of obesity. *Horm Mol Biol Clin Investig*, 24, 65-72.
- MUNNUR, U., DE BOISBLANC, B. & SURESH, M. S. 2005. Airway problems in pregnancy. *Crit Care Med*, 33, S259-68.

- MUSA, S. S., BELLO, U. M., ZHAO, S., ABDULLAHI, Z. U., LAWAN, M. A. & HE, D. 2021. Vertical Transmission of SARS-CoV-2: A Systematic Review of Systematic Reviews. *Viruses*, 13.
- NAKAGAWA, K., LOKUGAMAGE, K. G. & MAKINO, S. 2016. Viral and Cellular mRNA Translation in Coronavirus-Infected Cells. *Adv Virus Res*, 96, 165-192.
- NAM, Y., KIM, J. H., SEO, M., KIM, J. H., JIN, M., JEON, S., SEO, J. W., LEE, W. H., BING, S. J., JEE, Y., LEE, W. K., PARK, D. H., KOOK, H. & SUK, K. 2014. Lipocalin-2 protein deficiency ameliorates experimental autoimmune encephalomyelitis: the pathogenic role of lipocalin-2 in the central nervous system and peripheral lymphoid tissues. *J Biol Chem*, 289, 16773-89.
- NAPOLITANO, A. P., DEAN, D. M., MAN, A. J., YOUSSEF, J., HO, D. N., RAGO, A. P., LECH, M. P. & MORGAN, J. R. 2007. Scaffold-free three-dimensional cell culture utilizing micromolded nonadhesive hydrogels. *Biotechniques*, 43, 494, 496-500.
- NARASARAJU, T., NG, H. H., PHOON, M. C. & CHOW, V. T. K. 2010. MCP-1 Antibody Treatment Enhances Damage and Impedes Repair of the Alveolar Epithelium in Influenza Pneumonitis. *American Journal of Respiratory Cell and Molecular Biology*, 42, 732-743.
- NEGAMI, A. I. & TOMINAGA, T. 1991. Effects of prolactin on cultured human endometrial cells. *Horm Res*, 35 Suppl 1, 50-7.
- NEVES, L. A., STOVALL, K., JOYNER, J., VALDÉS, G., GALLAGHER, P. E., FERRARIO, C. M., MERRILL, D. C. & BROSNIHAN, K. B. 2008. ACE2 and ANG-(1-7) in the rat uterus during early and late gestation. *Am J Physiol Regul Integr Comp Physiol*, 294, R151-61.
- NG, S. W., NORWITZ, G. A., PAVLICEV, M., TILBURGS, T., SIMÓN, C. & NORWITZ, E. R. 2020. Endometrial Decidualization: The Primary Driver of Pregnancy Health. *Int J Mol Sci*, 21.
- NISHIDA, M. 2002. The Ishikawa cells from birth to the present. *Human Cell*, 15, 104-117.
- NISHIDA, M., KASAHARA, K., KANEKO, M., IWASAKI, H. & HAYASHI, K. 1985. [Establishment of a new human endometrial adenocarcinoma cell line, Ishikawa cells, containing estrogen and progesterone receptors]. *Nihon Sanka Fujinka Gakkai zasshi*, 37, 1103-1111.
- NORWITZ, E. R. & CAUGHEY, A. B. 2011. Progesterone supplementation and the prevention of preterm birth. *Rev Obstet Gynecol*, 4, 60-72.
- OCHOA-BERNAL, M. A. & FAZLEABAS, A. T. 2020. Physiologic Events of Embryo Implantation and Decidualization in Human and Non-Human Primates. *Int J Mol Sci*, 21.
- ODA, H., YOSHIDA, Y., KAWAMURA, A. & KAKINUMA, A. 2008. Cell shape, cell-cell contact, cell-extracellular matrix contact and cell polarity are all required for the maximum induction of CYP2B1 and CYP2B2 gene expression by phenobarbital in adult rat cultured hepatocytes. *Biochem Pharmacol*, 75, 1209-17.
- OKADA, H., TSUZUKI, T. & MURATA, H. 2018. Decidualization of the human endometrium. *Reprod Med Biol*, 17, 220-227.

- OKTEM, O. & OKTAY, K. 2008. The Ovary. *Annals of the New York Academy of Sciences*, 1127, 1-9.
- ONG, C. S., ZHOU, X., HAN, J., HUANG, C. Y., NASHED, A., KHATRI, S., MATTSON, G., FUKUNISHI, T., ZHANG, H. & HIBINO, N. 2018. In vivo therapeutic applications of cell spheroids. *Biotechnol Adv*, 36, 494-505.
- ONG, S. W. X., CHIEW, C. J., ANG, L. W., MAK, T. M., CUI, L., TOH, M., LIM, Y. D., LEE, P. H., LEE, T. H., CHIA, P. Y., MAURER-STROH, S., LIN, R. T. P., LEO, Y. S., LEE, V. J., LYE, D. C. & YOUNG, B. E. 2021. Clinical and virological features of SARS-CoV-2 variants of concern: a retrospective cohort study comparing B.1.1.7 (Alpha), B.1.315 (Beta), and B.1.617.2 (Delta). *Clin Infect Dis*.
- ORSINI, A., CORSI, M., SANTANGELO, A., RIVA, A., PERONI, D., FOIADELLI, T., SAVASTA, S. & STRIANO, P. 2020. Challenges and management of neurological and psychiatric manifestations in SARS-CoV-2 (COVID-19) patients. *Neurol Sci*, 41, 2353-2366.
- OSBORN, M. 1983. Intermediate Filaments as Histologic Markers: An Overview. *Journal of Investigative Dermatology*, 81, S104-S109.
- OU, X., LIU, Y., LEI, X., LI, P., MI, D., REN, L., GUO, L., GUO, R., CHEN, T., HU, J., XIANG, Z., MU, Z., CHEN, X., CHEN, J., HU, K., JIN, Q., WANG, J. & QIAN, Z. 2020. Characterization of spike glycoprotein of SARS-CoV-2 on virus entry and its immune cross-reactivity with SARS-CoV. *Nat Commun*, 11, 1620.
- PAIVA, P., LOCKHART, M. G., GIRLING, J. E., OLSHANSKY, M., WOODROW, N., MARINO, J. L., HICKEY, M. & ROGERS, P. A. W. 2016. Identification of genes differentially expressed in menstrual breakdown and repair. *Molecular Human Reproduction*, 22, 898-912.
- PALMEIRA, P., QUINELLO, C., SILVEIRA-LESSA, A. L., ZAGO, C. A. & CARNEIRO-SAMPAIO, M. 2012. IgG placental transfer in healthy and pathological pregnancies. *Clin Dev Immunol*, 2012, 985646.
- PAMPALONI, F., REYNAUD, E. G. & STELZER, E. H. 2007. The third dimension bridges the gap between cell culture and live tissue. *Nat Rev Mol Cell Biol*, 8, 839-45.
- PAN, C. Q., ZHU, B. S., XU, J. P., LI, J. X., SUN, L. J., TIAN, H. X., ZHANG, X. H., LI, S. W. & DAI, E. H. 2022. Pregnancy and fetal outcomes of chronic hepatitis C mothers with viremia in China. *World J Gastroenterol*, 28, 5023-5035.
- PAN, J. L., YUAN, D. Z., ZHAO, Y. B., NIE, L., LEI, Y., LIU, M., LONG, Y., ZHANG, J. H., BLOK, L. J., BURGER, C. W. & YUE, L. M. 2017. Progesterone-induced miR-133a inhibits the proliferation of endometrial epithelial cells. *Acta Physiol (Oxf)*, 219, 683-692.
- PARK, C., BAE, H., BAZER, F. W., SONG, G. & LIM, W. 2019. Activation of CCL20 and its receptor CCR6 promotes endometrium preparation for implantation and placenta development during the early pregnancy period in pigs. *Developmental & Comparative Immunology*, 92, 35-42.
- PARK, D. W., CHOI, D. S., RYU, H. S., KWON, H. C., JOO, H. & MIN, C. K. 2003. A well-defined in vitro three-dimensional culture of human endometrium and its applicability to endometrial cancer invasion. *Cancer Lett*, 195, 185-92.

- PARTIDA-SÁNCHEZ, S., COCKAYNE, D. A., MONARD, S., JACOBSON, E. L., OPPENHEIMER, N., GARVY, B., KUSSER, K., GOODRICH, S., HOWARD, M., HARMSSEN, A., RANDALL, T. D. & LUND, F. E. 2001. Cyclic ADP-ribose production by CD38 regulates intracellular calcium release, extracellular calcium influx and chemotaxis in neutrophils and is required for bacterial clearance in vivo. *Nature Medicine*, 7, 1209-1216.
- PATEL, V. B., ZHONG, J. C., GRANT, M. B. & OUDIT, G. Y. 2016. Role of the ACE2/Angiotensin 1-7 Axis of the Renin-Angiotensin System in Heart Failure. *Circ Res*, 118, 1313-26.
- PAWAR, S., LAWS, M. J., BAGCHI, I. C. & BAGCHI, M. K. 2015. Uterine Epithelial Estrogen Receptor- α Controls Decidualization via a Paracrine Mechanism. *Molecular Endocrinology*, 29, 1362-1374.
- PEI, L., CASTRILLO, A., CHEN, M., HOFFMANN, A. & TONTONOZ, P. 2005. Induction of NR4A orphan nuclear receptor expression in macrophages in response to inflammatory stimuli. *J Biol Chem*, 280, 29256-62.
- PÉRILLAUD-DUBOIS, C., BELHADI, D., LAOUÉNAN, C., MANDELBROT, L., PICONE, O. & VAULOUP-FELLOUS, C. 2021. Current practices of management of maternal and congenital Cytomegalovirus infection during pregnancy after a maternal primary infection occurring in first trimester of pregnancy: Systematic review. *PLoS One*, 16, e0261011.
- PETRENKO, A. P., CASTELO-BRANCO, C., MARSHALOV, D. V., KULIGIN, A. V., MYSOVSKAYA, Y. S., SHIFMAN, E. M. & ABDULAEV, A. M. R. 2021. Physiology of intra-abdominal volume during pregnancy. *J Obstet Gynaecol*, 41, 1016-1022.
- PHELAN, D. E., SHIGEMURA, M., ALDHAFIRI, S., MOTA, C., HALL, T. J., SZNAJDER, J. I., MURPHY, E. P., CREAN, D. & CUMMINS, E. P. 2021. Transcriptional Profiling of Monocytes Deficient in Nuclear Orphan Receptors NR4A2 and NR4A3 Reveals Distinct Signalling Roles Related to Antigen Presentation and Viral Response. *Frontiers in immunology*, 12, 676644-676644.
- PIERRO, E., MINICI, F., ALESIANI, O., MICELI, F., PROTO, C., SCREPANTI, I., MANCUSO, S. & LANZONE, A. 2001. Stromal-Epithelial Interactions Modulate Estrogen Responsiveness in Normal Human Endometrium1. *Biology of Reproduction*, 64, 831-838.
- PILARSKA, I., BIZON, M. & SAWICKI, W. 2023. Influence of COVID-19 infection on placental function. *Ginekol Pol*, 94, 79-83.
- POMAR, L., LAMBERT, V., MATHEUS, S., POMAR, C., HCINI, N., CARLES, G., ROUSSET, D., VOUGA, M., PANCHAUD, A. & BAUD, D. 2021. Prolonged Maternal Zika Viremia as a Marker of Adverse Perinatal Outcomes. *Emerg Infect Dis*, 27, 490-498.
- PRINCE, L. R., PROSEDA, S. D., HIGGINS, K., CARLRING, J., PRESTWICH, E. C., OGRYZKO, N. V., RAHMAN, A., BASRAN, A., FALCIANI, F., TAYLOR, P., RENSHAW, S. A., WHYTE, M. K. B. & SABROE, I. 2017. NR4A orphan nuclear receptor family members, NR4A2 and NR4A3, regulate neutrophil number and survival. *Blood*, 130, 1014-1025.
- PROCTOR, A., HURST, B. S., MARSHBURN, P. B. & MATTHEWS, M. L. 2006. Effect of progesterone supplementation in early pregnancy on the

- pregnancy outcome after in vitro fertilization. *Fertility and Sterility*, 85, 1550-1552.
- QIN, X., SUN, W., WANG, C., LI, M., ZHAO, X., LI, C. & ZHANG, H. 2021. Mifepristone inhibited the expression of B7-H2, B7-H3, B7-H4 and PD-L2 in adenomyosis. *Reproductive Biology and Endocrinology*, 19, 114.
- QIU, L., LIU, X., XIAO, M., XIE, J., CAO, W., LIU, Z., MORSE, A., XIE, Y., LI, T. & ZHU, L. 2020. SARS-CoV-2 Is Not Detectable in the Vaginal Fluid of Women With Severe COVID-19 Infection. *Clin Infect Dis*, 71, 813-817.
- RAGAB, D., SALAH ELDIN, H., TAEIMAH, M., KHATTAB, R. & SALEM, R. 2020. The COVID-19 Cytokine Storm; What We Know So Far. *Front Immunol*, 11, 1446.
- RAHI, M. S., JINDAL, V., REYES, S. P., GUNASEKARAN, K., GUPTA, R. & JAIYESIMI, I. 2021. Hematologic disorders associated with COVID-19: a review. *Ann Hematol*, 100, 309-320.
- RAHMATI, M., YON, D. K., LEE, S. W., BUTLER, L., KOYANAGI, A., JACOB, L., SHIN, J. I. & SMITH, L. 2023. Effects of COVID-19 vaccination during pregnancy on SARS-CoV-2 infection and maternal and neonatal outcomes: A systematic review and meta-analysis. *Rev Med Virol*, 33, e2434.
- RAINE, C., AUSTIN, K. & GILES, I. 2020. Mechanisms determining the amelioration of rheumatoid arthritis in pregnancy: A systematic review. *Semin Arthritis Rheum*, 50, 1357-1369.
- RAMBAUT, A., HOLMES, E. C., O'TOOLE, A., HILL, V., MCCRONE, J. T., RUIS, C., DU PLESSIS, L. & PYBUS, O. G. 2020. A dynamic nomenclature proposal for SARS-CoV-2 lineages to assist genomic epidemiology. *Nature Microbiology*, 5, 1403-1407.
- REN, X., GLENDE, J., AL-FALAH, M., DE VRIES, V., SCHWEGMANN-WESSELS, C., QU, X., TAN, L., TSCHERNIG, T., DENG, H., NAIM, H. Y. & HERRLER, G. 2006. Analysis of ACE2 in polarized epithelial cells: surface expression and function as receptor for severe acute respiratory syndrome-associated coronavirus. *J Gen Virol*, 87, 1691-1695.
- RICHARDS, Z., MCCRAY, T., MARSILI, J., ZENNER, M. L., MANLUCU, J. T., GARCIA, J., KAJDACSZY-BALLA, A., MURRAY, M., VOISINE, C., MURPHY, A. B., ABDULKADIR, S. A., PRINS, G. S. & NONN, L. 2019. Prostate Stroma Increases the Viability and Maintains the Branching Phenotype of Human Prostate Organoids. *iScience*, 12, 304-317.
- ROBERTS, D. K., PARMLEY, T. H., WALKER, N. J. & HORBELT, D. V. 1992. Ultrastructure of the microvasculature in the human endometrium throughout the normal menstrual cycle. *Am J Obstet Gynecol*, 166, 1393-406.
- ROBINSON, E. E., FOTY, R. A. & CORBETT, S. A. 2004. Fibronectin matrix assembly regulates alpha5beta1-mediated cell cohesion. *Mol Biol Cell*, 15, 973-81.
- ROBINSON, N. B., KRIEGER, K., KHAN, F. M., HUFFMAN, W., CHANG, M., NAIK, A., YONGLE, R., HAMEED, I., KRIEGER, K., GIRARDI, L. N. & GAUDINO, M. 2019. The current state of animal models in research: A review. *Int J Surg*, 72, 9-13.

- ROBSON, A., HARRIS, L. K., INNES, B. A., LASH, G. E., ALJUNAIDY, M. M., APLIN, J. D., BAKER, P. N., ROBSON, S. C. & BULMER, J. N. 2012. Uterine natural killer cells initiate spiral artery remodeling in human pregnancy. *Faseb j*, 26, 4876-85.
- ROSSI, G., MANFRIN, A. & LUTOLF, M. P. 2018. Progress and potential in organoid research. *Nat Rev Genet*, 19, 671-687.
- ROTTENSTREICH, A., TSUR, A., BRAVERMAN, N., KABIRI, D., PORAT, S., BENENSON, S., OSTER, Y., KAM, H. A., WALFISCH, A., BART, Y., MEYER, R., LIFSHITZ, S. J., AMIKAM, U., BIRON-SHENTAL, T., COHEN, G., SCIAKY-TAMIR, Y., SHACHAR, I. B., YINON, Y. & REUBINOFF, B. 2021. Vaginal delivery in SARS-CoV-2-infected pregnant women in Israel: a multicenter prospective analysis. *Arch Gynecol Obstet*, 303, 1401-1405.
- ROTTENSTREICH, A., VORONTSOV, O., ALFI, O., ZARBIV, G., OIKNINE-DJIAN, E., ZIGRON, R., KLEINSTERN, G., MANDELBOIM, M., PORAT, S. & WOLF, D. G. 2022. Maternal and Neonatal SARS-CoV-2 Omicron Variant Neutralization after Antenatal mRNA Vaccination. *Clinical Infectious Diseases*.
- ROUAUD, F., MÉAN, I. & CITI, S. 2022. The ACE2 Receptor for Coronavirus Entry Is Localized at Apical Cell—Cell Junctions of Epithelial Cells. *Cells*, 11, 627.
- RUETALO, N., BUSINGER, R., ALTHAUS, K., FINK, S., RUOFF, F., POGODA, M., IFTNER, A., GANZENMÜLLER, T., HAMPRECHT, K., FLEHMIG, B., BAKCHOUL, T., TEMPLIN, M. F. & SCHINDLER, M. 2021. Antibody Response against SARS-CoV-2 and Seasonal Coronaviruses in Nonhospitalized COVID-19 Patients. *mSphere*, 6.
- RUSSELL, P., SACKS, G., TREMELLEN, K. & GEE, A. 2013. The distribution of immune cells and macrophages in the endometrium of women with recurrent reproductive failure. III: Further observations and reference ranges. *Pathology*, 45, 393-401.
- RUTANEN, E. M. 1998. Insulin-like growth factors in endometrial function. *Gynecological Endocrinology*, 12, 399-406.
- RYU, N. E., LEE, S. H. & PARK, H. 2019. Spheroid Culture System Methods and Applications for Mesenchymal Stem Cells. *Cells*, 8.
- SACHS, L. & SHELESNYAK, M. C. 1955. The development and suppression of polyploidy in the developing and suppressed deciduoma in the rat. *J Endocrinol*, 12, 146-51.
- SAINI, A., MAHAJAN, S., AHUJA, N., BHAGYARAJ, E., KALRA, R., JANMEJA, A. K. & GUPTA, P. 2018. An Accord of Nuclear Receptor Expression in M. tuberculosis Infected Macrophages and Dendritic Cells. *Scientific Reports*, 8, 2296.
- SAITO, S., KASAHARA, T., SAKAKURA, S., UMEKAGE, H., HARADA, N. & ICHIJO, M. 1994. Detection and localization of interleukin-8 mRNA and protein in human placenta and decidual tissues. *Journal of Reproductive Immunology*, 27, 161-172.
- SALAHUDEEN, A. A., CHOI, S. S., RUSTAGI, A., ZHU, J., VAN UNEN, V., DE LA O, S. M., FLYNN, R. A., MARGALEF-CATALÀ, M., SANTOS, A. J. M., JU, J., BATISH, A., USUI, T., ZHENG, G. X. Y., EDWARDS, C. E.,

- WAGAR, L. E., LUCA, V., ANCHANG, B., NAGENDRAN, M., NGUYEN, K., HART, D. J., TERRY, J. M., BELGRADER, P., ZIRALDO, S. B., MIKKELSEN, T. S., HARBURY, P. B., GLENN, J. S., GARCIA, K. C., DAVIS, M. M., BARIC, R. S., SABATTI, C., AMIEVA, M. R., BLISH, C. A., DESAI, T. J. & KUO, C. J. 2020. Progenitor identification and SARS-CoV-2 infection in human distal lung organoids. *Nature*, 588, 670-675.
- SALAMONSEN, L. A. & LATHBURY, L. J. 2000. Endometrial leukocytes and menstruation. *Human Reproduction Update*, 6, 16-27.
- SALKER, M. S., NAUTIYAL, J., STEEL, J. H., WEBSTER, Z., SUĆUROVIĆ, S., NICOU, M., SINGH, Y., LUCAS, E. S., MURAKAMI, K., CHAN, Y. W., JAMES, S., ABDALLAH, Y., CHRISTIAN, M., CROY, B. A., MULAC-JERICEVIC, B., QUENBY, S. & BROSENS, J. J. 2012. Disordered IL-33/ST2 activation in decidualizing stromal cells prolongs uterine receptivity in women with recurrent pregnancy loss. *PLoS One*, 7, e52252.
- SALZBERGER, B., BUDER, F., LAMPL, B., EHRENSTEIN, B., HITZENBICHLER, F., HOLZMANN, T., SCHMIDT, B. & HANSES, F. 2021. Epidemiology of SARS-CoV-2. *Infection*, 49, 233-239.
- SAMSOON, G. L. & YOUNG, J. R. 1987. Difficult tracheal intubation: a retrospective study. *Anaesthesia*, 42, 487-90.
- SAMUDRALA, P. K., KUMAR, P., CHOUDHARY, K., THAKUR, N., WADEKAR, G. S., DAYARAMANI, R., AGRAWAL, M. & ALEXANDER, A. 2020. Virology, pathogenesis, diagnosis and in-line treatment of COVID-19. *Eur J Pharmacol*, 883, 173375.
- SANTINI, M. T. & RAINALDI, G. 1999. Three-dimensional spheroid model in tumor biology. *Pathobiology*, 67, 148-57.
- SAPPENFIELD, E., JAMIESON, D. J. & KOURTIS, A. P. 2013. Pregnancy and susceptibility to infectious diseases. *Infect Dis Obstet Gynecol*, 2013, 752852.
- SARIS, A., REIJNDERS, T. D. Y., REIJM, M., HOLLANDER, J. C., DE BUCK, K., SCHUURMAN, A. R., DUITMAN, J., HEUNKS, L., AMAN, J., BOGAARD, H. J., NOSSENT, E. J., VAN DER POLL, T. & BONTKES, H. J. 2021. Enrichment of CCR6(+) CD8(+) T cells and CCL20 in the lungs of mechanically ventilated patients with COVID-19. *Eur J Immunol*, 51, 1535-1538.
- SCHATZ, F. & LOCKWOOD, C. J. 1993. Progesterin regulation of plasminogen activator inhibitor type 1 in primary cultures of endometrial stromal and decidual cells. *J Clin Endocrinol Metab*, 77, 621-5.
- SCHIAVONI, I., SCAGNOLARI, C., HORENSTEIN, A. L., LEONE, P., PIERANGELI, A., MALAVASI, F., AUSIELLO, C. M. & FEDELE, G. 2018. CD38 modulates respiratory syncytial virus-driven proinflammatory processes in human monocyte-derived dendritic cells. *Immunology*, 154, 122-131.
- SCHWEINFURTH, J. M. & MEYERS, C. 2006. Organotypic (raft) culture of biopsy-derived upper respiratory epithelium. *Laryngoscope*, 116, 1600-2.
- SEASELY, A. R., BLANCHARD, C. T., ARORA, N., BATTARBEE, A. N., CASEY, B. M., DIONNE-ODOM, J., LEAL, S. M., JR., MOATES, D. B., SINKEY, R. G., SZYCHOWSKI, J. M., TITA, A. T. & SUBRAMANIAM, A.

2021. Maternal and Perinatal Outcomes Associated With the Severe Acute Respiratory Syndrome Coronavirus 2 (SARS-CoV-2) Delta (B.1.617.2) Variant. *Obstet Gynecol*, 138, 842-844.
- SHAH, M. & WOO, H. G. 2021. Omicron: A Heavily Mutated SARS-CoV-2 Variant Exhibits Stronger Binding to ACE2 and Potently Escapes Approved COVID-19 Therapeutic Antibodies. *Front Immunol*, 12, 830527.
- SHAH, N. M., IMAMI, N. & JOHNSON, M. R. 2018. Progesterone Modulation of Pregnancy-Related Immune Responses. *Frontiers in Immunology*, 9.
- SHANG, J., YE, G., SHI, K., WAN, Y., LUO, C., AIHARA, H., GENG, Q., AUERBACH, A. & LI, F. 2020. Structural basis of receptor recognition by SARS-CoV-2. *Nature*, 581, 221-224.
- SHARMA, S., GODBOLE, G. & MODI, D. 2016. Decidual Control of Trophoblast Invasion. *American Journal of Reproductive Immunology*, 75, 341-350.
- SHENDE, P., GAIKWAD, P., GANDHEWAR, M., UKEY, P., BHIDE, A., PATEL, V., BHAGAT, S., BHOR, V., MAHALE, S., GAJBHIYE, R. & MODI, D. 2021. Persistence of SARS-CoV-2 in the first trimester placenta leading to transplacental transmission and fetal demise from an asymptomatic mother. *Hum Reprod*, 36, 899-906.
- SHIMAZUI, T., SCHALKEN, J. A., KAWAI, K., KAWAMOTO, R., VAN BOCKHOVEN, A., OOSTERWIJK, E. & AKAZA, H. 2004. Role of complex cadherins in cell-cell adhesion evaluated by spheroid formation in renal cell carcinoma cell lines. *Oncol Rep*, 11, 357-60.
- SHIOTA, A., YAMAMOTO, K., OHISHI, M., TATARA, Y., OHNISHI, M., MAEKAWA, Y., IWAMOTO, Y., TAKEDA, M. & RAKUGI, H. 2010. Loss of ACE2 accelerates time-dependent glomerular and tubulointerstitial damage in streptozotocin-induced diabetic mice. *Hypertens Res*, 33, 298-307.
- SHULLA, A., HEALD-SARGENT, T., SUBRAMANYA, G., ZHAO, J., PERLMAN, S. & GALLAGHER, T. 2011. A transmembrane serine protease is linked to the severe acute respiratory syndrome coronavirus receptor and activates virus entry. *J Virol*, 85, 873-82.
- SIMBAR, M., NAZARPOUR, S. & SHEIDAEI, A. 2023. Evaluation of pregnancy outcomes in mothers with COVID-19 infection: a systematic review and meta-analysis. *J Obstet Gynaecol*, 43, 2162867.
- SIMCOX, L. E., ORMESHER, L., TOWER, C. & GREER, I. A. 2015. Thrombophilia and Pregnancy Complications. *Int J Mol Sci*, 16, 28418-28.
- SINGH, S., ANSHITA, D. & RAVICHANDIRAN, V. 2021. MCP-1: Function, regulation, and involvement in disease. *Int Immunopharmacol*, 101, 107598.
- SMITH, E. R., OAKLEY, E., GRANDNER, G. W., FERGUSON, K., FAROOQ, F., AFSHAR, Y., AHLBERG, M., AHMADZIA, H., AKELO, V., ALDROVANDI, G., TIPPETT BARR, B. A., BEVILACQUA, E., BRANDT, J. S., BROUTET, N., FERNÁNDEZ BUHIGAS, I., CARRILLO, J., CLIFTON, R., CONRY, J., COSMI, E., CRISPI, F., CROVETTO, F., DELGADO-LÓPEZ, C., DIVAKAR, H., DRISCOLL, A. J., FAVRE, G., FLAHERMAN, V. J., GALE, C., GIL, M. M., GOTTLIEB, S. L.,

- GRATACÓS, E., HERNANDEZ, O., JONES, S., KALAFAT, E., KHAGAYI, S., KNIGHT, M., KOTLOFF, K., LANZONE, A., LE DOARE, K., LEES, C., LITMAN, E., LOKKEN, E. M., LAURITA LONGO, V., MADHI, S. A., MAGEE, L. A., MARTINEZ-PORTILLA, R. J., MCCLURE, E. M., METZ, T. D., MILLER, E. S., MONEY, D., MOUNGMAITHONG, S., MULLINS, E., NACHEGA, J. B., NUNES, M. C., ONYANGO, D., PANCHAUD, A., POON, L. C., RAITEN, D., REGAN, L., RUKUNDO, G., SAHOTA, D., SAKOWICZ, A., SANIN-BLAIR, J., SÖDERLING, J., STEPHANSSON, O., TEMMERMAN, M., THORSON, A., TOLOSA, J. E., TOWNSON, J., VALENCIA-PRADO, M., VISENTIN, S., VON DADELSZEN, P., ADAMS WALDORF, K., WHITEHEAD, C., YASSA, M. & TIELSCH, J. M. 2023a. Adverse maternal, fetal, and newborn outcomes among pregnant women with SARS-CoV-2 infection: an individual participant data meta-analysis. *BMJ Glob Health*, 8.
- SMITH, E. R., OAKLEY, E., GRANDNER, G. W., RUKUNDO, G., FAROOQ, F., FERGUSON, K., BAUMANN, S., ADAMS WALDORF, K. M., AFSHAR, Y., AHLBERG, M., AHMADZIA, H., AKELO, V., ALDROVANDI, G., BEVILACQUA, E., BRACERO, N., BRANDT, J. S., BROUTET, N., CARRILLO, J., CONRY, J., COSMI, E., CRISPI, F., CROVETTO, F., DEL MAR GIL, M., DELGADO-LÓPEZ, C., DIVAKAR, H., DRISCOLL, A. J., FAVRE, G., FERNANDEZ BUHIGAS, I., FLAHERMAN, V., GALE, C., GODWIN, C. L., GOTTLIEB, S., GRATACÓS, E., HE, S., HERNANDEZ, O., JONES, S., JOSHI, S., KALAFAT, E., KHAGAYI, S., KNIGHT, M., KOTLOFF, K. L., LANZONE, A., LAURITA LONGO, V., LE DOARE, K., LEES, C., LITMAN, E., LOKKEN, E. M., MADHI, S. A., MAGEE, L. A., MARTINEZ-PORTILLA, R. J., METZ, T. D., MILLER, E. S., MONEY, D., MOUNGMAITHONG, S., MULLINS, E., NACHEGA, J. B., NUNES, M. C., ONYANGO, D., PANCHAUD, A., POON, L. C., RAITEN, D., REGAN, L., SAHOTA, D., SAKOWICZ, A., SANIN-BLAIR, J., STEPHANSSON, O., TEMMERMAN, M., THORSON, A., THWIN, S. S., TIPPETT BARR, B. A., TOLOSA, J. E., TUG, N., VALENCIA-PRADO, M., VISENTIN, S., VON DADELSZEN, P., WHITEHEAD, C., WOOD, M., YANG, H., ZAVALA, R. & TIELSCH, J. M. 2023b. Clinical risk factors of adverse outcomes among women with COVID-19 in the pregnancy and postpartum period: a sequential, prospective meta-analysis. *Am J Obstet Gynecol*, 228, 161-177.
- SOJKA, D. K., YANG, L. & YOKOYAMA, W. M. 2019. Uterine Natural Killer Cells. *Front Immunol*, 10, 960.
- SONG, P., LI, W., XIE, J., HOU, Y. & YOU, C. 2020. Cytokine storm induced by SARS-CoV-2. *Clinica chimica acta; international journal of clinical chemistry*, 509, 280-287.
- SONG, Y., BURNS, G. W., JOSHI, N. R., ARORA, R., KIM, J. J. & FAZLEABAS, A. T. 2023. Spheroids as a model for endometriotic lesions. *JCI Insight*, 8.
- SOUYRIS, M., CENAC, C., AZAR, P., DAVIAUD, D., CANIVET, A., GRUNENWALD, S., PIENKOWSKI, C., CHAUMEIL, J., MEJÍA, J. E. & GUÉRY, J. C. 2018. TLR7 escapes X chromosome inactivation in immune cells. *Sci Immunol*, 3.

- SPINATO, G., FABBRIS, C., POLESEL, J., CAZZADOR, D., BORSETTO, D., HOPKINS, C. & BOSCOLO-RIZZO, P. 2020. Alterations in Smell or Taste in Mildly Symptomatic Outpatients With SARS-CoV-2 Infection. *Jama*, 323, 2089-2090.
- SROGA, J. M., MA, X. & DAS, S. K. 2012. Developmental regulation of decidual cell polyploidy at the site of implantation. *Front Biosci (Schol Ed)*, 4, 1475-86.
- STADNYTSKYI, V., BAX, C. E., BAX, A. & ANFINRUD, P. 2020. The airborne lifetime of small speech droplets and their potential importance in SARS-CoV-2 transmission. *Proc Natl Acad Sci U S A*, 117, 11875-11877.
- STAFF, A. C., FJELDSTAD, H. E., FOSHEIM, I. K., MOE, K., TUROWSKI, G., JOHNSEN, G. M., ALNAES-KATJAVIVI, P. & SUGULLE, M. 2022. Failure of physiological transformation and spiral artery atherosclerosis: their roles in preeclampsia. *Am J Obstet Gynecol*, 226, S895-s906.
- STOIKOS, C. J., HARRISON, C. A., SALAMONSEN, L. A. & DIMITRIADIS, E. 2008. A distinct cohort of the TGFbeta superfamily members expressed in human endometrium regulate decidualization. *Hum Reprod*, 23, 1447-56.
- STRAFACI, G., SELMIN, A., ZANARDO, V., DE SANTIS, M., ERCOLI, A. & SCAMBIA, G. 2012. Herpes simplex virus infection in pregnancy. *Infect Dis Obstet Gynecol*, 2012, 385697.
- SUH, W.-K., WANG, S., DUNCAN, G. S., MIYAZAKI, Y., CATES, E., WALKER, T., GAJEWSKA, B. U., DEENICK, E., DAWICKI, W., OKADA, H., WAKEHAM, A., ITIE, A., WATTS, T. H., OHASHI, P. S., JORDANA, M., YOSHIDA, H. & MAK, T. W. 2006. Generation and Characterization of B7-H4/B7S1/B7x-Deficient Mice. *Molecular and Cellular Biology*, 26, 6403-6411.
- SUN, K., GU, L., MA, L. & DUAN, Y. 2021. Atlas of ACE2 gene expression reveals novel insights into transmission of SARS-CoV-2. *Heliyon*, 7, e05850.
- SUN, T. T., EICHNER, R., NELSON, W. G., TSENG, S. C., WEISS, R. A., JARVINEN, M. & WOODCOCK-MITCHELL, J. 1983. Keratin classes: molecular markers for different types of epithelial differentiation. *J Invest Dermatol*, 81, 109s-15s.
- SUN, X., XIE, H., ZHANG, H., LI, Z., QI, H., YANG, C., LIU, X., REN, L., JIANG, Y. & HU, X. 2022. B7-H4 reduction induced by Toxoplasma gondii infection results in dysfunction of decidual dendritic cells by regulating the JAK2/STAT3 pathway. *Parasites & Vectors*, 15, 157.
- SUTHAPORN, S., JAYAPRAKASAN, K., THORNTON, J. G., WALKER, K. F., CASTELLANOS, M., MAY, S., HERNANDEZ-MEDRANO, J. & MAALOUF, W. E. 2021. Evaluating the influence of progesterone concentration and time of exposure on in vitro endometrial decidualisation. *Mol Cell Endocrinol*, 111242.
- SZECSI, P. B., JØRGENSEN, M., KLAJNBARD, A., ANDERSEN, M. R., COLOV, N. P. & STENDER, S. 2010. Haemostatic reference intervals in pregnancy. *Thromb Haemost*, 103, 718-27.
- TABIBZADEH, S., SATYASWAROOP, P. G., VON WOLFF, M. & STROWITZKI, T. 1999. Regulation of TNF- α mRNA expression in

- endometrial cells by TNF- α and by oestrogen withdrawal. *Molecular Human Reproduction*, 5, 1141-1149.
- TAKMAZ, O., KAYA, E., ERDI, B., UNSAL, G., SHARIFLI, P., AGAOGLU, N. B., OZBASLI, E., GENCER, S. & GUNGOR, M. 2021. Severe acute respiratory syndrome coronavirus (SARS-CoV-2) is not detected in the vagina: A prospective study. *PLoS One*, 16, e0253072.
- TAN, E. K. & TAN, E. L. 2013. Alterations in physiology and anatomy during pregnancy. *Best Pract Res Clin Obstet Gynaecol*, 27, 791-802.
- TAN, J., KAN, A., HITKARI, J., TAYLOR, B., TALLON, N., WARRAICH, G., YUZPE, A. & NAKHUDA, G. 2018. The role of the endometrial receptivity array (ERA) in patients who have failed euploid embryo transfers. *J Assist Reprod Genet*, 35, 683-692.
- TANG, B. & GURPIDE, E. 1993. Direct effect of gonadotropins on decidualization of human endometrial stroma cells. *J Steroid Biochem Mol Biol*, 47, 115-21.
- TANG, M., XU, Y., JULIAN, J., CARSON, D. & TABIBZADEH, S. 2005. Lefty is expressed in mouse endometrium in estrous cycle and peri-implantation period. *Human Reproduction*, 20, 872-880.
- TANG, S., MAO, Y., JONES, R. M., TAN, Q., JI, J. S., LI, N., SHEN, J., LV, Y., PAN, L., DING, P., WANG, X., WANG, Y., MACINTYRE, C. R. & SHI, X. 2020. Aerosol transmission of SARS-CoV-2? Evidence, prevention and control. *Environ Int*, 144, 106039.
- TEIJEIRA, A., GARASA, S., OCHOA, M. D. C., CIRELLA, A., OLIVERA, I., GLEZ-VAZ, J., ANDUEZA, M. P., MIGUELIZ, I., ALVAREZ, M., RODRÍGUEZ-RUIZ, M. E., ROUZAUT, A., BERRAONDO, P., SANMAMED, M. F., PEREZ GRACIA, J. L. & MELERO, I. 2021. Differential Interleukin-8 thresholds for chemotaxis and netosis in human neutrophils. *Eur J Immunol*, 51, 2274-2280.
- TEILMANN, S. C., CLEMENT, C. A., THORUP, J., BYSKOV, A. G. & CHRISTENSEN, S. T. 2006. Expression and localization of the progesterone receptor in mouse and human reproductive organs. *J Endocrinol*, 191, 525-35.
- TEKLENBURG, G., SALKER, M., MOLOKHIA, M., LAVERY, S., TREW, G., AOJANEPONG, T., MARDON, H. J., LOKUGAMAGE, A. U., RAI, R., LANGLES, C., ROELEN, B. A., QUENBY, S., KUIJK, E. W., KAVELAARS, A., HEIJNEN, C. J., REGAN, L., BROSENS, J. J. & MACKLON, N. S. 2010. Natural selection of human embryos: decidualizing endometrial stromal cells serve as sensors of embryo quality upon implantation. *PLoS One*, 5, e10258.
- TERRAULT, N. A., LEVY, M. T., CHEUNG, K. W. & JOURDAIN, G. 2021. Viral hepatitis and pregnancy. *Nat Rev Gastroenterol Hepatol*, 18, 117-130.
- THELLIN, O., COUMANS, B., ZORZI, W., IGOUT, A. & HEINEN, E. 2000. Tolerance to the foeto-placental 'graft': ten ways to support a child for nine months. *Current Opinion in Immunology*, 12, 731-737.
- THELLIN, O. & HEINEN, E. 2003. Pregnancy and the immune system: between tolerance and rejection. *Toxicology*, 185, 179-84.
- THIELE, K., HIERWEGER, A. M., RIQUELME, J. I. A., SOLANO, M. E., LYDON, J. P. & ARCK, P. C. 2019. Impaired Progesterone-

- Responsiveness of CD11c(+) Dendritic Cells Affects the Generation of CD4(+) Regulatory T Cells and Is Associated With Intrauterine Growth Restriction in Mice. *Front Endocrinol (Lausanne)*, 10, 96.
- THIRUCHELVAM, U., DRANSFIELD, I., SAUNDERS, P. T. & CRITCHLEY, H. O. 2013. The importance of the macrophage within the human endometrium. *J Leukoc Biol*, 93, 217-25.
- THORNBURG, K. L., JACOBSON, S. L., GIRAUD, G. D. & MORTON, M. J. 2000. Hemodynamic changes in pregnancy. *Semin Perinatol*, 24, 11-4.
- TIBBETTS, T. A., DEMAYO, F., RICH, S., CONNEELY, O. M. & O'MALLEY, B. W. 1999. Progesterone receptors in the thymus are required for thymic involution during pregnancy and for normal fertility. *Proc Natl Acad Sci U S A*, 96, 12021-6.
- TICCONI, C., PIETROPOLLI, A., DI SIMONE, N., PICCIONE, E. & FAZLEABAS, A. 2019. Endometrial Immune Dysfunction in Recurrent Pregnancy Loss. *Int J Mol Sci*, 20.
- TORLONI, M. R., BONET, M., BETRÁN, A. P., RIBEIRO-DO-VALLE, C. C. & WIDMER, M. 2020. Quality of medicines for life-threatening pregnancy complications in low- and middle-income countries: A systematic review. *PLoS One*, 15, e0236060.
- TÖRNBLOM, S. A., KLIMAVICIUTE, A., BYSTRÖM, B., CHROMEK, M., BRAUNER, A. & EKMAN-ORDEBERG, G. 2005. Non-infected preterm parturition is related to increased concentrations of IL-6, IL-8 and MCP-1 in human cervix. *Reproductive Biology and Endocrinology*, 3, 39.
- TORRES-TORRES, J., MARTINEZ-PORTILLA, R. J., ESPINO, Y. S. S., ESTRADA-GUTIERREZ, G., SOLIS-PAREDES, J. M., VILLAFAN-BERNAL, J. R., MEDINA-JIMENEZ, V., RODRIGUEZ-MORALES, A. J., ROJAS-ZEPEDA, L. & POON, L. C. 2021. Comorbidities, poverty and social vulnerability as risk factors for mortality in pregnant women with confirmed SARS-CoV-2 infection: analysis of 13 062 positive pregnancies including 176 maternal deaths in Mexico. *Ultrasound Obstet Gynecol*.
- TSENG, L. & ZHU, H. H. 1998. Progestin, estrogen, and insulin-like growth factor-I stimulate the prolactin receptor mRNA in human endometrial stromal cells. *J Soc Gynecol Investig*, 5, 149-55.
- TURCO, M. Y., GARDNER, L., HUGHES, J., CINDROVA-DAVIES, T., GOMEZ, M. J., FARRELL, L., HOLLINSHEAD, M., MARSH, S. G. E., BROSENS, J. J., CRITCHLEY, H. O., SIMONS, B. D., HEMBERGER, M., KOO, B. K., MOFFETT, A. & BURTON, G. J. 2017. Long-term, hormone-responsive organoid cultures of human endometrium in a chemically defined medium. *Nat Cell Biol*, 19, 568-577.
- TWOHIG, K. A., NYBERG, T., ZAIDI, A., THELWALL, S., SINNATHAMBY, M. A., ALIABADI, S., SEAMAN, S. R., HARRIS, R. J., HOPE, R., LOPEZ-BERNAL, J., GALLAGHER, E., CHARLETT, A., DE ANGELIS, D., PRESANIS, A. M. & DABRERA, G. 2022. Hospital admission and emergency care attendance risk for SARS-CoV-2 delta (B.1.617.2) compared with alpha (B.1.1.7) variants of concern: a cohort study. *Lancet Infect Dis*, 22, 35-42.

- UCHIMA, F. D., EDERY, M., IGUCHI, T. & BERN, H. A. 1991. Growth of mouse endometrial luminal epithelial cells in vitro: functional integrity of the oestrogen receptor system and failure of oestrogen to induce proliferation. *J Endocrinol*, 128, 115-20.
- VALDÉS, G., CORTHORN, J., BHARADWAJ, M. S., JOYNER, J., SCHNEIDER, D. & BROSNIHAN, K. B. 2013. Utero-placental expression of angiotensin-(1-7) and ACE2 in the pregnant guinea-pig. *Reprod Biol Endocrinol*, 11, 5.
- VALDÉS, G., NEVES, L. A., ANTON, L., CORTHORN, J., CHACÓN, C., GERMAIN, A. M., MERRILL, D. C., FERRARIO, C. M., SARAO, R., PENNINGER, J. & BROSNIHAN, K. B. 2006. Distribution of angiotensin-(1-7) and ACE2 in human placentas of normal and pathological pregnancies. *Placenta*, 27, 200-7.
- VALDESPINO-VÁZQUEZ, M. Y., HELGUERA-REPETTO, C. A., LEÓN-JUÁREZ, M., VILLAVICENCIO-CARRISOZA, O., FLORES-PLIEGO, A., MORENO-VERDUZCO, E. R., DÍAZ-PÉREZ, D. L., VILLEGAS-MOTA, I., CARRASCO-RAMÍREZ, E., LÓPEZ-MARTÍNEZ, I. E., GIRALDO-GÓMEZ, D. M., LIRA, R., YOCUPICIO-MONROY, M., RODRÍGUEZ-BOSCH, M., SEVILLA-REYES, E. E., CORTÉS-BONILLA, M., ACEVEDO-GALLEGOS, S., MERCHANT-LARIOS, H., CARDONA-PÉREZ, J. A. & IRLES, C. 2021. Fetal and placental infection with SARS-CoV-2 in early pregnancy. *J Med Virol*.
- VAZ-SILVA, J., CARNEIRO, M. M., FERREIRA, M. C., PINHEIRO, S. V. B., SILVA, D. A., SILVA, A. L., WITZ, C. A., REIS, A. M., SANTOS, R. A. & REIS, F. M. 2009. The Vasoactive Peptide Angiotensin-(1—7), Its Receptor Mas and the Angiotensin-converting Enzyme Type 2 are Expressed in the Human Endometrium. *Reproductive Sciences*, 16, 247-256.
- VENTO-TORMO, R., EFREMOVA, M., BOTTING, R. A., TURCO, M. Y., VENTO-TORMO, M., MEYER, K. B., PARK, J. E., STEPHENSON, E., POLAŃSKI, K., GONCALVES, A., GARDNER, L., HOLMQVIST, S., HENRIKSSON, J., ZOU, A., SHARKEY, A. M., MILLAR, B., INNES, B., WOOD, L., WILBREY-CLARK, A., PAYNE, R. P., IVARSSON, M. A., LISGO, S., FILBY, A., ROWITCH, D. H., BULMER, J. N., WRIGHT, G. J., STUBBINGTON, M. J. T., HANIFFA, M., MOFFETT, A. & TEICHMANN, S. A. 2018. Single-cell reconstruction of the early maternal-fetal interface in humans. *Nature*, 563, 347-353.
- VERDECCHIA, P., CAVALLINI, C., SPANEVELLO, A. & ANGELI, F. 2020. The pivotal link between ACE2 deficiency and SARS-CoV-2 infection. *Eur J Intern Med*, 76, 14-20.
- VERDONK, K., VISSER, W., VAN DEN MEIRACKER, A. H. & DANSER, A. H. 2014. The renin-angiotensin-aldosterone system in pre-eclampsia: the delicate balance between good and bad. *Clin Sci (Lond)*, 126, 537-44.
- VILELLA, F., WANG, W., MORENO, I., ROSON, B., QUAKE, S. R. & SIMON, C. 2021. Single-cell RNA sequencing of SARS-CoV-2 cell entry factors in the preconceptional human endometrium. *Hum Reprod*, 36, 2709-2719.
- VILLA, P., TRIULZI, S., CAVALIERI, B., DI BITONDO, R., BERTINI, R., BARBERA, S., BIGINI, P., MENNINI, T., GELOSA, P., TREMOLI, E.,

- SIRONI, L. & GHEZZI, P. 2007. The Interleukin-8 (IL-8/CXCL8) Receptor Inhibitor Reparixin Improves Neurological Deficits and Reduces Long-term Inflammation in Permanent and Transient Cerebral Ischemia in Rats. *Molecular Medicine*, 13, 125-133.
- VIVANTI, A. J., VAULOUP-FELLOUS, C., PREVOT, S., ZUPAN, V., SUFFEE, C., DO CAO, J., BENACHI, A. & DE LUCA, D. 2020. Transplacental transmission of SARS-CoV-2 infection. *Nat Commun*, 11, 3572.
- VON BEEK, C., WAERN, I., ERIKSSON, J., MELO, F. R., ROBINSON, C., WALLER, A. S., SELLIN, M. E., GUSS, B. & PEJLER, G. 2019. Streptococcal sagA activates a proinflammatory response in mast cells by a sublytic mechanism. *Cell Microbiol*, 21, e13064.
- VOUSDEN, N., RAMAKRISHNAN, R., BUNCH, K., MORRIS, E., SIMPSON, N. A. B., GALE, C., O'BRIEN, P., QUIGLEY, M., BROCKLEHURST, P., KURINCZUK, J. J. & KNIGHT, M. 2022. Severity of maternal infection and perinatal outcomes during periods of SARS-CoV-2 wildtype, alpha, and delta variant dominance in the UK: prospective cohort study. *BMJ Medicine*, 1, e000053.
- WAGNER, T. R., SCHNEPF, D., BEER, J., RUETALO, N., KLINGEL, K., KAISER, P. D., JUNKER, D., SAUTER, M., TRAENKLE, B., FRECOT, D. I., BECKER, M., SCHNEIDERHAN-MARRA, N., OHNEMUS, A., SCHWEMMLE, M., SCHINDLER, M. & ROTHBAUER, U. 2022. Biparatopic nanobodies protect mice from lethal challenge with SARS-CoV-2 variants of concern. *EMBO Rep*, 23, e53865.
- WAN, C., LATTER, J. L., AMIRSHAHI, A., SYMONDS, I., FINNIE, J., BOWDEN, N., SCOTT, R. J., CUNNINGHAM, K. A., TIMMS, P. & BEAGLEY, K. W. 2014. Progesterone activates multiple innate immune pathways in Chlamydia trachomatis-infected endocervical cells. *Am J Reprod Immunol*, 71, 165-77.
- WANG, C. L., LIU, Y. Y., WU, C. H., WANG, C. Y., WANG, C. H. & LONG, C. Y. 2021. Impact of COVID-19 on Pregnancy. *Int J Med Sci*, 18, 763-767.
- WANG, H., PILLA, F., ANDERSON, S., MARTÍNEZ-ESCRIBANO, S., HERRER, I., MORENO-MOYA, J. M., MUSTI, S., BOCCA, S., OEHNINGER, S. & HORCAJADAS, J. A. 2012a. A novel model of human implantation: 3D endometrium-like culture system to study attachment of human trophoblast (Jar) cell spheroids. *Mol Hum Reprod*, 18, 33-43.
- WANG, J., JIANG, M., CHEN, X. & MONTANER, L. J. 2020a. Cytokine storm and leukocyte changes in mild versus severe SARS-CoV-2 infection: Review of 3939 COVID-19 patients in China and emerging pathogenesis and therapy concepts. *J Leukoc Biol*, 108, 17-41.
- WANG, K., GHEBLAWI, M. & OUDIT, G. Y. 2020b. Angiotensin Converting Enzyme 2: A Double-Edged Sword. *Circulation*, 142, 426-428.
- WANG, M. Y., ZHAO, R., GAO, L. J., GAO, X. F., WANG, D. P. & CAO, J. M. 2020c. SARS-CoV-2: Structure, Biology, and Structure-Based Therapeutics Development. *Front Cell Infect Microbiol*, 10, 587269.
- WANG, X., HAO, J., METZGER, D. L., MUI, A., AO, Z., AKHOUNDSADEGH, N., LANGERMANN, S., LIU, L., CHEN, L., OU, D., VERCHERE, C. B. &

- WARNOCK, G. L. 2011. Early treatment of NOD mice with B7-H4 reduces the incidence of autoimmune diabetes. *Diabetes*, 60, 3246-55.
- WANG, Y., PRINGLE, K. G., SYKES, S. D., MARQUES, F. Z., MORRIS, B. J., ZAKAR, T. & LUMBERS, E. R. 2012b. Fetal sex affects expression of renin-angiotensin system components in term human decidua. *Endocrinology*, 153, 462-8.
- WARNER, F. J., LEW, R. A., SMITH, A. I., LAMBERT, D. W., HOOPER, N. M. & TURNER, A. J. 2005. Angiotensin-converting enzyme 2 (ACE2), but not ACE, is preferentially localized to the apical surface of polarized kidney cells. *J Biol Chem*, 280, 39353-62.
- WATKINS, J. C., TOROUS, V. F. & ROBERTS, D. J. 2021. Defining Severe Acute Respiratory Syndrome Coronavirus 2 (SARS-CoV-2) Placentitis: A Report of 7 Cases With Confirmatory In Situ Hybridization, Distinct Histomorphologic Features, and Evidence of Complement Deposition. *Archives of Pathology & Laboratory Medicine*, 145, 1341-1349.
- WEATHERBEE, B. A. T., GLOVER, D. M. & ZERNICKA-GOETZ, M. 2020. Expression of SARS-CoV-2 receptor ACE2 and the protease TMPRSS2 suggests susceptibility of the human embryo in the first trimester. *Open Biol*, 10, 200162.
- WEBER, A. M., WALTERS, M. D., SCHOVER, L. R. & MITCHINSON, A. 1995. Vaginal anatomy and sexual function. *Obstetrics & Gynecology*, 86, 946-949.
- WEI, J., LOKE, P., ZANG, X. & ALLISON, J. P. 2011. Tissue-specific expression of B7x protects from CD4 T cell-mediated autoimmunity. *J Exp Med*, 208, 1683-94.
- WEI, S. Q., BILODEAU-BERTRAND, M., LIU, S. & AUGER, N. 2021. The impact of COVID-19 on pregnancy outcomes: a systematic review and meta-analysis. *Canadian Medical Association Journal*, cmaj.202604.
- WEIMAR, C. H., MACKLON, N. S., POST UITERWEER, E. D., BROSENS, J. J. & GELLERSEN, B. 2013a. The motile and invasive capacity of human endometrial stromal cells: implications for normal and impaired reproductive function. *Hum Reprod Update*, 19, 542-57.
- WEIMAR, C. H., POST UITERWEER, E. D., TEKLENBURG, G., HEIJNEN, C. J. & MACKLON, N. S. 2013b. In-vitro model systems for the study of human embryo-endometrium interactions. *Reprod Biomed Online*, 27, 461-76.
- WEISWALD, L. B., GUINEBRETIERE, J. M., RICHON, S., BELLET, D., SAUBAMÉA, B. & DANGLES-MARIE, V. 2010. In situ protein expression in tumour spheres: development of an immunostaining protocol for confocal microscopy. *BMC Cancer*, 10, 106.
- WEN, W. H., CHANG, M. H., ZHAO, L. L., NI, Y. H., HSU, H. Y., WU, J. F., CHEN, P. J., CHEN, D. S. & CHEN, H. L. 2013. Mother-to-infant transmission of hepatitis B virus infection: significance of maternal viral load and strategies for intervention. *J Hepatol*, 59, 24-30.
- WERLER, M. M., MITCHELL, A. A., HERNANDEZ-DIAZ, S. & HONEIN, M. A. 2005. Use of over-the-counter medications during pregnancy. *Am J Obstet Gynecol*, 193, 771-7.

- WESTIN, S. N., FELLMAN, B., SUN, C. C., BROADDUS, R. R., WOODALL, M. L., PAL, N., URBAUER, D. L., RAMONDETTA, L. M., SCHMELER, K. M., SOLIMAN, P. T., FLEMING, N. D., BURZAWA, J. K., NICK, A. M., MILBOURNE, A. M., YUAN, Y., LU, K. H., BODURKA, D. C., COLEMAN, R. L. & YATES, M. S. 2021. Prospective phase II trial of levonorgestrel intrauterine device: nonsurgical approach for complex atypical hyperplasia and early-stage endometrial cancer. *Am J Obstet Gynecol*, 224, 191.e1-191.e15.
- WHO. 2020. *WHO Director-General's opening remarks at the media briefing on COVID-19 - 11 March 2020* [Online]. Available: <https://www.who.int/director-general/speeches/detail/who-director-general-s-opening-remarks-at-the-media-briefing-on-covid-19---11-march-2020> [Accessed May 10 2022].
- WHO. 2023a. *Updated working definitions and primary actions for SARS-CoV-2 variants, 4 October 2023* [Online]. Available: <https://www.who.int/publications/m/item/updated-working-definitions-and-primary-actions-for--sars-cov-2-variants> [Accessed November 22 2023].
- WHO. 2023b. *WHO COVID-19 Dashboard* [Online]. Geneva. Available: <https://covid19.who.int/> [Accessed November 22 2023].
- WIDDERS, A., BROOM, A. & BROOM, J. 2020. SARS-CoV-2: The viral shedding vs infectivity dilemma. *Infect Dis Health*, 25, 210-215.
- WIERSINGA, W. J., RHODES, A., CHENG, A. C., PEACOCK, S. J. & PRESCOTT, H. C. 2020. Pathophysiology, Transmission, Diagnosis, and Treatment of Coronavirus Disease 2019 (COVID-19): A Review. *Jama*, 324, 782-793.
- WITRY, S. W. 1992. Pulmonary edema in pregnancy. *J Obstet Gynecol Neonatal Nurs*, 21, 177-84.
- WOLFF, M. V., THALER, C. J., STROWITZKI, T., BROOME, J., STOLZ, W. & TABIBZADEH, S. 2000. Regulated expression of cytokines in human endometrium throughout the menstrual cycle: dysregulation in habitual abortion. *Molecular Human Reproduction*, 6, 627-634.
- WOLTER, N., JASSAT, W., WALAZA, S., WELCH, R., MOULTRIE, H., GROOME, M., AMOAKO, D. G., EVERATT, J., BHIMAN, J. N., SCHEEPERS, C., TEBEILA, N., CHIWANDIRE, N., DU PLESSIS, M., GOVENDER, N., ISMAIL, A., GLASS, A., MLISANA, K., STEVENS, W., TREURNICHT, F. K., MAKATINI, Z., HSIAO, N. Y., PARBOOSING, R., WADULA, J., HUSSEY, H., DAVIES, M. A., BOULLE, A., VON GOTTBERG, A. & COHEN, C. 2022. Early assessment of the clinical severity of the SARS-CoV-2 omicron variant in South Africa: a data linkage study. *Lancet*, 399, 437-446.
- WÖRSDÖRFER, P., I, T., ASAHINA, I., SUMITA, Y. & ERGÜN, S. 2020. Do not keep it simple: recent advances in the generation of complex organoids. *Journal of Neural Transmission*, 127, 1569-1577.
- WRAY, S. & PRENDERGAST, C. 2019. The Myometrium: From Excitation to Contractions and Labour. *Adv Exp Med Biol*, 1124, 233-263.
- WU, H., ZHANG, S., LIN, X., HE, J., WANG, S. & ZHOU, P. 2021. Pregnancy-related complications and perinatal outcomes following progesterone supplementation before 20 weeks of pregnancy in spontaneously

- achieved singleton pregnancies: a systematic review and meta-analysis. *Reprod Biol Endocrinol*, 19, 165.
- WU, Z. & MCGOOGAN, J. M. 2020. Characteristics of and Important Lessons From the Coronavirus Disease 2019 (COVID-19) Outbreak in China: Summary of a Report of 72 314 Cases From the Chinese Center for Disease Control and Prevention. *Jama*, 323, 1239-1242.
- XIE, X., MURUATO, A., LOKUGAMAGE, K. G., NARAYANAN, K., ZHANG, X., ZOU, J., LIU, J., SCHINDEWOLF, C., BOPP, N. E., AGUILAR, P. V., PLANTE, K. S., WEAVER, S. C., MAKINO, S., LEDUC, J. W., MENACHERY, V. D. & SHI, P. Y. 2020. An Infectious cDNA Clone of SARS-CoV-2. *Cell Host Microbe*, 27, 841-848.e3.
- XIONG, Y., LIU, Y., CAO, L., WANG, D., GUO, M., JIANG, A., GUO, D., HU, W., YANG, J., TANG, Z., WU, H., LIN, Y., ZHANG, M., ZHANG, Q., SHI, M., LIU, Y., ZHOU, Y., LAN, K. & CHEN, Y. 2020. Transcriptomic characteristics of bronchoalveolar lavage fluid and peripheral blood mononuclear cells in COVID-19 patients. *Emerg Microbes Infect*, 9, 761-770.
- XU, J., ZHAO, Y. H., CHEN, Y. P., YUAN, X. L., WANG, J., ZHU, H. & LU, C. M. 2014. Maternal circulating concentrations of tumor necrosis factor-alpha, leptin, and adiponectin in gestational diabetes mellitus: a systematic review and meta-analysis. *ScientificWorldJournal*, 2014, 926932.
- XU, X., WANG, Q., DENG, B., WANG, H., DONG, Z., QU, X. & KONG, B. 2012. Monocyte Chemoattractant Protein-1 Secreted by Decidual Stromal Cells Inhibits NK Cells Cytotoxicity by Up-Regulating Expression of SOCS3. *PLOS ONE*, 7, e41869.
- XUE, H., MA, L., XUE, J., SUN, X., LI, M., LU, H., ZHOU, Y., GUO, Y., ZHANG, Y. & BAI, J. 2017. Low Expression of LEFTY1 in Placental Villi Is Associated with Early Unexplained Miscarriage. *J Reprod Med*, 62, 305-10.
- YAN, J., GUO, J., FAN, C., JUAN, J., YU, X., LI, J., FENG, L., LI, C., CHEN, H., QIAO, Y., LEI, D., WANG, C., XIONG, G., XIAO, F., HE, W., PANG, Q., HU, X., WANG, S., CHEN, D., ZHANG, Y., POON, L. C. & YANG, H. 2020. Coronavirus disease 2019 in pregnant women: a report based on 116 cases. *Am J Obstet Gynecol*, 223, 111.e1-111.e14.
- YANG, D., CHEN, Q., HOOVER, D. M., STALEY, P., TUCKER, K. D., LUBKOWSKI, J. & OPPENHEIM, J. J. 2003. Many chemokines including CCL20/MIP-3alpha display antimicrobial activity. *J Leukoc Biol*, 74, 448-55.
- YANG, Q., WANG, W., LIU, C., WANG, Y. & SUN, K. 2016. Compartmentalized localization of 11 β -HSD 1 and 2 at the feto-maternal interface in the first trimester of human pregnancy. *Placenta*, 46, 63-71.
- YANG, S., THIEL, K. W. & LESLIE, K. K. 2011. Progesterone: the ultimate endometrial tumor suppressor. *Trends in Endocrinology & Metabolism*, 22, 145-152.
- YAO, X. H., LUO, T., SHI, Y., HE, Z. C., TANG, R., ZHANG, P. P., CAI, J., ZHOU, X. D., JIANG, D. P., FEI, X. C., HUANG, X. Q., ZHAO, L., ZHANG, H., WU, H. B., REN, Y., LIU, Z. H., ZHANG, H. R., CHEN, C.,

- FU, W. J., LI, H., XIA, X. Y., CHEN, R., WANG, Y., LIU, X. D., YIN, C. L., YAN, Z. X., WANG, J., JING, R., LI, T. S., LI, W. Q., WANG, C. F., DING, Y. Q., MAO, Q., ZHANG, D. Y., ZHANG, S. Y., PING, Y. F. & BIAN, X. W. 2021. A cohort autopsy study defines COVID-19 systemic pathogenesis. *Cell Res*, 31, 836-846.
- YOCKEY, L. J. & IWASAKI, A. 2018. Interferons and Proinflammatory Cytokines in Pregnancy and Fetal Development. *Immunity*, 49, 397-412.
- YONG, Y., HUNTER-CHANG, S., STEPANOVA, E. & DEPPMANN, C. 2021. Axonal spheroids in neurodegeneration. *Mol Cell Neurosci*, 117, 103679.
- YOU, Y., STELZL, P., ZHANG, Y., PORTER, J., LIU, H., LIAO, A. H., ALDO, P. B. & MOR, G. 2019. Novel 3D in vitro models to evaluate trophoblast migration and invasion. *Am J Reprod Immunol*, 81, e13076.
- YOUNG, S. L., SAVARIS, R. F., LESSEY, B. A., SHARKEY, A. M., BALTHAZAR, U., ZAINO, R. J., SHERWIN, R. A. & FRITZ, M. A. 2017. Effect of randomized serum progesterone concentration on secretory endometrial histologic development and gene expression. *Human Reproduction*, 32, 1903-1914.
- YUAN, D. Z., LEI, Y., ZHAO, D., PAN, J. L., ZHAO, Y. B., NIE, L., LIU, M., LONG, Y., ZHANG, J. H. & YUE, L. M. 2019. Progesterone-Induced miR-145/miR-143 Inhibits the Proliferation of Endometrial Epithelial Cells. *Reprod Sci*, 26, 233-243.
- ZANONI, M., CORTESI, M., ZAMAGNI, A., ARIENTI, C., PIGNATTA, S. & TESEI, A. 2020. Modeling neoplastic disease with spheroids and organoids. *J Hematol Oncol*, 13, 97.
- ZENG, H., XU, C., FAN, J., TANG, Y., DENG, Q., ZHANG, W. & LONG, X. 2020. Antibodies in Infants Born to Mothers With COVID-19 Pneumonia. *Jama*, 323, 1848-1849.
- ZHANG, L., LIU, X., LIANG, J., WU, J., TAN, D. & HU, W. 2020. Lefty-1 inhibits renal epithelial–mesenchymal transition by antagonizing the TGF- β /Smad signaling pathway. *Journal of Molecular Histology*, 51, 77-87.
- ZHANG, W.-B., CHENG, M.-J., HUANG, Y.-T., JIANG, W., CONG, Q., ZHENG, Y.-F. & XU, C.-J. 2012. A study in vitro on differentiation of bone marrow mesenchymal stem cells into endometrial epithelial cells in mice. *European Journal of Obstetrics & Gynecology and Reproductive Biology*, 160, 185-190.
- ZHANG, Y. & ZHENG, J. 2020. Functions of immune checkpoint molecules beyond immune evasion. *Regulation of Cancer Immune Checkpoints*, 201-226.
- ZHANG, Y. Z. & HOLMES, E. C. 2020. A Genomic Perspective on the Origin and Emergence of SARS-CoV-2. *Cell*, 181, 223-227.
- ZHAO, L., FU, J., DING, F., LIU, J., LI, L., SONG, Q. & FU, Y. 2021. IL-33 and Soluble ST2 Are Associated With Recurrent Spontaneous Abortion in Early Pregnancy. *Front Physiol*, 12, 789829.
- ZHAO, L., XIA, J., WANG, X. & XU, F. 2014. Transcriptional regulation of CCL20 expression. *Microbes and Infection*, 16, 864-870.
- ZHENG, X., WANG, Q., YUAN, X., ZHOU, Y., CHU, H., WANG, G., LI, X., WANG, Y., WEI, L., WANG, L. & LI, X. 2020. B7-H4 Inhibits the

- Development of Primary Sjögren's Syndrome by Regulating Treg Differentiation in NOD/Ltj Mice. *J Immunol Res*, 2020, 4896727.
- ZHOU, F., YU, T., DU, R., FAN, G., LIU, Y., LIU, Z., XIANG, J., WANG, Y., SONG, B., GU, X., GUAN, L., WEI, Y., LI, H., WU, X., XU, J., TU, S., ZHANG, Y., CHEN, H. & CAO, B. 2020a. Clinical course and risk factors for mortality of adult inpatients with COVID-19 in Wuhan, China: a retrospective cohort study. *Lancet*, 395, 1054-1062.
- ZHOU, P., YANG, X. L., WANG, X. G., HU, B., ZHANG, L., ZHANG, W., SI, H. R., ZHU, Y., LI, B., HUANG, C. L., CHEN, H. D., CHEN, J., LUO, Y., GUO, H., JIANG, R. D., LIU, M. Q., CHEN, Y., SHEN, X. R., WANG, X., ZHENG, X. S., ZHAO, K., CHEN, Q. J., DENG, F., LIU, L. L., YAN, B., ZHAN, F. X., WANG, Y. Y., XIAO, G. F. & SHI, Z. L. 2020b. A pneumonia outbreak associated with a new coronavirus of probable bat origin. *Nature*, 579, 270-273.
- ZHOU, Q., YAN, G., DING, L., LIU, J., YU, X., KONG, S., ZHANG, M., WANG, Z., LIU, Y., JIANG, Y., KONG, N., SUN, J. & SUN, H. 2019a. EHD1 impairs decidualization by regulating the Wnt4/ β -catenin signaling pathway in recurrent implantation failure. *EBioMedicine*, 50, 343-354.
- ZHOU, Y., ZHOU, B., PACHE, L., CHANG, M., KHODABAKHSHI, A. H., TANASEICHUK, O., BENNER, C. & CHANDA, S. K. 2019b. Metascape provides a biologist-oriented resource for the analysis of systems-level datasets. *Nat Commun*, 10, 1523.
- ZHU, G., AUGUSTINE, M. M., AZUMA, T., LUO, L., YAO, S., ANAND, S., RIETZ, A. C., HUANG, J., XU, H., FLIES, A. S., FLIES, S. J., TAMADA, K., COLONNA, M., VAN DEURSEN, J. M. & CHEN, L. 2009. B7-H4-deficient mice display augmented neutrophil-mediated innate immunity. *Blood*, 113, 1759-67.
- ZIEGLER, C. G. K., ALLON, S. J., NYQUIST, S. K., MBANO, I. M., MIAO, V. N., TZOUANAS, C. N., CAO, Y., YOUSIF, A. S., BALS, J., HAUSER, B. M., FELDMAN, J., MUUS, C., WADSWORTH, M. H., 2ND, KAZER, S. W., HUGHES, T. K., DORAN, B., GATTER, G. J., VUKOVIC, M., TALIAFERRO, F., MEAD, B. E., GUO, Z., WANG, J. P., GRAS, D., PLAISANT, M., ANSARI, M., ANGELIDIS, I., ADLER, H., SUCRE, J. M. S., TAYLOR, C. J., LIN, B., WAGHRAY, A., MITSIALIS, V., DWYER, D. F., BUCHHEIT, K. M., BOYCE, J. A., BARRETT, N. A., LAIDLAW, T. M., CARROLL, S. L., COLONNA, L., TKACHEV, V., PETERSON, C. W., YU, A., ZHENG, H. B., GIDEON, H. P., WINCHELL, C. G., LIN, P. L., BINGLE, C. D., SNAPPER, S. B., KROPSKI, J. A., THEIS, F. J., SCHILLER, H. B., ZARAGOSI, L. E., BARBRY, P., LESLIE, A., KIEM, H. P., FLYNN, J. L., FORTUNE, S. M., BERGER, B., FINBERG, R. W., KEAN, L. S., GARBER, M., SCHMIDT, A. G., LINGWOOD, D., SHALEK, A. K. & ORDOVAS-MONTANES, J. 2020. SARS-CoV-2 Receptor ACE2 Is an Interferon-Stimulated Gene in Human Airway Epithelial Cells and Is Detected in Specific Cell Subsets across Tissues. *Cell*, 181, 1016-1035.e19.

8 Appendix

8.1 Supplementary Data: Materials and Methods

Supplementary Table 8-1: Endometrial Organoids Medium, for 30 ml

Material	Amount
FGF-10, 20 µg/ml	15 µl
EGF, 100 µg/ml	15 µl
A 83-01, 5 mM	3 µl
N2 supplement, 100X	300 µl
B27 supplement 100X	600 µl
<i>N</i> -Acetyl-L-cystein, 500 mM	75 µl
Nicotinamide, 1 M	60 µl
SB202190, 5 mM	6 µl
Y-27632, 10 mM	30 µl
LWRN 10% conditioned medium (RN8)	3 ml
Advanced DMEM/F-12 (containing 10 mM HEPES, 1% GlutaMAX and 1% antibiotic/antimycotic solution)	25.92 ml

Supplementary Table 8-2: Tri-Sodium Citrate Buffer, pH 6

Material	Amount
Tri-sodium citrate dihydrate	2.94 g
Distilled water	Fill up to 1000 ml
HCl	Adjust pH to 6
Tween 20	2.5 ml

Supplementary Table 8-3: Laemmli Buffer 2X, for 50 ml

Material	Amount
0.5 M Tris buffer (pH 6.8)	10 ml
20% SDS solution	5 ml
Distilled water	19 ml
Glycerol	10 ml
0.1% Bromophenol blue	1 ml
2-mercaptoethanol	5 ml

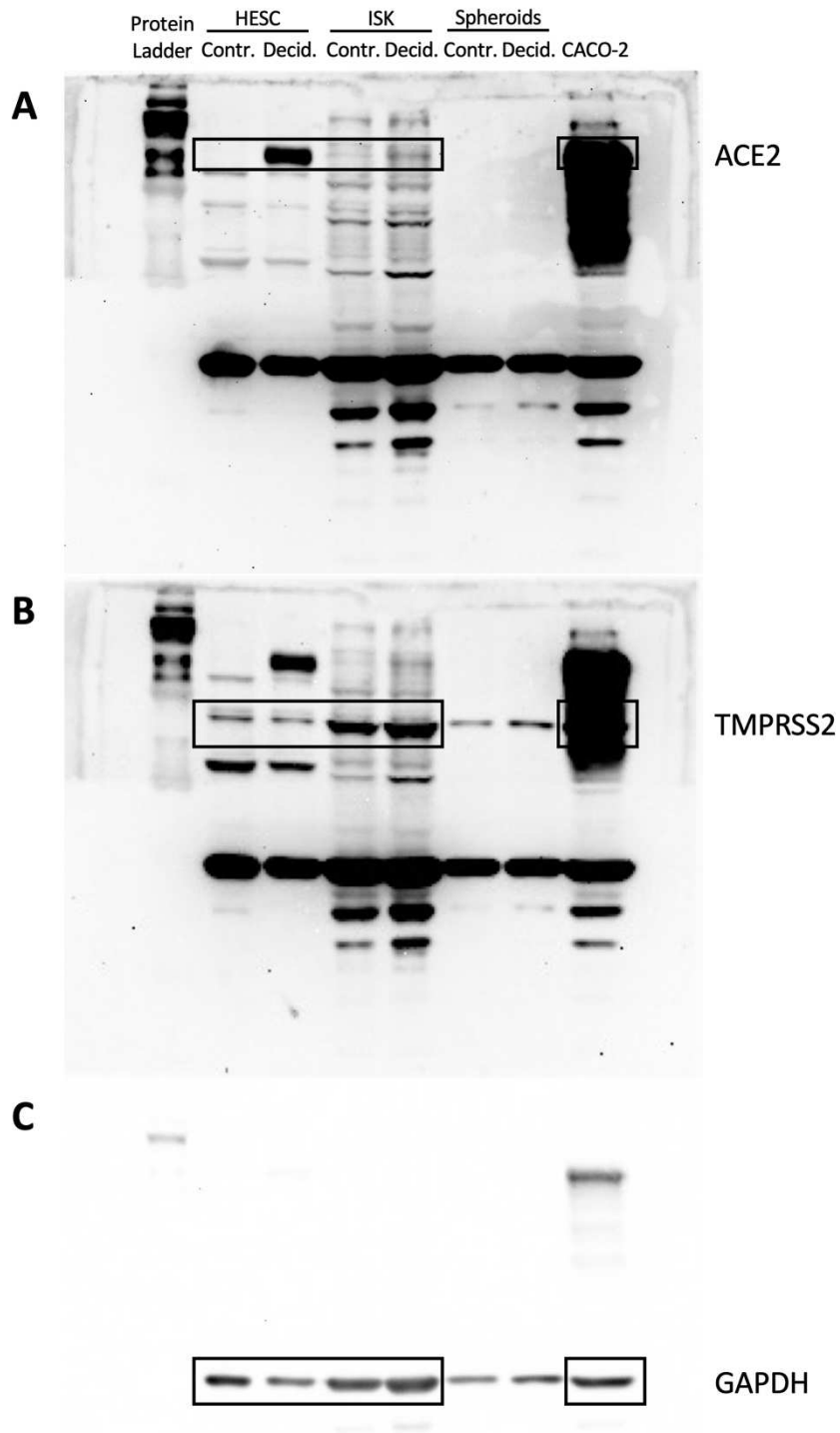
Supplementary Table 8-4: Hand Casted Electrophoresis Gel, Volume for Two Gels

Material	Amount
Gel cassettes	2
Separating Gel (10%)	
Acrylamide/Bis-solution	6.6 ml
2 M Tris buffer (pH 8.8)	4 ml
Distilled water	9.2 ml
20% SDS solution	100 μ l
10% APS	100 μ l
TEMED	40 μ l
Stacking Gel (4%)	
Acrylamide/Bis-solution	1.33 ml
0.5 M Tris buffer (pH 6.8)	2.5 ml
Distilled water	6.1 ml
20% SDS solution	50 μ l
10% APS	66.7 μ l
TEMED	20 μ l

Supplementary Table 8-5: Tris Buffered Saline Tween 20 (TBST)

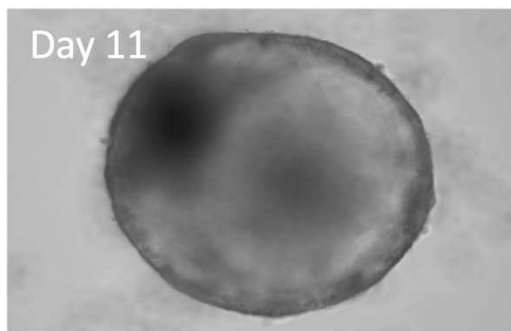
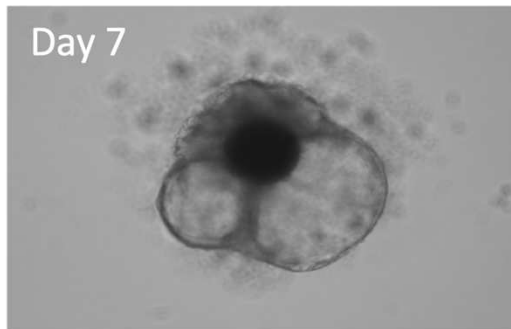
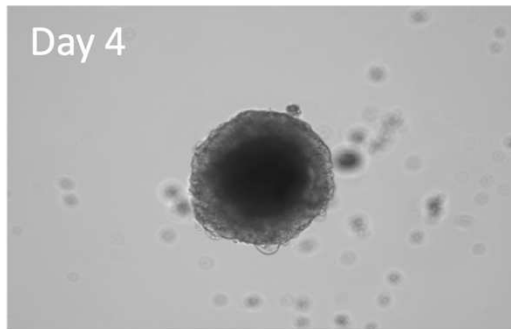
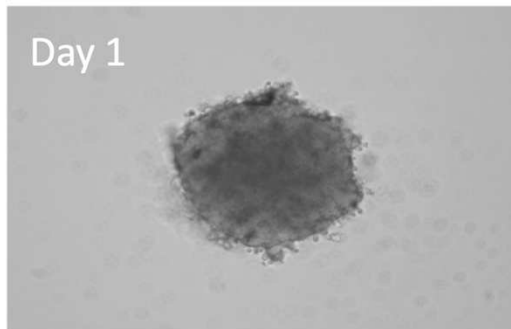
Material	Amount
Sodium chloride (NaCl)	17.5 g
Trizma base	4.8 g
Tween 20	2 ml
Distilled water	2 L

8.2 Supplementary Data: Results

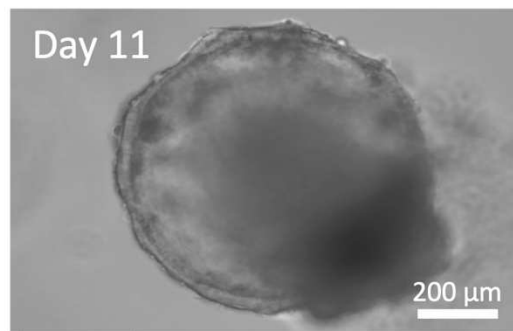
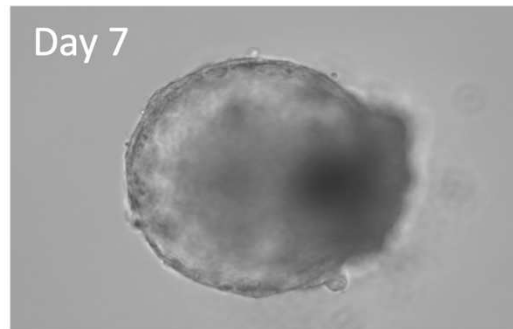
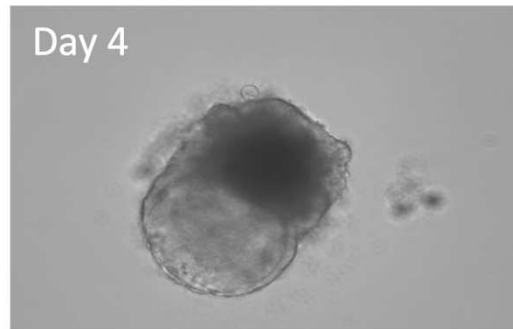
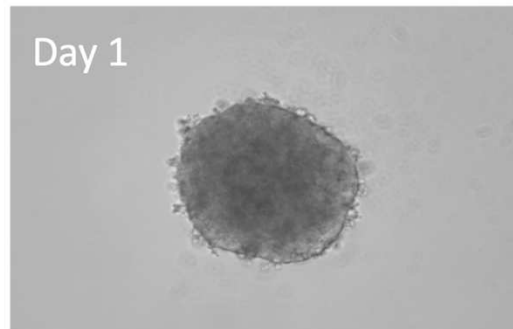


Supplementary Figure 8-1: Full Western Blot for ACE2 and TMPRSS2 in 2D HESC and ISK Cells. Control (Contr.) and decidualized (Decid.) HESC and ISK were cultured in a monolayer. A western blot was performed for ACE2 (A, 120 kDa) and TMPRSS2 (B, 70 kDa) with GAPDH (C, 37 kDa) as a loading control and CACO-2 cells as a positive control. Rectangles indicate sections chosen for Figure 3-3.

Agarose-coated wells

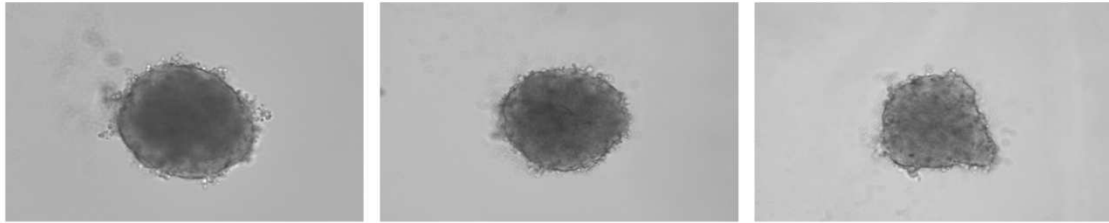


Ultra-low attachment wells

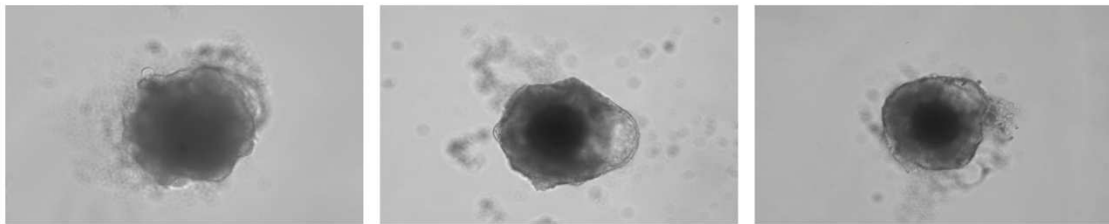


Supplementary Figure 8-2: Comparison of Endometrial Spheroids Grown in Agarose-Coated or Ultra-Low Attachment Wells. Endometrial spheroids were cultured using the liquid-overlay technique either in agarose-coated wells (left) or in commercially available ultra-low attachment wells (right). Spheroids were imaged for 11 days through phase-contrast microscopy. The scale bar is 200 μm .

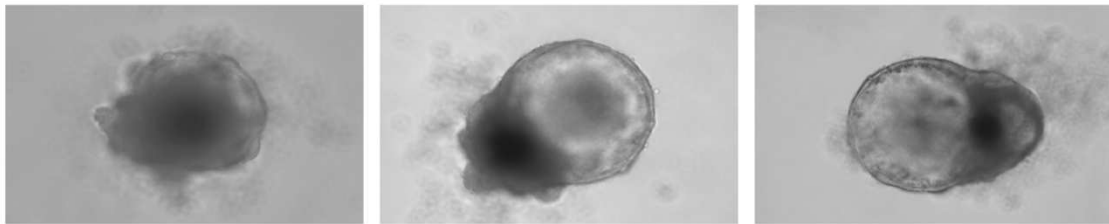
Day 1



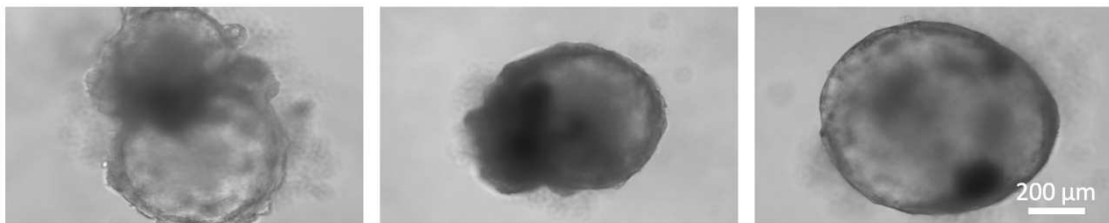
Day 4



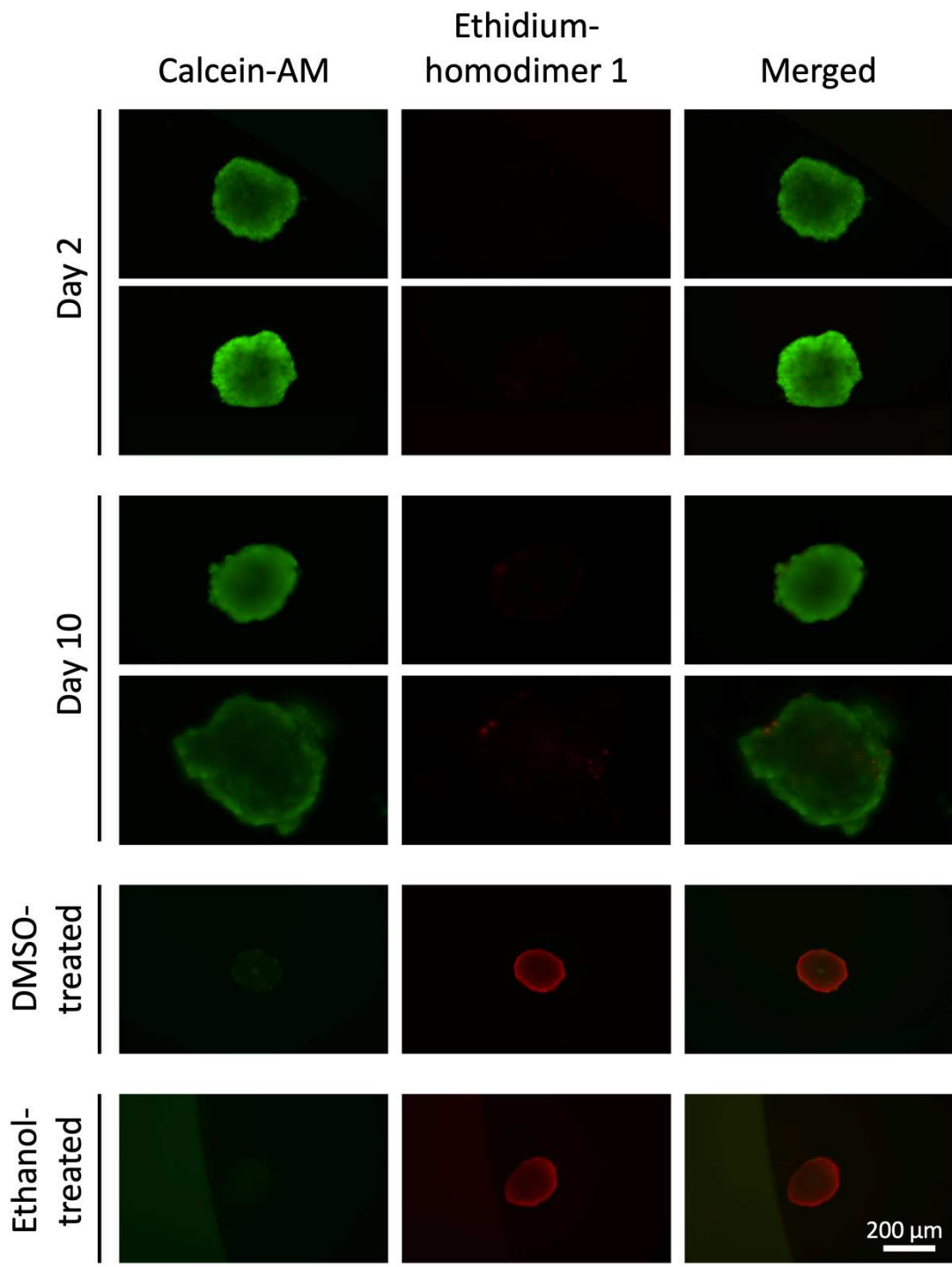
Day 8



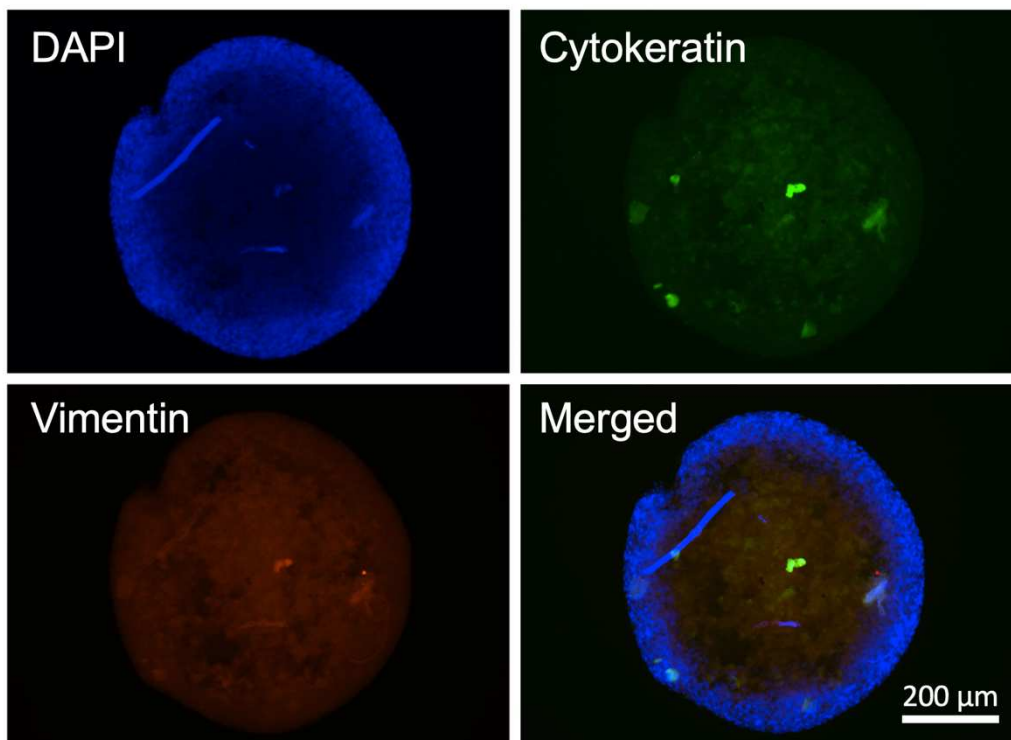
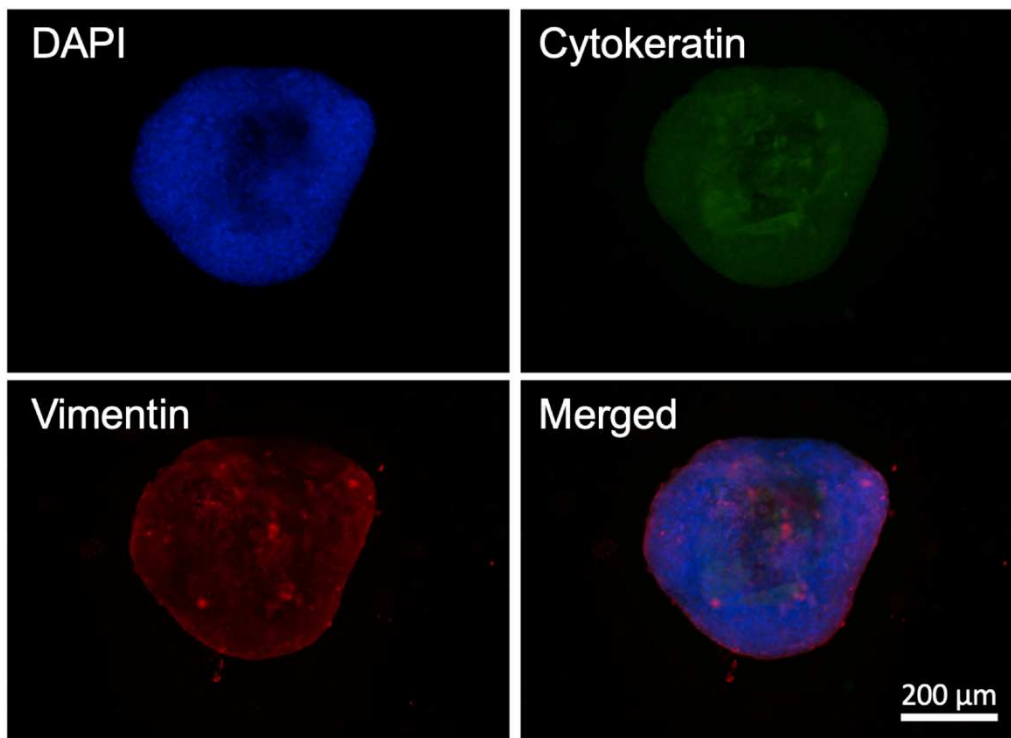
Day 11



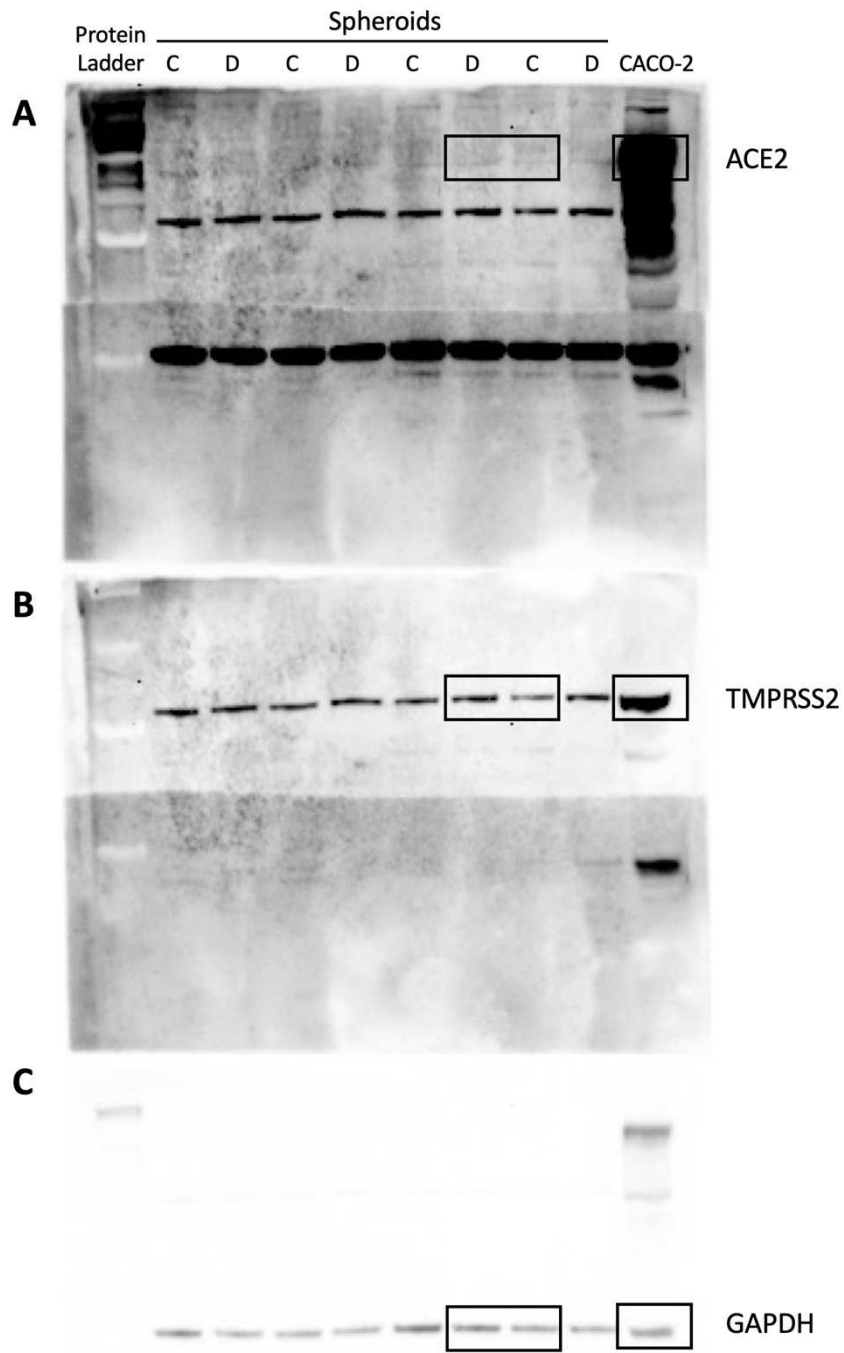
Supplementary Figure 8-3: Additional Images of the Growth of Endometrial Spheroids. For 11 days, the growth of endometrial spheroids was monitored through phase-contrast microscopy. Images in one row represent one time point and images in one column represent the growth of a single spheroid. The scale bar is 200 μm . Images are representative of at least 100 spheroids.



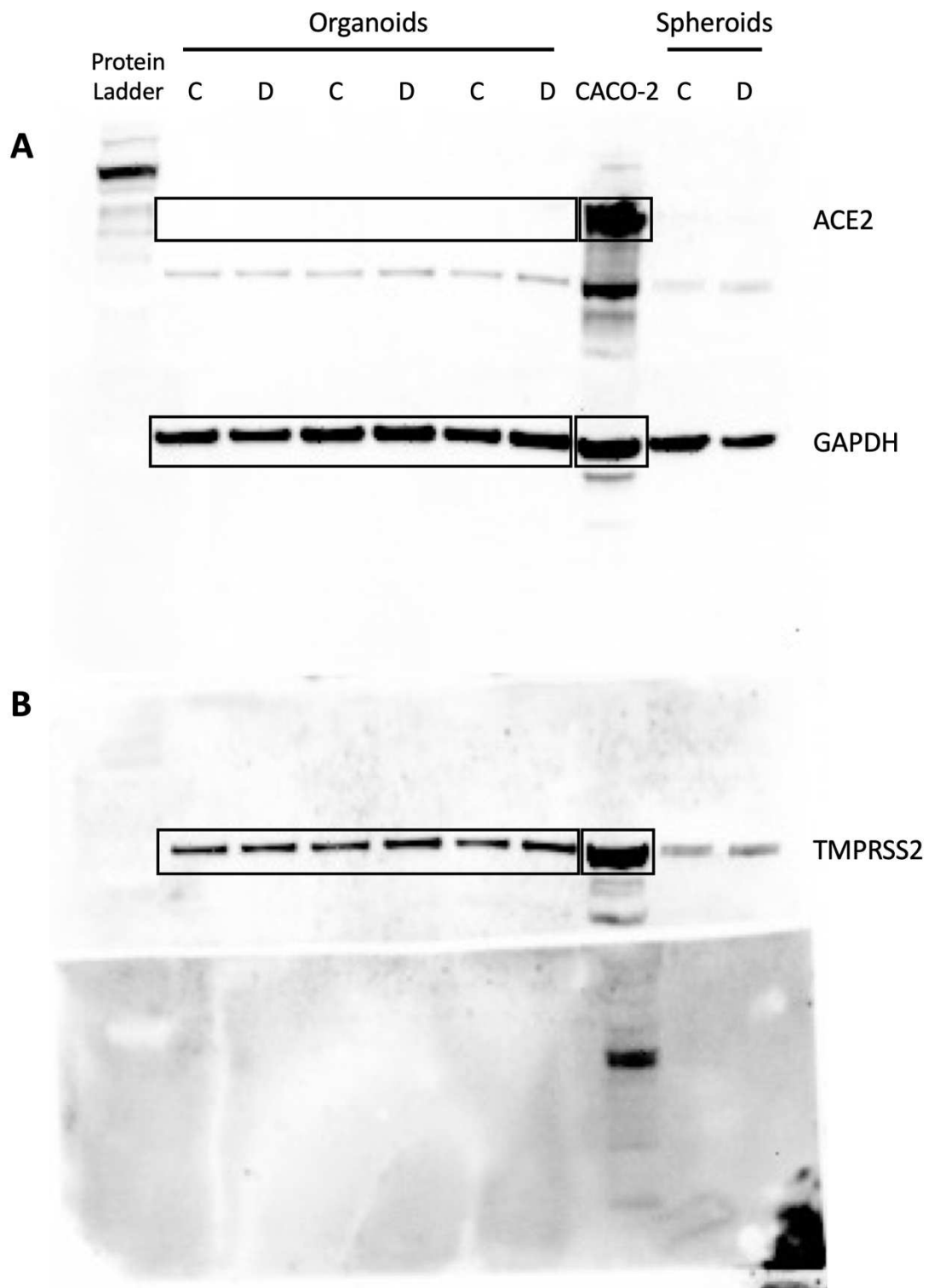
Supplementary Figure 8-4: Additional Images of Viability Assay of Endometrial Spheroids. After 2 and 10 days in culture, respectively, endometrial spheroids were tested for viability using the LIVE/DEAD Viability/Cytotoxicity Kit. Live cells were stained with calcein-AM (green) and dead cells were stained with ethidium-homodimer-1 (red). DMSO- or ethanol-treated spheroids were used as dead control. The scale bar is 200 μm .



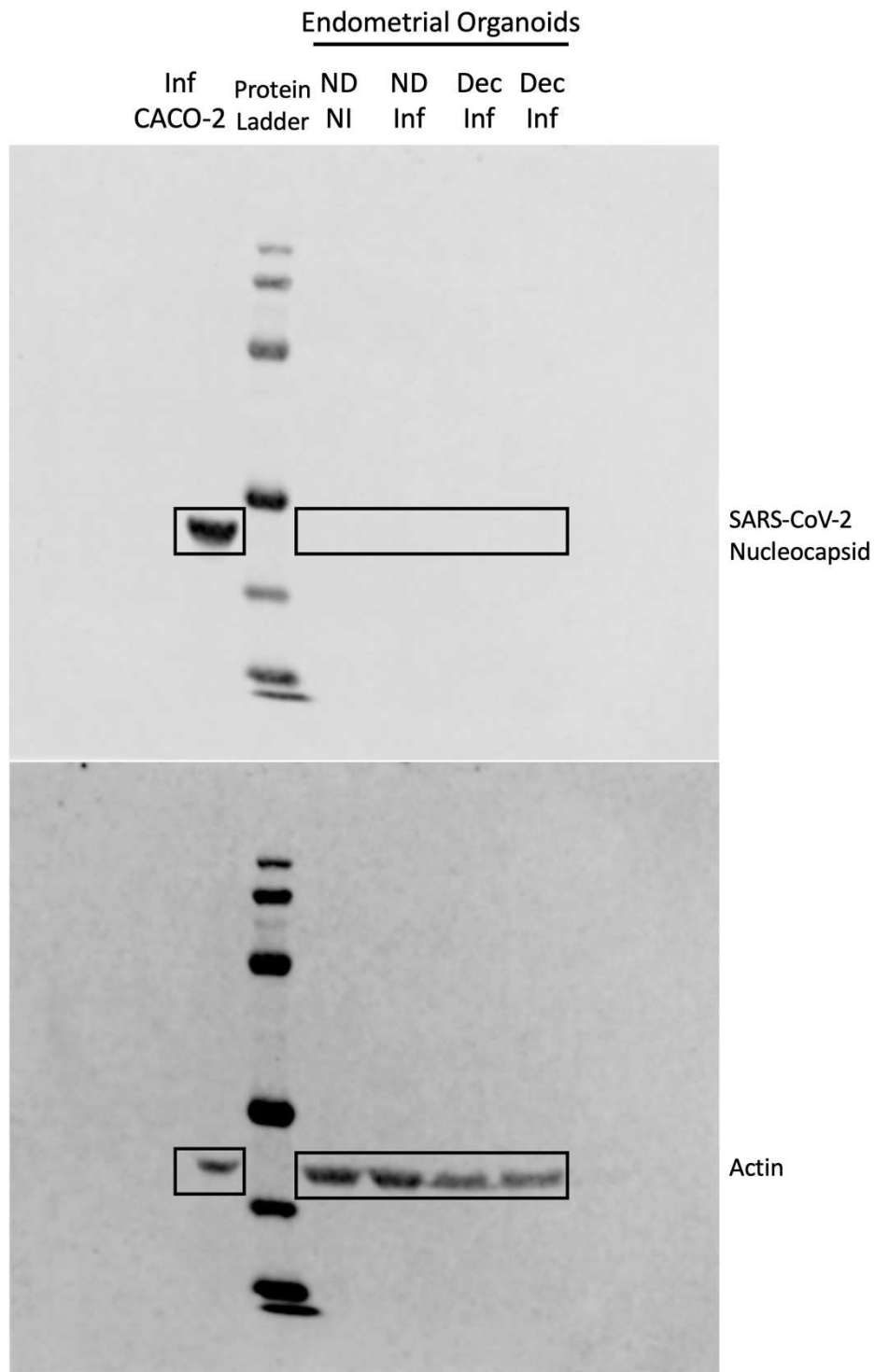
Supplementary Figure 8-5: Additional Images of Immunostaining of Endometrial Spheroids for Cytokeratin 7 and Vimentin. Endometrial spheroids cultured for 7 days were stained for epithelial cell marker cytokeratin 7 (green) and stromal cell marker vimentin (red). The nuclei were counterstained with DAPI (blue). The scale bar is 200 μm.



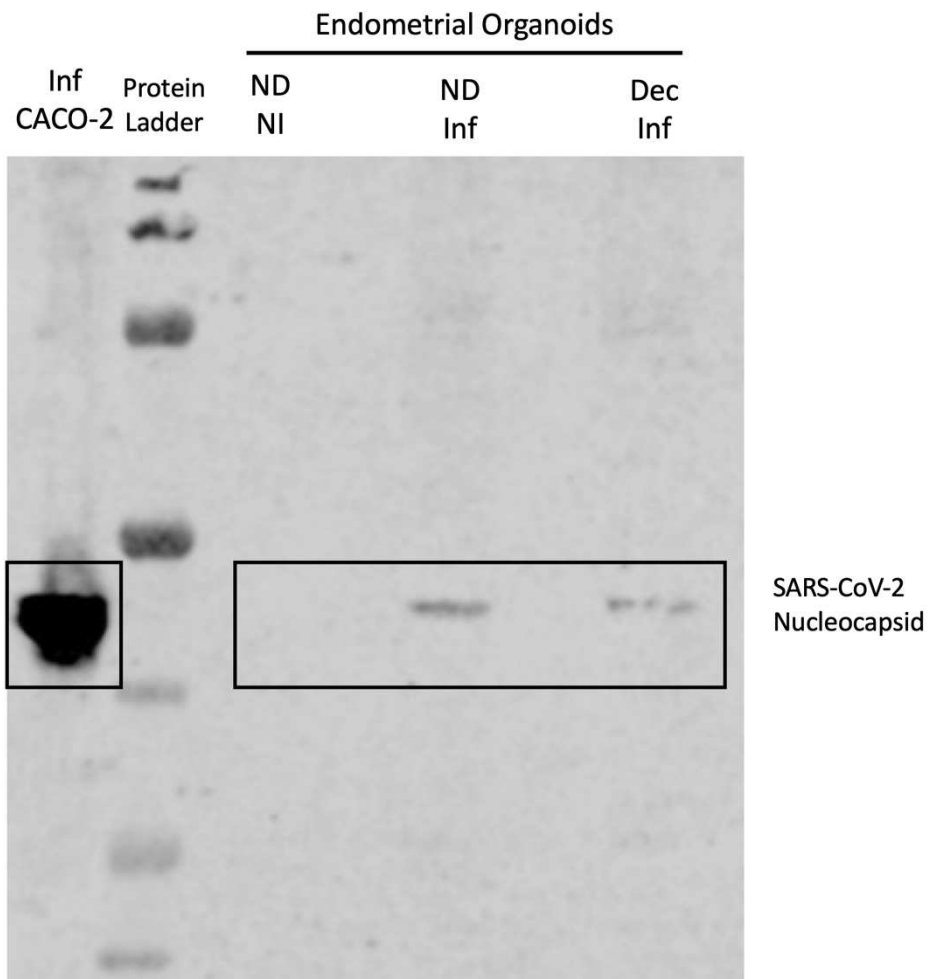
Supplementary Figure 8-6: Full Western Blot for ACE2 and TMPRSS2 in Endometrial Spheroids. A western blot was performed using protein isolates of control (C) and decidualized (D) endometrial spheroids. ACE2 (A, 120 kDa) and TMPRSS2 (B, 70 kDa) were determined. GAPDH (C, 37 kDa) was used as a loading control and CACO-2 cells as a positive control. Rectangles indicate sections chosen for Figure 3-12.



Supplementary Figure 8-7: Full Western Blot for ACE2 and TMPRSS2 in Endometrial Organoids. A western blot was performed using protein isolates of control (C) and decidualized (D) endometrial organoids. ACE2 (A, 120 kDa) and TMPRSS2 (B, 70 kDa) were determined. GAPDH (A, 37 kDa) was used as a loading control and CACO-2 cells as a positive control. Rectangles indicate sections chosen for Figure 3-16.

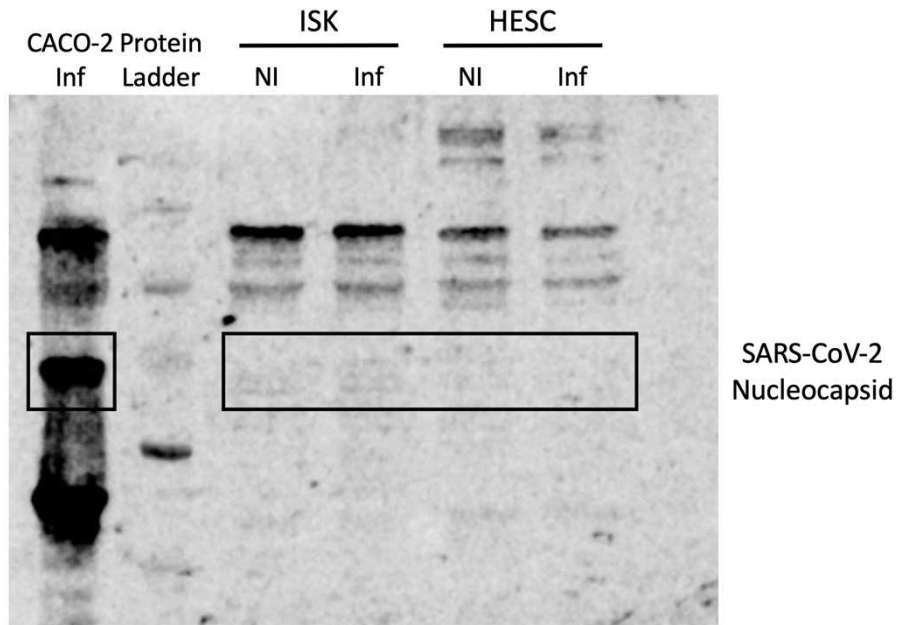


Supplementary Figure 8-8: Full Western Blot for SARS-CoV-2 Nucleocapsid Protein in Infected Basal Out Organoids. Non-decidualized (ND) and decidualized (Dec) basal out endometrial organoids were non-infected (NF) or infected (Inf) with SARS-CoV-2 B.1. Western blot was performed for SARS-CoV-2 nucleocapsid protein (A, 49 kDa) with Actin (B, 42 kDa) as loading control. Rectangles indicate sections chosen for **Figure 3-16**.

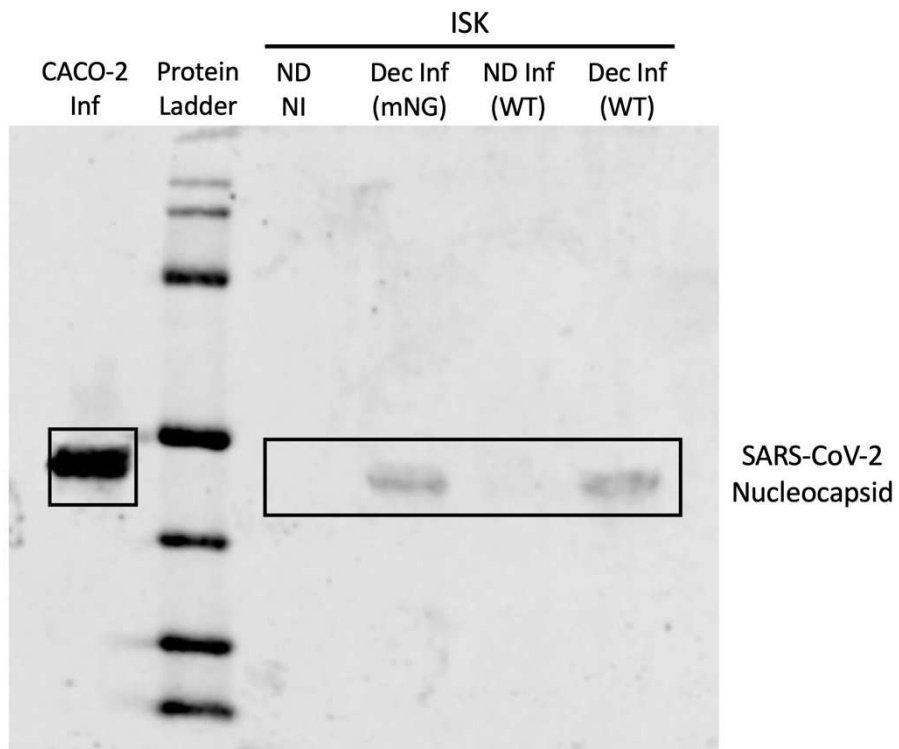


Supplementary Figure 8-9: Full Western Blot for SARS-CoV-2 Nucleocapsid Protein in Infected Apical Out Organoids. Non-decidualized (ND) and decidualized (Dec) apical out endometrial organoids were non-infected (NI) or infected (Inf) with SARS-CoV-2 B.1.617.2. Western blot was performed for SARS-CoV-2 nucleocapsid protein (A, 49 kDa). Rectangles indicate sections chosen for **Figure 3-17**.

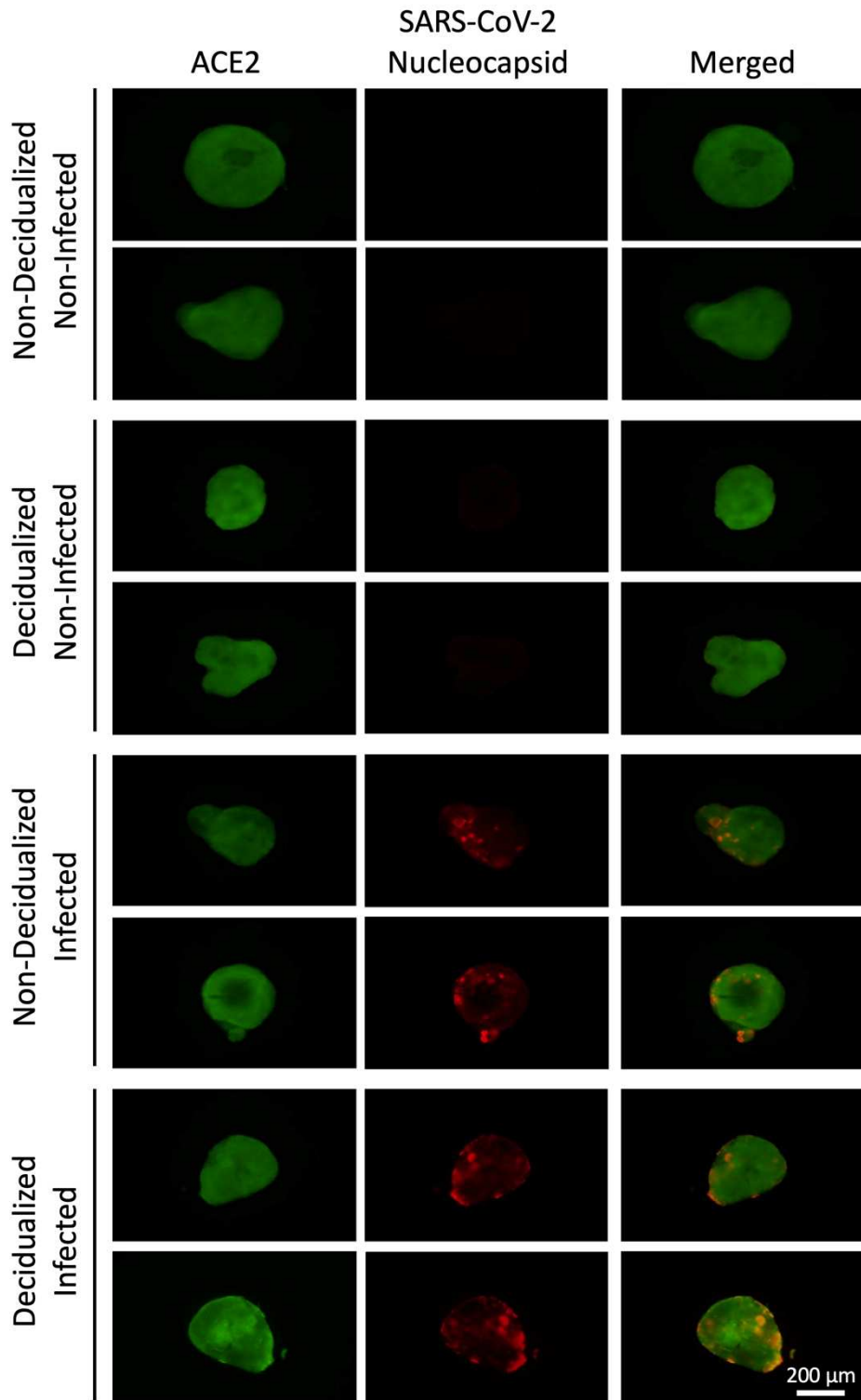
A Non-Decidualized 2D Cells



B ISK

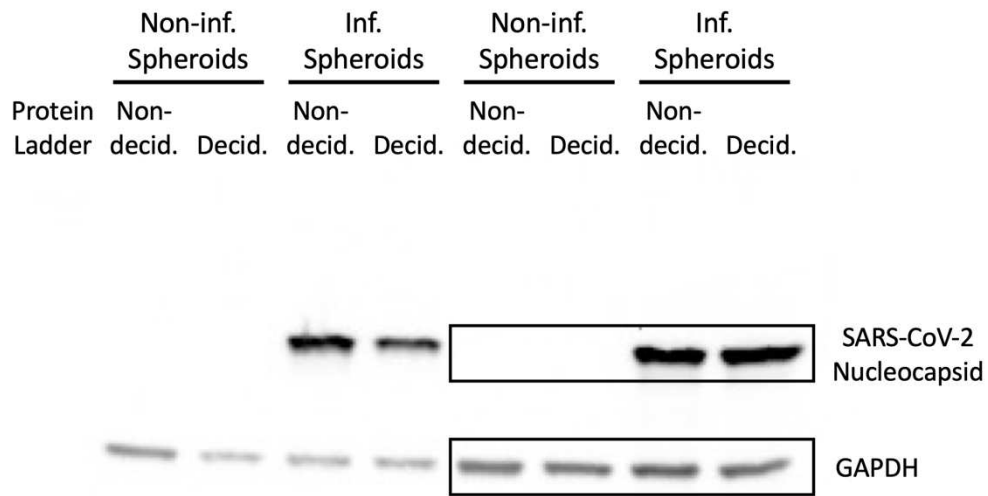


Supplementary Figure 8-10: Full Western Blot for SARS-CoV-2 Nucleocapsid Protein in Infected 2D Cells. HESC and ISK cells cultured in a monolayer were non-infected (NF) or infected (Inf) with SARS-CoV-2 B.1 (A). Non-decidualized (ND) and decidualized (Dec) ISK were non-infected (NF) or infected (Inf) with ic-SARS-CoV-2-mNG (mNG) or SARS-CoV-2 B.1 (WT). Western blot was performed for SARS-CoV-2 nucleocapsid protein (49 kDa). Rectangles indicate sections chosen for **Figure 3-18**.

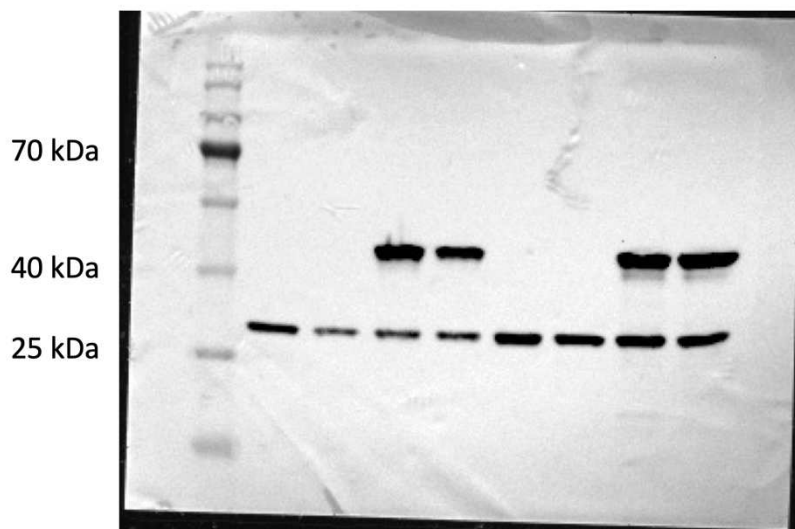


Supplementary Figure 8-11: Additional Images of Non-Infected and Infected Endometrial Spheroids. After 48 h of infection, endometrial spheroids were fixed and stained for ACE2 (green) and SARS-CoV-2 nucleocapsid protein (red). The scale bar is 200 μm .

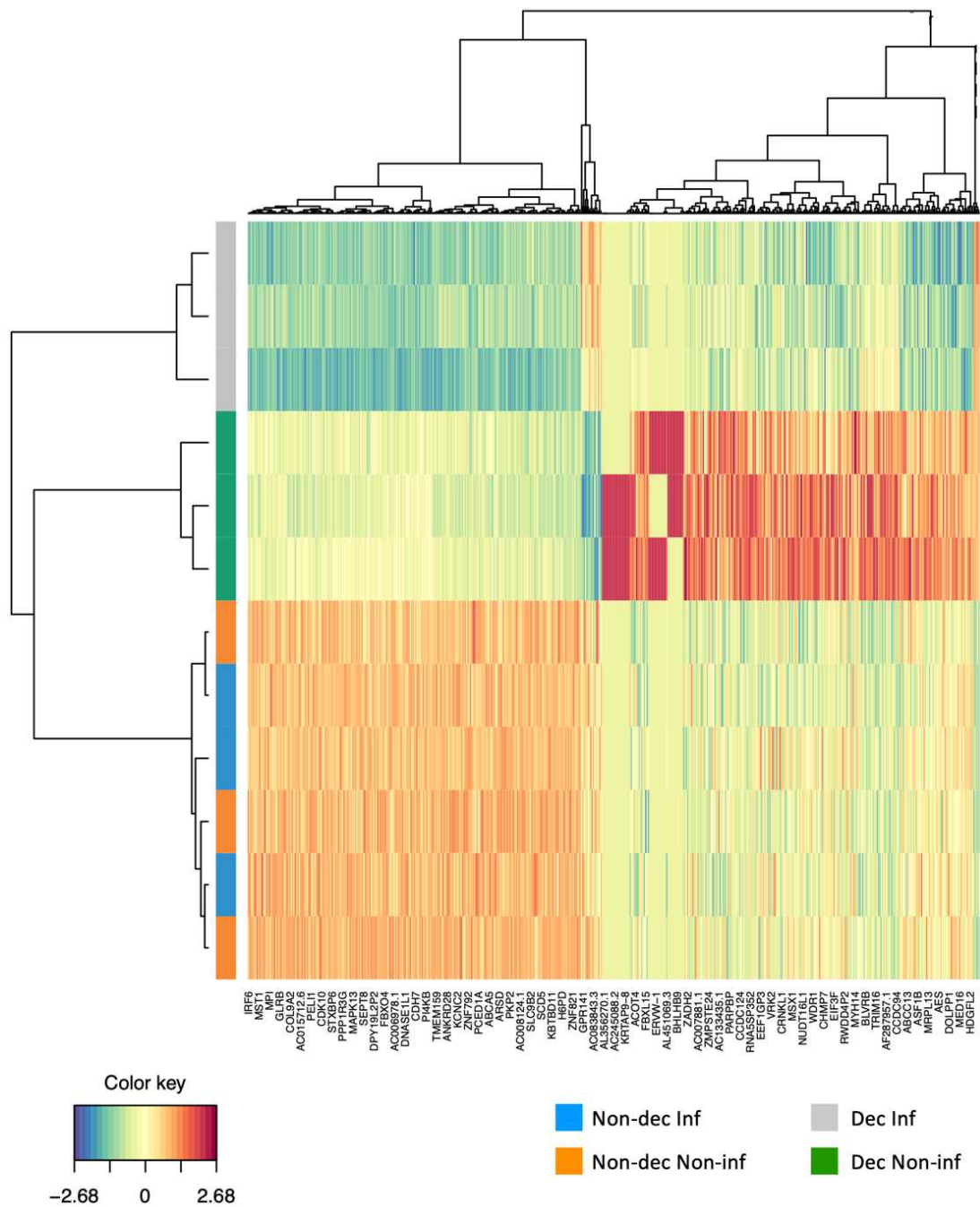
A



B



Supplementary Figure 8-12: Full Western Blot for SARS-CoV-2 Nucleocapsid Protein in Infected Endometrial Spheroids. Non-decidualized (Non-decid.) and decidualized (Decid.) endometrial spheroids were non-infected (Non-inf.) or infected (Inf.) with SARS-CoV-2 B.1.617.2. Western blot was performed for SARS-CoV-2 nucleocapsid protein (A, 49 kDa) with GAPDH (37 kDa) as a loading control. Overlay image (B) shows the protein ladder for reference. Rectangles indicate sections chosen for Figure 3-21.



Supplementary Figure 8-13: Heat Map with Dendrogram of DEGs from Endometrial Spheroids Infected with SARS-CoV-2. A subset of selected DEGs from RNA-seq analysis are displayed as a heat map with each row representing an individual gene and each column representing a pairwise comparison of two experimental groups. A dendrogram shows similarity between the groups. The color scale indicates the gene expression levels, with red indicating upregulation and blue indicating downregulation.

9 Erklärung zum Eigenanteil

Die Arbeit wurde am Forschungsinstitut für Frauengesundheit der Universitätsfrauenklinik Tübingen unter Betreuung von Frau Prof. Sara Y. Brucker und Frau Dr. Madhuri S. Salker durchgeführt.

Die Konzeption der Studie erfolgte in Zusammenarbeit mit Frau Dr. Madhuri S. Salker, Herr Dr. Yogesh Singh und Herr Prof. Michael Schindler.

Mit Ausnahme der im Folgenden genannten Schritte wurden sämtliche Versuche von mir eigenständig durchgeführt: Bereitstellen der Organoid-Linien durch Herr Dr. André Koch, Paraffin-Einbettung und Schneiden der Organoide durch Frau Ingrid Teufel, Infektionen mit SARS-CoV-2 im S3 Labor sowie Mikroskopie und Western Blot für Figure 3-17 und 3-18 durch Frau Dr. Natalia Ruetalo-Buschinger, Inaktivieren des Überstands mittels UV-Strahlung durch Frau Miriam Hohner, Bedienung des Durchflusszytometers durch Herr Dr. Yogesh Sing, Durchführung der RNA-Sequenzierung am Institut für Medizinische Genetik und Angewandte Genomik und bioinformatische Auswertung der RNA-Sequenzierungsdaten durch Herr Miguel Camarena-Sainz.

Die statistische Auswertung erfolgte eigenständig durch mich.

Teile der Einleitung wurden aus der Publikation „Molecular and Physiological Aspects of SARS-CoV-2 Infection in Women and Pregnancy“ übernommen, für die ich den ursprünglichen Entwurf geschrieben und die Abbildungen mittels BioRender.com erstellt habe. Die Ko-Autoren Frau Dr. Madhuri S. Salker, Frau Janet Raja Xavier, Herr Dr. Yogesh Singh und Frau Prof. Sara Y. Brucker unterstützten mich mit Ihrem Rat bei der Literaturrecherche, bei der Erstellung sowie beim Korrekturlesen der Publikation.

Ich versichere, das Manuskript selbständig verfasst zu haben und keine weiteren als die von mir angegebenen Quellen verwendet zu haben.

Holzheim, den 04.12.2023

10 Publications

Parts of this thesis have been previously published in:

Liu A, Raja Xavier J, Singh Y, Brucker SY, Salker MS. **Molecular and Physiological Aspects of SARS-CoV-2 Infection in Women and Pregnancy.** Front Glob Womens Health. 2022 Feb 24;3:756362.
doi: 10.3389/fgwh.2022.756362. PMID: 35284910; PMCID: PMC8908006.

Oral presentation at the 14th Congress of the European Society of Gynecology (Venice, Italy, 2021) and publication of the abstract in:

Liu A, Raja Xavier J, Singh Y, Koch A, Brucker SY, Salker MS. **Use of 3D endometrial spheroids and organoids to understand vertical transmission of COVID-19.** EGO European Gynecology and Obstetrics (2021); 2021/03, Supplement 1, p. 49

The results of this thesis are part of an unpublished manuscript:

Liu A, Ruetalo N, Raja Xavier J, Brucker SY, Singh Y, Schindler M, Salker MS. **Human Endometrial Spheroids and Monolayers Provide Insights into SARS-CoV-2 Infection during Early Pregnancy.** *In Preparation.*

11 Acknowledgments

I would like to express my deepest gratitude to my supervisors Prof. Sara Y. Brucker and Dr. Madhuri S. Salker for their support, guidance and invaluable feedback throughout the entire process of researching and writing this thesis. Their expertise and insightful comments greatly improved this thesis.

Further, I am thankful to Prof. Daniel Sauter for his interest in my thesis, his flexibility and the exciting discussion.

Special thanks go to Dr. Yogesh Singh, whose ideas, support and intellectual input were indispensable to the successful completion of this study.

I extend my appreciation to Prof. Michael Schindler and Dr. Natalia Ruetalo-Buschinger at the Institute for Medical Virology for the great inspiration and collaboration essential to this study.

I am grateful for the help I received from the Institute for Medical Genetics and Applied Genomics and from Miguel Camarena-Sainz.

Special thanks go to Janet Raja Xavier for teaching me essential laboratory techniques, for a great time in Venice and for her friendship.

I am sincerely grateful to Dr. André Koch and his team for their support, shared knowledge and critical discussions.

I am indebted to my family and my partner for their unwavering support and encouragement throughout this academic journey. Their love and understanding have been a constant source of motivation.

Finally, I want to express my gratitude to my friends who encouraged me, shared their perspectives and supported me during challenging times.

This thesis would not have been possible without the collective contributions and support of these individuals and for that, I am truly grateful.